Small regulatory RNAs in vascular remodeling and atherosclerosis

Ingen, E. van

Small regulatory RNAs in Vascular Remodeling and Atherosclerosis

Eva van Ingen

Small regulatory RNAs in Vascular Remodeling and Atherosclerosis

Eva van Ingen

Cover photo	Eva van Ingen | *In vitro* cultured human macrophages (edited)
Cover design	Tom van Ingen
Lay-out	Eva van Ingen
Print	Ridderprint | www.ridderprint.nl
ISBN	978-94-6458-246-8

Small regulatory RNAs in Vascular Remodeling and Atherosclerosis

Proefschrift

ter verkrijging van
de graad van doctor aan de Universiteit Leiden,
op gezag van rector magnificus prof.dr.ir. H. Bijl,
volgens besluit van het college voor promoties
te verdedigen op donderdag 9 juni 2022
klokke 15.00 uur

door

Eva van Ingen

geboren te Utrecht
in 1992

Promotor:	Prof. dr. P.H.A. Quax
Copromotor:	Dr. A.Y. Nossent
Leden promotiecommissie:	Prof. dr. M.J.T.H. Goumans
	Prof. dr. P.C.N. Rensen
	Prof. dr. R.A. Boon (Amsterdam UMC)
	Dr. I. Bot (Leiden University)

The research described in this thesis was supported by a grant from the Rembrandt Institute of Cardiovascular Science (2016). Financial support by the Dutch Heart Foundation for the publication of this thesis is gratefully acknowledged.

Table of contents

Chapter 1

General Introduction

General introduction

Cardiovascular disease

Cardiovascular disease (CVD) is a major cause of death worldwide, representing 31% of all global deaths[1]. The heart and blood vessels, called the cardiovascular system, circulate blood through the body in order to deliver oxygen and nutrients and to remove waste products. CVD is a collective term for multiple diseases affecting the cardiovascular system, including myocardial infarction, ischemic stroke and peripheral arterial disease (PAD).

Atherosclerosis

The underlying cause of most CVD is atherosclerosis. Atherosclerosis is a chronic inflammatory disease, characterized by progressive plaque build-up in the arterial wall. Plaques are composed of lipids and inflammatory cells, and develop in the subendothelial intimal layer in large- and medium-sized arteries[2, 3]. Most plaques that develop during a person's life remain clinically silent. Patients generally only start developing symptoms when the artery becomes severely narrowed (stenosis of over 70%) or when a plaque ruptures. The latter causes acute occlusion of the artery and patients often present with more severe symptoms that can even be fatal, i.e. a myocardial infarction and ischemic stroke. Full rupture of a plaque or plaque erosion (this is when a superficial piece of the plaque breaks off) triggers thrombus formation in the artery. The thrombus partially or completely occludes the artery, blocks blood flow downstream and causes acute lack of oxygen and nutrients in the affected area, called an infarction[4-6]. Oxygen and nutrients are crucial for tissue survival and function[3, 8]. Immediate action is therefore needed to restore blood flow and to limit adverse consequences, including cell death and permanent damage in the ischemic tissues[10, 11].

Risk factors and current therapies

Risk factors for atherosclerosis-induced CVD are hypercholesterolemia, diabetes, obesity, genetic predisposition, hypertension and age[11]. Many of these risk factors can be the result of an unhealthy lifestyle, such as high fat, cholesterol and salt intake, smoking and lack of physical activity. Healthy lifestyle changes can therefore help in the prevention of CVD. Plasma lipid lowering drugs (e.g. statins), platelet inhibitors and antihypertensives are examples of widely used medications to lower the risk of a (recurrent) cardiovascular event[11-13]. Once a cardiovascular event has occurred, therapies are aimed at restoring blood flow in order to prevent recurrence and support the affected organ, such as the heart.

Thrombus dissolving drugs (thrombolytics) and surgical interventions are current therapies to remove the arterial blockage[4, 10, 14].

Balloon angioplasty with or without stent placement is often used to treat a myocardial infarction[10]. These endovascular interventions can restore blood flow quickly. A disadvantage of these endovascular interventions however, is the high risk of recurrent occlusions. An alternative surgical procedure is bypass placement. Bypass surgery is less favorable in the acute situation, but can be performed when endovascular interventions are not successful (e.g. recurrent occlusions) or possible. Often the saphenous vein from the patient's own leg is used as a bypass graft. Bypasses made from venous vessels are more easily available than arterial vessels. A disadvantage of venous bypasses however, is the high risk of reocclusion of the vein graft. In this case a second intervention is required, although this is not always possible[15-17].

An endarterectomy of the carotid artery in the neck is performed to prevent an ischemic stroke. An endarterectomy is a surgical procedure to remove the plaque from the arterial wall. This is a risky surgical procedure and therefore only performed if the potential benefit of the intervention outweighs the potential adverse peri-operative risks. Criteria are when the plaque is causing significant stenosis (>70%) or when the plaque is symptomatic and causes transient ischemic attacks (TIAs). In many cases, however, symptoms occur during an ischemic stroke, making prevention no longer possible. Once a patient is diagnosed with ischemic stroke, often thrombolytics are used to dissolve the thrombus that blocks blood supply to part of the brain[4].

The presentation of PAD varies and includes acute and chronic presentations. In PAD patients, symptoms are caused by acute blockage or gradual narrowing (i.e. chronic limb ischemia) of a peripheral artery. Blockage of the artery leads to distal ischemia with symptoms such as severe pain during exercise or even in rest, coldness and numbness in the affected limb and non-healing ulcers. Neovascularization is the formation of new blood vessels and the body's own capacity to restore blood flow. In the more severe PAD patients, however, this capacity is not sufficient to restore blood flow. Surgical interventions are required to restore blood flow in these patients. Prolonged lack of blood supply may eventually lead to cell death, non-healing wounds and gangrene in the affected limb. Amputation of the affected limb is then needed to release a patient from pain and to prevent life-threatening sepsis[14, 18].

Even though current therapeutic strategies succeed in restoring blood flow and contribute to reduce the risk of (recurrent) cardiovascular events, a need remains to improve clinical outcome.

Pathogenesis of atherosclerosis

Traditionally, atherosclerosis was seen as a cholesterol storage disease in the intimal layer of arteries. Nowadays, it is increasingly recognized that atherosclerosis is largely driven by inflammation too[2, 3, 19]. In the initial phase of plaque development low-density lipoprotein (LDL) particles enter the intima and start to accumulate in the arterial wall, where they become oxidized (oxLDL). Endothelial cells lining the inner layer of the vessel wall undergo inflammatory activation. Circulating monocytes and other leukocytes bind to the endothelium and extravasate into the lesion. Once in the lesion, these inflammatory cells start secreting chemokines in order to recruit more inflammatory cells. Monocytes that entered the lesion from the blood stream differentiate into tissue macrophages, which then start to internalize oxLDL and eventually can become lipid-laden foam cells. Foam cells are a hallmark of an atherosclerotic plaque. Dying foam cells form the necrotic core, which is often located in the center of the plaque. In the growing plaque, smooth muscle cells (SMCs) start to proliferate and migrate towards the outer layer of the plaque to form a fibrous cap. The fibrous cap is the structural support of the plaque and is predominantly composed of SMCs and extracellular matrix proteins produced by these SMCs, such as collagen and elastin. Local intra-plaque inflammation however, triggers secretion of matrix metalloproteinases (MMPs). MMPs degrade the matrix in the fibrous cap, thus reducing the structural barrier of the plaque and increasing the risk of plaque rupture. A growing necrotic core, a thinning fibrous cap and persistent inflammation contribute to a vulnerable plaque phenotype[20, 21].

Inhibiting plaque progression and increasing stability of existing atherosclerotic plaques are potential therapeutic strategies to reduce the risk of rupture and its clinical consequences. Reducing intra-plaque inflammation and presence of a thick fibrous cap makes a plaque less vulnerable and thus, less prone to rupture[6]. Since atherosclerosis is a complex, multifactorial disease, most likely therapeutic strategies targeting multiple aspects of the disease are needed rather than single-factor therapeutics to reduce atherosclerosis and thereby the risk of a (recurrent) cardiovascular event.

Many cell types of both the innate and adaptive immune system are involved in the development and progression of atherosclerosis[3]. In this thesis, we focused on two different cell types in atherosclerosis, namely macrophages and blood platelets.

Macrophages

Macrophages play a key role in the onset and progression of atherosclerosis. After differentiation from monocytes, macrophages can polarize into different subtypes within the plaque. Macrophages continuously adapt their functional phenotype in response to environmental stimuli. At the broadest sense, macrophage subsets are classified into proinflammatory M1 or anti-inflammatory M2 macrophages. However, macrophage phenotypes *in vivo* are rather a continuum than either M1 or M2, and many different intermediate subtypes exist[22-24]. Macrophages expressing M1 markers are the predominant subtype in atherosclerotic plaques and promote plaque progression. M2 macrophages counteract inflammation and are associated with an anti-atherogenic response[25].

Because of their dynamic plasticity and key role in atherosclerosis, macrophages are an attractive therapeutic target to potentially resolve atherosclerosis. Several cellular pathways have been shown to either promote or inhibit inflammatory phenotypes of macrophages[26, 27]. For instance, activation of Toll-like receptor 4 (TLR4) induces the nuclear factor κB (NF-κB) signaling pathway and promotes proinflammatory M1 polarization[28]. On the other hand, the interleukin-4 (IL-4)/ signal transducer and activator of transcription (STAT) 6 pathway regulates the expression of pro-resolving genes (i.e. the mannose receptor CD206) and promotes M2 polarization[29, 30]. Inhibiting M1 polarization and enhancing M2 polarization, e.g. via macrophage activation and polarization pathways, is both favorable in reducing plaque development and increasing stability.

Blood platelets

Blood platelets are well-known from their function in hemostasis and blood coagulation, but their function goes beyond that. In fact, platelets are highly involved in proinflammatory responses[31]. Platelets are cells without a nucleus. They derive from a large precursor cell, the megakaryocyte. Anuclear platelets lack novel gene transcription, but are capable of splicing and protein synthesis with their repertoire of (pre)mRNAs derived from the megakaryocyte[32]. The lifespan of a human platelet is between 8 and 12 days. Senescent platelets are removed from the circulation and mostly degraded by the liver and spleen[33].
In atherogenesis, platelets can bind to the activated endothelium, secret chemokines to boost inflammation and facilitate extravasation of immune cells, like monocytes and

neutrophils, into the lesion[34-36]. These insights from basic science indicate that treatment with antiplatelet drugs would be beneficial in reducing the risk of a cardiovascular event. However, the use of antiplatelet drugs is limited by the increased risk of bleeding[31]. Yet, no recommendation for the use of antiplatelet drugs in primary prevention of CVD exists, though the identification of novel targets to reduce platelet inflammation without increasing bleeding risk, may be promising for future treatments.

Noncoding RNAs

Noncoding RNAs (ncRNAs) are RNAs that are not translated into protein. Over 97% of the human transcriptome consists of ncRNAs. For years, parts of the human genome that do not encode proteins were considered junk DNA. However, over the past 2 decades there has been increasing evidence that ncRNAs are crucial in regulating gene expression and fulfill functions in different pathologies, including CVD[37, 38]. NcRNAs target and regulate expression of other RNAs. Based on their size, ncRNA species are classified in either small or long ncRNAs (either shorter or longer than 200 nucleotides in length, respectively)[39]. There are many different types of ncRNAs, which perform various functions. This thesis will focus on microRNAs, small nucleolar RNAs (snoRNAs) and transfer RNAs (tRNAs).

MicroRNAs

A type of ncRNA that received much attention over the past few years in CVD are microRNAs. MicroRNAs regulate expression of their target genes at the posttranscriptional level. MicroRNAs are small molecules of about 22 nucleotides in length[40]. An overview of the microRNA biogenesis is shown in **Figure 1**. The biogenesis of microRNAs starts with transcription of a microRNA gene by RNA polymerase II or III. The resulting transcript, a primary microRNA, is processed into precursor microRNA. The precursor microRNA is exported out of the nucleus into the cytoplasm, where it is further processed into a microRNA duplex with two mature microRNA strands. One strand of the mature microRNA is incorporated in the RNA-induced silencing complex (RISC). Once in RISC, microRNAs hybridize with their seed sequence to complementary sequences in the 3' untranslated region (3'UTR) of their target messenger RNAs (mRNAs). This binding inhibits translation of target mRNAs into protein[41, 42]. MicroRNAs down tune expression of their target genes rather than completely silencing them. However, one microRNA has multiple target genes. Therefore, changing expression of one microRNA affects expression levels of multiple target genes simultaneously[40]. Modulating microRNA expression can thereby have major impact on complex cellular pathways and multifactorial diseases, including atherosclerosis.

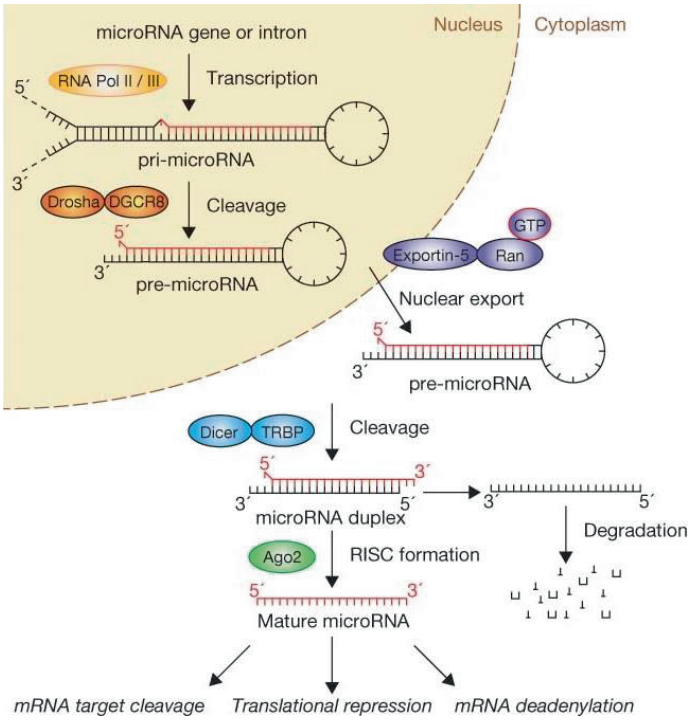

Figure 1. Schematic overview of microRNA processing. The biogenesis of microRNAs starts with transcription of a microRNA gene by RNA polymerase II or III, forming a primary microRNA transcript (pri-microRNA). Pri-microRNA is cleaved into precursor microRNA (pre-microRNA) by the microprocessor complex Drosha-DGCR8 in the nucleus. The pre-microRNA is exported out of the nucleus by Exportin-5-RAN-GPT. Dicer-TRBP complex processes the pre-microRNA to its mature length by cleaving the hairpin structure. The functional strand (in red) is loaded into the RNA-induced silencing complex (RISC) together with Argonaute 2 (Ago2), where it performs its function through mRNA cleavage, translational repression and mRNA deadenylation. The other strand (in black) is degraded. Figure adapted from Winter et al[9].

Small nucleolar RNAs

SnoRNAs are a relatively unexplored type of small ncRNA in the cardiovascular field. Their presence in both eukaryotes and archaea indicate a common ancestor, implying that snoRNAs are one of the most evolutionarily ancient types of RNA. Furthermore, the canonical function of snoRNAs and the set of proteins they associate with, is the same in archaea and all eukaryotic lineages[43-45]. SnoRNAs mediate site-specific RNA modifications of their target RNAs. SnoRNAs are 60-300 nucleotides in length and are classified as either C/D box or H/ACA box snoRNAs. A schematic overview of both snoRNA structures is shown in **Figure 2**. Most snoRNAs contain two sets of conserved C/D or two sets of conserved H/ACA boxes, and two sets of antisense boxes. Both snoRNA species have a specific topology and

form a complex with ribonucleoproteins to mediate RNA modifications. C/D box snoRNAs guide 2'-O-ribose methylation (2'Ome) and H/ACA snoRNAs guide RNA pseudoridylation (Ψ). Both types of RNA modifications are abundantly present on target RNAs[44, 46, 47].

C/D box snoRNAs associate with ribonucleoproteins NHP2L1, NOP56, NOP58 and Fibrillarin (FBL). FBL is a methyltransferase that catalyzes 2'Ome. SnoRNAs hybridize to target RNA via Watson-Crick base-pairing with their antisense box. The 5th nucleotide upstream of D or D' box is positioned for 2'Ome by FBL. A canonical C/D box snoRNA target is ribosomal RNA (rRNA), but many C/D box snoRNAs antisense sequences do not match with known rRNA 2'Ome sites. These snoRNAs have no known targets and thus are considered orphan[47, 48].
The canonical function of snoRNAs is well-known, however, other non-canonical targets and functions are currently being discovered. Some suggest that orphan snoRNAs can perform 2'Ome on other, non-canonical targets, like mRNA[49]. Others demonstrate that orphan snoRNAs can perform entirely different functions than guiding 2'Ome, such as mediating alternative splicing and 3'UTR processing[50, 51]. Some C/D box snoRNAs are processed into smaller fragments and exert microRNA-like functions by binding to mRNA 3'UTRs and inhibiting translation[52]. Dysregulation of snoRNAs is associated with clinically relevant events, including CVD[53], which implies that they have a regulatory role in diseases. In-depth research into their mechanism of action is needed to investigate whether orphan snoRNAs could serve as novel therapeutical targets.

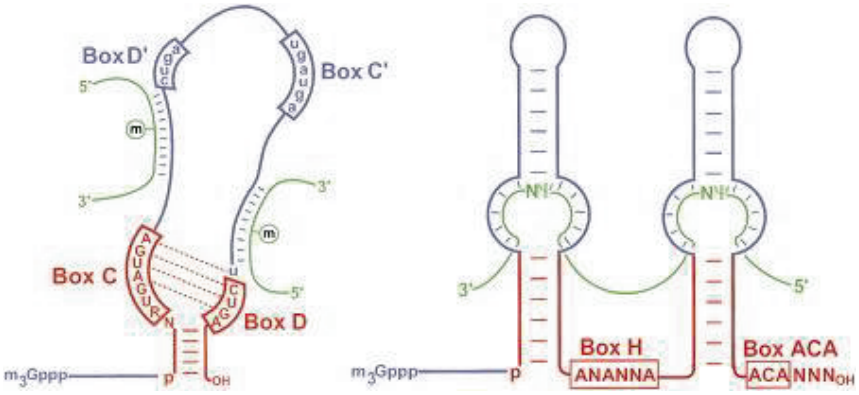

Figure 2. Schematic structure of C/D box and H/ACA box small nucleolar RNAs. (Left) C/D box snoRNA containing box C and D motifs. The C' and D' boxes represent internal copies of the C and D boxes. The two antisense boxes are located upstream of the D and D' box. The 2'-O-methylation site is marked with a circled m. Nucleotides interacting in the C and D boxes are indicated with a dashed line. (Right) H/ACA snoRNA containing H and ACA boxes. The unpaired uridine of the target RNA is located about 15 nucleotides from the H or ACA box of the snoRNA. The pseudoridylation site is marked with Ψ. Target RNA is shown in green. Regions essential for snoRNA location and processing are highlighted in red. Figure adapted from Kiss[7].

Transfer RNAs

The tRNA plays a fundamental role in protein translation by delivering amino acids to the growing peptide chain. However, advances in RNA sequencing enabled the identification of a new class of small RNAs, namely tRNA derived small fragments (tRFs), suggesting that tRNAs can also perform functions other than carrying amino acids. Fragments of tRNAs were first disregarded as degradation products, but are now recognized to have a biologically active function in regulating gene expression. These tRFs originate from different parts of their parental mature tRNA and range from ~18-50 nucleotides in size. An overview of tRNA-derived fragments is shown in **Figure 3**. The production of tRFs is conserved throughout evolution[54, 55]. Angiogenin is an enzyme belonging to the RNAse A family and is a known tRNA-processing endonuclease. Cellular stress-induced activation of Angiogenin results in increased formation of tRFs[56, 57].

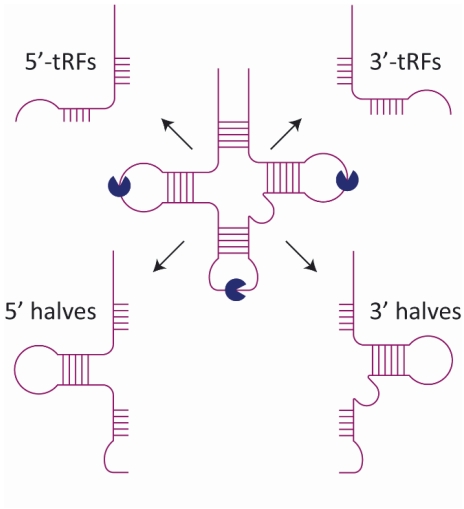

Figure 3. Schematic overview of tRNA-derived fragments. The mature tRNA can be cleaved into different sized fragments. Shorter fragments (<26 nucleotides) are called tRFs. Fragments derived from cleavage at the anticodon site are called tRNA halves. tRFs and tRNA halves are called 5' or 3', depending on the location they were generated from.

The mature tRNA is heavily decorated with modifications. These modifications may both protect against and direct tRNA cleavage. Some modifications may be guided by orphan snoRNAs. For example, orphan SNORD97 has a 2'Ome site on the wobble cytidine C34 of $tRNA^{Met}$(CAT), which is protected against Angiogenin-induced fragmentation[58, 59]. However, little is still known about tRF biogenesis and, in particular, their role in cardiovascular disease.

The 14q32 locus

MicroRNA and snoRNA genes are often located in clusters in the human genome. Advances in bioinformatics have led to prediction algorithms for targets of microRNAs, snoRNAs and tRFs[60-62]. In previous work from our group, reversed target prediction (RTP) identified microRNAs that were predicted to regulate expression of genes involved in neovascularization and atherosclerosis[63, 64]. Remarkably, RTP identified 27 microRNAs with

enrichment of putative binding sites, which were all encoded by a single microRNA cluster located on the long arm of human chromosome 14 (14q32). The 14q32 locus, also named DLK1-DIO3 locus by its protein coding genes DLK1 and DIO3, is an imprinted locus containing numerous maternally expressed ncRNAs. The 14q32 cluster is highly conserved in human and mice. The equivalent in mice is located on chromosome 12 (12F1). The 14q32 cluster encodes besides its 3 protein coding genes and 54 microRNAs, a cluster of 41 C/D box snoRNAs, 3 long noncoding RNAs (lncRNAs), MEG3, MEG8 and MEG9, and Piwi-interacting RNAs (piRNAs)[63, 65, 66]. Genetic association analyses demonstrated that the 14q32 microRNAs, snoRNAs and lncRNAs are, independently of each other, strongly linked to CVD[53].

MicroRNA-494-3p and microRNA-329-3p

One of the 14q32 microRNAs that is highly involved in different processes of vascular remodeling is miR-494-3p[63, 64, 67, 68]. In a murine model for early atherosclerosis, inhibition of miR-494-3p resulted in reduced initial lesion development, increased plaque stability and decreased plasma cholesterol levels[64]. These findings demonstrate the potential of miR-494-3p as a therapeutical target to reduce atherosclerosis and subsequently, the risk of a cardiovascular event. However, this first study focused on initial lesion development, while patients at risk of atherosclerotic complications generally present in the clinic with advanced and unstable lesions. Also, most patients at risk of a (recurrent) cardiovascular event receive plasma cholesterol lowering drugs[11, 69]. Therefore, a second study using mice with advanced lesions and including plasma cholesterol lowering in addition to treatment with miR-494-3p inhibitors, would more closely translate these findings to a human clinical setting.

Another 14q32 microRNA that is highly involved in vascular remodeling is miR-329-3p[63, 67, 68]. Just as miR-494-3p, miR-329-3p was predicted to regulate expression of genes involved in neovascularization and inhibition of miR-329-3p indeed improved neovascularization and blood flow recovery in a murine model for PAD[63]. However, its role in the development and progression of atherosclerosis is unknown.

The increased plaque stability that was observed in mice treated with miR-494-3p inhibitors, may indicate a shift in macrophage subsets from proinflammatory M1 towards an anti-inflammatory M2 phenotype. Downregulation of miR-494-3p resulted in upregulated expression of miR-494-3p targets metalloproteinase inhibitor 3 (TIMP3), interleukin 33 (IL-33) and transforming growth factor beta 2 (TGFB2) in the carotid artery[64]. Expression of these genes contributes to a decrease in local plaque inflammation. Furthermore, in a

murine model for intimal hyperplasia, miR-494-3p inhibition reduced macrophage influx in the intima[67]. Investigations into whether miR-494-3p directly influences macrophage activation and polarization and if so, via which specific activation pathways, are needed to answer these research questions.

Orphan 14q32 snoRNAs

The 14q32 locus encodes a cluster of 41 C/D box snoRNAs, named SNORD112, SNORD113 1-9 and SNORD114 1-31. Compared to 14q32 microRNAs, much less is known about the 14q32 snoRNAs. However, previous findings do suggest a regulatory role in CVD. Genetic association analysis demonstrated that the 14q32 snoRNAs associate stronger to CVD than 14q32 microRNAs and lncRNAs[53]. All seven measured 14q32 snoRNAs could be detected in both plasma of end-stage PAD patients and cycling athletes, and four of them, SNORD112, SNORD113.2, SNORD113.6 and SNORD114.1, were highly expressed in end-stage PAD patients in particular[70]. In a second study, PAD patients suffering from intermittent claudication but without critical limb ischemia were included. SNORD112, SNORD113.2, SNORD113.6 and SNORD114.1 were highly expressed, demonstrating that these snoRNAs are elevated in all PAD patients and not just the severe cases. Also, SNORD113.2 and SNORD114.1 appeared strongly linked to platelet activation, which is an important determinant of long-term outcome in PAD[71].

Bioinformatic tools predict that all 14q32 snoRNAs lack a rRNA binding site, making all 14q32 C/D box snoRNAs 'orphan', as their targets are unknown[47, 48]. However, binding to FBL indicates that they do perform canonical functions, but likely on non-canonical targets, such as mRNAs and tRNAs[53]. In-depth research is needed to lift the orphan status of 14q32 snoRNAs and to investigate their therapeutic potential in treatment of CVD.

Emerging therapeutic potentials

The importance of the inflammatory component in atherosclerosis is increasingly being recognized. The canakinumab anti-inflammatory thrombosis outcome study (CANTOS) trial showed for the first time that targeting inflammation reduced cardiovascular events, independent of lowering plasma cholesterol. Canakinumab is a monoclonal antibody that targets proinflammatory IL-1β[19]. Since then, more clinical trials are focusing on the inflammatory aspect of the disease. Colchicine is well-established anti-inflammatory medication for the treatment of gout and pericarditis. Several clinical trials have investigated the use of colchicine to reduce CVD, including the Low Dose Colchicine for Secondary Prevention of Cardiovascular Disease (LoDoCo) and a larger second trial

LoDoCo2, Colchicine Cardiovascular Outcomes Trial (COLCOT) and Colchicine in Patients With Acute Coronary Syndromes (COPS)[72-75]. Outcomes of these trials indicate that using colchicine in addition to standard therapies is promising to prevent a recurrent cardiovascular event in patients with coronary artery disease and hence emphasize the importance of reducing inflammation in CVD.

Noncoding RNAs as therapeutic targets

NcRNAs are emerging as novel therapeutic targets for potential CVD treatments. MicroRNAs in particular are being widely investigated in preclinical studies of CVD[37]. As microRNAs regulate expression of numerous target genes, they have the potential to simultaneously target multiple aspects of the disease, including inflammation[40]. MicroRNAs are expressed and thus active, in various cell types in the cardiovascular system, such as endothelial cells, smooth muscle cells, fibroblasts and leukocytes[40]. Changes in gene expression profiles, which can be facilitated by manipulation of one microRNA, can direct fate of cellular pathways and ultimately change cellular behavior. Therefore, one microRNA can act as a master switch on a multicellular level and has the potential to target all different aspects of CVD, including inflammation and cholesterol regulation, which subsequently may affect the course of CVD.

Expression of microRNAs can be modulated by using antisense oligonucleotides (ASOs), small interfering RNA (siRNA), mimics or viral vectors. To investigate its therapeutic potential in atherosclerosis, mostly mice with LDLr$^{-/-}$ or ApoE$^{-/-}$ background on a high fat diet, with surgical interventions, are used to induce atherosclerosis[76]. Several studies show encouraging results in reducing atherosclerosis via targeting ncRNAs[37]. For example, systemic delivery of miR-181b mimics inhibited activation of the NF-κB pathway and reduced vascular inflammation and atherosclerotic lesion formation[77]. Deficiency of miR-155 in ApoE$^{-/-}$ mice resulted in decreased atherogenesis via reduced inflammatory responses of macrophages[78]. As yet, modulation of microRNAs and other ncRNAs in CVD have not been studied in clinical trials, except for miR-132-3p in heart failure patients. MiR-132-3p has been shown to affect signaling pathways involved in cardiomyocyte growth, autophagy, calcium handling and contractility. One target of miR-132-3p is Forkhead box O3 (FOXO3), a pro-autophagic transcription factor[79]. CDR132L is a synthetic locked nucleic acid ASO inhibitor, with a fully phosphorylated backbone, against miR-132-3p. A first-in-human Phase 1b study showed that CDR132L is safe and well-tolerated, had linear plasma pharmacokinetics and suggests improvements in cardiac function[80]. This clinical trial is

limited by the small number of patients, but results are promising for future follow-up clinical studies of miR-132-3p and other ncRNAs.

Thesis outline

The aim of this thesis is to elucidate the molecular mechanism of action of 14q32 microRNAs and snoRNAs, and to evaluate the therapeutic potential of targeting 14q32 microRNAs and snoRNAs in CVD.

The first part of the thesis focuses on 14q32 microRNAs in atherosclerosis.

Chapter 2 demonstrates the therapeutic potential of single 14q32 microRNA inhibition, miR-494-3p and miR-329-3p, in a murine model for atherosclerosis. We used a clinically relevant murine model with advanced, established atherosclerotic lesions, induced by a 10-week high fat diet and collar placement around both carotid arteries. After 10 weeks of high fat diet, diet was switched to regular chow to mimic plasma cholesterol lowering treatments. Simultaneously, mice received third-generation antisense treatment against miR-494-3p (3GA-494), miR-329-3p (3GA-329) or an antisense control (3GA-ctrl), and at week 12 and 14. We show that treatment with 3GA-494 and, in part, 3GA-329 halted plaque progression. Furthermore, plaque stability was increased in 3GA-494 treated mice compared to 3GA-ctrl. Pro-atherogenic cells in the circulation, including $Ly6C^{hi}$ monocytes, neutrophils and blood platelets were decreased upon miR-494-3p and, in part, miR-329-3p inhibition.

Based on results from chapter 2, we hypothesized that miR-494-3p directly influences macrophage polarization and activation.

Chapter 3 shows that 3GA-494 treatment dampens proinflammatory M1 polarization, while enhancing anti-inflammatory M2 polarization. Proinflammatory marker CCR2 was reduced in plaques of 3GA-494 treated hypercholesterolemic mice. Furthermore, pathway analysis predicted that miR-494-3p targets genes involved in Wnt signaling. 3GA-494 treatment indeed activated Wnt signaling both in cultured M1 macrophages and in plaques of hypercholesterolemic mice, which at least in part, dampened M1 polarization. 3GA-494 could therefore be a potential therapeutic agent for stabilizing vulnerable lesions and reducing the risk of a cardiovascular event.

The second part of the thesis focuses on the function of human 14q32 snoRNA SNORD113-6 and its equivalent AF357425 in mice.

Chapter 4 shows that formerly orphan SNORD113-6/AF357425 targets mRNAs and acts via two mechanisms, namely pre-mRNA processing and 2'O-ribose methylation (2'Ome).

Several pre-mRNAs with conserved AF357425/SNORD113-6 D'-seed binding sites in the last exon/3'UTR were identified, which directed pre-mRNA processing and splice-variant-specific protein expression. Identified genes from pulldown of methyltransferase fibrillarin, were enriched for genes in the integrin pathway. 2'Ome of 6 integrin pathway mRNAs was confirmed, which appeared important for mRNA stability. Furthermore, primary human umbilical arterial fibroblasts (HUAFs) barrier function was altered under SNORD113-6 inhibition, indicating that SNORD113-6 is important for vascular function. SNORD113-6 could therefore be a novel therapeutic target for treating CVD. However, more research into remaining target RNAs, its second seed sequence and other 14q32 snoRNAs remains to be done.

Based on findings in chapter 4, we aimed to investigate whether AF357425/SNORD113-6 can also target small RNAs.

Chapter 5 demonstrates that AF357425/SNORD113-6 targets tRNAs via 2'Ome and thereby protects the tRNA from cleavage into small fragments. Small RNA sequencing of murine fibroblasts in which AF357425 was overexpressed or inhibited, showed that expression of tRNA fragments (tRFs) was predominantly regulated. We focused on tRNA Leucine anti-codon TAA ($tRNA^{Leu}$(TAA)) that has a conserved predicted binding site for AF357425/SNORD113-6. Adjacent to this site, $tRNA^{Leu}$(TAA) is cleaved and its dominant fragment, $tRF^{Leu\ 47\text{-}64}$, is formed. 2'Ome by AF357425/SNORD113-6 prevented formation of $tRF^{Leu\ 47\text{-}64}$. Exposing fibroblasts to oxidative stress or hypoxic stress induced $tRNA^{Leu}$(TAA) and AF357425/SNORD113-6 expression, but AF357425/SNORD113-6 knockdown did not increase $tRF^{Leu\ 47\text{-}64}$ formation under stress even further. Thus, independent of cellular stress, AF357425/SNORD113-6 directs fragmentation of $tRNA^{Leu}$(TAA) via 2'Ome.

Chapter 6 describes a summary of all results shown in this thesis and discusses future perspectives of this research.

References

1. Organization, W.H. (2017). https://www.who.int/news-room/fact-sheets/detail/cardiovascular-diseases-(cvds).
2. Wolf, D., and Ley, K. (2019). Immunity and Inflammation in Atherosclerosis. *Circulation research* **124**: 315-327.
3. Gisterå, A., and Hansson, G.K. (2017). The immunology of atherosclerosis. *Nat Rev Nephrol* **13**: 368-380.
4. Bonati, L.H., Dobson, J., Featherstone, R.L., Ederle, J., van der Worp, H.B., de Borst, G.J., Mali, W.P., Beard, J.D., Cleveland, T., Engelter, S.T., et al. (2015). Long-term outcomes after stenting versus endarterectomy for treatment of symptomatic carotid stenosis: the International Carotid Stenting Study (ICSS) randomised trial. *Lancet (London, England)* **385**: 529-538.
5. Herrington, W., Lacey, B., Sherliker, P., Armitage, J., and Lewington, S. (2016). Epidemiology of Atherosclerosis and the Potential to Reduce the Global Burden of Atherothrombotic Disease. *Circulation research* **118**: 535-546.
6. Hansson, G.K., Libby, P., and Tabas, I. (2015). Inflammation and plaque vulnerability. *J Intern Med* **278**: 483-493.
7. Kiss, T. (2002). Small nucleolar RNAs: an abundant group of noncoding RNAs with diverse cellular functions. *Cell* **109**: 145-148.
8. Timmis, A., Townsend, N., Gale, C., Grobbee, R., Maniadakis, N., Flather, M., Wilkins, E., Wright, L., Vos, R., Bax, J., et al. (2018). European Society of Cardiology: Cardiovascular Disease Statistics 2017. *European heart journal* **39**: 508-579.
9. Winter, J., Jung, S., Keller, S., Gregory, R.I., and Diederichs, S. (2009). Many roads to maturity: microRNA biogenesis pathways and their regulation. *Nat Cell Biol* **11**: 228-234.
10. Braunwald, E. (2012). The treatment of acute myocardial infarction: the Past, the Present, and the Future. *Eur Heart J Acute Cardiovasc Care* **1**: 9-12.
11. Arnett, D.K., Blumenthal, R.S., Albert, M.A., Buroker, A.B., Goldberger, Z.D., Hahn, E.J., Himmelfarb, C.D., Khera, A., Lloyd-Jones, D., McEvoy, J.W., et al. (2019). 2019 ACC/AHA Guideline on the Primary Prevention of Cardiovascular Disease: A Report of the American College of Cardiology/American Heart Association Task Force on Clinical Practice Guidelines. *Circulation* **140**: e596-e646.
12. Karmali, K.N., Lloyd-Jones, D.M., Berendsen, M.A., Goff, D.C., Jr., Sanghavi, D.M., Brown, N.C., Korenovska, L., and Huffman, M.D. (2016). Drugs for Primary Prevention of Atherosclerotic Cardiovascular Disease: An Overview of Systematic Reviews. *JAMA Cardiol* **1**: 341-349.
13. Valgimigli, M., Bueno, H., Byrne, R.A., Collet, J.P., Costa, F., Jeppsson, A., Jüni, P., Kastrati, A., Kolh, P., Mauri, L., et al. (2018). 2017 ESC focused update on dual antiplatelet therapy in coronary artery disease developed in collaboration with EACTS: The Task Force for dual antiplatelet therapy in coronary artery disease of the European Society of Cardiology (ESC) and of the European Association for Cardio-Thoracic Surgery (EACTS). *European heart journal* **39**: 213-260.
14. Gerhard-Herman, M.D., Gornik, H.L., Barrett, C., Barshes, N.R., Corriere, M.A., Drachman, D.E., Fleisher, L.A., Fowkes, F.G., Hamburg, N.M., Kinlay, S., et al. (2017). 2016 AHA/ACC Guideline on the Management of Patients With Lower Extremity Peripheral Artery Disease: Executive Summary: A Report of the American College of Cardiology/American Heart Association Task Force on Clinical Practice Guidelines. *Circulation* **135**: e686-e725.
15. Bonati, L.H., Gregson, J., Dobson, J., McCabe, D.J.H., Nederkoorn, P.J., van der Worp, H.B., de Borst, G.J., Richards, T., Cleveland, T., Müller, M.D., et al. (2018). Restenosis and risk of stroke after stenting or endarterectomy for symptomatic carotid stenosis in the International Carotid Stenting Study (ICSS): secondary analysis of a randomised trial. *Lancet Neurol* **17**: 587-596.

16. Ward, A.O., Caputo, M., Angelini, G.D., George, S.J., and Zakkar, M. (2017). Activation and inflammation of the venous endothelium in vein graft disease. *Atherosclerosis* **265**: 266-274.
17. Mawhinney, J.A., Mounsey, C.A., and Taggart, D.P. (2018). The potential role of external venous supports in coronary artery bypass graft surgery. *Eur J Cardiothorac Surg* **53**: 1127-1134.
18. Annex, B.H., and Cooke, J.P. (2021). New Directions in Therapeutic Angiogenesis and Arteriogenesis in Peripheral Arterial Disease. *Circulation research* **128**: 1944-1957.
19. Ridker, P.M., Everett, B.M., Thuren, T., MacFadyen, J.G., Chang, W.H., Ballantyne, C., Fonseca, F., Nicolau, J., Koenig, W., Anker, S.D., et al. (2017). Antiinflammatory Therapy with Canakinumab for Atherosclerotic Disease. *The New England journal of medicine* **377**: 1119-1131.
20. Libby, P. (2002). Inflammation in atherosclerosis. *Nature* **420**: 868-874.
21. Geovanini, G.R., and Libby, P. (2018). Atherosclerosis and inflammation: overview and updates. *Clin Sci (Lond)* **132**: 1243-1252.
22. Willemsen, L., and de Winther, M.P. (2020). Macrophage subsets in atherosclerosis as defined by single-cell technologies. *J Pathol* **250**: 705-714.
23. Depuydt, M.A.C., Prange, K.H.M., Slenders, L., Örd, T., Elbersen, D., Boltjes, A., de Jager, S.C.A., Asselbergs, F.W., de Borst, G.J., Aavik, E., et al. (2020). Microanatomy of the Human Atherosclerotic Plaque by Single-Cell Transcriptomics. *Circulation research* **127**: 1437-1455.
24. Stoger, J.L., Gijbels, M.J., van der Velden, S., Manca, M., van der Loos, C.M., Biessen, E.A., Daemen, M.J., Lutgens, E., and de Winther, M.P. (2012). Distribution of macrophage polarization markers in human atherosclerosis. *Atherosclerosis* **225**: 461-468.
25. de Gaetano, M., Crean, D., Barry, M., and Belton, O. (2016). M1- and M2-Type Macrophage Responses Are Predictive of Adverse Outcomes in Human Atherosclerosis. *Frontiers in immunology* **7**: 275.
26. Canfran-Duque, A., Rotllan, N., Zhang, X., Fernandez-Fuertes, M., Ramirez-Hidalgo, C., Araldi, E., Daimiel, L., Busto, R., Fernandez-Hernando, C., and Suarez, Y. (2017). Macrophage deficiency of miR-21 promotes apoptosis, plaque necrosis, and vascular inflammation during atherogenesis. *EMBO molecular medicine* **9**: 1244-1262.
27. Wei, Y., Zhu, M., Corbalan-Campos, J., Heyll, K., Weber, C., and Schober, A. (2015). Regulation of Csf1r and Bcl6 in macrophages mediates the stage-specific effects of microRNA-155 on atherosclerosis. *Arteriosclerosis, thrombosis, and vascular biology* **35**: 796-803.
28. Moore, K.J., Sheedy, F.J., and Fisher, E.A. (2013). Macrophages in atherosclerosis: a dynamic balance. *Nature reviews Immunology* **13**: 709-721.
29. Van Dyken, S.J., and Locksley, R.M. (2013). Interleukin-4- and interleukin-13-mediated alternatively activated macrophages: roles in homeostasis and disease. *Annu Rev Immunol* **31**: 317-343.
30. Weinstock, A., Rahman, K., Yaacov, O., Nishi, H., Menon, P., Nikain, C.A., Garabedian, M.L., Pena, S., Akbar, N., Sansbury, B.E., et al. (2021). Wnt signaling enhances macrophage responses to IL-4 and promotes resolution of atherosclerosis. *Elife* **10**.
31. Nording, H., Baron, L., and Langer, H.F. (2020). Platelets as therapeutic targets to prevent atherosclerosis. *Atherosclerosis* **307**: 97-108.
32. Denis, M.M., Tolley, N.D., Bunting, M., Schwertz, H., Jiang, H., Lindemann, S., Yost, C.C., Rubner, F.J., Albertine, K.H., Swoboda, K.J., et al. (2005). Escaping the nuclear confines: signal-dependent pre-mRNA splicing in anucleate platelets. *Cell* **122**: 379-391.
33. Li, R., Hoffmeister, K.M., and Falet, H. (2016). Glycans and the platelet life cycle. *Platelets* **27**: 505-511.
34. Badrnya, S., Schrottmaier, W.C., Kral, J.B., Yaiw, K.C., Volf, I., Schabbauer, G., Soderberg-Naucler, C., and Assinger, A. (2014). Platelets mediate oxidized low-density lipoprotein-

induced monocyte extravasation and foam cell formation. *Arteriosclerosis, thrombosis, and vascular biology* **34**: 571-580.
35. da Costa Martins, P., Garcia-Vallejo, J.J., van Thienen, J.V., Fernandez-Borja, M., van Gils, J.M., Beckers, C., Horrevoets, A.J., Hordijk, P.L., and Zwaginga, J.J. (2007). P-selectin glycoprotein ligand-1 is expressed on endothelial cells and mediates monocyte adhesion to activated endothelium. *Arteriosclerosis, thrombosis, and vascular biology* **27**: 1023-1029.
36. Lisman, T. (2018). Platelet-neutrophil interactions as drivers of inflammatory and thrombotic disease. *Cell Tissue Res* **371**: 567-576.
37. Poller, W., Dimmeler, S., Heymans, S., Zeller, T., Haas, J., Karakas, M., Leistner, D.M., Jakob, P., Nakagawa, S., Blankenberg, S., et al. (2018). Non-coding RNAs in cardiovascular diseases: diagnostic and therapeutic perspectives. *European heart journal* **39**: 2704-2716.
38. (2012). An integrated encyclopedia of DNA elements in the human genome. *Nature* **489**: 57-74.
39. Mattick, J.S., Taft, R.J., and Faulkner, G.J. (2010). A global view of genomic information--moving beyond the gene and the master regulator. *Trends Genet* **26**: 21-28.
40. Welten, S.M., Goossens, E.A., Quax, P.H., and Nossent, A.Y. (2016). The multifactorial nature of microRNAs in vascular remodelling. *Cardiovascular research* **110**: 6-22.
41. Lee, Y., Jeon, K., Lee, J.T., Kim, S., and Kim, V.N. (2002). MicroRNA maturation: stepwise processing and subcellular localization. *The EMBO journal* **21**: 4663-4670.
42. Treiber, T., Treiber, N., and Meister, G. (2019). Regulation of microRNA biogenesis and its crosstalk with other cellular pathways. *Nat Rev Mol Cell Biol* **20**: 5-20.
43. Baldini, L., Charpentier, B., and Labialle, S. (2021). Emerging Data on the Diversity of Molecular Mechanisms Involving C/D snoRNAs. *Noncoding RNA* **7**.
44. Dieci, G., Preti, M., and Montanini, B. (2009). Eukaryotic snoRNAs: a paradigm for gene expression flexibility. *Genomics* **94**: 83-88.
45. Hoeppner, M.P., and Poole, A.M. (2012). Comparative genomics of eukaryotic small nucleolar RNAs reveals deep evolutionary ancestry amidst ongoing intragenomic mobility. *BMC Evol Biol* **12**: 183.
46. Watkins, N.J., and Bohnsack, M.T. (2012). The box C/D and H/ACA snoRNPs: key players in the modification, processing and the dynamic folding of ribosomal RNA. *Wiley Interdiscip Rev RNA* **3**: 397-414.
47. Kiss, T. (2001). Small nucleolar RNA-guided post-transcriptional modification of cellular RNAs. *The EMBO journal* **20**: 3617-3622.
48. Falaleeva, M., Welden, J.R., Duncan, M.J., and Stamm, S. (2017). C/D-box snoRNAs form methylating and non-methylating ribonucleoprotein complexes: Old dogs show new tricks. *Bioessays* **39**.
49. Elliott, B.A., Ho, H.T., Ranganathan, S.V., Vangaveti, S., Ilkayeva, O., Abou Assi, H., Choi, A.K., Agris, P.F., and Holley, C.L. (2019). Modification of messenger RNA by 2'-O-methylation regulates gene expression in vivo. *Nature communications* **10**: 3401.
50. Kishore, S., Khanna, A., Zhang, Z., Hui, J., Balwierz, P.J., Stefan, M., Beach, C., Nicholls, R.D., Zavolan, M., and Stamm, S. (2010). The snoRNA MBII-52 (SNORD 115) is processed into smaller RNAs and regulates alternative splicing. *Human molecular genetics* **19**: 1153-1164.
51. Huang, C., Shi, J., Guo, Y., Huang, W., Huang, S., Ming, S., Wu, X., Zhang, R., Ding, J., Zhao, W., et al. (2017). A snoRNA modulates mRNA 3' end processing and regulates the expression of a subset of mRNAs. *Nucleic Acids Res* **45**: 8647-8660.
52. Brameier, M., Herwig, A., Reinhardt, R., Walter, L., and Gruber, J. (2011). Human box C/D snoRNAs with miRNA like functions: expanding the range of regulatory RNAs. *Nucleic Acids Res* **39**: 675-686.
53. Håkansson, K.E.J., Goossens, E.A.C., Trompet, S., van Ingen, E., de Vries, M.R., van der Kwast, R., Ripa, R.S., Kastrup, J., Hohensinner, P.J., Kaun, C., et al. (2019). Genetic associations and

regulation of expression indicate an independent role for 14q32 snoRNAs in human cardiovascular disease. *Cardiovascular research* **115**: 1519-1532.
54. Krishna, S., Raghavan, S., DasGupta, R., and Palakodeti, D. (2021). tRNA-derived fragments (tRFs): establishing their turf in post-transcriptional gene regulation. *Cell Mol Life Sci* **78**: 2607-2619.
55. Keam, S.P., and Hutvagner, G. (2015). tRNA-Derived Fragments (tRFs): Emerging New Roles for an Ancient RNA in the Regulation of Gene Expression. *Life (Basel)* **5**: 1638-1651.
56. Fu, H., Feng, J., Liu, Q., Sun, F., Tie, Y., Zhu, J., Xing, R., Sun, Z., and Zheng, X. (2009). Stress induces tRNA cleavage by angiogenin in mammalian cells. *FEBS Lett* **583**: 437-442.
57. Yamasaki, S., Ivanov, P., Hu, G.F., and Anderson, P. (2009). Angiogenin cleaves tRNA and promotes stress-induced translational repression. *J Cell Biol* **185**: 35-42.
58. Vitali, P., and Kiss, T. (2019). Cooperative 2'-O-methylation of the wobble cytidine of human elongator tRNA(Met)(CAT) by a nucleolar and a Cajal body-specific box C/D RNP. *Genes & development* **33**: 741-746.
59. Nostramo, R.T., and Hopper, A.K. (2019). Beyond rRNA and snRNA: tRNA as a 2'-O-methylation target for nucleolar and Cajal body box C/D RNPs. *Genes & development* **33**: 739-740.
60. Peterson, S.M., Thompson, J.A., Ufkin, M.L., Sathyanarayana, P., Liaw, L., and Congdon, C.B. (2014). Common features of microRNA target prediction tools. *Front Genet* **5**: 23.
61. Kehr, S., Bartschat, S., Stadler, P.F., and Tafer, H. (2011). PLEXY: efficient target prediction for box C/D snoRNAs. *Bioinformatics* **27**: 279-280.
62. Li, N., Shan, N., Lu, L., and Wang, Z. (2021). tRFtarget: a database for transfer RNA-derived fragment targets. *Nucleic Acids Res* **49**: D254-d260.
63. Welten, S.M., Bastiaansen, A.J., de Jong, R.C., de Vries, M.R., Peters, E.A., Boonstra, M.C., Sheikh, S.P., La Monica, N., Kandimalla, E.R., Quax, P.H., et al. (2014). Inhibition of 14q32 MicroRNAs miR-329, miR-487b, miR-494, and miR-495 increases neovascularization and blood flow recovery after ischemia. *Circulation research* **115**: 696-708.
64. Wezel, A., Welten, S.M., Razawy, W., Lagraauw, H.M., de Vries, M.R., Goossens, E.A., Boonstra, M.C., Hamming, J.F., Kandimalla, E.R., Kuiper, J., et al. (2015). Inhibition of MicroRNA-494 Reduces Carotid Artery Atherosclerotic Lesion Development and Increases Plaque Stability. *Annals of surgery* **262**: 841-847; discussion 847-848.
65. Enfield, K.S., Martinez, V.D., Marshall, E.A., Stewart, G.L., Kung, S.H., Enterina, J.R., and Lam, W.L. (2016). Deregulation of small non-coding RNAs at the DLK1-DIO3 imprinted locus predicts lung cancer patient outcome. *Oncotarget* **7**: 80957-80966.
66. Molina-Pinelo, S., Salinas, A., Moreno-Mata, N., Ferrer, I., Suarez, R., Andrés-León, E., Rodríguez-Paredes, M., Gutekunst, J., Jantus-Lewintre, E., Camps, C., et al. (2018). Impact of DLK1-DIO3 imprinted cluster hypomethylation in smoker patients with lung cancer. *Oncotarget* **9**: 4395-4410.
67. Welten, S.M.J., de Jong, R.C.M., Wezel, A., de Vries, M.R., Boonstra, M.C., Parma, L., Jukema, J.W., van der Sluis, T.C., Arens, R., Bot, I., et al. (2017). Inhibition of 14q32 microRNA miR-495 reduces lesion formation, intimal hyperplasia and plasma cholesterol levels in experimental restenosis. *Atherosclerosis* **261**: 26-36.
68. Welten, S.M.J., de Vries, M.R., Peters, E.A.B., Agrawal, S., Quax, P.H.A., and Nossent, A.Y. (2017). Inhibition of Mef2a Enhances Neovascularization via Post-transcriptional Regulation of 14q32 MicroRNAs miR-329 and miR-494. *Molecular therapy Nucleic acids* **7**: 61-70.
69. Stone, N.J., Robinson, J.G., Lichtenstein, A.H., Bairey Merz, C.N., Blum, C.B., Eckel, R.H., Goldberg, A.C., Gordon, D., Levy, D., Lloyd-Jones, D.M., et al. (2014). 2013 ACC/AHA guideline on the treatment of blood cholesterol to reduce atherosclerotic cardiovascular risk in adults: a report of the American College of Cardiology/American Heart Association Task Force on Practice Guidelines. *Circulation* **129**: S1-45.

70. Håkansson, K.E.J., Sollie, O., Simons, K.H., Quax, P.H.A., Jensen, J., and Nossent, A.Y. (2018). Circulating Small Non-coding RNAs as Biomarkers for Recovery After Exhaustive or Repetitive Exercise. *Front Physiol* **9**: 1136.
71. Nossent, A.Y., Ektefaie, N., Wojta, J., Eichelberger, B., Kopp, C., Panzer, S., and Gremmel, T. (2019). Plasma Levels of snoRNAs are Associated with Platelet Activation in Patients with Peripheral Artery Disease. *Int J Mol Sci* **20**.
72. Nidorf, S.M., Eikelboom, J.W., Budgeon, C.A., and Thompson, P.L. (2013). Low-dose colchicine for secondary prevention of cardiovascular disease. *Journal of the American College of Cardiology* **61**: 404-410.
73. Nidorf, S.M., Fiolet, A.T.L., Eikelboom, J.W., Schut, A., Opstal, T.S.J., Bax, W.A., Budgeon, C.A., Tijssen, J.G.P., Mosterd, A., Cornel, J.H., et al. (2019). The effect of low-dose colchicine in patients with stable coronary artery disease: The LoDoCo2 trial rationale, design, and baseline characteristics. *American heart journal* **218**: 46-56.
74. Tardif, J.C., Kouz, S., Waters, D.D., Bertrand, O.F., Diaz, R., Maggioni, A.P., Pinto, F.J., Ibrahim, R., Gamra, H., Kiwan, G.S., et al. (2019). Efficacy and Safety of Low-Dose Colchicine after Myocardial Infarction. *The New England journal of medicine* **381**: 2497-2505.
75. Tong, D.C., Quinn, S., Nasis, A., Hiew, C., Roberts-Thomson, P., Adams, H., Sriamareswaran, R., Htun, N.M., Wilson, W., Stub, D., et al. (2020). Colchicine in Patients With Acute Coronary Syndrome: The Australian COPS Randomized Clinical Trial. *Circulation* **142**: 1890-1900.
76. Emini Veseli, B., Perrotta, P., De Meyer, G.R.A., Roth, L., Van der Donckt, C., Martinet, W., and De Meyer, G.R.Y. (2017). Animal models of atherosclerosis. *European journal of pharmacology* **816**: 3-13.
77. Sun, X., He, S., Wara, A.K.M., Icli, B., Shvartz, E., Tesmenitsky, Y., Belkin, N., Li, D., Blackwell, T.S., Sukhova, G.K., et al. (2014). Systemic delivery of microRNA-181b inhibits nuclear factor-κB activation, vascular inflammation, and atherosclerosis in apolipoprotein E-deficient mice. *Circulation research* **114**: 32-40.
78. Du, F., Yu, F., Wang, Y., Hui, Y., Carnevale, K., Fu, M., Lu, H., and Fan, D. (2014). MicroRNA-155 deficiency results in decreased macrophage inflammation and attenuated atherogenesis in apolipoprotein E-deficient mice. *Arteriosclerosis, thrombosis, and vascular biology* **34**: 759-767.
79. Foinquinos, A., Batkai, S., Genschel, C., Viereck, J., Rump, S., Gyöngyösi, M., Traxler, D., Riesenhuber, M., Spannbauer, A., Lukovic, D., et al. (2020). Preclinical development of a miR-132 inhibitor for heart failure treatment. *Nature communications* **11**: 633.
80. Täubel, J., Hauke, W., Rump, S., Viereck, J., Batkai, S., Poetzsch, J., Rode, L., Weigt, H., Genschel, C., Lorch, U., et al. (2021). Novel antisense therapy targeting microRNA-132 in patients with heart failure: results of a first-in-human Phase 1b randomized, double-blind, placebo-controlled study. *European heart journal* **42**: 178-188.

Chapter 2

Antisense oligonucleotide inhibition of microRNA-494 halts atherosclerotic plaque progression and promotes plaque stabilization

Eva van Ingen[1,2], Amanda C. Foks[3], Mara J. Kröner[3], Johan Kuiper[3], Paul H.A. Quax[1,2], Ilze Bot[3]*, A. Yaël Nossent[1,2,4,5]*

Molecular Therapy Nucleic Acids. 2019 Dec 6;18:638-649

[1]Department of Surgery and [2]Einthoven Laboratory for Experimental Vascular Medicine, Leiden University Medical Center, Leiden, The Netherlands. [3]Division BioTherapeutics, Leiden Academic Centre for Drug Research, Leiden University, Leiden, The Netherlands. [4]Department of Internal Medicine II and [5]Department of Laboratory Medicine, Medical University of Vienna, Vienna, Austria. *These authors contributed equally.

Abstract

We have previously shown that 3rd Generation Antisense (3GA)- inhibition of 14q32 microRNA (miRNA)-494 reduced early development of atherosclerosis. However, patients at risk of atherosclerotic complications generally present with advanced and unstable lesions. Here, we administered 3GAs against 14q32 miRNA-494 (3GA-494), miRNA-329 (3GA-329) or a control (3GA-ctrl) to mice with advanced atherosclerosis. Atherosclerotic plaque formation in $LDLr^{-/-}$ mice was induced by a 10-week high-fat diet and simultaneous carotid artery-collar placement. Parallel to 3GA-treatment, hyperlipidemia was normalized by a diet-switch to regular chow for an additional 5 weeks. We show that, even though plasma cholesterol levels were normalized after diet-switch, carotid artery plaque progression continued in 3GA-ctrl mice. However, treatment with 3GA-494 and, in part, 3GA-329 halted plaque progression. Furthermore, in the aortic root, intra-plaque collagen content was increased in 3GA-494 mice, accompanied by a reduction in the intra-plaque macrophage content. Proatherogenic cells in the circulation, including inflammatory $Ly6C^{hi}$ monocytes, neutrophils and blood platelets were decreased upon miRNA-329 and miRNA-494 inhibition. Taken together, treatment with 3GA-494, and in part with 3GA-329, halts atherosclerotic plaque progression and promotes stabilization of advanced lesions, which is highly relevant for human atherosclerosis.

Introduction

Atherosclerosis is a chronic inflammatory disease characterized by progressive plaque buildup in the arterial wall. Most plaques that develop during one's life remain clinically silent. However, lesion progression and disruption of a vulnerable plaque may result in a cardiovascular event, such as an ischemic stroke or myocardial infarction.[1] Surgical interventions to prevent, for example, ischemic stroke are carotid endarterectomy or stenting, but due to the perioperative risks, these are only performed when a plaque causes a stenosis of the carotid artery of more than 70% or when the plaque is symptomatic, i.e. causing transient ischemic attacks (TIAs).[2]

An established therapeutic strategy is plasma lipid lowering by statins. Lipid-lowering strategies have been shown to contribute to increased plaque stability and reduce the risk of (recurrent) cardiovascular events, including myocardial infarction.[3-5] Independent of lipid lowering, targeting inflammation is also important in reducing the incidence of recurrent cardiovascular events, as was demonstrated in the Canakinumab Anti-Inflammatory Thrombosis Outcome Study (CANTOS) trial.[6] Although current therapeutic strategies contribute to reducing the risk of recurrent cardiovascular events, a clinical need remains for novel noninvasive therapies targeting multiple aspects of atherosclerosis and improving clinical outcome. Therapeutic strategies increasing stabilization of vulnerable plaques, alone or complemented by existing lipid lowering treatments, would be of great clinical value in reducing the risk of thrombotic events in the carotid, coronary and peripheral arteries.

MicroRNAs (miRNAs) are post-transcriptional negative regulators of gene-expression. Because of their ability to fine-tune expression of multiple target genes, miRNAs are promising drug targets for complex diseases, including atherosclerosis.[7] Several studies have focused on the therapeutic potential of miRNA-modulation in atherosclerosis. For example, the miRNA-33 family, including miRNA-33a and miRNA-33b, regulates cholesterol metabolism by targeting cholesterol transporter ABCA1. Inhibition of miRNA-33 resulted in decreased very low-density lipoprotein (VLDL), whereas high-density lipoprotein (HDL) was increased in the plasma.[8-10] More recently, it was shown that miRNA-33 inhibition also promotes cholesterol efflux from arterial macrophages and thereby directly regulates atherosclerotic plaque formation.[11] Inflammation in atherosclerosis was reduced via miRNA-155 inhibition. MiRNA-155 is predominantly expressed in pro-inflammatory macrophages. Inhibition of miRNA-155 resulted in smaller atherosclerotic lesions containing fewer lipid-laden macrophages via increasing expression of its target BCL6, which attenuates pro-inflammatory nuclear factor kB (NF-kB) signaling.[12] Furthermore, plaque stability was shown to increase

upon overexpressing miRNA-210. MiRNA-210 inhibits adenomatous polyposis coli (APC) expression in smooth muscle cells (SMCs) and thereby enhances intra-plaque SMC survival and, thus, intraplaque collagen synthesis.[13] However, as one miRNA can have multiple target genes, single miRNAs also have the potential to target all aspects of atherosclerosis at once. For example, inhibition of miRNAs transcribed from the 14q32 cluster (12F1 in mice), targeted multiple aspects in atherosclerosis, including lipid hemostasis, inflammation and concomitant plaque development, as we have shown previously.[14]

The 14q32 cluster is the largest known miRNA gene cluster in humans and contains more than 50 miRNA genes. We have evaluated the therapeutic inhibition of 14q32 miRNAs in different vascular remodeling processes.[14-17] In two different murine models of vascular remodeling, one for intimal hyperplasia and one for accelerated atherosclerosis, we showed that inhibition of 14q32 miRNAs reduced initial lesion development, increased plaque stability and decreased plasma cholesterol levels.[14, 16] Importantly, inhibition of 14q32 miRNAs reduced macrophage influx in the intima in the intimal hyperplasia model.[16] These studies, however, focused on the effects of 14q32 miRNA inhibition in initial lesion development[14], where most patients present in the clinic with advanced, symptomatic atherosclerotic lesions.

In the current study, we therefore aimed to investigate the effects of 14q32 miRNA inhibition on advanced lesions. We used 3rd Generation Antisense (3GA) to inhibit two different 14q32 miRNAs, miRNA-494 and miRNA-329. Parallel to 3GA-treatment, we included a diet-switch from high-fat high cholesterol to regular chow to normalize hyperlipidemia, in order to closely mimic routine lipid lowering treatment.

First, we show that inhibition of 14q32 miRNAs, particularly miRNA-494, halted atherosclerotic plaque progression and increased plaque stability in mice with advanced atherosclerotic lesions. Second, we show that plasma cholesterol levels show a modest, but further reduction after miRNA-494 and miRNA-329 inhibition. Third, we show that pro-atherogenic cells in the circulation, including inflammatory Ly6C^{hi} monocytes, neutrophils and platelets were decreased upon miRNA-329 and miRNA-494 inhibition, which is highly relevant in further reducing the risk of atherosclerotic complications.

Results

3GA-494 and 3GA-329 treatment reduces plasma cholesterol levels and body weight

The timeline of the study is shown in Sup. Fig. 1. Plasma cholesterol levels showed a clear decrease in all groups after diet-replacement (Fig. 1A). Both 3GA-494 and -329 treated groups showed a further reduction in total plasma cholesterol levels compared to the 3GA-control five weeks after diet switch (3GA-494: 155±6 mg/dL, 3GA-329: 168±11 mg/dL versus 3GA-ctrl: 214±13 mg/dL, P<0.05; Fig. 1B). Similar to as shown previously[18], body weight did not significantly differ after diet switch in the 3GA-ctrl group as compared to baseline, but showed a reduction in 3GA-494 or 3GA-329-treated mice compared to 3GA-ctrl (Fig. 1C). Subsequently, all groups increased in body weight during the remainder of the study, independent of the treatment, but body weight levels of 3GA-494 and 3GA-329-treated mice remained decreased compared to 3GA-ctrl. The size of the spleen was increased in all of the 3GA-494-treated mice and in half of the 3GA-329-treated mice, as is further described below. All other organs appeared normal and mice did not show any pathological changes.

3GA-494 treatment halts plaque progression in the carotid artery

In the carotid arteries, miRNA-494 and miRNA-329 expression were inhibited in both 3GA-494 and 3GA-329, respectively, compared to 3GA-ctrl (Fig. 2A). MiRNA-494 and miRNA-329 target gene expression levels (miRNA-494: IL33, TIMP3 and TLR4; miRNA-329: VEGFA, Mef2A and TLR4), however, were not significantly different compared to the control one week after final 3GA injections (Sup. Fig. 2A, B). 3GA-ctrl-treated mice showed increased carotid artery

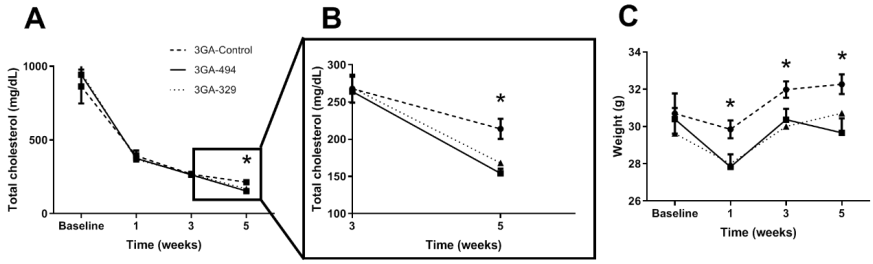

Figure 1. Total cholesterol levels and bodyweight levels of LDLr$^{-/-}$ mice treated with 3GA-ctrl, 3GA-494 or 3GA-329. Mice received 3GA-treatment immediately after (baseline), two and four weeks after diet replacement from high-fat high cholesterol to regular chow. All mice were sacrificed at week five. (A) Total cholesterol (TC) levels in milligrams per decilitre (mg/dL) measured in the serum of 3GA-ctrl, 3GA-494 and 3GA-329 treated mice, quantified by using enzymatic procedures, at baseline and up to five weeks after diet-replacement. (B) Zoomed in graph of TC at week three and five. (C) Bodyweight levels in grams (g) after diet-replacement. A two-tailed Student's t-test was performed to compare single treatment to the 3GA-ctrl group at each time point. *P<0.05 compared to 3GA-ctrl. 3GA-ctrl (N=10), 3GA-494 (N=10) and 3GA-329 (N=8) Data are represented as mean ± SEM.

average plaque size compared to baseline, indicating continued atherogenesis, even after lowering plasma cholesterol levels by diet-replacement (baseline: 18±4*10^3 µm^2 versus 3GA-ctrl: 32±10*10^3 µm^2; Fig. 2B, D). At the site of maximal stenosis, plaque size was increased in 3GA-ctrl compared to baseline (baseline: 30±8*10^3 µm^2 versus 3GA-ctrl: 56±16*10^3 µm^2; Fig. 2C). In 3GA-494 mice, carotid artery plaque size was significantly decreased compared to 3GA-ctrl. In fact, 3GA-494 mice had similar plaque sizes to baseline mice in both average plaque sizes (baseline: 18±4*10^3 µm^2, 3GA-ctrl: 32±10*10^3 µm^2 versus 3GA-494: 13±3*10^3 µm^2, P<0.05; Fig. 2B, D) and at the site of maximal stenosis (baseline: 30±8*10^3 µm^2, 3GA-ctrl: 56±16*10^3 µm^2 versus 3GA-494: 23±7*10^3 µm^2, P<0.05; Fig. 2C). 3GA-329 treated mice showed a trend towards a smaller average plaque size and at the site of maximal stenosis (average: 3GA-329: 15±1*10^3 µm^2 P=0.09, maximal stenosis: 3GA-329: 21±3*10^3 µm^2, P=0.1; Fig. 2B-D). Due to the small size, most plaques showed a fatty streak phenotype rather than an advanced atherosclerotic plaque phenotype. Advanced atherosclerotic plaque features, such as a fibrous cap and necrotic core, were lacking in most plaques and therefore we were unable to quantify and compare this among the groups.

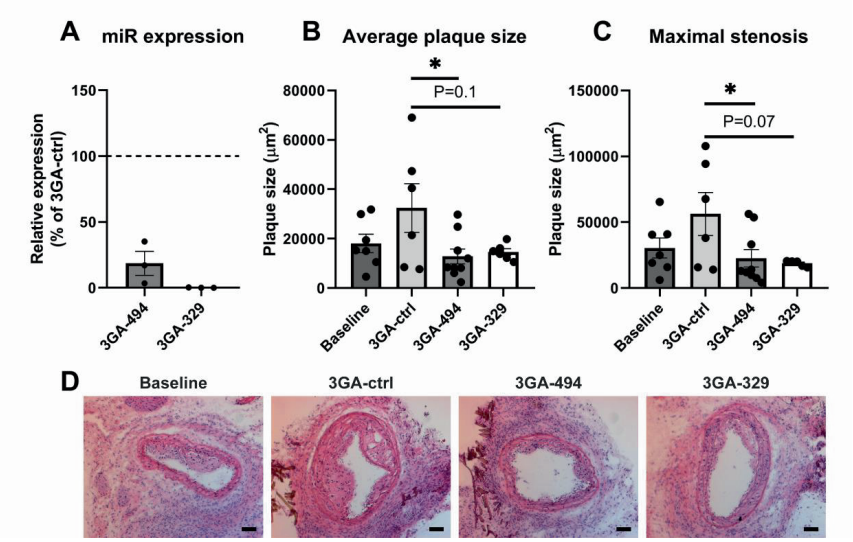

Figure 2. Inhibition of miRNA-494 and miRNA-329 in atherosclerotic lesions in the carotid artery. (A) Levels of miRNA-494 (N=3) and miRNA-329 (N=3) in carotid arteries of LDLr$^{-/-}$ mice one week after the final injection of 3GA-494 and 3GA-329, respectively, normalized to miRNA-494 and miRNA-329 expression in mice treated with 3GA-ctrl (100%; N=3). MiRNA-191 was used as a reference gene. (B) Average plaque size (calculated as the size average of plaque sections taken 100 um apart) in the carotid arteries of baseline (N=7), 3GA-ctrl (N=6), 3GA-494 (N=8) and 3GA-329 mice (N=6) and (C) plaque size at the site of maximal stenosis in µm^2 in the carotid arteries of baseline (N=7), 3GA-ctrl (N=6), 3GA-494 (N=8) and 3GA-329 mice (N=6). (D) Representative images of all groups. Scale bar 100 µm. A two-tailed Student's t-test was performed to compare single treatment to the 3GA-ctrl group. A Grubbs' test was used to identify significant outliers (α<0.05). *P<0.05 compared to 3GA-ctrl. Data are represented as mean ± SEM.

Inhibition of miRNA-494 increases plaque stability in advanced plaques

In the aortic root, plaque size and necrotic core size did not differ between groups (Fig. 3A, B). Other markers for plaque stability, however, were increased after miRNA-494 and, in part, miRNA-329 inhibition (Fig. 3C, E). Intra-plaque collagen content was strongly increased in 3GA-494 mice compared to the control (3GA-ctrl: 37±3% versus 3GA-494: 55±3%, P<0.0005; Fig. 3C). Treatment with 3GA-329 resulted in four mice in increased collagen content, whereas the other four showed similar collagen content as baseline mice (baseline: 15±2% versus 3GA-329: 34±9%; Fig. 3C). SMCs are the main source of collagen synthesis in atherosclerotic plaques, but the SMC-content was similar in all groups (baseline: 12±1%; 3GA-ctrl: 14±1%; 3GA-494: 11±1%; 3GA-329: 13±1%; Fig. 3D). Relative intra-plaque macrophage area was reduced upon diet switch from diet with high-fat high-cholesterol to regular chow (baseline: 22±2% versus 3GA-ctrl: 17±2%; Fig. 3E). In 3GA-494 mice, a further reduction in intra-plaque macrophage content was shown (3GA-ctrl: 17±2% versus 3GA-494: 12±1%, P<0.05; Fig. 3E), which is another marker of increased plaque stability. For the 3GA-329 treated mice, the relative macrophage area remained similar to control levels (3GA-329: 17±2%; Fig. 3E). Numbers of intra-plaque neutrophils were very small and not different among the groups (data not shown). Plaque necrotic core sizes were not significantly different between groups as well (Fig. 3E).

Blood, spleen and lymph node analyses of LDLr$^{-/-}$ mice treated with 3GA-494, 3GA-329 or 3GA-control

Blood analysis by Sysmex and flow cytometry revealed altered numbers of circulating cells upon 3GA-494 and 3GA-329 treatment compared to 3GA-ctrl (Fig. 4 and Sup. Fig. 3). White blood cells (WBCs) remained similar after miRNA-494 inhibition, but were decreased after miRNA-329 inhibition (Fig. 4A). Myeloid cells, as defined by CD11b^{+} and CD11c^{+}CD11b^{+} were elevated in 3GA-494 mice, whereas CD11b^{+} cells were decreased in 3GA-329 mice (Sup. Fig. 3A, B). More specifically, we observed that neutrophils (Ly6C^{+}Ly6G^{int}), which are part of the myeloid compartment of WBCs, were decreased after miRNA-494 and miRNA-329 inhibition (Fig. 4B, C). Total monocyte count, also part of the myeloid compartment of WBCs, was not significantly altered, although we did observe differences in the pro-inflammatory subset (Ly6C^{+}Ly6G^{-}) quantified by FACS analysis (Fig. 4D, E).

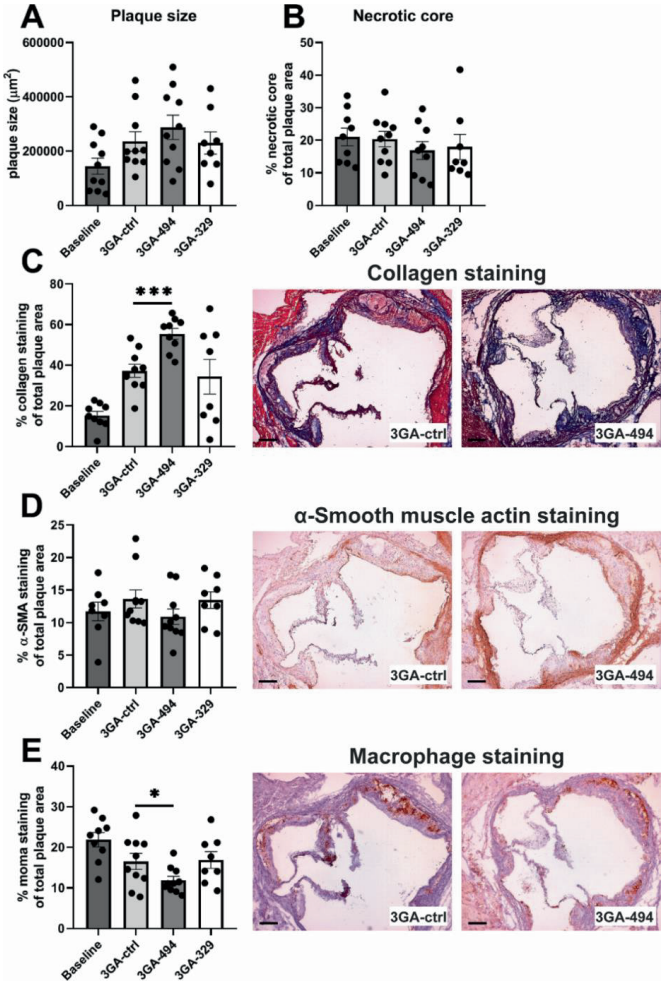

Figure 3. 3GA-494 treatment increased plaque stability in aortic root plaques. (A) Plaque size in µm^2 of aortic root plaques, calculated from at least five 10 µm thick section of the three-valve area. (B) Necrotic core area, defined as an acellular area, measured in the lesions stained with Masson's Trichrome, (C) collagen content, stained with Massons's Trichrome, (D) SMC cell content, stained with an antibody against α-smooth muscle actin (α-SMA), (E) macrophage content, stained with anti-monocyte-macrophage (Moma)-2 antibody. Amount of staining is shown as a percentage of total plaque area quantified in baseline (N=10), 3GA-ctrl (N=10), 3GA-494 (N=10) and 3GA-329 (N=8). (C-E) Scale bar 250 µm. A two-tailed Student's t-test was performed to compare single treatment to the 3GA-ctrl group. A Grubbs' test was used to identify significant outliers (α<0.05). *P<0.05, ***P<0.0005 compared to 3GA-ctrl. Data are represented as mean ± SEM.

Although total amounts of lymphocytes were similar, $CD19^+$ B-cells were reduced in 3GA-494 mice and $CD4^+$ and $CD8^+$ T-cells were slightly increased in 3GA-329 mice (Fig. 4F and Sup. Fig. 3C-E). Furthermore, miRNA-494 inhibition decreased red blood cell and, in particular, strongly reduced platelet count (Fig. 4G, H). In the 3GA-329 treated mice, three mice showed reduced platelet counts, whereas platelet counts were normal in the remaining mice (Fig. 4H).

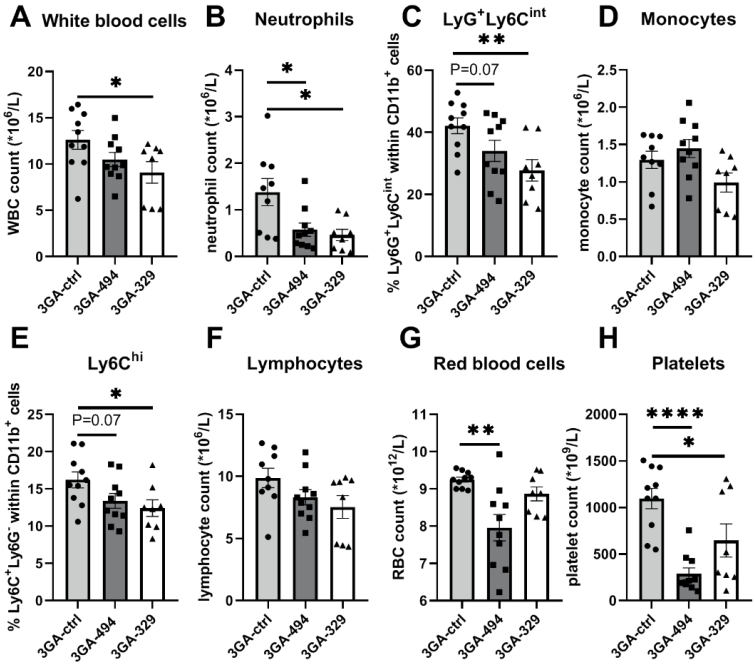

Figure 4. Blood analysis of mice treated with 3GA-494, 3GA-329 or 3GA-ctrl one week after final injection. Amount of circulating (A) white blood cells (WBC; 10^6/L), (B) neutrophils (10^6/L) and (C) neutrophil marker lymphocyte antigen 6 complex, locus G6D ($Ly6G^+$) lymphocyte antigen 6 complex, locus C1 $(Ly6C)^{int}$ cells defined as a percentage within $CD11b^+$ cells, (D) monocytes (10^6/L) and (E) inflammatory subset of monocytes $Ly6G^-Ly6C^{hi}$ cells as a percentage within $CD11b^+$ cells, (F) lymphocytes (10^6/L), (G) red blood cells (RBC; 10^{12}/L) and (H) platelets (10^9/L). (A, C, E-H) Blood cell analysis on whole blood quantified by Sysmex. (C, E) Flow cytometric analysis (FACS) analysis performed on the blood of 3GA-ctrl, 3GA-494 and 3GA-329 mice after red blood cells were removed using lysis buffer. A two-tailed Student's t-test was performed to compare single treatment to the 3GA-ctrl group. A Grubbs' test was used to identify significant outliers ($\alpha<0.05$). *P<0.05, **P<0.005, ****P<0.0001 compared to 3GA-ctrl. 3GA-ctrl (N=10), 3GA-494 (N=10) and 3GA-329 (N=8). Data are represented as mean ± SEM.

Percentages of $CD4^+$ and $CD8^+$ T-cells in the spleen were decreased in 3GA-494-treated mice and showed a trend towards a reduction in 3GA-329-treated mice (Sup. Fig. 3F, G). However, since the spleens were enlarged due to proliferation of other cell types, as discussed below, the absolute numbers of $CD4^+$ and $CD8^+$ T-cells may be similar among all groups. $CD4^+$ and $CD8^+$ T-cells in the draining lymph nodes were not different among all groups (Sup. Fig. 3H, I).

Splenic megakaryocyte retention

As mentioned above, all 3GA-494 mice and half of the 3GA-329 mice showed splenomegaly compared to 3GA-ctrl and baseline mice (Fig. 5A, B). Staining for Von Willebrand factor (VWF) revealed strongly elevated numbers of megakaryocytes in the enlarged spleens of 3GA-494 mice compared to 3GA-ctrl, indicating increased megakaryopoiesis (Fig. 5A, C). In 3GA-329 mice, only the mice with low platelet counts showed splenomegaly, accompanied by strongly elevated megakaryocyte numbers (Fig. 5B). Despite the administration of a miRNA-494 inhibitor, splenic expression of miRNA-494 was upregulated one week after the final 3GA-injection (Fig. 5C). Increased expression of megakaryocyte/platelet markers, i.e. glycoprotein Ib platelet subunit alpha (GPIbα) and subunit beta (GpIbβ), both part of the platelet receptor complex for VWF, and integrin subunit beta 3 (Itgb3), in the spleen of 3GA-494 mice confirmed indeed increased megakaryopoiesis (Fig. 5D-F). Megakaryocytes and erythrocytes derive from a bipotent erythrocytic-megakaryocyte progenitor. Transcription factors involved in commitment of erythrocytic-megakaryocyte progenitor cells towards megakaryocyte progenitors and platelet production were also increased upon 3GA-494 treatment (Fig. 5G-I)[19]. Expression of transcription factors involved in hematopoietic stem cell (HSC) proliferation and differentiation, which are putative targets of miRNA-494 and conserved in both human and mice, as was predicted by www.targetscan.org (release 7.2), was similar in both 3GA-494 and 3GA-ctrl treated mice (Sup. Fig. 2C)[20-23]. In the spleen of 3GA-329 mice, no significant differences in megakaryocyte/platelet markers nor transcription factor expression was shown compared to 3GA-ctrl mice (Fig. 5D-I).

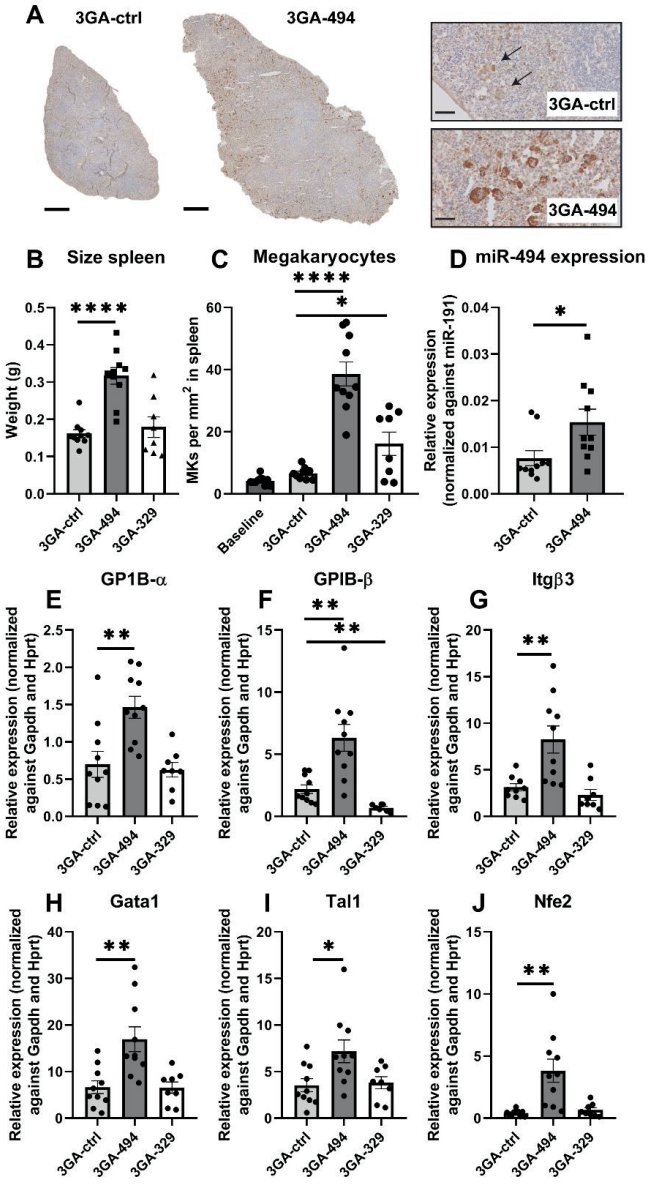

Figure 5. Megakaryocyte accumulation in the spleen upon 3GA-494 and 3GA-329 treatment. (A) Representative images of splenomegaly in 3GA-494 treated mice with megakaryocyte accumulation compared to 3GA-ctrl. Megakaryocytes were stained with an antibody against Von Willebrand factor. Scale bar 500 µm. Zoomed in image scale bar 50 µm. (B) Weight in grams (g) of the spleens of 3GA-ctrl (N=10), 3GA-494 (N=10) and 3GA-329 mice (N=8). (C) Amount of megakaryocytes per mm^2 spleen. (D) miRNA-494 expression in the spleen of 3GA-ctrl and 3GA-494 mice, relative to miRNA-191 expression. (E) Three different platelet/ megakaryocyte markers quantified by qPCR in the spleen; Glycoprotein Ib platelet subunit alpha (GP1b-α), (F) beta (GP1b-β) chain and (G) integrin subunit beta

3 (Itgb3) normalized to Gapdh and Hprt. (H-J) Transcription factors involved in megakaryocyte differentiation in the spleen. Gata binding protein 1 (Gata1), TAL bHLH transcription factor 1, erythroid differentiation factor (Tal1), nuclear factor, erythroid 2 (Nfe2). A two-tailed Student's t-test was performed to compare single treatment to the 3GA-ctrl group. A Grubbs' test was used to identify significant outliers (α<0.05). *P<0.05, **P<0.005, ****P<0.0001 compared to 3GA-ctrl. 3GA-ctrl (N=10), 3GA-494 (N=10) and 3GA-329 (N=8). Data are represented as mean ± SEM.

A previous study showed that in primary myelofibrosis, overexpression of miRNA-494 in HSCs promotes megakaryopoiesis via downregulation of suppressor of cytokine signaling 6 (SOCS6).[24] We quantified SOCS6 expression in the spleen. However, SOCS6 expression showed a trend towards upregulation compared to 3GA-ctrl instead of downregulation (Sup. Fig. 2D). As the bone marrow is also a source of megakaryopoiesis, we stimulated freshly isolated murine bone marrow cells with either 3GA-ctrl or 3GA-494. Although the miRNA-494 expression was downregulated in bone marrow cells after 3GA-494 treatment, we did not observe differences in SOCS6 expression nor in expression of transcription factors for megakaryocyte commitment and GPIbα and GpIbβ expression (Sup. Fig. 2E, F).

Increased hepatic platelet markers

Platelets can be cleared by hepatocytes and liver macrophages (Kuppfer cells).[25] Expression of miRNA-494 in the liver was similar in both 3GA-494 and 3GA-ctrl mice (Fig. 6A). MiRNA-329 was not expressed at all in the liver of either 3GA-329 or 3GA-ctrl mice (data not shown). Expression levels of platelet markers quantified by qPCR were upregulated in the liver of 3GA-494 treated mice, suggesting increased platelet clearance compared to 3GA-ctrl (Fig. 6B-D). In 3GA-329 mice, only the mice with low platelet counts showed increased expression of platelet markers in the liver (Fig. 6B-D).

Increased expression of platelet receptors upon 3GA-494 treatment

We further investigated whether 3GA-494 treatment could lead to miRNA-494 inhibition in anucleate platelets. Compared to 3GA-ctrl, mature miRNA-494 expression was first downregulated after one hour and then upregulated after four hours of incubation with 3GA-494 (Fig. 7A). As platelets have no transcription, upregulation of miRNA-494 was accompanied by depletion of the primary miRNA-494 transcript, pri-miRNA-494, indicating rapid processing of the pri-miRNA upon miRNA-494 downregulation (Fig. 7B). Changes in the intermediate pre-miRNA-494 were less pronounced (Fig. 7C).

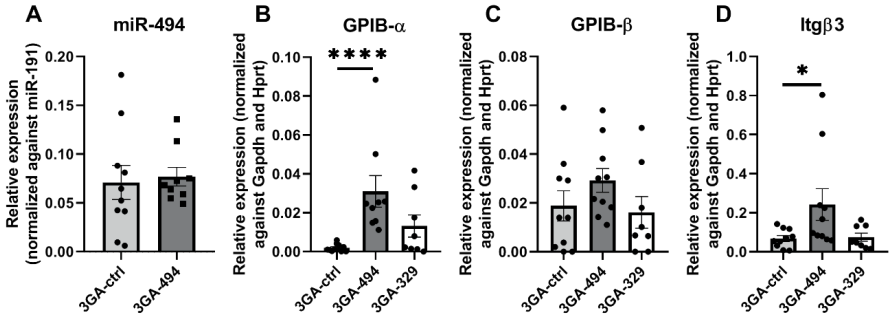

Figure 6. Increased platelet receptor expression in the liver of 3GA-494 mice. (A) MiRNA-494 expression in the liver of mice treated with 3GA-494 (N=9) or 3GA-ctrl (N=10), relative to miRNA-191. (B) Relative expression of three different platelet/megakaryocyte markers quantified by quantitative polymerase chain reaction (qPCR) in the liver of 3GA-ctrl (N=10), 3GA-494 (N=10) and 3GA-329 (N=8) mice; glycoprotein Ib platelet subunit alpha (GP1b-α), (C), beta chain (GPIb-β) and (D) integrin subunit beta 3 (Itgβ3) normalized to GAPDH and Hprt. (B-D) A Mann-Whitney U test was performed to compare single treatment to the 3GA-ctrl group. A Grubbs' test was used to identify significant outliers (α<0.05). *P<0.05, ****P<0.0001, compared to 3GA-ctrl. Data are represented as mean ± SEM.

Genes that we initially tested as housekeeping genes, including GAPDH, U6 and YWHAE, appeared to be unstable in 3GA-treated platelets (Sup. Fig. 4B-D).[26] Pre-ITGB3 showed stable expression and was, therefore, used as a housekeeping gene (Sup. Fig. 4A). Pro-survival genes BCL2 and MCL1 are putative targets of miRNA-494, as was predicted by www.targetscan.org (release 7.2). Since miRNA-494 was upregulated in platelets, we checked whether BCL2 and MCL1 were downregulated, leading to more apoptosis and subsequently to more clearance. MCL1 appeared downregulated in 3GA-494, but BCL2 did not (Sup. Fig. 4E, F).

Next, we quantified expression of platelet GPIBα and integrin subunit ITGB3, both part of platelet receptors involved in platelet activation, and found upregulation after four hours of 3GA-494 treatment compared to 3GA-ctrl (Fig. 7D-F). Since splicing occurs upon platelet activation, we measured pre-mRNA levels of MCL1, GAPDH and GPIBα.[27, 28] Pre-mRNA levels were declined in 3GA-494 treated platelets compared to 3GA-ctrl, indicating increased splicing and hence increased platelet activation in 3GA-494 treated platelets (Sup. Fig. 4G-I).

Time points from 8 hours on were excluded, since all platelets, independent of their treatment, were hyper-activated in culture.

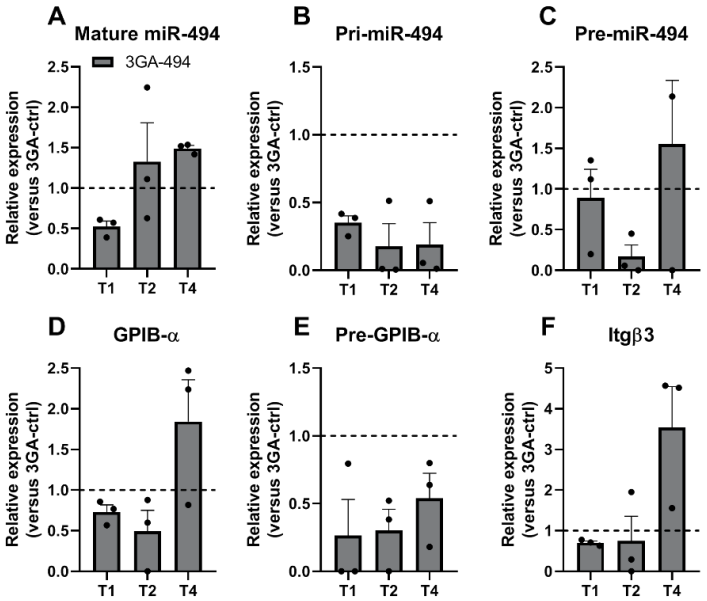

Figure 7. Upregulation of miRNA-494 expression following 3GA-494 treatment led to hyper-activation of platelets. Human platelets were incubated up to four hours in PAS-III buffer with 30-35% plasma with either 3GA-494 or 3GA-ctrl (in triplos). Platelets were kept in an incubator at 22ºC with 5% CO_2 at continuously swirling. (A) Mature miRNA-494 expression, relative to miRNA-126. (B) Pri-miRNA-494 and (C) pre-miRNA-494 relative to pre- integrin subunit beta 3 (Itgβ3) expression. (D) Expression levels of platelet receptors glycoprotein Ib platelet subunit alpha (GP1b-α), (E), beta chain (GPIb-β) and (F) Itgβ3, relative to pre-Itgβ3 expression. All expression levels were normalized to 3GA-ctrl (100%). Data are represented as mean ± SEM.

Discussion

In this study, we first show that inhibition of 14q32 miRNAs, particularly miRNA-494, in mice with advanced atherosclerotic lesions halted carotid atherosclerotic plaque progression and promoted plaque stability in the aortic root of LDLr$^{-/-}$ mice. Second, plasma cholesterol levels were lowered further by 14q32 miRNA inhibition than by diet switch alone. Third, pro-atherogenic cells in the circulation, including pro-inflammatory monocytes (Ly6C^{hi}), neutrophils and platelets were decreased after miRNA-329 and miRNA-494 inhibition.

Even though plasma cholesterol was lowered by diet-switch, plaques in the carotid artery continued to grow in 3GA-ctrl mice. With 3GA-494 treatment and, in part, 3GA-329 treatment, we managed to halt plaque progression in the carotid artery. Although we combined 3GA treatment with plasma lipid lowering, plaque sizes from 3GA-494 and 3GA-329-treated mice were not significantly reduced compared to baseline, indicating that plaque regression did not occur in this setup. Unlike for the carotid artery lesions, neither 3GA-494 treatment, nor 3GA-329 treatment, resulted in reduced plaque sizes in the aortic root compared to 3GA-ctrl treatment. We have previously established that the expression of 14q32 miRNAs differs between sites of lesion development in mice[14] and more recently, we demonstrated that expression of 14q32 miRNAs, including miRNA-494 and miRNA-329 and their targets, varies widely across the human vasculature as well.[29] Differences in response to miRNA inhibition in carotid artery plaques and aortic root plaques are, therefore, likely caused by differences in local miRNA and target gene expression. Although plaque size was not affected in the aortic root, plaque stability was clearly affected and increased after miRNA-494 inhibition, which is particularly relevant in reducing the risk of cardiovascular events. These results indicate that 3GA-494 treatment would be relevant for treating different types of plaques, developing at different sites in the vasculature.

Collagen provides structural support in the fibrotic cap and in our study, particularly miRNA-494 inhibition increased intra-plaque collagen content in advanced lesions. Collagen is synthesized by SMCs, however, we have previously shown that miRNA-494 does not affect collagen synthesis.[14] Furthermore, even though miRNA-494 does affect proliferation of myofibroblasts[15], neither miRNA-494, nor miRNA-329 inhibition affected the intraplaque SMC content, which indicates that another mechanism caused the enhanced collagen deposition. We previously validated tissue inhibitor of metalloproteinases 3 (TIMP3) as a target of miRNA-494.[14] TIMP3 inhibits collagen degradation by matrix metalloproteinases (MMPs) and, therefore, more TIMP3 expression likely contributed to the observed increase in collagen content. Since macrophages produce MMPs, the reduced intra-plaque macrophage content

may also have contributed to the increased collagen content in the plaques. Lipid lowering strategies have been described to contribute to fewer intra-plaque macrophages.[30] Fewer intra-plaque macrophages are associated with a more stable plaque phenotype. In our study, macrophages in advanced plaques of 3GA-ctrl mice were decreased compared with baseline mice, which was likely an effect of plasma lipid lowering by diet-switch and additional treatment with 3GA-494 even further reduced intra-plaque macrophage numbers. Circulating inflammatory monocytes (Ly6C^{hi}) are associated with promoting plaque progression after extravasation into the lesion and here, both miRNA-494 and miRNA-329 inhibition resulted in a reduction in circulating pro-inflammatory Ly6C^{hi} monocytes, which may have caused the reduction in plaque macrophages. In addition, platelets have been described to mediate monocyte activation, recruitment and extravasation into the lesion.[31] Therefore, the strongly reduced blood platelet levels in 3GA-494 mice may also have contributed to a reduction in macrophage extravasation into the lesion.

Particularly 3GA-494 mice showed reduced levels of circulating inflammatory cells, including neutrophils, red blood cells and platelets, all of which originate from a common early myeloid progenitor cell. Decreased expression of miRNA-494 has been reported to drive chronic myeloid leukemia, a stem cell derived malignant disorder in human.[32] We measured whether transcription factors involved in HSC proliferation and differentiation were targeted by increased miRNA-494 expression in the spleen. However, expression levels were not affected, indicating that this was not primary cause of reduced levels of circulating neutrophils, red blood cells and platelets in 3GA-494 mice. Others have also described a role for 14q32 miRNAs, including miRNA-494, in human erythropoiesis and, therefore, proper development of erythrocytes in our murine model may have been targeted by 3GA-494 treatment.[33] Exact mechanisms on how myeloid cells in the circulation are reduced, however, remains to be determined in future research.

In previous studies, we have shown that multiple miRNAs transcribed from the 14q32 cluster are involved in different processes of vascular remodeling.[14-17] Inhibition of 14q32 miRNAs miRNA-494, miRNA-329, miRNA-487b and miRNA-495 improved neovascularization and blood flow recovery in a hindlimb ischemia model.[15] Neovascularization requires a pro-inflammatory response, whereas an anti-inflammatory response is favorable for atherosclerosis. Stimulation of neovascularization often leads to aggravation of atherosclerosis and vice versa.[34] This effect is often referred to as the Janus phenomenon, after the two-faced Roman god.[35] In contrast to the Janus-phenomenon, 14q32 miRNA

inhibition both increases neovascularization and reduces atherosclerosis and, therefore, play a unique role in vascular remodeling.
Strongly increased megakaryocyte content and increased expression of transcription factors in the spleen of 3GA-494 mice clearly showed increased commitment toward the megakaryocyte lineage. Since SOCS6 expression was not affected upon 3GA-494 treatment in either the spleen or bone marrow cells, this indicates that megakaryocyte differentiation was not targeted by 3GA-494 treatment. Increased splenic megakaryocyte differentiation in 3GA-494 mice is, therefore, likely a compensatory mechanism to prevent severe thrombocytopenia. Others have also demonstrated that mice show increased megakaryocyte differentiation as a response to lower platelet counts.[36]

The underlying mechanism of platelet exhaustion may be an increased hepatic clearance. We found increased platelet receptor expression in the liver. Apoptotic platelets are recognized and cleared by the liver.[37] However, pro-survival genes Mcl-1 and Bcl-2 were not clearly affected by miRNA-494 expression in the platelets and were therefore unlikely the key contributors to increased platelet clearance. Activation of the platelet receptor GPIb-IX can also lead rapid hepatic clearance and differential expression of the 14q32 cluster has previously been linked to platelet reactivity.[37-39] Indeed, we found that upregulation of miRNA-494 expression following 3GA-494 treatment led to hyper-activation of platelets. Also, as miRNA-494 expression in the liver itself was not affected by 3GA-494, it is most likely that increased platelet clearance is caused by platelet activation in response to 3GA-494 treatment, rather than by upregulation of clearance pathways in the liver.

A surprising observation in this study is the fact that in both platelets and in the spleen, 3GA-494 treatment resulted in short-term miRNA-494 inhibition followed by a clear miRNA-494 upregulation. The upregulation was accompanied by rapid depletion of miRNA-494 precursors in platelets. RNA binding proteins, which are regulated by miRNAs themselves, are able to regulate miRNA-processing in a cell-specific manner. In a previous study, we have demonstrated post-transcriptional regulation of miRNA-494 by Mef2A, which directly binds to pri-miRNA-494.[17] However, which precise mechanism underlies the cell- and tissue-specific autoregulation of miRNA-494 in LDLr$^{-/-}$ mice remains to be determined.

Since each cell type has its own specific miRNA and target gene expression pattern, single miRNA inhibition has distinct effects in each cell type.[29, 40, 41] Above, we have discussed the effects of miRNA-494 and miRNA-329 inhibition on SMCs and myofibroblasts, on macrophages, and on megakaryocyte cells and platelets, but also the endothelial cell is of

importance in atherosclerosis development and progression. We have shown in the past that inhibition of miRNA-494 had little effect on proliferation of human arterial endothelial cells. Inhibition of miRNA-329, however, increased proliferation of endothelial cells.[15] Whether inhibition of miRNA-329 affects plaque size and composition via increased proliferation of endothelial cells, remains for future research.

In our study, we used a scrambled 3GA as control, and in a previous study we have established that this 3GA-ctrl does not show significant differences as compared to vehicle controls.[15] Non-specific effects of this 3GA-ctrl in this study are thus highly unlikely; however, they cannot be completely excluded. In addition, in this study, we used LDLr$^{-/-}$, which is a strain that allows plasma lipid lowering in response to a diet switch. Previously, we have shown therapeutic effects of 3GA-494 in an ApoE$^{-/-}$ mouse model, in which atherosclerosis develops in response to elevated lipid levels, which cannot be lowered using a diet switch. The data from these two studies may thus not be directly comparable due to strain differences, however in both models 3GA-494 treatment improved lesion size and stability. The most important strength of this study is that we used a murine model with fully established lesions and started 3GA-treatment after advanced plaques had been formed, while most studies focus on initial lesion development. Additionally, we included a lipid lowering strategy by changing the diet from high-fat high cholesterol to regular chow. Since most patients present in the clinic with advanced and unstable atherosclerosis and receive routine lipid lowering treatment, we more closely mimicked the clinical situation in this study.

Conclusions

In conclusion, inhibition of 14q32 miRNAs, and particularly of miRNA-494, halts plaque progression and increases plaque stability in mice with established advanced atherosclerotic lesions. Plasma cholesterol levels were lowered further by 14q32 miRNA inhibition than by diet switch alone. Furthermore, pro-atherogenic cells, including inflammatory Ly6C^{hi} monocytes, neutrophils and platelets, were reduced in the circulation. Inhibition of miRNA-494 would therefore be a potential therapeutic target for stabilizing vulnerable lesions in patients and may even prevent surgical interventions in some cases.

Material and Methods

Mice and experimental design

All animal work was performed conform the guidelines from the Dutch government and the Directive 2010/63/EU of the European Parliament and all experiments were approved by the local animal ethics committee (DEC number 14103). Male LDLr$^{-/-}$ mice, aged 8 to 9 weeks, were obtained from our in-house breeding facility (Gorlaeus Laboratories, Leiden University, Leiden, the Netherlands). Food and water were available *ad libitum*.

The timeline of the study is shown in Sup. Fig. 1. All mice were fed a Western-type diet (WTD) containing 0.25% cholesterol and 15% cacao butter (SDS, Sussex, United Kingdom) for 10 weeks to induce advanced atherosclerotic lesions, as described previously.[42] Four weeks after start of the WTD, mice underwent surgical interventions in order to induce carotid artery plaque formation. As described previously, semi-constrictive collars were placed around both carotid arteries.[14] Mice were anaesthetized by subcutaneous injection of ketamine (60 mg/kg, Eurovet Animal Health, Bladel, The Netherlands), fentanyl citrate and fluanisone (1.26 mg/kg and 2 mg/kg respectively, Janssen Animal Health, Sauderton, UK).

Six weeks after collar placement, mice were age-, cholesterol-, and weight-matched, to ensure an equal distribution over all groups before start of the treatment. At that time-point, a subset of mice (n=10) was sacrificed as baseline control. The remaining mice were placed on a regular chow diet to lower plasma cholesterol levels and 3GAs against miRNA-494 (3GA-494; n=10), miRNA-329 (3GA-329; n=10) or negative control (3GA-ctrl; n=10) were administered via the tail vein (i.v.) at a concentration of 1 mg/mouse. 3GAs were designed with perfect reverse complementary to the mature target miRNA sequence and synthesized by Idera Pharmaceuticals (Cambridge, MA, USA). The same sequences of 3GAs (formerly named Gene Silencing Oligonucleotides; GSOs) against miRNA-494 and miRNA-329 were used as described previously.[15] As a negative control, a scrambled sequence was used, designed not to target any known murine miRNA. Sequences of the miRNAs and 3GAs are shown in Table 1. Second and third injections were given two and four weeks after diet switch. During the experiment, total serum cholesterol levels were quantified by enzymatic procedures using Precipath (Roche Diagnostics GmbH, Mannheim, Germany). One week after the final 3GA injection, mice were anaesthetized by a subcutaneous injection of a cocktail containing ketamine (40 mg/mL), atropine (50 µg/mL), and sedazine (6.25 mg/mL). Mice were subsequently perfused with phosphate-buffered saline (PBS) through the left cardiac ventricle, after which carotid arteries and other organs were collected, frozen and used for

further analysis. At sacrifice, whole blood was analyzed on a Sysmex XT-2000i analyzer (Goffin Meyvis, Etten Leur, The Netherlands).

Flow cytometric analysis

At sacrifice, blood, spleen and the mediastinal lymph nodes near the heart (HLN) were isolated. Single-cell suspensions of spleen and HLN were obtained by squeezing the organs through a 70 µm cell strainer. Red blood cells were removed using Ammonium-Chloride-Potassium (ACK) lysis buffer (0.15 M NH4Cl, 10 mM NaHCO3, 0.1 mM EDTA, pH 7.3). Immune cells were analyzed with flow cytometry: T cells ($CD4^+$, $CD8^+$), B cells ($CD19^+$) neutrophils ($CD11b^+Ly6G^+$) and inflammatory monocytes ($CD11b^+Ly6G^-Ly6C^{high}$). Flow cytometric analysis was performed on a FACSCantoII (BD Biosciences) and data was analyzed with FlowJo software (Treestar).

RNA isolation and RT/qPCR

Frozen tissues were crushed by use of pestle and mortar while immersed in liquid nitrogen. After homogenizing and complete evaporation of the liquid nitrogen, TRIzol (ThermoFisher, Bleiswijk, the Netherlands) was added to the samples. For carotid artery RNA isolation, carotid artery segments from three to four mice were pooled and homogenized with a pellet crusher in TRIzol. Total RNA was isolated by standard TRIzol-chloroform extraction. RNA concentration and purity were measured on the Nanodrop (Nanodrop® Technologies).

For microRNAs, microRNA specific Taqman qPCR kits (ThermoFisher, Bleiswijk, the Netherlands) were used for reversed transcription and quantification by qPCR according to the manufacturers protocol. For mRNA, RNA was reverse transcribed using 'high-capacity RNA to cDNA' kit (ThermoFisher, Bleiswijk, the Netherlands). SybrGreen reagents (Qiagen Benelux, Venlo, the Netherlands) were used for the qPCR. The data was normalized using a stably expressed endogenous control. MiRNA-191 was used for microRNAs and Gapdh and Hprt for mRNA. qPCR was performed on the VIIa7 (Applied Biosystems).

Immunohistochemistry

Frozen sections of carotid arteries (10 µm thick) were fixed with Formal-Fixx (ThermoFisher, Bleiswijk, the Netherlands) for 30 min and subsequently stained with hematoxylin and eosin to determine plaque size. Analysis was performed on sections throughout the atherosclerotic lesion (100 µm apart, resulting in the average plaque size value) and at the site of maximal stenosis, this is the site/section of the plaque that has the largest plaque size, using Leica Qwin software, as described previously.[43] Mice with plaques containing a reorganized thrombus

were excluded from the plaque size analysis (three mice in baseline, four mice in 3GA-ctrl, one mouse in 3GA-494 and one mouse in 3GA-329).

To determine lesion size in the three-valve area, cryosections (10 µm thick) of the aortic root were stained with oil red O and hematoxylin (Sigma-Aldrich, Zwijndrecht, the Netherlands). Lesion size was calculated from at least five 10 µm thick sections of the three-valve area. Masson's trichrome staining was used to visualize collagen and determine necrotic core area. Plaque macrophages were stained using a MOMA-2 antibody at a 1:1000 concentration (rat IgG2b, Serotec Ltd., Kidlington, UK). SMCs were stained with α-smooth muscle actin antibody (Clone 1A4, 1:1000, Abcam, Cambridge, UK). Neutrophils were stained using the Naphthol AS-D Chloroacetate Kit (Sigma-Aldrich, Zwijndrecht, the Netherlands). Collagen, necrotic core size, SMCs, macrophages and neutrophils were defined as percentage of total plaque area using Leica Qwin software.

Frozen cross-sections of spleen and liver were prepared (6 µm thickness) and fixed in ice-cold acetone. An antibody against Von Willebrand factor (A0082, 1:1000, Dako, Santa Clara, CA, USA) was used to visualize megakaryocytes in the spleen. Megakaryocytes were counted manually. ImageJ software was used for area measurements.

Bone marrow cells

To isolate BM cells, femurs and tibias of C57Bl/6 mice were dissected and the bone marrow was flushed with PBS. BM cells were filtered through 70 µm cell strainer, centrifuged at 300g for 15 min, and suspended in RPMI 1640 medium containing L-glutamine supplemented with 10% heat-inactivated fetal calf serum (FCSi) and 1% penicillin/streptomycin (P/S). BM cells were plated at a concentration of 1.8 x 10^6 cells/mL and stimulated with 3GA-494 or 3GA-ctrl at a concentration of 10 ng/µl for 48 hours in an incubator at 37ºC with 5% CO^2. After 48 hours of incubation, cells were washed with PBS and resuspended in TRIzol for subsequent RNA isolations.

Human platelets

Platelets, pooled from five different healthy donors with blood type O and Rh positive, were obtained from a blood bank facility (Sanquin, Amsterdam, the Netherlands). The same conditions as used for storage in platelet transfusion were used in the experiment. Platelets in PAS-III buffer with 30-35% plasma were transferred from the transfusion bag into 6-well plates and kept in an incubator at 22ºC with 5% CO^2 at continuously swirling. Platelet concentration was 0,9-1,3 10^9/ mL and contained <1 10^6 leukocytes. Platelets were untreated

or 3GA-494 or 3GA-ctrl was added at a concentration of 10 ng/µl, and incubated for up to 48 hours. As a quality control, pH was measured at each time point and platelet parameters were measured by Sysmex. To pellet the platelets after treatments, platelets were centrifuged at 800 g for 15 min at room temperature and subsequently resuspended in TRIzol.

Statistical Analyses

Results are expressed as mean ± SEM. A Kolmogorov-SmiRNAnov Test was performed to check normal distribution of values. When values were normally distributed, a two-tailed Student's t-test was used to compare single treatment group with the control group. When values were not normally distributed, a Mann-Whitney U test was performed to compare single treatment with the control group. $P<0.05$ was considered significant. A Grubbs' test was used to identify significant outliers ($\alpha<0.05$).

Acknowledgements

This study was supported by a grant from the Rembrandt Institute of Cardiovascular Science (2016), the Dutch Hart Foundation [grant number 2018T051], the CVON GENIUS II program, the LUMC Johanna Zaaijer Fund (2017) and the Austrian Science Fund FWF [Lise Meitner Grant, grant number M2578-B30]. We acknowledge S. Agrawal, B. Boersma and G. Beerends for their technical support.

Conflicts of Interest

There are no conflicts of interest.

Author Contributions

E.V.I., A.C.F., I.B., A.Y.N. designed the experiments; E.V.I., A.C.F., M.J.K, I.B., A.Y.N. conducted the experiments; E.V.I., A.C.F., I.B., A.Y.N., J.K., P.H.A.Q., wrote, reviewed and edited the paper; I.B. and A.Y.N. acquired funding; I.B., A.Y.N. and P.H.A.Q. supervised.

References

1. Libby, P, Ridker, PM, and Hansson, GK (2011). Progress and challenges in translating the biology of atherosclerosis. *Nature* **473**: 317-325.
2. Bonati, LH, Dobson, J, Featherstone, RL, Ederle, J, van der Worp, HB, de Borst, GJ*, et al.* (2015). Long-term outcomes after stenting versus endarterectomy for treatment of symptomatic carotid stenosis: the International Carotid Stenting Study (ICSS) randomised trial. *Lancet (London, England)* **385**: 529-538.
3. Stone, NJ, Robinson, JG, Lichtenstein, AH, Bairey Merz, CN, Blum, CB, Eckel, RH*, et al.* (2014). 2013 ACC/AHA guideline on the treatment of blood cholesterol to reduce atherosclerotic cardiovascular risk in adults: a report of the American College of Cardiology/American Heart Association Task Force on Practice Guidelines. *Circulation* **129**: S1-45.
4. Steen, DL, Khan, I, Ansell, D, Sanchez, RJ, and Ray, KK (2017). Retrospective examination of lipid-lowering treatment patterns in a real-world high-risk cohort in the UK in 2014: comparison with the National Institute for Health and Care Excellence (NICE) 2014 lipid modification guidelines. *BMJ open* **7**: e013255.
5. Crisby, M, Nordin-Fredriksson, G, Shah, PK, Yano, J, Zhu, J, and Nilsson, J (2001). Pravastatin treatment increases collagen content and decreases lipid content, inflammation, metalloproteinases, and cell death in human carotid plaques: implications for plaque stabilization. *Circulation* **103**: 926-933.
6. Ridker, PM, Everett, BM, Thuren, T, MacFadyen, JG, Chang, WH, Ballantyne, C*, et al.* (2017). Antiinflammatory Therapy with Canakinumab for Atherosclerotic Disease. *The New England journal of medicine* **377**: 1119-1131.
7. Welten, SM, Goossens, EA, Quax, PH, and Nossent, AY (2016). The multifactorial nature of microRNAs in vascular remodelling. *Cardiovascular research* **110**: 6-22.
8. Najafi-Shoushtari, SH, Kristo, F, Li, Y, Shioda, T, Cohen, DE, Gerszten, RE*, et al.* (2010). MicroRNA-33 and the SREBP host genes cooperate to control cholesterol homeostasis. *Science (New York, NY)* **328**: 1566-1569.
9. Rayner, KJ, Sheedy, FJ, Esau, CC, Hussain, FN, Temel, RE, Parathath, S*, et al.* (2011). Antagonism of miRNA-33 in mice promotes reverse cholesterol transport and regression of atherosclerosis. *The Journal of clinical investigation* **121**: 2921-2931.
10. Rayner, KJ, Suarez, Y, Davalos, A, Parathath, S, Fitzgerald, ML, Tamehiro, N*, et al.* (2010). MiRNA-33 contributes to the regulation of cholesterol homeostasis. *Science (New York, NY)* **328**: 1570-1573.
11. Price, NL, Rotllan, N, Canfran-Duque, A, Zhang, X, Pati, P, Arias, N*, et al.* (2017). Genetic Dissection of the Impact of miRNA-33a and miRNA-33b during the Progression of Atherosclerosis. *Cell reports* **21**: 1317-1330.
12. Nazari-Jahantigh, M, Wei, Y, Noels, H, Akhtar, S, Zhou, Z, Koenen, RR*, et al.* (2012). MicroRNA-155 promotes atherosclerosis by repressing Bcl6 in macrophages. *The Journal of clinical investigation* **122**: 4190-4202.
13. Eken, SM, Jin, H, Chernogubova, E, Li, Y, Simon, N, Sun, C*, et al.* (2017). MicroRNA-210 Enhances Fibrous Cap Stability in Advanced Atherosclerotic Lesions. *Circulation research* **120**: 633-644.
14. Wezel, A, Welten, SM, Razawy, W, Lagraauw, HM, de Vries, MR, Goossens, EA*, et al.* (2015). Inhibition of MicroRNA-494 Reduces Carotid Artery Atherosclerotic Lesion Development and Increases Plaque Stability. *Annals of surgery* **262**: 841-847; discussion 847-848.
15. Welten, SM, Bastiaansen, AJ, de Jong, RC, de Vries, MR, Peters, EA, Boonstra, MC*, et al.* (2014). Inhibition of 14q32 MicroRNAs miRNA-329, miRNA-487b, miRNA-494, and miRNA-495 increases neovascularization and blood flow recovery after ischemia. *Circulation research* **115**: 696-708.

16. Welten, SMJ, de Jong, RCM, Wezel, A, de Vries, MR, Boonstra, MC, Parma, L*, et al.* (2017). Inhibition of 14q32 microRNA miRNA-495 reduces lesion formation, intimal hyperplasia and plasma cholesterol levels in experimental restenosis. *Atherosclerosis* **261**: 26-36.
17. Welten, SMJ, de Vries, MR, Peters, EAB, Agrawal, S, Quax, PHA, and Nossent, AY (2017). Inhibition of Mef2a Enhances Neovascularization via Post-transcriptional Regulation of 14q32 MicroRNAs miRNA-329 and miRNA-494. *Molecular therapy Nucleic acids* **7**: 61-70.
18. Foks, AC, van Puijvelde, GH, Bot, I, ter Borg, MN, Habets, KL, Johnson, JL*, et al.* (2013). Interruption of the OX40-OX40 ligand pathway in LDL receptor-deficient mice causes regression of atherosclerosis. *Journal of immunology (Baltimore, Md : 1950)* **191**: 4573-4580.
19. Fuhrken, PG, Chen, C, Apostolidis, PA, Wang, M, Miller, WM, and Papoutsakis, ET (2008). Gene Ontology-driven transcriptional analysis of CD34+ cell-initiated megakaryocytic cultures identifies new transcriptional regulators of megakaryopoiesis. *Physiological genomics* **33**: 159-169.
20. Magnusson, M, Brun, AC, Miyake, N, Larsson, J, Ehinger, M, Bjornsson, JM*, et al.* (2007). HOXA10 is a critical regulator for hematopoietic stem cells and erythroid/megakaryocyte development. *Blood* **109**: 3687-3696.
21. Tanabe, O, Shen, Y, Liu, Q, Campbell, AD, Kuroha, T, Yamamoto, M*, et al.* (2007). The TR2 and TR4 orphan nuclear receptors repress Gata1 transcription. *Genes & development* **21**: 2832-2844.
22. Chen, Z, Yi, W, Morita, Y, Wang, H, Cong, Y, Liu, JP*, et al.* (2015). Wip1 deficiency impairs haematopoietic stem cell function via p53 and mTORC1 pathways. *Nature communications* **6**: 6808.
23. Nemeth, MJ, Kirby, MR, and Bodine, DM (2006). Hmgb3 regulates the balance between hematopoietic stem cell self-renewal and differentiation. *Proceedings of the National Academy of Sciences of the United States of America* **103**: 13783-13788.
24. Rontauroli, S, Norfo, R, Pennucci, V, Zini, R, Ruberti, S, Bianchi, E*, et al.* (2017). miRNA-494-3p overexpression promotes megakaryocytopoiesis in primary myelofibrosis hematopoietic stem/progenitor cells by targeting SOCS6. *Oncotarget* **8**: 21380-21397.
25. Sorensen, AL, Rumjantseva, V, Nayeb-Hashemi, S, Clausen, H, Hartwig, JH, Wandall, HH*, et al.* (2009). Role of sialic acid for platelet life span: exposure of beta-galactose results in the rapid clearance of platelets from the circulation by asialoglycoprotein receptor-expressing liver macrophages and hepatocytes. *Blood* **114**: 1645-1654.
26. Mossberg, K, Svensson, PA, Gidlof, O, Erlinge, D, Jern, S, and Brogren, H (2016). Normalization of qPCR in platelets - YWHAE a potential genericreference gene. *Platelets* **27**: 729-734.
27. Denis, MM, Tolley, ND, Bunting, M, Schwertz, H, Jiang, H, Lindemann, S*, et al.* (2005). Escaping the nuclear confines: signal-dependent pre-mRNA splicing in anucleate platelets. *Cell* **122**: 379-391.
28. Nassa, G, Giurato, G, Cimmino, G, Rizzo, F, Ravo, M, Salvati, A*, et al.* (2018). Splicing of platelet resident pre-mRNAs upon activation by physiological stimuli results in functionally relevant proteome modifications. *Scientific reports* **8**: 498.
29. Goossens, EAC, de Vries, MR, Simons, KH, Putter, H, Quax, PHA, and Nossent, AY (2019). miRNAMap: Profiling 14q32 microRNA Expression and DNA Methylation Throughout the Human Vasculature **6**.
30. Feig, JE, Parathath, S, Rong, JX, Mick, SL, Vengrenyuk, Y, Grauer, L*, et al.* (2011). Reversal of hyperlipidemia with a genetic switch favorably affects the content and inflammatory state of macrophages in atherosclerotic plaques. *Circulation* **123**: 989-998.
31. Badrnya, S, Schrottmaier, WC, Kral, JB, Yaiw, KC, Volf, I, Schabbauer, G*, et al.* (2014). Platelets mediate oxidized low-density lipoprotein-induced monocyte extravasation and foam cell formation. *Arteriosclerosis, thrombosis, and vascular biology* **34**: 571-580.
32. Salati, S, Salvestrini, V, Carretta, C, Genovese, E, Rontauroli, S, Zini, R*, et al.* (2017). Deregulated expression of miRNA-29a-3p, miRNA-494-3p and miRNA-660-5p affects

sensitivity to tyrosine kinase inhibitors in CML leukemic stem cells. *Oncotarget* **8**: 49451-49469.
33. Lessard, S, Beaudoin, M, Orkin, SH, Bauer, DE, and Lettre, G (2018). 14q32 and let-7 microRNAs regulate transcriptional networks in fetal and adult human erythroblasts. *Human molecular genetics* **27**: 1411-1420.
34. Parma, L, Baganha, F, Quax, PHA, and de Vries, MR (2017). Plaque angiogenesis and intraplaque hemorrhage in atherosclerosis. *European journal of pharmacology* **816**: 107-115.
35. Epstein, SE, Stabile, E, Kinnaird, T, Lee, CW, Clavijo, L, and Burnett, MS (2004). Janus phenomenon: the interrelated tradeoffs inherent in therapies designed to enhance collateral formation and those designed to inhibit atherogenesis. *Circulation* **109**: 2826-2831.
36. Barwari, T, Eminaga, S, Mayr, U, Lu, R, Armstrong, PC, Chan, MV*, et al.* (2018). Inhibition of profibrotic microRNA-21 affects platelets and their releasate. *JCI insight* **3**.
37. Quach, ME, Chen, W, and Li, R (2018). Mechanisms of platelet clearance and translation to improve platelet storage. *Blood* **131**: 1512-1521.
38. Deng, W, Xu, Y, Chen, W, Paul, DS, Syed, AK, Dragovich, MA*, et al.* (2016). Platelet clearance via shear-induced unfolding of a membrane mechanoreceptor. *Nature communications* **7**: 12863.
39. Edelstein, LC, Simon, LM, Montoya, RT, Holinstat, M, Chen, ES, Bergeron, A*, et al.* (2013). Racial differences in human platelet PAR4 reactivity reflect expression of PCTP and miRNA-376c. *Nature medicine* **19**: 1609-1616.
40. Santulli, G (2015). microRNAs Distinctively Regulate Vascular Smooth Muscle and Endothelial Cells: Functional Implications in Angiogenesis, Atherosclerosis, and In-Stent Restenosis. *Advances in experimental medicine and biology* **887**: 53-77.
41. Rogg, EM, Abplanalp, WT, Bischof, C, John, D, Schulz, MH, Krishnan, J*, et al.* (2018). Analysis of Cell Type-Specific Effects of MicroRNA-92a Provides Novel Insights Into Target Regulation and Mechanism of Action. *Circulation* **138**: 2545-2558.
42. van Duijn, J, Kritikou, E, Benne, N, van der Heijden, T, van Puijvelde, GH, Kroner, MJ*, et al.* (2019). CD8+ T-cells contribute to lesion stabilization in advanced atherosclerosis by limiting macrophage content and CD4+ T-cell responses. *Cardiovascular research* **115**: 729-738.
43. Bot, I, Ortiz Zacarias, NV, de Witte, WE, de Vries, H, van Santbrink, PJ, van der Velden, D*, et al.* (2017). A novel CCR2 antagonist inhibits atherogenesis in apoE deficient mice by achieving high receptor occupancy. *Scientific reports* **7**: 52.

Supplementary data

Supplemental Figure 1. Timeline of the study. All mice were fed a Western type diet for ten weeks to induce atherosclerosis. After four weeks of diet, semi-constrictive collars were placed around both carotid arteries. At week ten, a subset of mice (N=10) was sacrificed as baseline control. The remaining mice were placed on a regular chow diet to normalize plasma cholesterol levels and 3GA treatment against miRNA-494 (3GA-494; N=10), miRNA-329 (3GA-329; N=10) or a scrambled sequence control (3GA-ctrl; N=10) were administered via the tail vein at a concentration of 1 mg/mouse. A second and third injection were given two and four weeks after diet replacement. One week after the final 3GA injection, all mice were sacrificed.

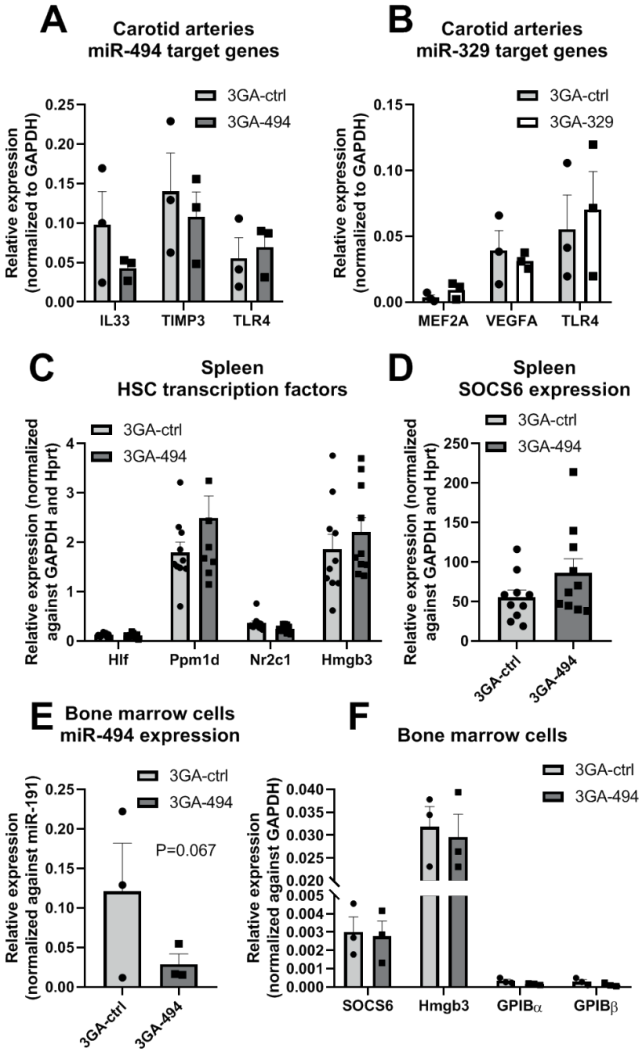

Supplemental Figure 2. MiRNA-494 and miRNA-329 target gene expression in the carotid arteries, spleen and bone marrow cells. (A) Relative expression levels of miRNA-494 and miRNA-329 target genes, interleukin 33 (IL33), TIMP metallopeptidase inhibitor 3 (TIMP3), toll like receptor 4 (TLR4) and myocyte enhancer factor 2A (MEF2A), vascular endothelial growth factor A (VEGFA), TLR4, respectively, one week after the final 3GA injection in the carotid arteries of 3GA-ctrl (N=3) and 3GA-494 mice (N=3). Expression levels were relative to glyceraldehyde-3-phosphate dehydrogenase (GAPDH). (C) Relative expression of transcription factors hepatic leukemia factor (Hlf), protein phosphatase, Mg2+Mn2+ dependent 1D (Ppm1d), nuclear receptor subfamily 2 group C member 1 (Nr2c1) and high mobility group box 3 (Hmgb3), involved in hematopoietic stem cell (HSC) proliferation and differentiation, measured in the spleen of 3GA-ctrl (N=10) and 3GA-494 mice (N=10). Expression is normalized to GAPDH and hypoxanthine guanine phophoribosyl transferase (Hprt). (D) Suppressor of cytokine signalling 6 (SOCS6) expression, normalized to GAPDH and Hprt, in the spleen

of 3GA-ctrl (N=10) and 3GA-494 mice (N=10). (E) Relative miRNA-494 expression in bone marrow (BM) cells treated with 3GA-494 or 3GA-ctrl for 48 hours (in triplo). Expression levels were normalized to miRNA-191. (F) SOCS6, Hmgb3, glycoprotein Ib platelet subunit alpha (GPIBα) and glycoprotein Ib platelet subunit beta (GPIBβ) expression, relative to GAPDH, in BM cells (in triplo). Data are represented as mean ± SEM.

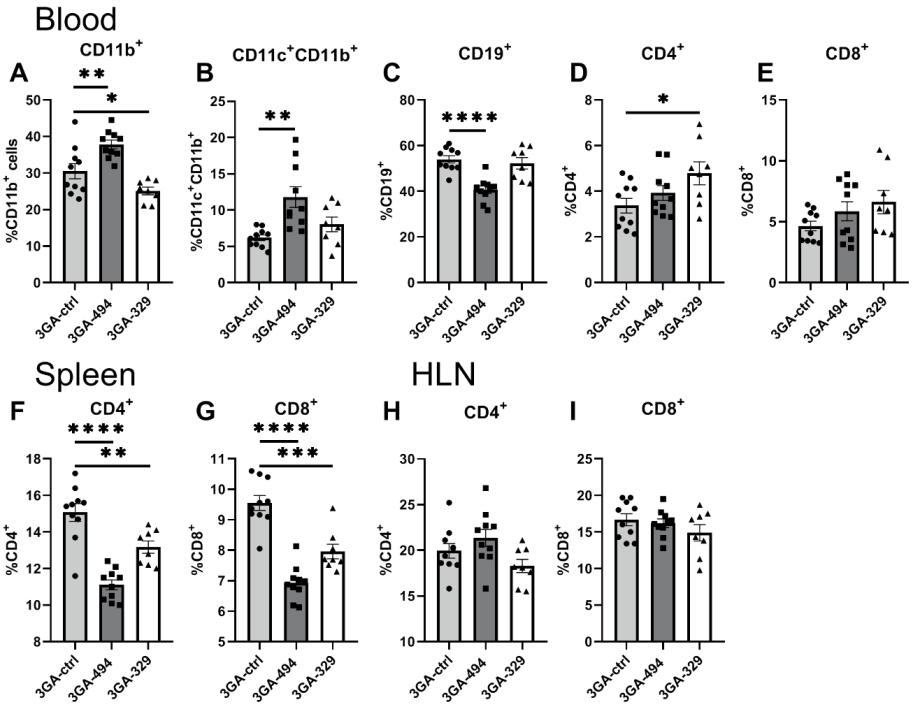

Supplemental Figure 3. Flow cytometric analysis of the blood, spleen and draining lymph nodes of mice treated with 3GA-ctrl, 3GA-494 or 3GA-329 one week after the final 3GA injection. (A) Percentage CD11b$^+$ cells of total input cells from the blood, (B) dendritic cells shown as percentage CD11c$^+$CD11b$^+$ within CD11b+ cells. (C) Percentage CD19$^+$ B cells, (D) CD4 and (E) CD8 T cells of total input cells from the blood. (F) Percentage CD4 and (G) CD8 T cells of total input cells from the spleen. (H) Percentage CD4 and (I) CD8 T cells of total input cells from draining lymph nodes. (A, C-I) Graphs show percentage of total cell input after red blood cell lysis. A two-tailed Student's t-test was performed to compare single treatment to the 3GA-ctrl group. A Grubbs' test was used to identify significant outliers (α<0.05). *P<0.05, **P<0.005, ***P<0.0005, ****P<0.0001 compared to 3GA-ctrl. 3GA-ctrl (N=10), 3GA-494 (N=10) and 3GA-329 (N=8). Data are represented as mean ± SEM.

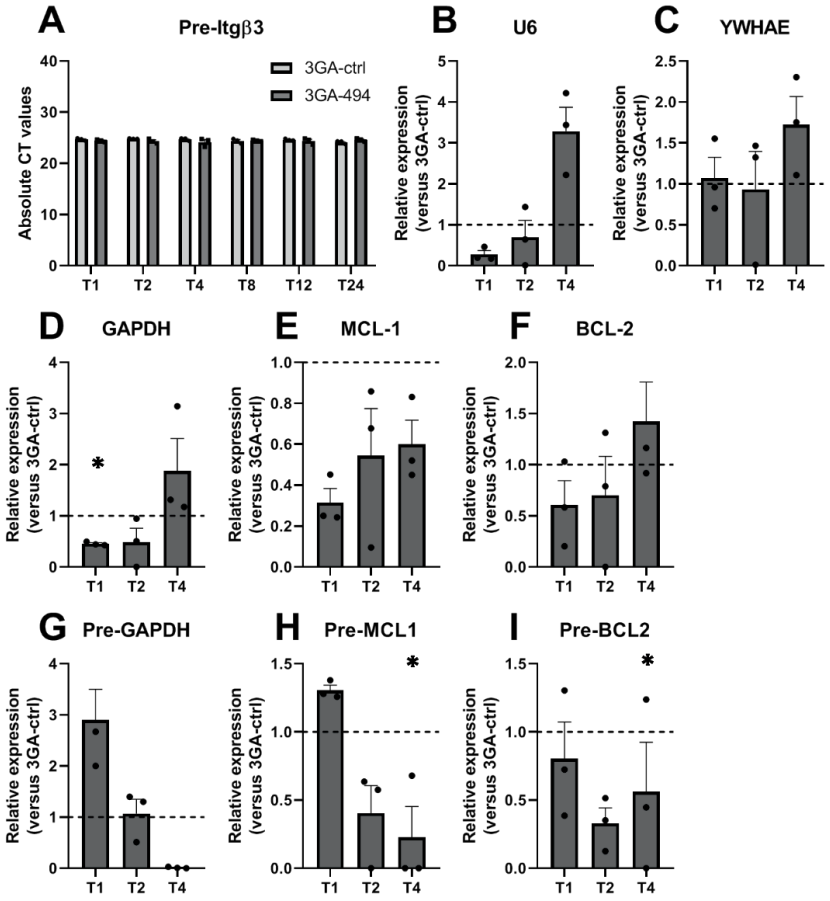

Supplemental Figure 4. Human platelets treated with 3GA-ctrl or 3GA-494. Human platelets were incubated up to four hours in PAS-III buffer with 30-35% plasma with either 3GA-494 or 3GA-ctrl (in triplos). Platelets were kept in an incubator at 22ºC with 5% CO_2 at continuously swirling. (A) Ct values of pre- integrin subunit beta 3 (ITGβ3) expression in 3GA-ctrl and 3GA-494 treated human platelets, incubated for 1, 2, 4, 8, 12 and 24 hours (in triplos). (B) Relative expression of U6, (C) tyrosine 3-monooxygenase/tryptophan 5-monooxygenase activation protein epsilon (YWHAE), (D) glyceraldehyde-3-phosphate dehydrogenase (GAPDH), (E) pro-survival genes and putative targets of miRNA-494 MCL1 apoptosis regulator (MCL1) and (F) BCL2 apoptosis regulator (BCL2), (G) pre-GAPDH, (H) pre-MCL1 and (I) pre-BCL2, relative to pre-ITGβ3 expression and normalized to 3GA-ctrl treated platelets (in triplos) at 1, 2 and 4 hours of incubation. A two-tailed Student's t-test was performed to compare 3GA-494 treatment to the 3GA-ctrl group. *P<0.05 compared to 3GA-ctrl. Data are represented as mean ± SEM.

MiRNA	**Sequence**
hsa/mmu-miRNA-494	5’-UGAAACAUACACGGGAAACCUC-3’
mmu-miRNA-329	5’-AACACACCCAGCUAACCUUUUU-3’
hsa-miRNA-329	5’-AACACACCUGGUUAACCUCUUU-3’
3GA	**Sequence**
hsa/mmu-3GA-494	3’-ACTTTGTATGTGCCCTTTGGAG-X-GAGGTTTCCCGTGTATGTTTCA-3’
mmu-3GA-329	3’-TTGTGTGGGTCGATTGGAAAAA-X-AAAAAGGTTAGCTGGGTGTGTT-3’
hsa-3GA-329	3’-TTGTGTGGACCAATTGGAGAAA-X-AAAGAGGTTAACCAGGTGTGTT-3’
negative control 3GA	3’-TGTACGACTCCATAACGGT-X-TGGCAATACCTCAGCATGT-3’

Table 1. Sequences of miRNAs and 3GAs. ‘X’: Phosphorothioate linker

Chapter 3

Inhibition of microRNA-494-3p activates Wnt signaling and reduces proinflammatory macrophage polarization in atherosclerosis

Eva van Ingen[1-3], Amanda C. Foks[3], Tamar Woudenberg[1,2], M. Leontien van der Bent[1,2], Alwin de Jong[1,2], Philipp J. Hohensinner[4], Johann Wojta[4,6], Ilze Bot[3], Paul. H.A. Quax[1,2], A. Yaël Nossent[1,2,4,5]

Molecular Therapy Nucleic Acids. 2021 Nov 4;26:1228-1239

[1]Department of Surgery and [2]Einthoven Laboratory for Experimental Vascular Medicine, Leiden University Medical Center, Leiden, The Netherlands. [3]Division of BioTherapeutics, Leiden Academic Centre for Drug Research, Leiden University, Leiden, The Netherlands. [4]Department of Internal Medicine II, Medical and [5]Department of Laboratory Medicine, University of Vienna, Vienna, Austria. [6]Ludwig Boltzmann Institute for Cardiovascular Research, Vienna, Austria.

Abstract

We have previously shown that treatment with third-generation antisense oligonucleotides against miR-494-3p (3GA-494) reduces atherosclerotic plaque progression and stabilizes lesions, both in early and established plaques, with reduced macrophage content in established plaques. Within the plaque, different subtypes of macrophages are present. Here, we aimed to investigate whether miR-494-3p directly influences macrophage polarization and activation. Human macrophages were polarized into either proinflammatory M1 or anti-inflammatory M2 macrophages, and simultaneously treated with 3GA-494 or a control antisense (3GA-ctrl). We show that 3GA-494 treatment inhibited miR-494-3p in M1 macrophages and dampened M1 polarization, while in M2 macrophages, miR-494-3p expression was induced and M2 polarization enhanced. The proinflammatory marker CCR2 was reduced in 3GA-494 treated atherosclerosis-prone mice. Pathway enrichment analysis predicted an overlap between miR-494-3p target genes in macrophage polarization and Wnt signaling. We demonstrate that miR-494-3p regulates expression levels of multiple Wnt signaling components, such as LRP6 and TBL1X. Wnt signaling appears activated upon treatment with 3GA-494, both in cultured M1 macrophages and in plaques of hypercholesterolemic mice. Taken together, 3GA-494 treatment dampened M1 polarization, at least in part via activated Wnt signaling, while M2 polarization was enhanced, which is both favorable in reducing atherosclerotic plaque formation and increasing plaque stability.

Introduction

Atherosclerosis is a chronic inflammatory disease, characterized by formation of lipid-rich plaques in the arterial wall. Vulnerable plaques may eventually rupture and result in a cardiovascular event, such as myocardial infarction or ischemic stroke[1]. Macrophages are cells of the innate immune system that play a central role in atherosclerosis. Circulating monocytes are recruited to the lesion site, where they differentiate into macrophages. Within the plaque, macrophages can polarize in response to signals from cytokines and chemokines, but also from bioactive lipids such as cholesterol and oxidized low-density lipoproteins (LDLs)[2-6].

In vivo, different subtypes of macrophages are present, each performing distinct functions. Historically, polarized macrophages were classified into M1 proinflammatory or M2 anti-inflammatory macrophages. *In vitro*, M1 macrophages polarize in response to interferon-γ IFNγ and lipopolysaccharide (LPS). M1 macrophages are considered to be potent effector cells that prime the immune system for action. Alternatively activated M2 macrophages polarize in response to interleukin (IL)-4 and IL-13. M2 macrophages induce an anti-inflammatory response whereby they counteract activation of the immune system[7-10]. The *in vitro* M1/M2 classification, however, is an oversimplification compared with the *in vivo* situation. Macrophage plasticity is highly dynamic and macrophages continuously adapt to the signals they receive from their environment[3, 9-11].

As macrophages are exposed to diverse stimuli in the plaque, it is unlikely pure M1 and M2 macrophages are present. However, markers for both M1 and M2 macrophages are present in plaques of mouse and human, with the M1 macrophage as the predominant phenotype[12-15]. The M1-like phenotype is associated with a proatherogenic response and located in rupture-prone, unstable regions. The M2-like phenotype is associated with an anti-atherogenic response and located in stable regions and in the surrounding adventitial tissue[4, 16, 17]. Because of their dynamic plasticity and key role in atherosclerosis, macrophages are an attractive therapeutic target to reduce inflammation and resolve atherosclerosis.

Several microRNAs have been described to regulate cellular pathways in macrophages, either by inhibiting or promoting inflammatory responses[18-20]. MicroRNAs are short noncoding RNAs which regulate gene expression at the post-transcriptional level. MicroRNAs facilitate degradation of mRNA or inhibition of protein translation by binding to the 3' untranslated region (UTR) of their target mRNA[21]. Because one microRNA has

multiple target mRNAs, changes in microRNA expression can have major impact on cellular processes, including complex signaling pathways.

A large noncoding RNA cluster located on the long arm of human chromosome 14, the 14q32 cluster (12F1 in mice), encodes more than 50 microRNAs. We have investigated inhibition of single 14q32 microRNAs in different models for vascular remodeling[21-26]. In murine models for intimal hyperplasia and early and advanced atherosclerosis, inhibition of 14q32 microRNAs, miR-494-3p in particular, resulted in smaller lesions with increased stability[23, 25, 26]. In both intimal hyperplasia and in advanced atherosclerosis, lesions contained fewer macrophages after miR-494-3p inhibition[23, 26]. Also, downregulation of miR-494-3p, resulted in upregulation of miR-494-3p targets, such as IL-33, metalloproteinase inhibitor 3 (TIMP3), and transforming growth factor beta 2 (TGFB2), in the carotid artery[25]. In addition, proatherogenic Ly6C^{hi} monocytes in the circulation were reduced when miR-494-3p was inhibited[26]. Based on these results, we hypothesized that miR-494-3p directly influences macrophage polarization and activation.

Here, we aimed to investigate whether miR-494-3p directly influences macrophage polarization in atherosclerosis. We show that endogenous miR-494-3p expression is regulated during macrophage polarization *in vitro*. Also, miR-494-3p regulates mRNA and protein levels of key polarization markers in macrophages. Inhibition of miR-494-3p reduces the proinflammatory response in macrophages *in vitro* and reduces the proinflammatory marker CCR2 in atherosclerotic plaques *in vivo*. Pathway enrichment analysis predicted that miR-494-3p has more than 70 targets involved in macrophage polarization, with most of these involved in Wnt signaling. We confirmed that miR-494-3p targets components of the Wnt signaling pathway and that treatment with 3rd Generation Antisense against miR-494-3p (3GA-494) activates Wnt signaling in cultured M1 macrophages. Also, in plaques of atherosclerotic mice, Wnt signaling appeared activated in response to 3GA-494 treatment.

Results

MiR-494-3p expression is regulated during macrophage polarization

To study miR-494-3p inhibition in different macrophage subsets, we utilized *in vitro* polarized macrophages, isolated and differentiated from different individual human blood donors or from murine bone marrow, with either LPS/IFNγ for M1 or IL-4/IL-13 for M2 polarization. Macrophages polarized toward M1 showed decreased miR-494-3p expression compared with M0 macrophages (P=0.02). In contrast, macrophages polarized toward M2 showed a trend toward increased miR-494-3p expression compared with M0 (P=0.1; Figure 1A). Treatment with microRNA inhibitor 3GA-494 decreased miR-494-3p expression in M0 and M1 macrophages compared with 3GA-ctrl (P=0.01 and P=0.003, respectively), as expected. In contrast, in M2 macrophages, miR-494-3p expression appeared upregulated after 24 hours treatment with 3GA-494 (P=0.06; Figure 1B). We have shown previously that expression of miR-494-3p upregulates in specific cell types and even whole tissues after treatment with 3GA-494[26], likely via an autoregulatory mechanism. 3GA-494 treated M2 macrophages also increased miR-494-3p secretion via extracellular vesicles (EVs; P=0.01), whereas in EVs from M0 and M1 macrophages, no differences were observed in miR-494-3p secretion between 3GA-ctrl and 3GA-494. Except for a general increased secretion by M1 macrophages treated with 3GA-494, for both miR-494-3p and U6 (P=0.1 and P=0.03, respectively; Supplemental Figure 1A-C). Expression patterns of miR-494-3p in murine macrophages treated with 3GA-494, were not as clear as in human macrophages, but showed a similar trend in 2 out of 3 mice (Supplemental Figure 1D). To confirm uptake of 3GAs by macrophages, we treated M0 macrophages with fluorescently-labeled 3GA-494 (Figure 1C) and observed a strong fluorescent signal in the cytoplasm, as expected.

MiR-494-3p regulates mRNA levels of key macrophage polarization markers

M1 and M2 polarization states are defined by expression of specific surface markers and secretory patterns[2-4]. To confirm whether our polarization strategy by LPS/IFNγ or IL-4/IL-13 was successful, we measured expression levels of key polarization markers. In human macrophages, treatment with LPS/IFNγ resulted in upregulated expression of M1 markers cluster of receptors differentiation 80 (CD80; 3GA-ctrl P=0.04 and 3GA-494 P=0.003), CD86

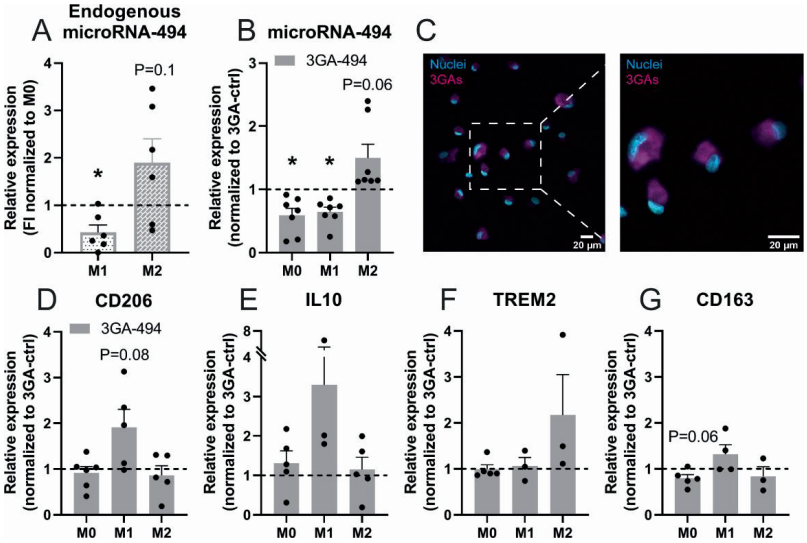

Figure 1. Expression of miR-494-3p and key polarization markers in human macrophages treated with 3GA-494 or 3GA-ctrl. (A) Endogenous miR-494-3p expression in primary human macrophages during M1 and M2 polarization, shown as fold increase (FI) normalized to miR-494-3p expression in M0 macrophages for each donor. (B) MiR-494-3p expression in resting M0 and M1 and M2 polarized macrophages treated with 3GA-494, normalized to 3GA-ctrl treated M0, M1 and M2 macrophages, respectively. (C) M0 macrophages treated with IRDye-800-CW-labeled 3GA-494 for 24 hours. Right image is a zoom-in image of the left image. Scale bar is 20 µm. (D) Expression levels of M2 markers cluster of receptors differentiation 206 (CD206), (E) interleukin 10 (IL10), triggering receptor on myeloid cells 2 (TREM2) and (G) receptor for hemoglobin-haptoglobin complexes CD163 (N=5). (D-G) Expression levels were normalized to 3GA-ctrl. U6 was used as a reference gene. A one-sample t-test was performed to compare single treatment with the control, within each individual donor. N is represented by the individual dots. Variations in N are caused by the exclusion criteria, as explained in the material and methods. Data are represented as mean ±SEM. *P<0.05, compared with M0 (A) 3GA-ctrl (B-D).

(3GA-ctrl P=0.02 and 3GA-494 P=0.02), chemokine ligand 9 (CXCL9; 3GA-ctrl P=0.03 and 3GA-494 P=0.04; Supplemental Figure 2A-C). In murine macrophages, expression of inducible oxide synthase (iNOS) appeared increased in M1 polarization (3GA-ctrl P=0.1 and 3GA-494 P=0.08), compared with M0 macrophages (Supplemental Figure 1E). Treatment with IL-4/IL-13 resulted in a trend toward increased expression of M2 marker mannose receptor CD206, anti-inflammatory cytokine, in human macrophages compared with M0 (3GA-ctrl P=0.1 and 3GA-494 P=0.09; Supplemental Figure 2E). IL-10 did not show differences compared with M0 in both groups and triggering receptor on myeloid cells 2 (TREM-2) only showed increased expression in 3GA-494 treated human macrophages compared with M0 (3GA-494 P=0.02); Supplemental Figure 2F and G). In murine macrophages CD206 expression increased in response to IL-4/IL-13 treatment (3GA-ctrl P=0.003 and 3GA-494 P=0.0004 Supplemental Figure 1F).

Next, we investigated how altered miR-494-3p expression affects mRNA levels of key polarization markers in both M1 and M2 macrophage subsets in human macrophages. Expression levels of M1 markers were not different between 3GA-ctrl and 3GA-494 M1 treated macrophages, except for cytokine interleukin 1-β (IL-1β), which showed a trend toward upregulation in 3GA-494 (P=0.09; Supplemental Figure 2A-E). However, expression of the M2 marker CD206 appeared increased in 3GA-494 M1 macrophages, compared with 3GA-ctrl (P=0.08; Figure 1D). Expression levels in M0 macrophages were not different between 3GA-494 and 3GA-ctrl, except for CD163, a receptor for hemoglobin-haptoglobin complexes, which showed a trend toward reduced expression in 3GA-494 M0 macrophages compared with 3GA-ctrl (P=0.06; Figure 1G and Supplemental Figure 2H).

3GA-494 treatment reduces proinflammatory macrophage polarization *in vitro* and *in vivo*

Since macrophage M1 and M2 polarization states are defined by the presence of specific intracellular and surface proteins[2-4], we performed flow cytometric analysis to further

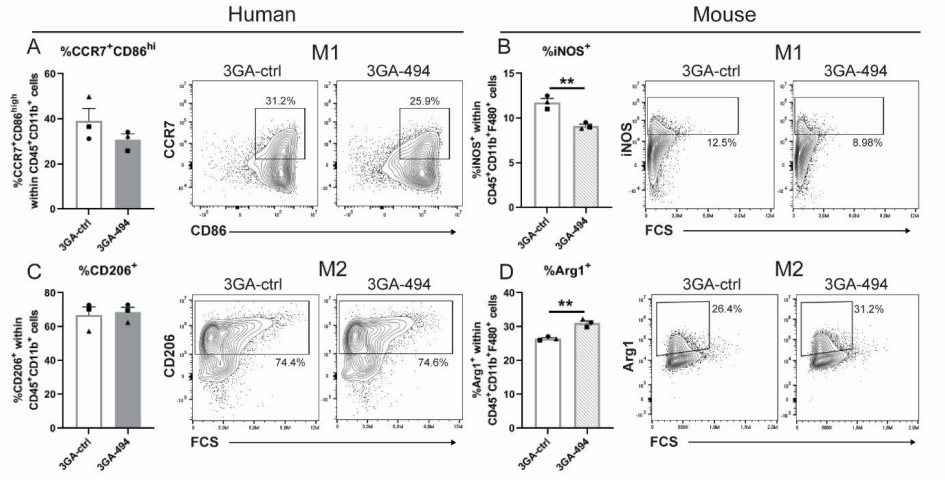

Figure 2. Flow cytometric analysis of human and murine polarized macrophages treated with 3GA-494 or 3GA-ctrl. Protein levels of M1 and M2 markers in human and murine *in vitro* polarized macrophages, treated with 3GA-494 or 3GA-ctrl for 24 hours during polarization, analyzed by flow cytometric analysis. Percentage of M1 markers (A) C-C chemokine receptor 7 (CCR7) and cluster of differentiation 86 (CD86) positive cells in human M1 macrophages. (B) Percentage of M1 marker inducible oxide synthase (iNOS) positive cells in murine M1 macrophages. (C) Percentage of M2 marker CD206 positive cells in human M2 macrophages. (D) Percentage of M2 marker Arginase-1 (Arg1) positive cells in murine M2 macrophages. (A-D) Percentage (%) of positive cells, within alive (A and C) $CD45^+CD11b^+$ or (B and D) $CD11b^+F4/80^+$ cells, in 3GA-ctrl or 3GA-494 treated cells. Representative plots of both groups are shown. N is represented by the individual symbols. A two-tailed unpaired t-test was performed to compare single treatment with the control. Data are represented as mean ±SEM. **P<0.01 compared with 3GA-ctrl.

determine the effects of 3GA-494 treatment during M1 and M2 polarization. Expression of M1 markers C-C chemokine receptor 7 (CCR7) and CD86 and M2 marker CD206 was increased in M1 and M2 macrophages compared with M0, respectively, and confirmed polarization in human cells (P=0.001 and P=0.005, respectively; Supplemental Figure 3A and 3B). In murine cells, intracellular expression of M1 marker iNOS and M2 marker Arginase-1 (Arg1) was increased in M1 and M2 macrophages compared with M0, respectively, and confirmed polarization in M1 and M2 subsets (P<0.0001; Supplemental Figure 3C and 3D).
Even though we did see differences on mRNA levels, we did not see differences between 3GA-494 and 3GA-ctrl in percentage of positive CCR7 and CD86 cells, CD206 cells nor in the mean fluorescent intensity (MFI) per cell in human macrophages, possibly due to inter-donor variability (Figure 2A and C, Supplemental Figure 3E-G). In murine M1 macrophages however, percentage of iNOS positive cells was significantly decreased in 3GA-494, compared with 3GA-ctrl (P=0.005; Figure 2B). In murine M2 macrophages, the percentage of Arg1 expressing cells was increased in 3GA-494 compared with 3GA-ctrl (P=0.003; Figure 2D). The MFIs of iNOS and Arg1 were not different between groups (Supplemental Figure 3H-I). 3GA-494 treatment thus attenuated M1 polarization in response to LPS/IFNγ stimulation and further increased M2 polarization in response to IL-4/IL-13, leading to an overall decrease in proinflammatory activity, in murine macrophages. To confirm these findings *in vivo*, we stained for the proinflammatory M1 marker C-C motif chemokine receptor-2 (CCR2) in carotid artery plaques of hypercholesterolemic $ApoE^{-/-}$ mice treated with 3GA-494 or 3GA-ctrl, as described previously[25]. CCR2 intensity, quantified in the plaque area, appeared decreased in 3GA-494 treated mice compared with 3GA-ctrl mice (P=0.06; Figure 3). This indicates that, in addition to the reduction in total plaque macrophages that we showed previously[23, 26], the proinflammatory activity of intraplaque macrophages may be reduced, also *in vivo*.

MiR-494-3p targets the Wnt signaling pathway

To study the underlying mechanisms of miR-494-3p in macrophage polarization, we performed pathway enrichment analysis on a set of putative miR-494-3p targets, as predicted by Targetscan.org (v7.2) and a set of genes involved in M1 and M2 polarization, extracted from publicly available RNA sequencing data[27]. We found that 70 genes overlapped between both gene sets. The top ten of pathways containing most assigned genes is shown in Figure 4A and B. Out of ten pathways, eight overlapped between the two gene sets. Most putative miR-494-3p targets were assigned to the Wnt signaling pathway (16%; 17 genes in total, Figure 4A). Of the genes involved in macrophage polarization, 41 genes (13.3%) were also assigned to the Wnt signaling pathway (Figure 4B). Indeed, genes

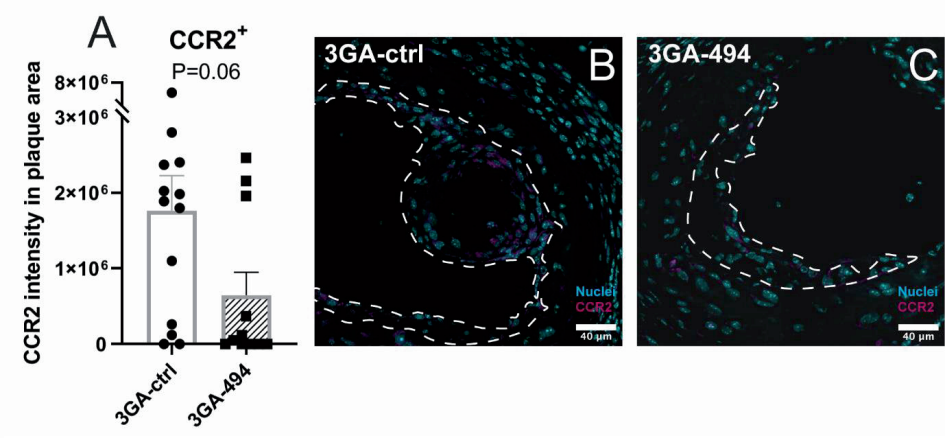

Figure 3. Proinflammatory marker CCR2 in carotid artery plaques of 3GA-494 or 3GA-ctrl treated ApoE$^{-/-}$ mice. Immunofluorescence staining of proinflammatory marker C-C motif chemokine receptor-2 (CCR2). (A) Quantifications of CCR2 intensity in the plaque area (N=13 and N=11 in 3GA-ctrl and 3GA-494, respectively). Representative cross sections of the carotid artery of mice treated with (B) 3GA-ctrl or (C) 3GA-494. Sections are stained with CCR2 (magenta) and Hoechst for nuclei (blue). Scale bar is 40 µm. Plaques are outlined with a dashed line. A two-tailed unpaired t-test was performed to compare single treatment with the control. Data are represented as mean ±SEM.

that were both putative miR-494-3p targets and components in the Wnt signaling pathway showed distinct expression patterns in each macrophage subset (Figure 4C-H). Expression of Frizzled class receptor 2 (FZD2) and LDL receptor related protein 6 (LRP6), both Wnt receptors, were significantly downregulated in 3GA-494 treated M2 macrophages compared with 3GA-ctrl (P=0.02 and P=0.007, respectively; Figure 4C and 4D). Activin A receptor type 1C (ACVR1C), was upregulated in 3GA-494 treated M1 macrophages (P=0.03; Figure 4E). During canonical Wnt activation, a β-catenin/TCF complex is formed and translocated in the nucleus to induce transcription[28]. Pygopus homolog 1 (PYGO1), transducing β-like 1 X-linked (TBL1X) and transcription factor 7 like 2 (TCF7L2) are all part of the β-catenin/TCF complex[29-31]. Inhibition of miR-494-3p significantly downregulated PYGO1 in M0 macrophages (P=0.008; Figure 4F). TBL1X and TCF7L2 were upregulated, significantly or a trend, (P=0.05; Figure 4G and P=0.1; Figure 4H, respectively) in 3GA-494 M1 macrophages compared with 3GA-ctrl. Overall, 3GA-494 treatment resulted in increased target gene expression in M1 macrophages and decreased target gene expression in M2 macrophages, in accordance with the observed 3GA-494 induced miR-494-3p downregulation in M1 and miR-494-3p upregulation in M2 macrophages.

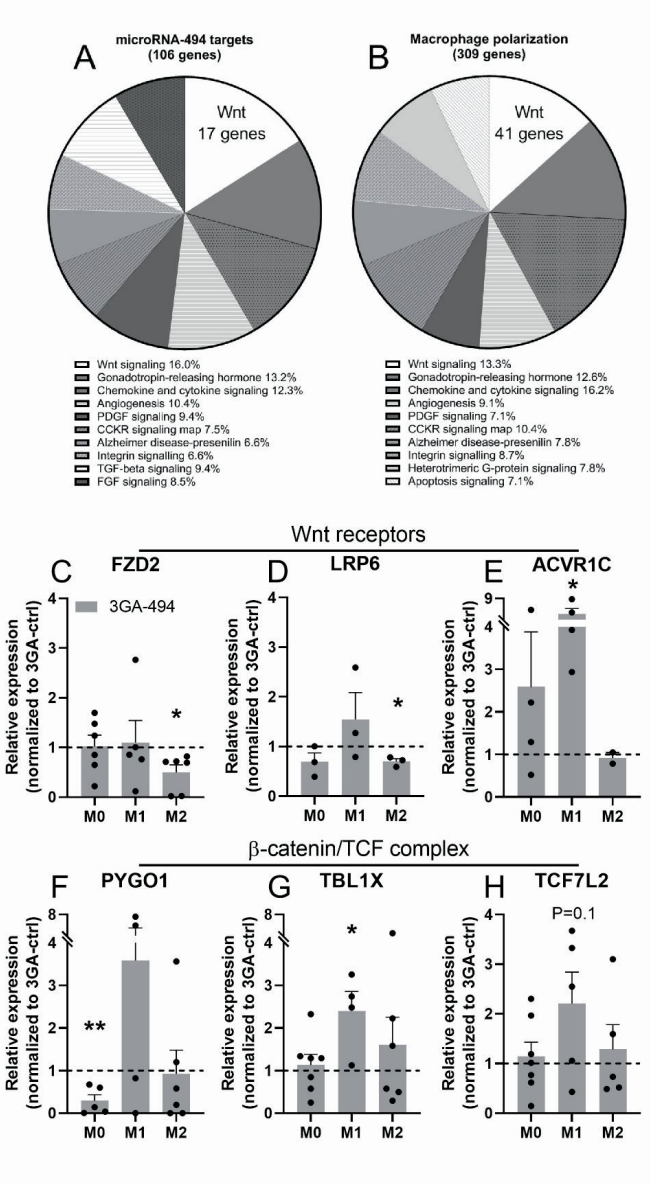

Figure 4. Pathway analysis and putative miR-494-3p target gene expression in the Wnt signaling pathway. (A) A set of putative miR-494-3p targets and (B) genes from transcriptome analysis of M1 and M2 polarized macrophages, were used in a pathway enrichment analysis. Top ten of pathways with most assigned genes are shown. Each part of the pie chart is represented as a percentage of the total genes in the top ten pathways. (C-H) Relative expression of genes, which are both putative miR-494-3p targets and components in the Wnt signaling pathway, in resting human M0, and polarized M1 and M2 macrophages, treated with 3GA-494 (N=5) or 3GA-ctrl (N=5). Wnt receptors, (C) Frizzled class receptor 2 (FZD2) (D) LDL receptor related protein 6 (LRP6) and (E) Activin A receptor type 1C (ACVR1C), and β-catenin/TCF complex genes, (F) Pygopus homolog 1 (PYGO1), (G) transducing β-like

1 X-linked (TBL1X) and (H) transcription factor 7 like 2 (TCF7L2), in 3GA-494 treated macrophages compared with 3GA-ctrl. Expression levels were normalized to 3GA-ctrl. U6 was used as a reference gene. A one-sample t-test was performed to compare single treatment with the control, within each individual donor. N is represented by the individual dots. Variations in N are caused by the exclusion criteria, as explained in the material and methods. Data are represented as mean ±SEM. *P<0.05, **P<0.01, compared with 3GA-ctrl.

MiR-494-3p inhibition activates Wnt signaling in M1 macrophages

We hypothesized that 3GA-494 treatment activates Wnt signaling in M1 macrophages and inhibits Wnt signaling in M0 and M2 macrophages. In canonical Wnt signaling, non-phosphorylated (non-phospho) β-catenin is translocated into the nucleus, where it forms a complex with TCF and induces transcription of downstream Wnt targets[28]. Therefore, we also measured β-catenin and downstream Wnt targets, even though they were not direct targets of miR-494-3p, both by immunohistochemistry and by RT/qPCR. The amount of non-phosho β-catenin appeared increased (P=0.06), in human M1 macrophages treated with 3GA-494, compared with 3GA-ctrl (Figure 5A-C). In addition, gene expression levels of β-catenin and two downstream transcription targets, signal of transducer and activator of transcription 3 (STAT3) and cyclin D1 (CCND1), showed a trend toward or a significant upregulation in 3GA-494 treated M1 macrophages (P=0.07, P=0.1 and P=0.02, respectively; Figure 5D-F). This shows that the canonical Wnt signaling pathway was indeed activated upon miR-494-3p inhibition.

We did not observe effects on downstream Wnt activation by 3GA-494 in M0 or M2 macrophages, with the exception of STAT3, which was downregulated in M0 macrophages compared with 3GA-ctrl (P=0.05; Supplemental Figure 4), indicating that miR-494-3p acts in a cell-type specific manner.

3GA-494 treatment activates Wnt signaling *in vivo*

To evaluate whether 3GA-494 treatment also leads to increased Wnt signaling in macrophages *in vivo*, we performed non-phospho β-catenin staining on plaques of ApoE$^{-/-}$ mice treated with 3GA-ctrl or 3GA-494. We noticed that, particularly in 3GA-494 treated mice, non-phospho β-catenin was present in, what are most likely, endothelial cells lining the plaque (Figure 6C). Because our focus was on Wnt signaling in macrophages, we excluded the endothelial layer from the quantification. Some plaques from 3GA-494 treated mice were too small[25] to perform quantification after exclusion of the endothelial layer and these were excluded from the analysis completely. Mice treated with 3GA-494 showed a trend toward increased intra-plaque non-phospho β-catenin expression compared with

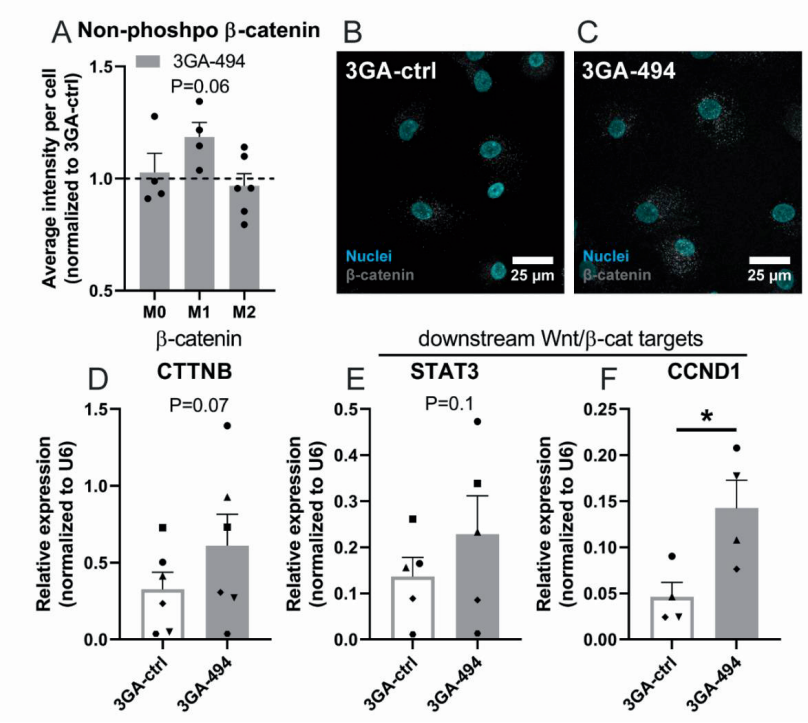

Figure 5. Active β-catenin and downstream Wnt target genes in human macrophages treated with 3GA-494 or 3GA-ctrl. M0 and polarized M1 and M2 macrophages, treated with 3GA-494 or 3GA-ctrl, were stained with an antibody against the non-phosphorylated (non-phospho) form of β-catenin, the functionally active form in the canonical Wnt signaling. (A) Quantifications of the average non-phosho β-catenin intensity per cell. Representative images of M1 macrophages treated with (B) 3GA-ctrl or (C) 3GA-494. Non-phosho β-catenin is shown in gray and nuclei are stained with Hoechst, shown in blue. Relative expression of (D) β-catenin and two downstream Wnt transcription targets, (E) signal of transducer and activator of transcription 3 (STAT3) and (F) cyclin D1 (CCND1) in 3GA-ctrl or 3GA-494 M1 macrophages. U6 was used as a reference gene. A ratio paired t-test was performed to compare single treatment with the control, within each individual donor. N is represented by the individual dots. Variations in N are caused by the exclusion criteria, as explained in the material and methods. Data are represented as mean ±SEM. *P<0.05, compared with 3GA-ctrl.

3GA-ctrl mice (P=0.1; Figure 6), indicating that macrophage Wnt signaling also appears activated *in vivo,* in response to 3GA-494 treatment.

In addition, we also stained for miR-494-3p, CD68 as macrophage marker and non-phospho β-catenin in human middle cerebral arteries from either a healthy, mildly atherosclerotic or severely atherosclerotic sections. Although this is purely anecdotal, non-phospho β-catenin and CD68 expression co-localized and expression of miR-494-3p increased in more advanced lesions (Supplemental Figure 5).

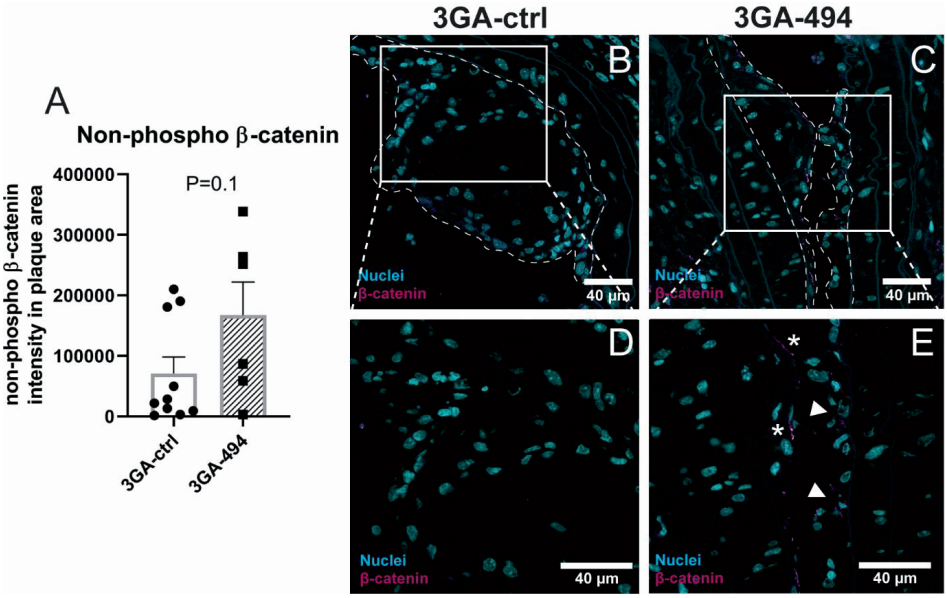

Figure 6. Active β-catenin in carotid artery plaques of 3GA-494 or 3GA-ctrl treated ApoE$^{-/-}$ mice. Immunofluorescence staining of non-phosphorylated (non-phospho) β-catenin. (A) Quantification of non-phospho β-catenin intensity in the plaque area. Representative cross sections of the carotid artery of mice treated with (B) 3GA-ctrl (N=10) or (C) 3GA-494 (N=6). Zoom-in images of (D) 3GA-ctrl and (E) 3GA-494 treated mice. Asterisks point at non-phospho β-catenin positive endothelial cells, which were excluded from the quantification analysis. Arrows point at non-phospho β-catenin positive cells in the plaque area of a 3GA-494 treated mouse, which were included in the analysis. Non-phospho β-catenin is shown in magenta and Hoechst for nuclei in blue. Scale bar is 40 µm. Plaques are outlined with a dashed line. A two-tailed unpaired t-test was performed to compare single treatment with the control. Data are represented as mean ±SEM.

Discussion

In this study, we show that endogenous miR-494-3p expression is regulated during macrophage polarization and that miR-494-3p regulates mRNA and protein levels of key polarization markers in macrophages. Furthermore, inhibition of miR-494-3p reduced the proinflammatory response in cultured macrophages *in vitro* and the proinflammatory marker CCR2 appeared reduced in atherosclerotic plaques *in vivo*. Finally, we show that miR-494-3p targets components of the Wnt signaling pathway and 3GA-494 treatment leads to activated Wnt signaling in cultured M1 macrophages as well as an apparent activation in plaques of atherosclerotic mice.

Our data show that miR-494-3p has a distinct role in each macrophage subtype, which becomes even more apparent upon treatment with 3GA-494. Both the increase in expression levels of anti-inflammatory receptors and cytokines, and the reduction of M1 markers in M1 macrophages, suggests that M1 polarization shifted toward a less inflammatory phenotype in response to miR-494-3p inhibition. This is consistent with the seemingly upregulated expression of STAT3, which suppresses immune responses in macrophages[32]. M2 polarization was further promoted by 3GA-494 treatment, as the anti-inflammatory marker TREM2 and, in murine macrophages, expression of the M2 marker Arg1 were further increased. Dampening M1 polarization, while enhancing M2 polarization, is both favorable in reducing inflammation and atherogenesis. Indeed, the proinflammatory marker CCR2 appeared reduced in proatherogenic mice treated with 3GA-494 compared with 3GA-ctrl mice. We have demonstrated previously that plaque size decreased and plaque stability increased correspondingly upon 3GA-494 treatment[25, 26]. Likely, the subtle shift in macrophage polarization from proinflammatory toward anti-inflammatory contributed to this clinically advantageous phenotype.

We used primary human macrophages, differentiated from peripheral blood mononuclear cells (PBMCs), to more closely translate our results to a human clinical setting. Biological differences between donors, however, led to greater variations in the response to 3GA-494 treatment than in murine macrophages, isolated and differentiated from mice with the same genetic background. Flow cytometric analysis showed clear differences in polarization in response to 3GA-494 in murine macrophages, with decreased M1 iNOS and increased M2 Arg1 expression in M1 and M2 macrophages, respectively. Although, human macrophages followed a similar pattern, the effects on polarization markers were more variable.

M2 polarization induced endogenous miR-494-3p expression, which was even further induced in response 3GA-494 treatment. We have previously shown that miR-494-3p expression increased unexpectedly in response to treatment with the miR-494-3p inhibitor 3GA-494 in certain cell types and tissues, likely via autoregulatory mechanisms[26]. In this study, we found that this phenomenon is even specific for differentially polarized subsets of the same cell type. MiRNA processing can be regulated by RNA binding proteins, which in turn are regulated by microRNAs themselves. Previously, we have demonstrated that the RNA binding protein Mef2A directly binds to pri-miR-494-3p, for example[24]. However, which precise mechanism underlies the miR-494-3p autoregulation in M2 macrophages, remains to be determined.

Pathway enrichment analysis predicted that eight out of the top ten pathways overlapped between a set of 106 putative miR-494-3p target genes and a set of 309 genes directly involved in macrophage polarization. As we observed the greatest overlap in the Wnt signaling pathway, we focused on canonical Wnt signaling, but of course it is likely that other pathways, including chemokine and cytokine signaling, also play important roles in shaping macrophage phenotypes under the influence of miR-494-3p.

We demonstrate here that miR-494-3p targets mRNA levels of multiple components in the Wnt signaling pathway, all upstream of gene transcription induced by the β-catenin/TCF complex. MicroRNAs downregulate the expression of their target genes, which is consistent with our observations for miR-494-3p in M1 versus M2 macrophages. In M1 macrophages, where miR-494-3p expression is downregulated in response to 3GA-494, Wnt components were upregulated. In contrast, in M2 macrophages, where miR-494-3p is upregulated in response to 3GA-494, Wnt components were downregulated. It is noteworthy that different Wnt components appeared to be targeted by miR-494-3p in the two different macrophage subtypes. MicroRNAs have cell type-specific target genes[33], which may help explain the distinct effects of 3GA-494 treatment on macrophage polarization within the two subtypes.
The Wnt signaling pathway has received little attention in the field of atherosclerosis so far, and is mostly known from cell development and differentiation, and its role in diseases such as cancer[28]. However, some studies suggest that Wnt signaling has a protective role against atherosclerosis[34-37]. The Wnt signaling pathway in macrophages has been described to be important for phagocytosis, clearance of LDLs and foam cell formation and, thus, may have a role in limiting cholesterol accumulation in atherosclerosis[36, 38-40]. WNT5A and LRP6 are both Wnt components that play a role in cholesterol metabolism[39, 40], and are both putative targets of miR-494-3p. WNT5A expression levels did not respond to 3GA-494 treatment

(Supplemental Figure 2), but expression of LRP6 was significantly decreased in 3GA-494 treated M2 macrophages. Another putative miR-494-3p target, involved in cholesterol synthesis, is 3-Hydroxy-3-methylglutaryl-coenzyme A (CoA) synthase 1 (HMGCS1). HMGCS1 showed differential expression, in three out of four human donors, in both M1 and M2 macrophages (Supplemental Figure 2). Finally, although not a direct target of miR-494-3p, TREM2, a marker for anti-inflammatory foamy lipid-laden macrophages involved in cholesterol metabolism, was increased in M2 macrophages in response to 3GA-494[41, 42]. These data suggest that miR-494-3p targets cholesterol metabolism, which corresponds to our findings in previous studies. For example, we have shown that in *in vitro* 3GA-494 treated macrophages, high density lipoprotein (HDL)-mediated efflux was increased compared with 3GA-ctrl treated macrophages[25]. Additionally, necrotic core sizes and plasma cholesterol levels in hypercholesterolemic mice treated with 3GA-494, were significantly reduced compared with 3GA-ctrl-treated mice[25, 26]. Precisely how the differential expression of Wnt targets in either macrophage subtype leads to altered cholesterol metabolism, remains to be determined.

A surprising observation in this study was the apparent increase in non-phospho β-catenin staining in the endothelium lining the carotid artery plaques in mice treated with 3GA-494. Although we did not look into this in detail, endothelial β-catenin has been reported to, via activation of Wnt signaling, to sustain endothelial integrity in atherosclerosis[43]. Also, enforced expression of endothelial β-catenin reduces leakage of the blood-brain barrier[44]. The apparently enhanced expression of endothelial β-catenin in 3GA-494 treated mice may indicate an improved endothelial barrier function, which would limit the development and progression of atherosclerosis even further.

It is a strength of this study that we were able to confirm the effects of 3GA-494 treatment in both murine and in human primary macrophages and that we could link these effects to Wnt signaling for the first time, again in both mice and in humans. To date however, it remains technically challenging to direct 3GA-494 treatment to specific cell types or subsets. MiR-494-3p, for example, clearly has a distinct effect in the different macrophage subsets. This technical restriction has important implications for the potential future use of therapeutics that target miR-494-3p, but also microRNAs in general, as different effects in different tissues, cell types and even cell subsets will have to be taken into account.

Taken together, 3GA-494 treatment inhibits miR-494-3p expression in M1 macrophages and dampens M1 polarization. Simultaneously, 3GA-494 treatment induces miR-494-3p

expression and enhances M2 polarization, which is favorable in both reducing atherosclerotic plaque formation and increasing plaque stability. Furthermore, inhibition of miR-494-3p reduces a proinflammatory response in M1 macrophages, at least in part via activated Wnt signaling. 3GA-494 could therefore be a potential therapeutic agent for stabilizing vulnerable lesions and reducing the risk of a cardiovascular event, such as myocardial infarction or ischemic stroke.

Material and methods

3rd Generation Antisense

3rd Generation Antisense (3GAs) were designed with perfect reverse complementary to the mature target microRNA sequence and synthesized by Idera Pharmaceuticals (Cambridge, MA, USA). The same sequences of 3GAs (formerly named Gene Silencing Oligonucleotides; GSOs) against miR-494 and a scrambled sequence control (3GA-ctrl) were used as described previously[22-26]. For *in vitro* experiments 3GAs were used at a concentration of 5 µg/ml medium. For *in vivo* experiments, a single dose of 1 mg/mouse in PBS was used.

Isolation and differentiation of human macrophages

Blood was obtained from healthy volunteers according to recommendations of the medical ethical board of the Leiden University Medical Center and the Medical University of Vienna. All donors gave informed consent. PBMCs were isolated from whole blood using density gradient medium Lymphoprep (Stem Cell Technologies, Vancouver, Canada, 07581). CD14 positive cells ($CD14^+$) were purified from the PBMCs using $CD14^+$ Microbeads (MACS, Miltenyi Biotec, Bergisch Gladbach, Germany, 130-050-201). $CD14^+$ cells were plated in 100 mm petridishes and cultured in RPMI containing L-glutamine (Gibco, Thermo Fisher, MA, USA, 11875093) supplemented with 25% heat-inactivated fetal calf serum (FCSi), 1% penicillin streptomycin (P/S; Lonza, Basel, Switzerland, DE17-602E) and 100 ng/mL mouse recombinant macrophage colony-stimulating factor (M-CSF; Peprotech, London, UK, 300-25). Medium was refreshed after five days. Ten days after isolation, differentiated resting macrophages (M0 macrophages) were washed with PBS and subsequently, RPMI with all other reagents described above supplemented with 100 ng/mL IFNγ (Peprotech, 300-02) and 100 ng/mL LPS for proinflammatory M1 and 20 ng/mL IL-4 (Peprotech, 400-04) and 20 ng/mL IL13 (Peprotech, 200-13) for anti-inflammatory M2 macrophages, were added for 24 hours, as described previously[7]. During M1 and M2 polarization, 3GA-494 or 3GA-ctrl at a concentration of 5 µg/ml medium was added to the media. M0 macrophages, without polarization cytokines added to the medium, were treated with 3GA-494 or 3GA-ctrl for 24 hours after differentiation with M-CSF. Accutase was used to detach the cells (BD Biosciences, NJ, USA, 561527). Thereafter, cells were harvested and used for further analysis.

The macrophages from two donors did not respond to our polarization strategy and were excluded from all analyses. Due to low RNA yields in some (subsets) of the donors, mRNA levels appeared below the detection limit for some targets. Only donors that showed

expression in both 3GA-ctrl and 3GA-494 treated macrophages, were included in the analyses.

Isolation and differentiation of mouse macrophages

Bone marrow cells were isolated from femurs and tibias of C57Bl/6 mice. After dissection, the bone marrow was flushed with PBS. Cells were filtered through a 70 µm cell strainer, centrifuged at 1200 rpm for 10 min and washed with PBS. The cell pellet was resuspended in Ammonium-Chloride-Potassium lysis buffer (Gibco, Thermo Fisher Scientific, MA, USA A1049201) and incubated on ice to lyse red blood cells. Subsequently, cells were centrifuged at 1200 rpm for 10 minutes and washed twice with PBS. Cells were plated in a 100 mm petri dish (Falcon, Corning, NY, USA, 353003) at a concentration of $8x10^6$ cells per dish. Cells were cultured in RPMI 1640 medium containing L-glutamine, supplemented with 25% FCSi and 1% P/S in a humidified incubator at 37ºC. To obtain bone marrow derived macrophages, cells were stimulated for 7 to 10 days with mouse recombinant macrophage colony stimulating factor (M-CSF; Peprotech, 315-02). Polarization conditions and 3GA treatments were the same as for human macrophages, but with murine cytokines IFNγ (Peprotech, 315-05), IL-4 (Peprotech, 214-04) and IL-13 (Peprotech, 210-13).

Mice and experimental design

All animal experiments were performed in compliance with the Dutch government guidelines and the Directive 2010/63/EU of the European Parliament. As described previously[25], male ApoE-/- mice, obtained from the local animal breeding facility (Gorlaeus Laboratories, Leiden University, Leiden, the Netherlands), were fed a Western type diet (WTD) for six weeks. Two weeks after start of WTD, semi-constrictive collars were placed around both left and right carotid arteries to induce carotid artery plaque formation. At four and 18 days after surgery, mice received an intravenous injection via the tail vein of 1 mg/mouse and 0,5 mg/mouse (in 200 µl PBS), respectively, of 3GA-494 or 3GA-ctrl. Four weeks after surgery, mice were sacrificed and carotid arteries were harvested for further analysis.

RNA isolation and RT/qPCR

Total RNA was isolated by standard TRIzol (ThermoFisher, 15596026) chloroform extraction. RNA concentration and purity were measured on the Nanodrop (Nanodrop® Technologies). For microRNAs, microRNA specific Taqman qPRC kits (ThermoFisher, 4427975) were used for reverse transcription and quantification by qPCR according to the manufacturers protocol. For mRNA, RNA was reverse transcribed using 'high-capacity RNA to cDNA' kit

(ThermoFisher, 4388950). SybrGreen reagents (Qiagen Benelux, Venlo, the Netherlands, 204145) were used for the qPCR. The data was normalized using a stably expressed endogenous control. U6 was used in human cells. In murine cells, miR-191 was used for microRNA normalization and Gapdh and ribosomal protein S18 for mRNAs. qPCR was performed on the VIIa7 (Applied Biosystems). A list of all primers used is shown in Table 1.

Extracellular vesicles

Media from 3GA-treated and simultaneously polarized macrophages was collected after 24 hours of incubation and ultracentrifuged at 17.500g for 70 minutes to enrich for EVs (Beckman Coulter Optima XE-90 Ultracentrifuge). The lowest fraction containing most EVs, was used for total RNA isolation using TRIzol liquid solution (LS) reagent (Thermo Fisher, 10296028), according to the manufacturers protocol.

3GA uptake

Human macrophages were seeded in chamber slides and treated with IRDye-800CW-labelled 3GA-494 (5 ng/µl; Idera Pharmaceuticals, Cambridge MA, USA) for 24 hours. Afterwards, cells were washed twice with PBS and fixed with 1.5% formaldehyde. Nuclei were stained with Dapi and slides were embedded in ProLong Gold antifade (Invitrogen, Thermo Fisher, P36930). Images were made under a Zeiss LSM700 confocal microscope.

Flow cytometric analysis

In vitro polarized macrophages, treated with 3GA-494 or 3GA-ctrl, were analyzed with flow cytometry to determine macrophage polarization phenotypes. Fc receptors were blocked using TruStain FcX (Biolegend) and an unconjugated anti-CD16/32 antibody (clone 2.4G2, BD Bioscience), for human and murine samples respectively. Living cells were selected using Fixable Viability Dye eFluor 780 (1:2000, eBioscience) and different cell populations were defined using anti-human and anti-mouse fluorochrome-conjugated antibodies. In human macrophages, the number of proinflammatory macrophages ($CCR7^{+}CD86^{hi}$) or anti-inflammatory macrophages ($CD206^{+}$) was quantified and shown as a percentage of positive cells within live $CD45^{+}CD11b^{+}$ cells. For murine macrophages, intracellular iNOS and Arg1 were stained using transcription factor fixation/permeabilization concentrate and diluent solutions (BD Biosciences). The number of proinflammatory macrophages ($iNOS^{+}$) or anti-inflammatory macrophages ($Arg1^{+}$) was quantified and shown as a percentage of positive cells within alive $CD11b^{+}F4/80^{+}$ cells. MFI per cell was also quantified. Flow cytometric analysis was performed on a Cytoflex S (Beckman Coulter) and the acquired data were analyzed using FlowJo software.

Collection of human middle cerebral arteries

Human middle cerebral arteries were collected from obduction material at the Department of Pathology of the Leiden University Medical Center. Collection, storage and processing of the samples were performed in compliance with the Medical Treatment Contracts Act (WBGO, 1995) and the Code of Conduct for Healthy Research using Body Material (Good Practice Code, Dutch Federation of Biomedical Scientific Societies, 2002) and the Dutch Personal Data Protection Act (WBP, 2001). Arterial tissues were fixed in formaldehyde and embedded in paraffin.

Immunofluorescence

For *in vitro* analyses, macrophages were seeded onto gelatin-coated glass coverslips on a 12-well plate. The next day, macrophages were polarized and/or treated with 3GAs. After 24 hours, cells were washed with PBS, fixed with 4% paraformaldehyde and again washed twice with PBS.

Murine tissues were fixed in formalin and embedded in paraffin. For murine *in vivo* analyses, paraffin sections (5 µm thick) of the carotid artery of 3GA-494 or 3GA-ctrl treated mice were used. For both murine and human tissues, sections were dewaxed and antigen retrieval was performed prior to stainings.

For CCR2 staining, directly labeled goat anti-mouse CCR2 AF647 (Biolegend, CA, USA, 150604) was used to stain CCR2 positive cells. Nuclei were stained with Hoechst.

For non-phospho β-catenin staining both in mouse and human, primary non-phospho β-Catenin (Ser33/37/Thr41) (D13A1) Rabbit monoclonal Antibody (Cell Signaling, MA, USA 8814) with secondary Donkey α-Rabbit Alexa Fluor 647 was used. Anti-CD68 (Dako, M0814 – clone name: KP1) with secondary Alexa Fluor 555 DαMouse (Invitrogen, A31570) was used to stain macrophages in human sections. Nuclei in murine sections were stained with oxazole yellow and in human sections with Hoechst.

After staining, slides were embedded in ProLong Gold antifade (Invitrogen, P36930) and images were made under a Zeiss LSM700 confocal microscope. Fiji was used to perform immunofluorescence analysis[45]. For murine *in vivo* sections, the plaque area was selected as the region of interest. Next, the integrated density, which is the sum of values of the pixels in the selected plaque area, was calculated. For *in vitro* analyses, the integrated density was calculated and normalized by the amount of nuclei.

Fluorescence in situ hybridization miR-494-3p

FISH was used for detection of miR-494-3p expression and distribution. A protocol described by Chaudhuri et al. with some modifications was used for FISH of miR-494-3p[46]. Briefly, formalin-fixed paraffin-embedded sections were dewaxed and an antigen retrieval step was performed. Next, sections were fixed in EDC (Sigma Aldrich, E1769) in methylimidazole solution for 1h. After washes with TBS, sections were prehybridized in 1xSSC buffer (Ultrapure SSC 20x, Thermo Fisher, 15557044) for 1h at 37°C. 1 µl of 10 µM miRCURY LNA microRNA detection probes against miR-494-3p or a scrambled sequence control (Qiagen, 339111) was added per 250 µl hybridization buffer and heated at 65°C for 5 min to ensure denaturation. Probes were added to the sections and hybridized overnight at 37°C. After stringency washes at 42°C, sections were incubated in blocking buffer containing 1% bovine serum albumin (BSA; Sigma Aldrich, B4287) and 3% normal goat serum in PBS for 1h. Next, anti-Digoxigenin-AP, Fab fragments (1:100 Roche, 11093274910) together with anti-α-smooth muscle actin (Dako, M0851) were diluted in blocking buffer and incubated on the sections overnight at 4°C. The next day, after 2 washes in TBS, Hoechst and secondary antibody AlexaFluor 555 DαMouse (Invitrogen, A31570) in blocking buffer was added for 1h at room temperature. After 2 washes in TBS, Cy5 from the Cy5-TSA kit (Perkin Elmer, NEL745E001KT) was diluted in the provided buffer (1:100) and incubated on the sections for 10 min. Finally, sections were embedded in ProLong Gold antifade (Invitrogen, P36930). Pictures were made under a Zeiss LSM700 confocal microscope.

Pathway analysis

Two datasets of genes were used in the pathway analysis using PANTHER 16.0. A list of putative miR-494-3p targets, 623 genes in total, was generated using Targetscan.org (v7.2). A list of top differentially expressed genes from RNA sequencing data comparing proinflammatory and anti-inflammatory macrophages, 2200 genes in total, performed by Gerrick et al.[27], was used to select genes involved in macrophage polarization. Of these genes, 275 and 926 of miR-494-3p putative targets and genes in macrophage polarization, respectively, were assigned to a pathway. Next, the top 10 pathways containing most assigned genes, were selected, with in total 106 and 309 genes of miR-494-3p putative targets and macrophage polarization genes, respectively.

Statistical analysis

Results are expressed as mean ± SEM. A two-tailed Student's t-test was used to compare single treatment group with the control group. For data normalized to 3GA-ctrl, a one-

sample t-test was performed. P<0.05 was considered significant. P<0.1 was considered a trend. A Grubbs' test was used to identify significant outliers (α<0.05).

Acknowledgements

We kindly acknowledge Dr. Sjoerd G. van Duinen, Annemieke J. van der Kroft, Julia Mayer, Martijn Willemsen and Pleun Engbers for their technical support.

Funding

The study was supported by funding from the Rembrandt Institute of Cardiovascular Science (E.V.I.) and the Austrian Science Fund (FWF) (A.Y.N., Lise Meitner grant M2578-B30).

Conflicts of Interest

There are no conflicts of interest.

Author Contributions

E.V.I., A.C.F., I.B., P.J.H., P.H.A.Q. and A.Y.N. designed the experiments; E.V.I., A.C.F., T.W., M.L.B., A.D.J, I.B. and A.Y.N. conducted the experiments; E.V.I., A.C.F., I.B., J.W., P.J.H., P.H.A.Q. and A.Y.N. wrote, reviewed and edited the paper; A.Y.N. acquired funding; A.Y.N. and P.H.A.Q. supervised.

References

1. Libby, P., Ridker, P.M., and Hansson, G.K. (2011). Progress and challenges in translating the biology of atherosclerosis. *Nature* **473**: 317-325.
2. Tabas, I., and Bornfeldt, K.E. (2016). Macrophage Phenotype and Function in Different Stages of Atherosclerosis. *Circulation research* **118**: 653-667.
3. Stremmel, C., Stark, K., and Schulz, C. (2019). Heterogeneity of Macrophages in Atherosclerosis. *Thrombosis and haemostasis* **119**: 1237-1246.
4. Stoger, J.L., Gijbels, M.J., van der Velden, S., Manca, M., van der Loos, C.M., Biessen, E.A., Daemen, M.J., Lutgens, E., and de Winther, M.P. (2012). Distribution of macrophage polarization markers in human atherosclerosis. *Atherosclerosis* **225**: 461-468.
5. Adamson, S., and Leitinger, N. (2011). Phenotypic modulation of macrophages in response to plaque lipids. *Current opinion in lipidology* **22**: 335-342.
6. Koelwyn, G.J., Corr, E.M., Erbay, E., and Moore, K.J. (2018). Regulation of macrophage immunometabolism in atherosclerosis. *Nature immunology* **19**: 526-537.
7. Hohensinner, P.J., Baumgartner, J., Kral-Pointner, J.B., Uhrin, P., Ebenbauer, B., Thaler, B., Doberer, K., Stojkovic, S., Demyanets, S., Fischer, M.B.*, et al.* (2017). PAI-1 (Plasminogen Activator Inhibitor-1) Expression Renders Alternatively Activated Human Macrophages Proteolytically Quiescent. *Arteriosclerosis, thrombosis, and vascular biology* **37**: 1913-1922.
8. Murray, P.J., Allen, J.E., Biswas, S.K., Fisher, E.A., Gilroy, D.W., Goerdt, S., Gordon, S., Hamilton, J.A., Ivashkiv, L.B., Lawrence, T.*, et al.* (2014). Macrophage activation and polarization: nomenclature and experimental guidelines. *Immunity* **41**: 14-20.
9. Moore, K.J., Sheedy, F.J., and Fisher, E.A. (2013). Macrophages in atherosclerosis: a dynamic balance. *Nature reviews Immunology* **13**: 709-721.
10. Mantovani, A., Garlanda, C., and Locati, M. (2009). Macrophage diversity and polarization in atherosclerosis: a question of balance. *Arteriosclerosis, thrombosis, and vascular biology* **29**: 1419-1423.
11. Wolfs, I.M., Donners, M.M., and de Winther, M.P. (2011). Differentiation factors and cytokines in the atherosclerotic plaque micro-environment as a trigger for macrophage polarisation. *Thrombosis and haemostasis* **106**: 763-771.
12. Bisgaard, L.S., Mogensen, C.K., Rosendahl, A., Cucak, H., Nielsen, L.B., Rasmussen, S.E., and Pedersen, T.X. (2016). Bone marrow-derived and peritoneal macrophages have different inflammatory response to oxLDL and M1/M2 marker expression - implications for atherosclerosis research. *Scientific reports* **6**: 35234.
13. de Gaetano, M., Crean, D., Barry, M., and Belton, O. (2016). M1- and M2-Type Macrophage Responses Are Predictive of Adverse Outcomes in Human Atherosclerosis. *Frontiers in immunology* **7**: 275.
14. Barrett, T.J. (2020). Macrophages in Atherosclerosis Regression. *Arteriosclerosis, thrombosis, and vascular biology* **40**: 20-33.
15. van Dijk, R.A., Rijs, K., Wezel, A., Hamming, J.F., Kolodgie, F.D., Virmani, R., Schaapherder, A.F., and Lindeman, J.H. (2016). Systematic Evaluation of the Cellular Innate Immune Response During the Process of Human Atherosclerosis. *Journal of the American Heart Association* **5**.
16. Chinetti-Gbaguidi, G., Colin, S., and Staels, B. (2015). Macrophage subsets in atherosclerosis. *Nature reviews Cardiology* **12**: 10-17.
17. Barlis, P., Serruys, P.W., Devries, A., and Regar, E. (2008). Optical coherence tomography assessment of vulnerable plaque rupture: predilection for the plaque 'shoulder'. *European heart journal* **29**: 2023.
18. Canfran-Duque, A., Rotllan, N., Zhang, X., Fernandez-Fuertes, M., Ramirez-Hidalgo, C., Araldi, E., Daimiel, L., Busto, R., Fernandez-Hernando, C., and Suarez, Y. (2017). Macrophage deficiency of miR-21 promotes apoptosis, plaque necrosis, and vascular inflammation during atherogenesis. *EMBO molecular medicine* **9**: 1244-1262.

19. Di Gregoli, K., Mohamad Anuar, N.N., Bianco, R., White, S.J., Newby, A.C., George, S.J., and Johnson, J.L. (2017). MicroRNA-181b Controls Atherosclerosis and Aneurysms Through Regulation of TIMP-3 and Elastin. *Circulation research* **120**: 49-65.
20. Nazari-Jahantigh, M., Wei, Y., Noels, H., Akhtar, S., Zhou, Z., Koenen, R.R., Heyll, K., Gremse, F., Kiessling, F., Grommes, J*., et al.* (2012). MicroRNA-155 promotes atherosclerosis by repressing Bcl6 in macrophages. *The Journal of clinical investigation* **122**: 4190-4202.
21. Welten, S.M., Goossens, E.A., Quax, P.H., and Nossent, A.Y. (2016). The multifactorial nature of microRNAs in vascular remodelling. *Cardiovascular research* **110**: 6-22.
22. Welten, S.M., Bastiaansen, A.J., de Jong, R.C., de Vries, M.R., Peters, E.A., Boonstra, M.C., Sheikh, S.P., La Monica, N., Kandimalla, E.R., Quax, P.H*., et al.* (2014). Inhibition of 14q32 MicroRNAs miR-329, miR-487b, miR-494, and miR-495 increases neovascularization and blood flow recovery after ischemia. *Circulation research* **115**: 696-708.
23. Welten, S.M.J., de Jong, R.C.M., Wezel, A., de Vries, M.R., Boonstra, M.C., Parma, L., Jukema, J.W., van der Sluis, T.C., Arens, R., Bot, I*., et al.* (2017). Inhibition of 14q32 microRNA miR-495 reduces lesion formation, intimal hyperplasia and plasma cholesterol levels in experimental restenosis. *Atherosclerosis* **261**: 26-36.
24. Welten, S.M.J., de Vries, M.R., Peters, E.A.B., Agrawal, S., Quax, P.H.A., and Nossent, A.Y. (2017). Inhibition of Mef2a Enhances Neovascularization via Post-transcriptional Regulation of 14q32 MicroRNAs miR-329 and miR-494. *Molecular therapy Nucleic acids* **7**: 61-70.
25. Wezel, A., Welten, S.M., Razawy, W., Lagraauw, H.M., de Vries, M.R., Goossens, E.A., Boonstra, M.C., Hamming, J.F., Kandimalla, E.R., Kuiper, J*., et al.* (2015). Inhibition of MicroRNA-494 Reduces Carotid Artery Atherosclerotic Lesion Development and Increases Plaque Stability. *Annals of surgery* **262**: 841-847; discussion 847-848.
26. van Ingen, E., Foks, A.C., Kroner, M.J., Kuiper, J., Quax, P.H.A., Bot, I., and Nossent, A.Y. (2019). Antisense Oligonucleotide Inhibition of MicroRNA-494 Halts Atherosclerotic Plaque Progression and Promotes Plaque Stabilization. *Molecular therapy Nucleic acids* **18**: 638-649.
27. Gerrick, K.Y., Gerrick, E.R., Gupta, A., Wheelan, S.J., Yegnasubramanian, S., and Jaffee, E.M. (2018). Transcriptional profiling identifies novel regulators of macrophage polarization. *PloS one* **13**: e0208602.
28. Nusse, R., and Clevers, H. (2017). Wnt/β-Catenin Signaling, Disease, and Emerging Therapeutic Modalities. *Cell* **169**: 985-999.
29. Schwab, K.R., Patterson, L.T., Hartman, H.A., Song, N., Lang, R.A., Lin, X., and Potter, S.S. (2007). Pygo1 and Pygo2 roles in Wnt signaling in mammalian kidney development. *BMC Biol* **5**: 15.
30. Li, J., and Wang, C.Y. (2008). TBL1-TBLR1 and beta-catenin recruit each other to Wnt target-gene promoter for transcription activation and oncogenesis. *Nat Cell Biol* **10**: 160-169.
31. Ip, W., Chiang, Y.T., and Jin, T. (2012). The involvement of the wnt signaling pathway and TCF7L2 in diabetes mellitus: The current understanding, dispute, and perspective. *Cell Biosci* **2**: 28.
32. Wang, F., Liu, Z., Park, S.H., Gwag, T., Lu, W., Ma, M., Sui, Y., and Zhou, C. (2018). Myeloid β-Catenin Deficiency Exacerbates Atherosclerosis in Low-Density Lipoprotein Receptor-Deficient Mice. *Arteriosclerosis, thrombosis, and vascular biology* **38**: 1468-1478.
33. Rogg, E.M., Abplanalp, W.T., Bischof, C., John, D., Schulz, M.H., Krishnan, J., Fischer, A., Poluzzi, C., Schaefer, L., Bonauer, A*., et al.* (2018). Analysis of Cell Type-Specific Effects of MicroRNA-92a Provides Novel Insights Into Target Regulation and Mechanism of Action. *Circulation* **138**: 2545-2558.
34. Cheng, W.L., Yang, Y., Zhang, X.J., Guo, J., Gong, J., Gong, F.H., She, Z.G., Huang, Z., Xia, H., and Li, H. (2017). Dickkopf-3 Ablation Attenuates the Development of Atherosclerosis in ApoE-Deficient Mice. *Journal of the American Heart Association* **6**.
35. Di, M., Wang, L., Li, M., Zhang, Y., Liu, X., Zeng, R., Wang, H., Chen, Y., Chen, W., Zhang, Y*., et al.* (2017). Dickkopf1 destabilizes atherosclerotic plaques and promotes plaque formation by

inducing apoptosis of endothelial cells through activation of ER stress. *Cell Death Dis* **8**: e2917.
36. Badimon, L., Luquero, A., Crespo, J., Peña, E., and Borrell-Pages, M. (2020). PCSK9 and LRP5 in macrophage lipid internalization and inflammation. *Cardiovascular research*.
37. Borrell-Pagès, M., Romero, J.C., and Badimon, L. (2015). LRP5 deficiency down-regulates Wnt signalling and promotes aortic lipid infiltration in hypercholesterolaemic mice. *Journal of cellular and molecular medicine* **19**: 770-777.
38. Boucher, P., Matz, R.L., and Terrand, J. (2020). atherosclerosis: gone with the Wnt? *Atherosclerosis* **301**: 15-22.
39. Ackers, I., Szymanski, C., Silver, M.J., and Malgor, R. (2020). Oxidized Low-Density Lipoprotein Induces WNT5A Signaling Activation in THP-1 Derived Macrophages and a Human Aortic Vascular Smooth Muscle Cell Line. *Front Cardiovasc Med* **7**: 567837.
40. Ye, Z.J., Go, G.W., Singh, R., Liu, W., Keramati, A.R., and Mani, A. (2012). LRP6 protein regulates low density lipoprotein (LDL) receptor-mediated LDL uptake. *J Biol Chem* **287**: 1335-1344.
41. Willemsen, L., and de Winther, M.P. (2020). Macrophage subsets in atherosclerosis as defined by single-cell technologies. *J Pathol* **250**: 705-714.
42. Depuydt, M.A.C., Prange, K.H.M., Slenders, L., Örd, T., Elbersen, D., Boltjes, A., de Jager, S.C.A., Asselbergs, F.W., de Borst, G.J., Aavik, E.*, et al.* (2020). Microanatomy of the Human Atherosclerotic Plaque by Single-Cell Transcriptomics. *Circulation research* **127**: 1437-1455.
43. Döring, Y., Noels, H., van der Vorst, E.P.C., Neideck, C., Egea, V., Drechsler, M., Mandl, M., Pawig, L., Jansen, Y., Schröder, K.*, et al.* (2017). Vascular CXCR4 Limits Atherosclerosis by Maintaining Arterial Integrity: Evidence From Mouse and Human Studies. *Circulation* **136**: 388-403.
44. Reis, M., Czupalla, C.J., Ziegler, N., Devraj, K., Zinke, J., Seidel, S., Heck, R., Thom, S., Macas, J., Bockamp, E.*, et al.* (2012). Endothelial Wnt/β-catenin signaling inhibits glioma angiogenesis and normalizes tumor blood vessels by inducing PDGF-B expression. *J Exp Med* **209**: 1611-1627.
45. Schindelin, J., Arganda-Carreras, I., Frise, E., Kaynig, V., Longair, M., Pietzsch, T., Preibisch, S., Rueden, C., Saalfeld, S., Schmid, B.*, et al.* (2012). Fiji: an open-source platform for biological-image analysis. *Nat Methods* **9**: 676-682.
46. Chaudhuri, A.D., Yelamanchili, S.V., and Fox, H.S. (2013). Combined fluorescent in situ hybridization for detection of microRNAs and immunofluorescent labeling for cell-type markers. *Front Cell Neurosci* **7**: 160.

Supplementary data

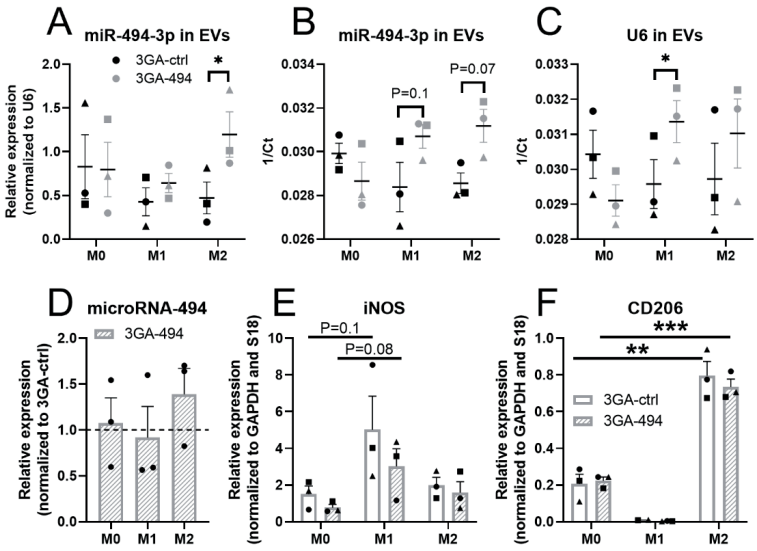

Supplemental Figure 1. Secretion of microRNA-494-3p in human extracellular vesicles and microRNA-494-3p expression and polarization markers in murine macrophages. (A-C) Expression of miR-494-3p in extracellular vesicles (EVs) secreted from M0, M1 and M2 human macrophages, treated with 3GA-ctrl or 3GA-494. (A) Relative expression of miR-494-3p normalized to U6. (B) 1 divided by absolute Ct value (1/Ct) of miR-494-3p and (C) 1/Ct of U6. (D) MiR-494-3p expression in resting M0 and polarized M1 and M2 murine macrophages treated with 3GA-494, normalized to 3GA-ctrl treated M0, M1 and M2 macrophages, respectively (N=3). Expression levels were normalized to 3GA-ctrl. MiR-191 was used as a reference gene. (E) Expression levels of M1 marker inducible oxide synthase (iNOS) and (F) M2 marker cluster of differentiation 206 (CD206) in M0, M1 and M2 macrophages (N=3). A two-tailed unpaired t-test was performed to compare single treatment with the control (3GA-ctrl or M0). (D-F) GAPDH and ribosomal protein S18 were used as a reference gene. Data are represented as mean ±SEM. ***P<0.001, **P<0.01, *P<0.05, compared with 3GA-ctrl or M0.

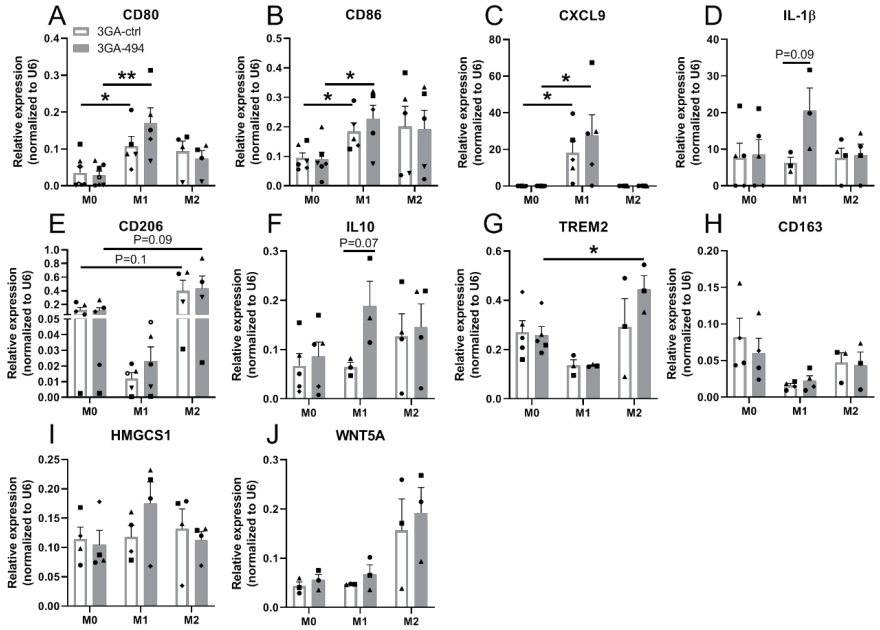

Supplemental Figure 2. Expression of key M1 and M2 polarization markers in human macrophages treated with 3GA-494 or 3GA-ctrl. Resting M0 and polarized M1 and M2 macrophages treated with 3GA-494 or 3GA-ctrl for 24 hours. Expression levels of M1 markers (A) cluster of differentiation (CD)80, (B) CD86, (C), chemokine ligand 9 (CXCL9) and (D) interleukin 1-β and expression levels of M2 markers (E) CD206, (F) interleukin 10 (IL10) and (G) triggering receptor on myeloid cells 2 (TREM-2). (H) Expression of CD163, a receptor for hemoglobin-haptoglobin complexes, (I) 3-Hydroxy-3-Methylglutaryl-CoA Synthase 1 (HMGCS1) and (J) Wnt family member 5A (WNT5A). A two-tailed unpaired t-test was performed to compare single treatment with the control (3GA-ctrl or M0). N is represented by the individual symbols. Variations in N are caused by the exclusion criteria, as explained in the material and methods. U6 was used as a reference gene. Data are represented as mean ±SEM. **P<0.01, *P<0.05, compared with 3GA-ctrl or M0.

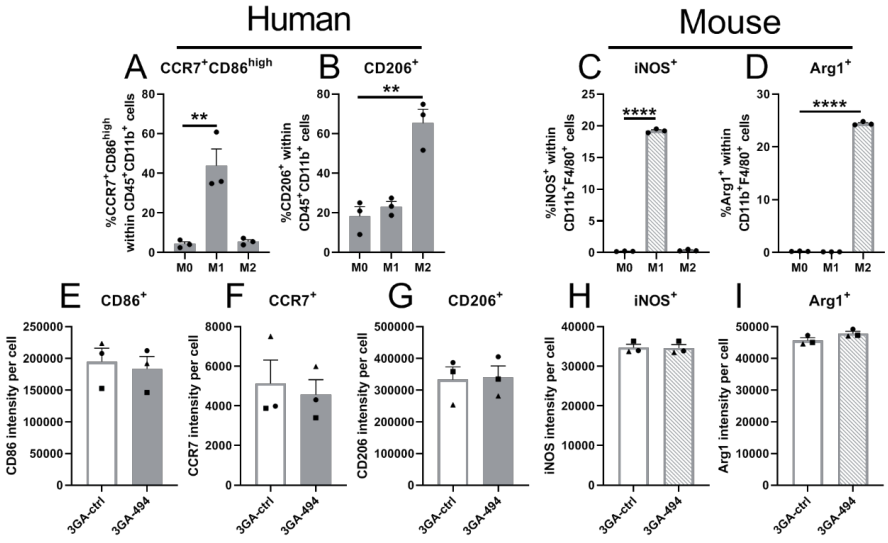

Supplemental Figure 3. Flow cytometric analysis of M1 and M2 markers in human and murine polarized macrophages. Protein levels of M1 and M2 markers in human and murine *in vitro* polarized macrophages (N=3). M1 polarization was induced with LPS and IFNγ. M2 polarization was induced with IL4 and IL13. Percentage of M1 markers (A) C-C chemokine receptor 7 (CCR7) and cluster of differentiation 86 (CD86) positive cells and percentage of M2 marker (B) CD206 positive cells in human M0 and polarized M1 and M2 macrophages. Percentage of M1 marker (C) inducible oxide synthase (iNOS) positive cells and (D) percentage of M2 marker Arginase-1 (Arg1) positive cells in murine M0 and polarized M1 and M2 macrophages. (E) CD86 and (F) CCR7 mean fluorescence intensity (MFI) per cell in human M1 macrophages and (G) CD206 MFI per cell in human M2 macrophages. (H) iNOS MFI in murine M1 macrophages and (I) Arg1 MFI in murine M2 macrophages. (A-D) Percentage (%) of positive cells within alive (A and B) $CD45^+CD11b^+$ or (C and D) $CD11b^+F4/80^+$ cells is shown. (E-I) MFI per cell, treated with 3GA-ctrl or 3GA-494. A two-tailed unpaired t-test was performed to compare single treatment with the control (M0). Data are represented as mean ±SEM. ****P<0.0001, **P<0.01, compared with M0.

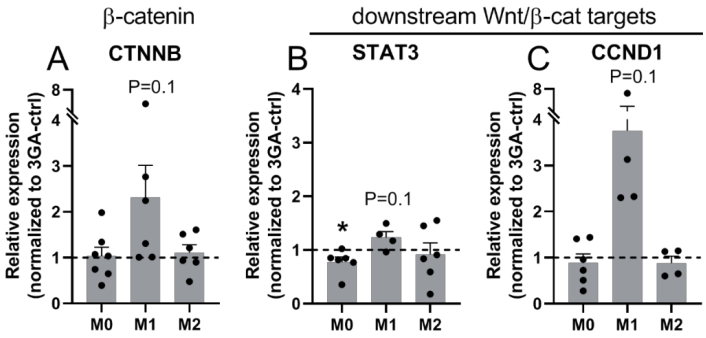

Supplemental Figure 4. Active β-catenin and downstream Wnt target genes in human macrophages treated with 3GA-494 or 3GA-ctrl. Relative expression levels of (A) β-catenin and two downstream Wnt transcription targets, (B) signal of transducer and activator of transcription 3 (STAT3) and (C) cyclin D1 (CCND1) in 3GA-ctrl or 3GA-494 treated M0 and polarized M1 and M2 human macrophages. Expression levels are normalized to 3GA-ctrl (1). U6 was used as a reference gene. A one-sample t-test was performed to compare single treatment with the control, within each individual donor. N is represented by the individual dots. Variations in N are caused by the exclusion criteria, as explained in the material and methods. Data are represented as mean ±SEM. *P<0.05, compared with 3GA-ctrl.

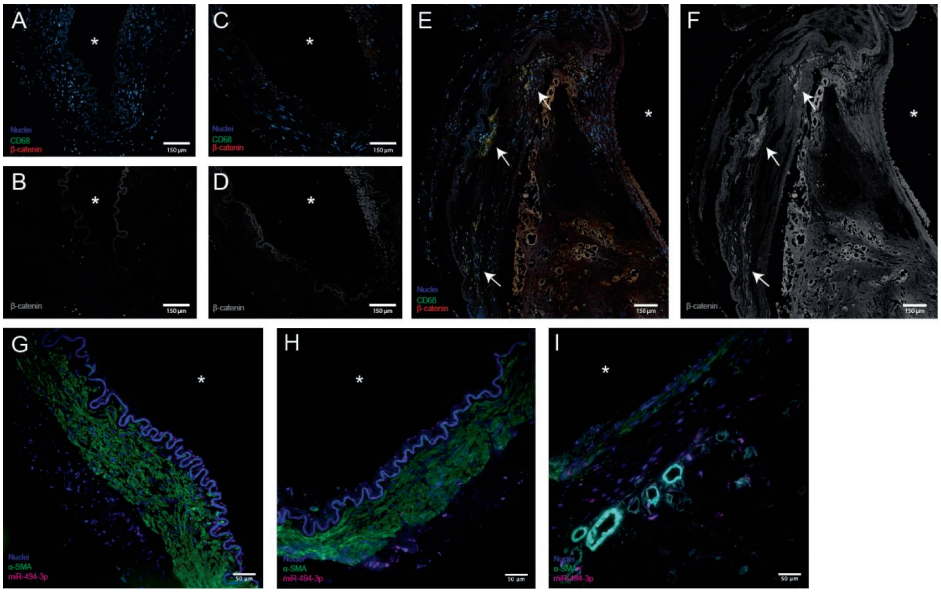

Supplemental Figure 5. Active β-catenin, CD68 and miR-494-3p in human middle cerebral arteries from either a healthy, mildly atherosclerotic or severely atherosclerotic section. (A, B) Healthy, (C,D) mildly atherosclerotic and (E,F) advanced atherosclerotic sections. (A, C, E) Sections were stained with an antibody against CD68 to stain for macrophages (green), the non-phosphorylated (non-phospho) form of β-catenin (red) and nuclei (blue). (B, D, F) β-catenin (grey) staining alone. (G) Healthy, (H) mildly atherosclerotic and (I) advanced atherosclerotic sections were stained with an antibody against α-smooth muscle actin (α-SMA; green) and with fluorescent in situ hybridization to stain for miR-494-3p (red). Nuclei are shown in blue. Arrows point at areas with both β-catenin and CD68 expression. Asterisks indicate the vessel lumen.

Chapter 4

C/D box snoRNA SNORD113-6/AF357425 plays a dual role in integrin signalling and arterial fibroblast function via pre-mRNA processing and 2'O-ribose methylation

Eva van Ingen[1,2*], Daphne A.L. van den Homberg[1,2*], M. Leontien van der Bent[1,2], H. Mei[3], Nikolina Papac-Milicevic[4], Veerle Kremer[5], Reinier A. Boon[5,6,7], Paul. H.A. Quax[1,2], Johann Wojta[8,9], A. Yaël Nossent[1,2,4,8]

Human Molecular Genetics. 2022 Mar 31;31(7):1051-1066

[1]Department of Surgery, [2]Einthoven Laboratory for Experimental Vascular Medicine and [3]Biomedical Data Sciences, Leiden University Medical Center, Leiden, the Netherlands. [4]Department of Laboratory Medicine, Medical University of Vienna, Vienna, Austria. [5]Department of Physiology, Amsterdam Cardiovascular Sciences, Vrije Universiteit, Amsterdam UMC location VUMC, Amsterdam, the Netherlands. [6]Institute for Cardiovascular Regeneration, Centre for Molecular Medicine, Goethe University and [7]German Center for Cardiovascular Research (DZHK), Frankfurt am Main, Germany. [8]Department of Internal Medicine II, Medical University of Vienna, Vienna, Austria. [9]Ludwig Boltzmann Institute for Cardiovascular Research, Vienna, Austria.
*These authors contributed equally.

Abstract

We have previously shown that C/D box small nucleolar RNAs (snoRNAs) transcribed from the DLK1-DIO3 locus on human chromosome 14 (14q32) are associated with cardiovascular disease. DLK1-DIO3 snoRNAs are 'orphan snoRNAs' that have no known targets. We aimed to identify RNA targets and elucidate the mechanism-of-action of human SNORD113-6 (AF357425 in mice). As AF357425-knockout cells were non-viable, we induced overexpression or inhibition of AF357425 in primary murine fibroblasts and performed RNA-Seq. We identified several pre-mRNAs with conserved AF357425/SNORD113-6 D'-seed binding sites in the last exon/3' untranslated region (3'UTR), which directed pre-mRNA processing and splice-variant-specific protein expression. We also pulled down the snoRNA-associated methyltransferase fibrillarin from AF357425-High versus AF357425-Low fibroblast lysates, followed by RNA isolation, ribosomal RNA depletion and RNA-Seq. Identifying mostly mRNAs, we subjected these to PANTHER pathway analysis and observed enrichment for genes in the integrin pathway. We confirmed 2'O-ribose methylation in six integrin pathway mRNAs (*MAP2K1*, *ITGB3*, *ITGA7*, *PARVB*, *NTN4* and *FLNB*). Methylation and mRNA expression were decreased while mRNA degradation was increased under AF357425/SNORD113-6 inhibition in both murine and human primary fibroblasts, but effects on protein expression were more ambiguous. Integrin signalling is crucial for cell-cell and cell-matrix interactions, and correspondingly, we observed altered human primary arterial fibroblast function upon SNORD113-6 inhibition.

Introduction

Small nucleolar RNAs (snoRNAs) are a class of noncoding RNAs that guide modifications of other RNA species, mostly of ribosomal RNAs (rRNAs)[1]. Typically, there are two types of snoRNAs, named after conserved sequence motives, namely H/ACA box snoRNAs that guide RNA pseudouridylation (Ψ) and C/D box snoRNAs that guide RNA 2'O-ribose methylation (2'Ome)[1]. These modifications are essential for normal rRNA processing and function, and thus for protein synthesis[2]. SnoRNAs bind their target RNAs via Watson-Crick base-pairing to their antisense boxes[1]. Most C/D box snoRNAs have two C box motifs, C and C', and two D box motifs, D and D'[1]. The ~9-20 nucleotides upstream of the D and D' boxes form the antisense boxes of C/D box snoRNAs[1]. In case of canonical C/D box snoRNA function, the snoRNA forms a small nucleolar ribonucleoprotein complex (snoRNP) with proteins NHP2L1, NOP56, NOP58 and the methyltransferase fibrillarin[1]. Binding of an antisense box to a target rRNA results in 2'Ome of the nucleotide bound to the 5th snoRNA-nucleotide upstream of the D or D' box[1]. Because of the strictly conserved base-pairing, rRNA targets can easily be predicted for approximately half of the known snoRNAs[3]. However, for the other half, no rRNA targets have been identified and thus, the function of these 'orphan' snoRNAs is still unknown[4].

We have previously shown that a cluster of 41 C/D box snoRNAs, SNORD112, SNORD113 1-9 and SNORD114 1-31, transcribed from the DLK1-DIO3 locus on the long arm of human chromosome 14 (14q32; 12F1 in murine cells) is strongly associated with human cardiovascular disease[5]. The 14q32 locus also encodes for two other types of noncoding RNAs, namely two long noncoding RNAs (lncRNAs), MEG3 and MEG8 and 54 microRNAs[6]. Both the lncRNAs and microRNAs also play a role in cardiovascular physiology and pathology[7-15], however genetic analyses showed that the role of the snoRNAs in cardiovascular disease is independent of and stronger than the 14q32 lncRNAs and microRNAs[5]. However, all 14q32 snoRNAs are orphan snoRNAs and their targets and mechanisms of action are still unknown[16].

The 14q32 snoRNA locus resembles the Prader-Willi locus, a large snoRNA gene cluster on human chromosome 15q11[17]. Both loci encode two clusters of highly similar C/D box snoRNAs, SNORD113 and SNORD114 on 14q32 and SNORD115 and SNORD116 on 15q11. Both loci are imprinted, however, where all 14q32 noncoding RNAs are transcribed from the maternal allele, the 15q11 snoRNAs are transcribed from the paternal allele[18]. The loss of imprinting or mutations and deletions in both loci leads to neuro-developmental disorders, Prader-Willi syndrome for 15q11 and either Temple or Kagami-Ogata syndrome for 14q32[19].

In contrast to the Prader-Willi locus however, no large deletions in the 14q32 snoRNA cluster have been reported; most mutations affect the upstream lncRNA MEG3 or one of three differentially methylated regions[19]. The lack of deletions in the snoRNA cluster hints at its importance for survival.

Besides 2'Ome of rRNAs, several non-canonical functions have been described for both canonical and orphan snoRNAs, including the 15q11 snoRNAs. The orphan SNORD115 for example, has been shown to direct alternative splicing, amongst others of the serotonin receptor *5HT2C*[20-22], where the canonical snoRNA SNORD27 directs alternative splicing of *E2F7*, for example[23]. C/D box snoRNAs can also direct processing of the 3'UTR of mRNAs and thereby affect protein expression[24]. Although the direction of alternative splicing and 3'-end processing appear to be 2'Ome-independent, it has also been shown that C/D box snoRNAs can induce 2'Ome of mRNAs. For example, the RPL13A-snoRNAs U32A and U51 can guide 2'Ome of the Peroxidasin mRNA, leading to mRNA stabilization and repression of translation, thereby increasing mRNA but decreasing protein levels[25]. Besides mRNAs, C/D box snoRNAs may also guide 2'Ome of other non-canonical RNA targets. For example, we showed in 2018 that a 14q32 microRNA, miR-487b is subject to 2'Ome in a fibrillarin-dependent, and thus likely in a C/D box snoRNA-dependent, manner[26]. Finally, it has also been shown that certain C/D box snoRNAs may be processed into smaller fragments that bind mRNA 3'UTRs and suppress translation in a microRNA-like fashion[27].

In order to elucidate the mechanisms of action of the 14q32 orphan C/D box snoRNAs, we focused on the murine snoRNA AF357425 and the human snoRNA SNORD113-6. The D'-antisense boxes of these two snoRNAs are fully conserved between the two species, are abundantly expressed in vascular tissue, and have been shown to play a role in vascular remodelling and cardiovascular disease[5, 28]. As the DLK1-DIO3 snoRNAs are expressed predominantly in fibroblasts[3], we used CRISPR/Cas9 in order to knock-out AF357425 in murine 3T3 fibroblasts. When this strategy proved unsuccessful as the snoRNA appears essential for cell survival, we used antisense technology in order to knockdown or overexpress AF357425 expression in primary murine fibroblasts (PMFs) followed by different RNA-Seq strategies, both with and without prior fibrillarin pulldown and rRNA depletion. Based on the RNA-Seq results, we followed up on multiple targets and mechanisms related to pre-mRNA processing, alternative splicing and RNA stability, in both murine and human fibroblasts.

Here, we describe that AF357425 / SNORD113-6 plays a dual role in the regulation of mRNA and protein expression via both pre-mRNA processing/splicing and via 2'Ome of mRNA targets, affecting amongst others, the integrin signalling pathway and primary human arterial fibroblast function.

Results

CRISPR/Cas9 knockout of AF357425

In order to elucidate the function of AF357425/SNORD113-6, we aimed to generate AF357425 knockout fibroblasts. We first transfected 3T3 cells with a single guide RNA, GA-AF357425-1+ (Supplemental Table 2), but all of the surviving clones were wildtype. We did observe multiple clones that ceased to proliferate and ultimately rounded up and died after 3-4 divisions, but with only 6-12 cells, we could not analyse these. We then used a combination of four vectors with four different guide RNAs, all aimed to target AF357425, but at different sites (Supplemental Table 2). We identified 34 single-cell clones, of which 9 ceased to proliferate and died after only a few divisions. The remaining 25 clones all showed normal expression of the mature AF357425 snoRNA by rt/qPCR. However, when analysing the genomic DNA PCR product on a 2.5% agarose gel, clone BF6 (plate B, well F6), showed two bands rather than one; the first band (BF6-L) appeared to be similar or slightly longer in length than the wildtype 3T3 band, and the second band (BF6-S) was clearly shorter (Supplemental Figure 1A). Sanger sequencing of the two alleles showed that the BF6-L allele has a single C-insert directly upstream of the shortest predicted D'-seed, whereas the D'-seed is almost completely deleted by a 9-nucleotide deletion in the BF6-S allele (Supplemental Figure 1B). Given that AF357425 expression was normal in the BF6, and the cells grow normal and appear in every way similar to wildtype 3T3 fibroblasts, we hypothesized that BF6-L is the maternal and expressed allele.

We then used a novel single guide RNA to knock out the BF6-L allele in the BF6 clone. We observed a ~99% lethality in the transfected cells, indicating that AF357425 is essential for cell proliferation and ultimately for cell survival.

Inhibition and overexpression of snoRNAs using oligonucleotides

SnoRNA expression was inhibited using gapmers (GM). As shown before, the efficiency of snoRNA inhibition was, however, variable[29] and appeared sensitive to factors including cell cycle, cell density and number of passages (the latter for primary cells only). Even though we controlled for these factors as much as possible, knockdown efficiency was checked for each individual experiment. SnoRNA knockdown was more efficient in primary cells, both human umbilical cord arterial fibroblasts (HUAFs) and primary murine skin fibroblasts (PMFs) than in human BJ and murine 3T3 and BF6 cells. For primary cells, a knockdown between 60-75% was deemed successful, for cell lines, a knockdown of 20-50% was deemed successful. Cells with less efficient or no knockdown were not used for further experiments or analyses.

Overexpression of the snoRNA AF357425 was achieved using 3rd generation antisense oligonucleotides (3GA) directed towards the 3'-end of the snoRNA. We have shown previously that 3GAs can efficiently induce snoRNA expression, most likely through protection from degradation by endonucleases[5]. Representative snoRNA inhibition and overexpression (in PMFs only) per cell line are shown in Supplemental Figure 2.

RNA-Seq of processing/splicing variants

As it was previously reported that snoRNAs can affect RNA processing and RNA stability[24, 30, 31], we isolated total RNA from the lysates of PMFs transfected with either 3GA-AF357425 (3GA-AF; AF357425-high) or GM-AF357425 (GM-AF; AF357425-low) and sent these to BGI for whole-transcriptome RNA-Seq. The 3GA/GM-induced upregulation/knockdown for this RNA-Seq experiment, as well as the RNA-binding protein immunoprecipitation (RIP)-Seq described later, is shown in Supplemental Figure 2A.

The data from this RNA-Seq experiment were used to identify changes in pre-mRNA processing. After selecting for the presence of a conserved AF357425/SNORD113-6 D' box seed antisense sequence, we identified 46 genes that showed differential expression of splice- or processing-variants between the AF357425-high and AF357425-low samples. Out of these, four genes had a binding site in the first exon, eight in an internal exon, nine had a binding site in an intron, and 31 genes had a binding site in the last exon, either in the coding sequence or in the 3'UTR (Figure 1A). We decided to focus on these last exon binding sites. Of these 31 genes, splice- or processing variants were also conserved in 20 human genes, which further narrowed down our selection (Figure 1B). In the human genes, we allowed for single-nucleotide mismatches in the D' box seed antisense sequence, except for nucleotides 4-6 upstream of the D' box. Although both binding sites and splice- or processing variants were conserved between mice and men, differences were observed in the location, including the 'last exon site', of the predicted snoRNA binding sites between the two species (Supplemental Figure 3).

RNA-Seq data are available in the Gene Expression Omnibus (GEO) under accession number GSE173099.

Validation of processing/splicing variants

PANTHER pathway analysis did not point towards pathways that are relevant for cardiovascular disease, so instead, we decided to follow-up on three genes, namely *JAG1*, *DUSP7* and *EBPL,* which were abundantly expressed in both murine 3T3 (and BF6) and

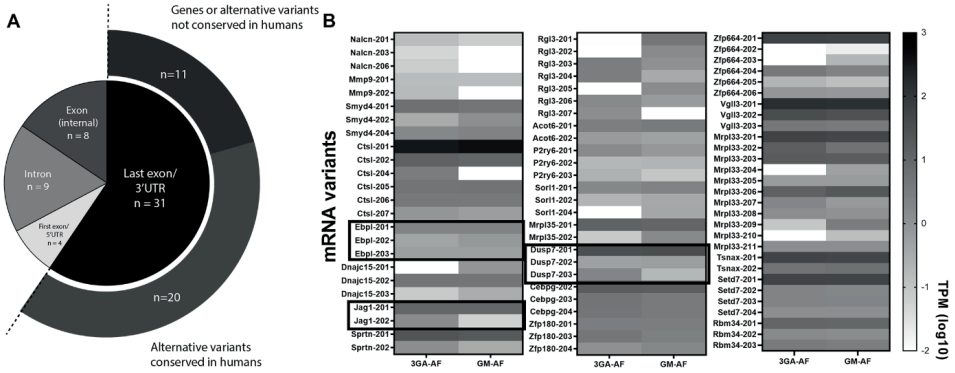

Figure 1. RNA-Seq. (A) Schematic representation of genes with multiple splice/processing variants that are differentially expressed between AF357425-High and AF357425-Low sample pool. Conservation between mice and humans is given for variants with D' box seed binding sites in the last exon/3'UTR of the dominant variant. (B) Heatmap of expression changes in variant expression in AF357425-High (3GA-AF) and AF357425-Low (GM-AF) sample pools of genes with conserved D' box seed binding sites in their last exon/3'UTR.

human BJ fibroblasts. Information on known splice variants was taken from the Ensembl Genome Browser (https://m.ensembl.org/; June 2020; Supplemental Figure 3). Supplemental Figure 3 also shows details on putative snoRNA binding sites, as well as binding sites for the primer sets that were used. As we chose to focus on the location of the binding site, variants with a binding site in the 3'UTR, or at least in an exon (in that order) were called variant 1. If both variants had similarly located binding sites, the variants that code for proteins were called variant 1. Finally, if both variants coded for a protein, the variant with the highest number of snoRNA binding sites was called variant 1 (Supplemental Figure 3).

JAG1 contains a single binding site for the D' box seed of SNORD113-6/AF357425, which is located towards the very end of the coding region towards the end of the last exon of transcript variant 1 (*JAG1-1*), both in the human and in the murine gene. Both in humans and in mice, *JAG1-1*, gives rise to a ~130 kDa protein. JAG1 transcript variant 2 (JAG1-2) has one snoRNA binding in the last exon in murine cells, and one site in the pre-last exon in human cells. *JAG1-2* is not translated in either mice or humans (Supplemental Figure 3). Looking at mRNA expression of the two variants, we observed that under snoRNA-inhibition, the ratio of mRNA *JAG1-1* over *JAG1-2* increased significantly in murine 3T3 and BF6 cells. We observed a similar trend in in human BJ cells (p=0.053) (Figure 2A-C).

DUSP7 has two transcript variants in both mice and humans that both give rise to a protein. In mice, variant 1, *DUSP7-1*, has a snoRNA binding site located in the 3'UTR and gives rise to a ~40-45 kDa protein. *DUSP7-2* gives rise to a ~24 kDa protein, but has no binding site for the D'-seed of AF357425. In humans, *DUSP7-1* has a binding site in the 3'UTR and gives rise to a ~30 kDa protein, whereas *DUSP7-2* has a binding site in the last intron of its pre-mRNA and gives rise to a ~40-45 kDa protein (Supplemental Figure 3). Looking at mRNA expression of the two variants, we observed that under snoRNA-inhibition, the ratio of mRNA *DUSP7-1* over *DUSP7-2* decreases significantly in murine 3T3 cells, but we observed the opposite in human BJ cells (Figure 2D-F).

EBPL has two splice variants in both mice and humans. In mice, *EBPL-1* gives rise to a ~23 kDa protein and has a binding site for the D'-seed of AF357425 in its 3'UTR. *EBPL-2* has no binding site, nor does it give rise to a protein. In humans, both *EBPL-1* and *EBPL-2* give rise to proteins, ~23 kDa and ~16 kDA, respectively, but *EBPL-1* has more binding sites for the D'-seed of SNORD113-6 (Supplemental Figure 3). Looking at mRNA expression of the two variants, we observed that under snoRNA-inhibition, the ratio of mRNA *EBPL-1* over *EBPL-2* shows a trend towards an increase in murine BF6 cells (p=0.064), and a significant increase in human BJ cells (Figure 2G-I).

Finally, although we identified them as potential 2'Ome targets via RIP-Seq (described below), *ITGB3*, *PARVB* and *MAP2K1* also have different processing variants in human cells combined with snoRNA binding sites towards the 3'-end of the gene (Supplemental Figure 3). The *ITGB3-1* pre-mRNA has a binding site for the D'-seed of SNORD113-6 in the last intron, whereas the *ITGB3-2* pre-mRNA lacks this intron and is marked for nonsense mediated decay (NMD; Ensembl). Inhibition of SNORD113-6 in HUAFs led to a trend towards a decreased ratio of the *ITGB3-1* mRNA over the *ITGB3-2* mRNA (p=0.07; Figure 2J). For MAP2K1, there are two variants that both have snoRNA binding sites in their introns, but MAP2K1-1 has more sites (12 sites) than the shorter MAP2K-2 (6 sites) and under snoRNA inhibition again the ratio of MAP2K1-1 over MAP2K-2 appeared decreased (p=0.068; Figure 2K). Finally, the human *PARVB-1* mRNA has a binding site in its 3'UTR, where *PARVB-2* has no binding site. However, here we did not observe changes in the ratio between the two variants (Figure 2L).

Overall, it appears as if snoRNA binding in the last exon and 3'UTR, but not in introns, affects pre-mRNA processing and possibly protects the (pre-)mRNA for degradation.

RNA Binding Protein – Immunoprecitation(RIP)-Seq and pathway analysis

As fibrillarin is the main C/D box snoRNA-associated methyltransferase[1], we also performed a fibrillarin pulldown followed by total RNA isolation on the lysates of AF357425-high and AF357425-low murine fibroblasts in order to identify novel RNA targets that are subject to AF357425-induced 2'Ome. Using both AF357425 overexpression and inhibition (Supplemental Figure 2A), we aimed to create the largest possible difference between cell pools, hypothesizing that transcripts enriched in the AF357425-high pool, are potential 2'Ome targets of AF357425. Samples from multiple transfections and pulldowns had to be pooled to obtain enough RNA for further analysis. Pooled RNA from AF257425-high or AF357425-low was sent to BGI for rRNA depletion followed by RNA-Seq. In total, we detected transcripts from 18.997 genes in the AF357425-High pool and 24.678 genes in the AF357425-Low pool. Within these genes, we selected all those with a conserved, nine-nucleotide antisense sequence for the AF357425 D' box seed sequence in the coding region and 3'UTR, which were enriched in the AF357425-High pool (407 genes). One mismatch in any position, except for nucleotides 4-6 upstream of the AF357425 D' box, was allowed. When conserved, these murine genes were converted to human genes (292 genes) and again all genes with a conserved antisense sequence of the SNORD113-6 D' box, now also in introns, were selected. A perfect antisense sequence was found in 161 genes. Allowing for one mismatch, except for nucleotides 4-6 upstream of the SNORD113-6 D' box, resulted in an additional 67 genes. We used these 228 genes in a PANTHER pathway analyses and found potential enrichment of multiple pathways, of which one, the integrin signalling pathway, stood out, with 7 out of 46 genes in the pathway enriched in the AF357425-high sample pool. Because of its importance in fibroblast function[32], we decided to follow up on the integrin signalling pathway target genes.

An overview of the number of genes and pathways identified is shown in Figure 3.

Validation of 2'Ome targets

We identified seven genes in the integrin signalling pathway as potential conserved fibrillarin-dependent targets for AF357425/SNORD113-6, namely *MAP2K1*, *ITGB3*, *ITGA7*, *FLNB*, *NTN4*, *PARVB* and *COL4A4*. In the murine *Itgb3*, *Flnb*, *Parvb* and *Col4a4* predicted binding sites were all located in the 3'UTR. Binding sites in *Map2k1*, *Itga7* and *Ntn4* were all located in exons. In the human *FLNB* and *PARVB*, binding sites were located in the 3'UTR. Binding sites in human *ITGB3* and *NTN4* were located in the last intron and in *ITGA7* in the last exon. Human M*AP2K1* and *COL4A4* had multiple predicted binding sites, 12 and 3, respectively, all located in introns. Binding site locations are indicated with an * in

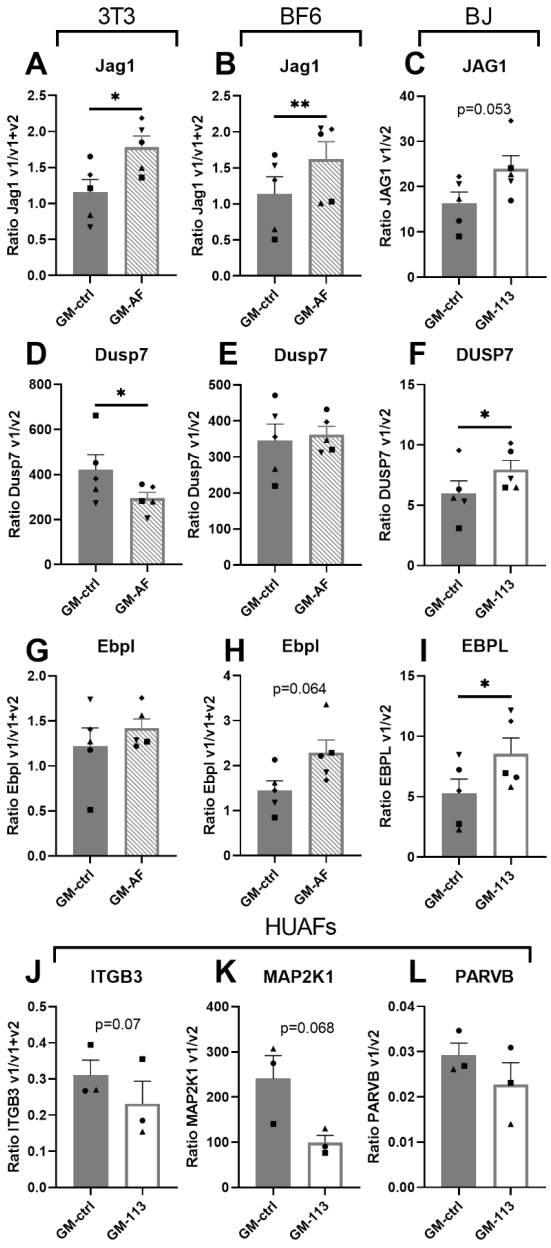

Supplemental Figure 3, those sites at which 2'Ome was measured are indicated with the full binding site sequence.

We performed Reverse Transcription at Low dNTP concentration followed by Quantitative PCR (RTL-Q[26]) in order to confirm and quantify methylation at the predicted site in both the murine and human genes in primary fibroblasts (PMFs and HUAFs, respectively). We indeed found 2'Ome in both the murine and human *MAP2K1*, *ITGA7* and *NTN4* mRNA (Figure 4B-D, G, I, K). We also found 2'Ome at the predicted site of the murine *Itgb3* mRNA (Figure 4A), as well as in the human *PARVB* and *FLNB* mRNA (Figure 4H, J). We then calculated the 'estimated methylated fraction' (EMF) for each of these sites. Although the EMF is an unprecise measure, an estimation by definition, we observed a trend towards reduction of the EMF upon inhibition of either AF357425 or SNORD113-6 for

Figure 2. Ratios of splice and processing variants with and without SNORD113-6/AF357425 binding sites. (A-I) Ratios of mRNA variants in murine 3T3 and BF6 and in human BJ fibroblasts and (J-L) in human umbilical arterial fibroblasts (HUAFs). Variant 1 was measured specifically, but depending on the primer binding sites (Supplemental Figure 3), we either measured variant 2 alone, or in combination with variant 1, as depicted on the y-axes. Expression levels are relative to GAPDH. A two-tailed paired t-test was performed to compare single treatment with the control, within each individual experiment. Data are represented as mean ±SEM. *p<0.05, compared with GM-ctrl.

Itgb3, Map2k1 and *Ntn4*, and in PMFs (Figure 4A, B, D) and for pre-*MAP2K1* in HUAFs (Figure 4G), indicating that the snoRNA indeed guides 2'Ome at these sites, but that a 60-80% snoRNA knockdown is not nearly enough to abolish all methylation at these sites.

In the remaining identified putative targets, *Col4a4*, *Flnb* and *Parvb* in PMFs and *COL4A4* and *pre-ITGB3* in HUAFs, expression was too low to confirm 2'Ome.

Although both RNA-Seq strategies provide different sorts of information, i.e. altered expression of different transcript versus snoRNA-induced binding to fibrillarin, both strategies provided us with potential AF357425 targets. Therefore, besides the integrin signalling pathway genes alone, we also measured potential 2'Ome in the AF357425 targets that were identified through the splicing/processing route described earlier. We confirmed 2'Ome at the predicted sites in the murine and human *DUSP7* mRNA (Figure 4F & 4L), in the murine *Jag1* mRNA (Figure 4E) and in the human *EBPL* mRNA (Figure 4M). In HUAFs, *JAG1* and in PMFs *Ebpl* expression were too low to quantify potential 2'Ome.

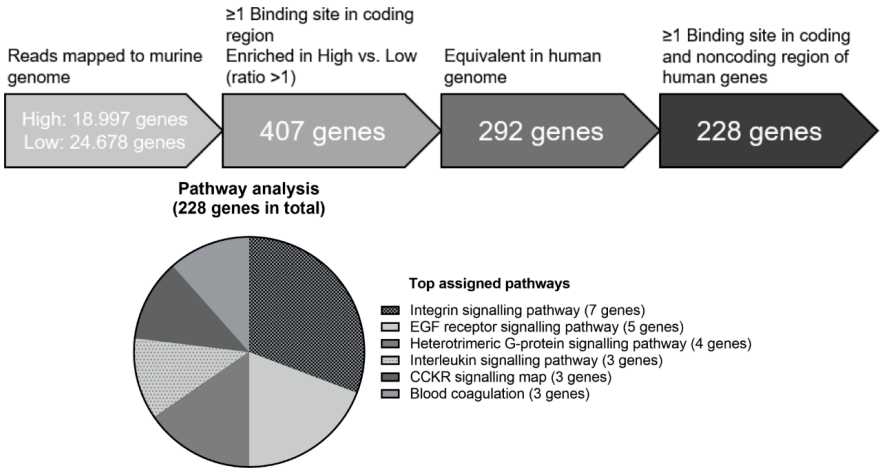

Figure 3. RIP-Seq and pathway analysis. Schematic representation for genes selected from the RIP-seq. RNA-seq was performed on RNA from pooled fibrillarin pulldowns of AF357425-High (3GA-AF) and AF357425-Low (GM-AF) treated PMFs. One mismatch in any position of the nine-nucleotide antisense sequence for the AF357425 D' box, except for nucleotides 4-6 upstream of the AF357425 D' box, was allowed. Similar criteria were used for SNORD113-6 binding sites in human genes. Pathway enrichment analysis was performed on the remaining set of potential target genes using PANTHER Classification System.

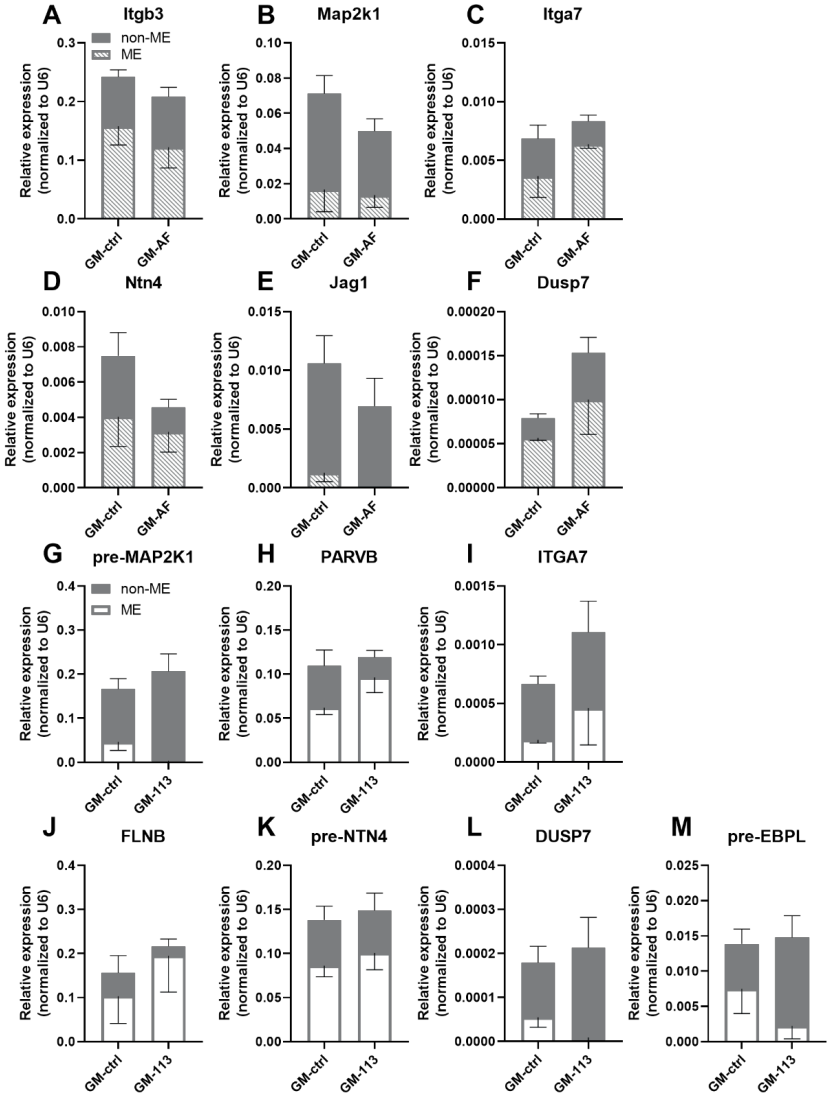

Figure 4. 2'-O-methylation at predicted SNORD113-6/AF357425 binding sites. For the detection of 2'-O-methyated nucleotides, Reversed Transcription at Low dNTP concentration followed by Quantitative PCR (RTL-Q) was performed. PMFs or HUAFs were transfected with GM-ctrl or GMs against murine AF357425 (GM-AF) or human SNORD113-6 (GM-113) for 24 h. The EMF was calculated and shown as part of the relative gene expression. Relative expression and EMF of murine targets (A) *Itgb3*, (B) *Map2k1*, (C) *Itga7*, (D) *Ntn4*, (E) *Jag1* and (F) *Dusp7* in PMFs transfected with GM-ctrl or GM-AF. Relative expression and EMF of human targets (G) pre-*MAP2K1*, (H) *PARVB*, (I) *ITGA7*, (J) *FLNB*, (K) pre-*NTN4*, (L) *DUSP7* and (M) *pre-EBPL* in HUAFs transfected with GM-ctrl or GM-113. Expression levels are relative to U6. Data are represented as mean ±SEM.

Effects of 2'Ome on mRNA stability

It has been postulated that 2'Ome can stabilize RNAs and thereby reduce RNA degradation rates[30, 31]. Therefore, after a 24-hour transfection with GMs, we treated HUAFs and PMFs with the transcription inhibitor Actinomycin D and measured mRNA levels after 2 and 6 hours, in order to determine the rate of mRNA degradation after snoRNA inhibition and decreased (pre-)mRNA 2'Ome. We used the same primer sets used to measure the EMF (earlier), however, we also measured mRNA degradation using the splice variant-specific primers sets (data shown in Supplemental Figure 4).

In murine cells, we confirmed 2'Ome in the *Itgb3*, *Map2k1*, *Itga7*, *Ntn4*, *Jag1 and Dusp7* mRNAs. Additionally, we observed that after transfection with GM-AF357425, total 2'Ome-mRNA was reduced for *Itgb3, Map2k1*, *Ntn4*, and *Jag1*, compared with GM control (GM-ctrl). In accordance, the *Itgb3* mRNA showed a trend towards increased degradation upon snoRNA inhibition (p=0.081; Figure 5A). *Map2k1, ItgA7*, *Ntn4*, and *Jag1* showed similar trends (p=0.079, p=0. 113, p=0.75, and p=0.130, respectively; Figure 5B-E), whereas degradation of the *Dusp7* mRNA was increased significantly (p=0.005; Figure 5F).

In human cells, we confirmed 2'Ome in the *pre-MAP2K1*, *PARVB*, *ITGA7*, *FLNB*, *pre-NTN4*, *DUSP7* and *pre-EBPL* (pre-)mRNAs. Moreover, we found that after transfection with GM-SNORD113-6, total 2'Ome-mRNA was reduced for *pre-MAP2K1*, *DUSP7* and *EBPL*, compared with GM-ctrl. In accordance, degradation of the *pre-MAP2K1*, *PARVB*, *ITGA7*, *pre-NTN4*, *DUSP7* and *pre-EBPL* (pre-)mRNAs was increased significantly (Figure 5G-M).

As discussed earlier, *DUSP7*, *JAG1* and *EBPL* have transcript variants with and without AF357425/SNORD113-6 binding sites. Human *MAP2K1* has two splice variants, which contains 12 and 6 intronic 2'Ome sites, respectively (Supplemental Figure 3). In human *MAP2K1, JAG1, and DUSP7* snoRNA inhibition resulted in, a trend or significant, increased degradation of the one variant, but not the other (Supplemental Figure 4I, J, M-P), confirming previous studies that showed that 2'Ome protects (pre-)mRNAs from degradation[25]. In mice, we observed the same effect for Jag1 and Dusp7-1 (Supplemental Figure 4A-D).

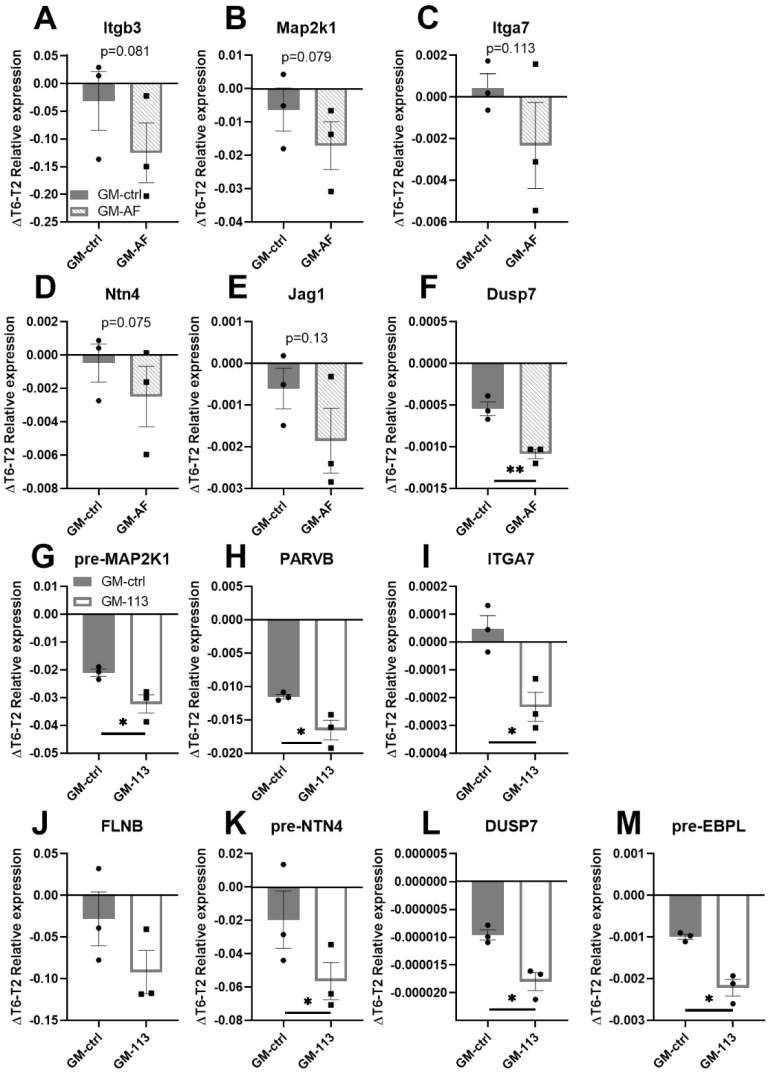

Figure 5. Stability of SNORD113-6/AF357425 target mRNAs in primary cells. PMFs or HUAFs were transfected with GM-ctrl or GMs against murine AF357425 (GM-AF) or human SNORD113-6 (GM-113) for 24 hours. After 24 hours, cells were treated with Actinomycin D to inhibit novel RNA transcription. mRNA levels of SNORD113-6/AF357425 targets were measured 2 (T2) and 6 (T6) hours after addition of Actinomycin D. The decline in mRNA was calculated over time as relative expression of T6 minus relative expression of T2 (ΔT6-T2). The decline in mRNA of murine targets (A) *Itgb3*, (B) *Map2k1*, (C) *Itga7,* (D) *Ntn4*, (E) *Jag1* and (F) *Dusp7* in PMFs transfected with GM-ctrl or GM-AF. The decline in mRNA of human targets (G) pre-*MAP2K1*, (H) *PARVB*, (I) *ITGA7*, (J) *FLNB*, (K) pre-*NTN4*, (L) *DUSP7* and (M) *pre-EBPL* in HUAFs transfected with GM-ctrl or GM-113.6. A one-tailed paired t-test was performed to compare increased decline in GM-AF/113 compared to GM-ctrl, within each individual experiment. Data are represented as mean ±SEM. *p<0.05, compared with GM-ctrl.

Protein expression

Based on our findings on (pre-)mRNA processing/splicing, 2'Ome, mRNA-stability and the availability of reliable antibodies, we used Western blotting to study the effects of AF357425/SNORD113-6 knockdown in primary human and murine fibroblasts on protein expression of JAG1, DUSP7, ITGB3 and MAP2K1 (Figure 6A-B).

Although we observed effects of snoRNA knockdown on pre-mRNA processing in both human and murine cells, and on methylation and mRNA degradation in murine cells, there was no effect on protein expression of JAG1 in either murine or human fibroblasts (Figure 6C and D). DUSP7 protein expression was also unaffected in murine primary fibroblasts (Figure 6E), but in human primary fibroblast, protein expression of DUSP7-2 (~40 kDa, Figure 6B) was upregulated under SNORD113-6 inhibition (p=0.052; Figure 6F), whereas DUSP7-1 (~30 kDa) was not detected by western blot. This is in conflict with the decrease in mRNA stability of *DUSP7-2* under snoRNA inhibition (Supplemental Figure 4P).

In murine cells, ITGB3 also showed a trend towards increased protein expression, whereas in human cells, ITGB3 protein expression was significantly reduced under snoRNA inhibition (Figure 6G and H). Like the human *(pre-)DUSP7*, the murine *Itgb3* mRNA is methylated and methylation is reduced under snoRNA inhibition. It has been shown previously that mRNA methylation can inhibit translation[25], which may explain the increased protein expression under snoRNA inhibition, an effect that is not seen for the unmethylated human *ITGB3*. In human cells, *ITGB3* was not methylated, but has at least two processing variants. Under snoRNA inhibition, we found that the mRNA ratio changes in favour of *ITGB3-2*, which is marked for NMD (Ensembl). This is confirmed by a decreased protein expression in HUAFs under SNORD113-6 inhibition.

Finally, we looked at protein expression of MAP2K1. MAP2K1 protein expression was significantly downregulated in murine fibroblasts under inhibition of AF357425 (Figure 6I). This is in accordance with the increased mRNA degradation, however it conflicts with notion that 2'Ome inhibits translation. The 2'Ome of the murine *Map2k1* mRNA is located in the coding region, whereas 2'Ome in *Itgb3* is located in the 3'UTR. Whether, and if so, how much, the location of 2'Ome affects translation remains to be determined. In contrast to murine fibroblasts, MAP2K1 protein expression showed a trend towards upregulation in human fibroblasts under SNORD113-6 inhibition (p=0.061; Figure 6J). However, in human cells, MAP2K1 has 2 splice variants that give rise to a protein. We were able to detect and quantify both variants. When we calculated the ratio MAP2K1-1:MAP2K1-2, this ratio was

significantly increased under snoRNA inhibition, which is in accordance to the change in mRNA ratios (Figure 6L). The human *MAP2K1-1* pre-mRNA only has intronic 2'Ome sites, which would not impact translation.

Effects of integrin pathway 2'Ome on fibroblast function

Clearly, the effects of AF357425/SNORD113-6 on protein expression of its target (pre-)mRNAs is complex and depends on among others the location of the binding site and whether binding leads to 2'Ome or not. Therefore, we aimed to look at effects of SNORD113-6 inhibition on fibroblast function, rather than merely on protein expression.

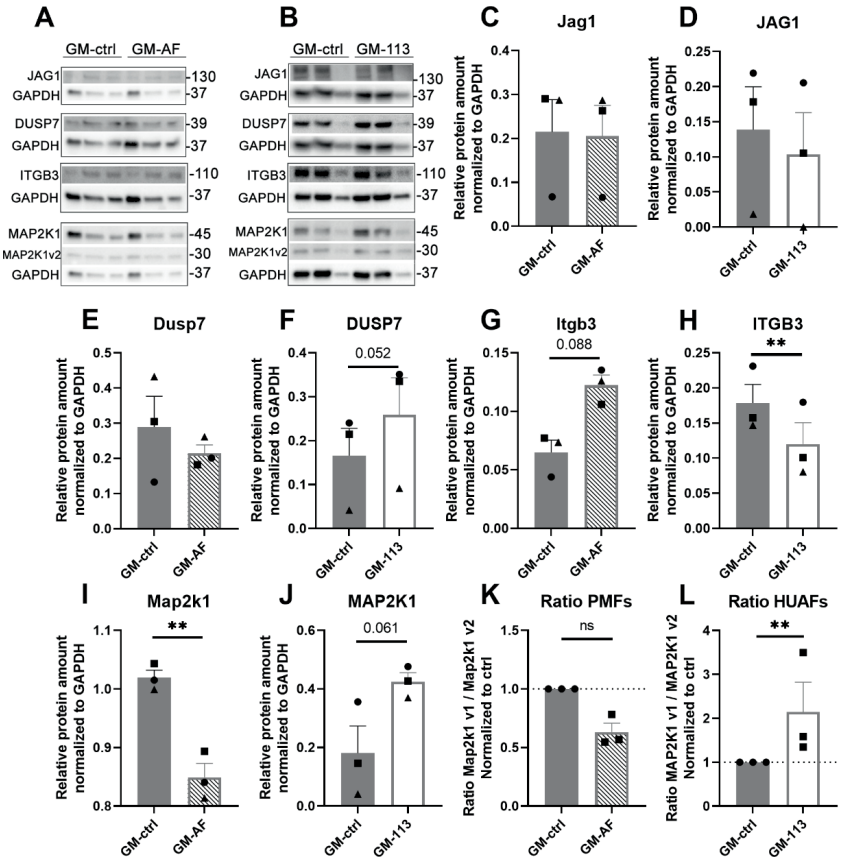

Figure 6. Protein expression in murine and human primary fibroblasts. (A) Western blots for JAG1, DUSP7, ITGB3 and MAP2K1, each with GAPDH, of three independent replicates (each band represents a pool of three technical triplicates) in PMFs. (B) Western blots for JAG1, DUSP7, ITGB3 and MAP2K1, with GAPDH of three independent replicates (each band represents a pool of three technical triplicates) in HUAFs. (C-L) Quantifications of protein band intensities, normalized to GAPDH. Data are represented as mean ±SEM. **p<0.01, compared with GM-ctrl.

Integrin signalling is an essential pathway in fibroblasts, affecting fibroblast interaction both with other fibroblasts and with the extracellular matrix[32]. We analysed the barrier function of HUAFs that were seeded in a monolayer. After seeding, there is a rapid peak in barrier function, which is caused by the initial adherence of the cells. This peak appears somewhat earlier and higher in GM-ctrl transfected HUAFs than in GM-113 transfected HUAFs, indicating that initial adherence is somewhat impaired under snoRNA inhibition. Over time, however, barrier function of HUAFs is maintained for longer at a higher level under SNORD113-6 inhibition, compared with the negative control (Figure 7A). There is a trend towards an increased barrier function after 24 hours, and a significant increase after 48 hours (Figure 7B and C). It should be noted that we cannot fully exclude effects of potential changes in cell proliferation rates between GM-113 and GM-ctrl treated cells.

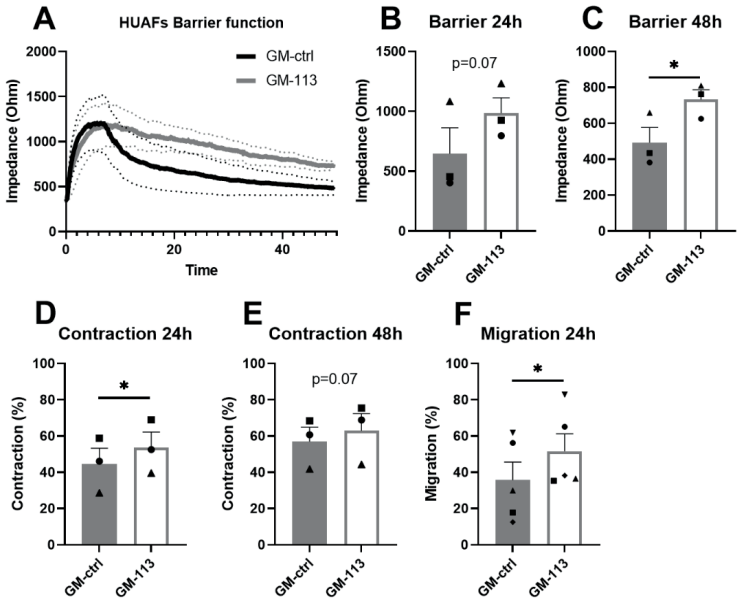

Figure 7. Primary human fibroblast function after SNORD113.6 inhibition. HUAFs transfected with gapmers against SNORD113.6 (GM-113) or GM-ctrl were plated in electrode plates for ECIS. Impedance (in Ohm) was measured over time for 50 hours in total. (A) HUAFs barrier function over time in GM-ctrl or GM-113 treated cells. (B) Impedance (in Ohm) at 24 h and (C) 48 h of incubation. HUAFs transfected with GM-113 or GM-ctrl were mixed into 2 mg/ml collagen gel cushion and cell-induced gel contraction was assessed. (D) Percentage of collagen gel contraction at 24 and (E) 48 h of incubation. (F) HUAFs transfected with GM-113 or GM-ctrl were seeded and subsequently a cross-sectional scratch wound was introduced and scratch wound closure (%) was assessed after 24 h and quantified. A two-tailed paired t-test was performed to compare single treatment with the control, within each individual experiment. Data are represented as mean ±SEM. *P<0.05, compared with GM-ctrl.

Therefore, we also assessed the effects of SNORD113-6 inhibition in a collagen contraction assay. Transfected fibroblasts were embedded in 2mg/ml collagen gels, which were allowed to float in culture medium. The extend of gel contraction was assessed after 24 and 48 hours. Already after 24 hours, we observed a 9% increase in gel contraction in cells treated with GM-113 compared to GM-ctrl ($p=0.02$; Figure 7D). After 48 hours we still observed a 6% increase in contraction ($p=0.075$; Figure 7E). Finally, we also assessed migratory properties of fibroblasts transfected with GM-113, using a scratch wound healing assay. After 24 hours, we observed a 16% increase in wound closure compared to GM-ctrl ($p=0.01$; Figure 7F).

Discussion

Because of their previously found association with cardiovascular disease[28], we aimed to identify targets for the orphan DLK1-DIO3 C/D box snoRNAs. We focused on the one of the most abundantly expressed snoRNAs from this locus with a fully conserved (D' box) seed in mice and humans, AF357425/SNORD113-6[28]. There are no known rRNA targets for this snoRNA[3], but here we show that AF357425/SNORD113-6 can target mRNAs and affects their expression via at least two different mechanisms. We confirm previous studies that showed that snoRNAs direct 3'end processing and splicing of pre-mRNAs[23, 24]. Our data further indicate that AF357425/SNORD113-6 directs fibrillarin towards specific mRNA targets to guide 2'Ome, which may lead to stabilization of the methylated (pre-)mRNA. The latter mechanism, 2'Ome appears better conserved between mice and humans than the pre-mRNA processing. Effects on protein expression; however were ambiguous and therefore we analysed the effects of SNORD113-6 on cell function in primary human fibroblasts and show that SNORD113-6 regulates cell-cell and cell-matrix interactions as well as cell migration, which is crucial for normal fibroblast function.

As it can be challenging to reliably knockdown snoRNAs using antisense oligonucleotides[29], we aimed initially to knockout the murine AF357425 in fibroblasts, using the easy-to-culture and easy-to-transfect NIH-3T3 fibroblast cell line. This strategy proved to be even more challenging than antisense knockdown, as we did not manage to obtain any surviving AF357425-knockout clones. We did however frequently observe clones that appeared normal for several divisions, but then stopped to divide, rounded up and ultimately died. Without surviving clones, we cannot prove that the dying clones were indeed knockouts for AF357425, it could simply be that our CRISPR/Cas9 strategy was not successful. However, it has been shown before that other snoRNAs can be knocked out effectively using CRISPR[33]. Furthermore, by looking at OFP expression, we found that the Cas9/sgRNA vector was transfected effectively every time. Finally, we did obtain a mutant clone, BF6, which proves that as long as expression and function are not severely affected, the AF357425 gene can be mutated using CRISPR/Cas9. We included the BF6 clone in our further analyses to see if under further snoRNA inhibition, the heterozygous knockout would make these cells behave differently. Imprinting of the locus appeared to be complete however, even under snoRNA inhibition, as the BF6 behaved very similar to the wildtype 3T3 fibroblasts. Together our findings implicate that AF357425 may be essential for cell survival.

Tightly controlling for cell number, confluency and cell cycle synchronization using KN-93[34] [serum starvation induces DLK1-DIO3 noncoding RNA expression[35]], we managed to

reproducibly induce and inhibit AF357425/SNORD113-6 expression using oligonucleotides. We performed RNA-Seq on AF357425-High versus AF357425-Low samples and found that there was an overrepresentation of (pre-)mRNAs with a snoRNA binding site in the last exon, particularly in the 3'UTR. It has been shown previously that snoRNAs can impact 3'end processing of pre-mRNAs[24] and we could confirm this finding for the AF357425-targets *Jag1*, *Dusp7* and *Ebpl*. However, although we checked for conservation of the SNORD113-6 binding sites in the human genes, these binding sites were not always located in the last exon. We therefore also confirmed a clear impact of snoRNA binding on the preference for specific splice variants, including for *EBPL* and *MAP2K1*, as has also been shown previously for other orphan snoRNAs[20-23].

Canonical C/D box snoRNAs act as guide RNAs for the methyltransferase fibrillarin to its rRNA targets[1]. Although the DLK1-DIO3 snoRNAs have no known rRNA targets, we have shown previously that they do associate with fibrillarin[5], indicating that they guide canonical 2'Ome of non-canonical target RNAs. Here we found that AF357425/SNORD113-6 indeed guides fibrillarin-induced 2'Ome of mRNAs. Similar to the way microRNAs target mRNAs[36, 37], AF357425/SNORD113-6 appears to have many different mRNA targets. However, these targets do appear to be enriched within specific gene pathways, supporting the concept that AF357425/SNORD113-6 plays a specific role in cellular function. Here we focused on the integrin signalling pathway, as it showed the strongest enrichment and as it plays an obvious role in fibroblast function specifically and in cardiovascular disease in general[32]. However, we also observed enrichment in various other cardiovascular relevant pathways, including blood coagulation and interleukin signalling. We now looked only at targets affected by the D' box seed of AF357425/SNORD113-6, but of course both the murine and the human snoRNA have a second seed sequence [which is not fully conserved between species[28]] with its own set of mRNA targets. Furthermore, here we looked at only one of the 34 murine and 41 human DLK1-DIO3 snoRNAs. The total number of mRNAs and gene pathways affected by the DLK1-DIO3 snoRNAs can only be guessed at this stage.

Although the full function of 2'Ome remains to be elucidated, it has been reported that 2'Ome leads to stabilization of the affected RNA molecule[30, 31]. In fact, synthetic oligonucleotides, including our 3GAs and GMs, are often 2'Ome-modified to increase stability[38]. When we inhibited novel transcription by actinomycin D, we indeed observed increased mRNA degradation under snoRNA knockdown. AF357425/SNORD113-6-guided 2'Ome indeed contributes to mRNA stability of its targets. The effects on protein expression however were quite ambiguous. Even though *Itgb3* mRNA methylation and expression are

reduced and degradation increased under AF357425 inhibition, Itgb3 protein expression is significantly increased in murine cells. A previous study by Elliot *et al* has shown that 2'Ome of the mRNA can inhibit translation[25], however, the human ITGB3 protein expression was decreased under snoRNA, and thus 2'Ome inhibition, as expected from the mRNA levels. This can be explained by the fact that under SNORD113-6 inhibition, there is a pre-mRNA processing preference for the mRNA variant that is marked for NMD (Ensemble Genome Browser). Clearly, effects of snoRNA binding on protein expression depend on multiple factors, including the location of the binding site (e.g. intron versus 3'UTR) and on whether binding leads to 2'Ome or not. We show here that multiple mechanisms of snoRNA-pre-mRNA interactions and consequences occur simultaneously within the same pathway.

Therefore, more relevant than effects on individual protein expression are effects on cell phenotype as a whole. The DIO3-DLK1 locus is predominantly expressed in fibroblasts[3] and we have also shown previously that DLK1-DIO3 noncoding RNAs are highly relevant to fibroblast phenotype in a cardiovascular setting[11, 26, 39, 40]. We show here that the inhibition of SNORD113-6 alters the barrier function of primary human fibroblasts seeded in a monolayer, as well as the ability of fibroblast to contract the extracellular matrix, which are likely the direct consequences of changes in the integrin signalling pathway that plays a crucial role in fibroblast cell-cell and cell-matrix interactions[32]. Fibroblast integrin signalling is a crucial pathway in various forms of cardiovascular remodelling that can lead to severe cardiovascular disease[41]. Understanding the molecular mechanisms that underlie changes in integrin signalling during the progression of cardiovascular disease and cancer, may therefore yield novel therapeutic targets.

In conclusion, we show here that DLK1-DIO3 snoRNA AF357425/SNORD113-6 targets a broad range of mRNAs, via two distinct mechanisms, namely pre-mRNA processing/splicing and via 2'Ome, which has a stabilizing effect on mRNA expression. Although AF357425/SNORD113-6 has a broad range of target mRNAs, we do observe clear enrichment of several pathways that play an important role in the progression of cardiovascular disease. AF357425/SNORD113-6 may no longer be a complete 'orphan' snoRNA: however, more research into its remaining target RNAs, its second seed sequence and into the other DLK1-DIO3 snoRNAs remains to be done.

Materials and Methods

Cell culture

All cells were cultured in a humidified incubator at 37°C under 5% CO_2. Cells were grown to 70-90% confluency and subsequently passaged. Fresh culture media was added every 2-3 days.

Cell lines

Murine NIH/3T3 embryonic fibroblasts were cultured in DMEM (Invitrogen, GIBCO, Auckland, New Zealand), with 10% heat-inactivated foetal calf serum (FCS; PAA, Pasching, Austria) and 1% penicillin/streptomycin (PenStrep; Lonza, Basel, Switzerland, Cat.Nr.DE17-602E). Human BJ foreskin fibroblasts (ATCC, Manassas, VA, USA) were cultured in MEM (Invitrogen, GIBCO), with 10% heat-inactivated FCS and 1% PenStrep.

Primary murine fibroblasts (PMFs)

PMFs were isolated from ear-clippings of C57BL/6-J mice, about 3 weeks of age. Ear tissues were cut into smaller pieces and embedded in 0.2% gelatine in 10 cm^2 plates. After embedding, DMEM containing 20% heat-inactivated FCS and 1% non-essential amino acids (NEAA; Gibco, Thermo Fisher, MA, USA, Cat.Nr.11140050) was added and tissues were kept in an incubator at 37°C under 5% CO_2. After approximately 7 days, cells were expanded up to passage 3 using culture media (DMEM with 10% heat-inactivated FCS and 1% PenStrep) and frozen down in liquid nitrogen for later use. Cells were used up to passage 5.

Primary human umbilical arterial fibroblasts (HUAFs)

Umbilical cords were collected from full-term pregnancies and stored in sterile PBS at 4°C and subsequently used for cell isolation within 7 days. The arteries were removed and cleaned from remaining connective tissue. Endothelial cells were removed by gently rolling the artery over a blunted needle. The tunica adventitia and tunica media were separated using surgical forceps. After overnight incubation in HUAF culture medium, (DMEM GlutaMAX™, 10% heat-inactivated FCS, 10% heat-inactivated human serum (PAA, Pasching, Austria), 1% PenStrep and 1% NEAA, the tunica adventitia was incubated in a 2mg/ml collagenase type II solution (Worthington; OH, USA, Cat.Nr.NC9693955) at 37 °C. Cell suspensions were filtered over a 70 µm cell strainer and centrifuged at 400g for 10 minutes. Cell pellets were resuspended and plated in culture medium. To remove slow-adhering non-fibroblast cells, the wells were washed with culture medium after 90 minutes. HUAFs were then cultured and used up to passage 6.

RNA isolation and RT/qPCR

For RNA isolation, culture media was removed and cells were washed in PBS. After that, cells were lysed with TRIzol (Thermo Fisher, MA, USA, Cat.Nr.15596026) and RNA was isolated by standard TRIzol-chloroform extraction. RNA concentration and purity were measured using Nanodrop (Nanodrop Technologies, DE, USA) or the Bioanalyzer (2100 Bioanalyzer Instrument, Agilent, CA, USA).

RNA was reverse transcribed using high-capacity RNA-to-cDNA reverse transcription kit (Applied Biosystems, Thermo Fisher, MA, USA, Cat.Nr.4388950) or the GoScript RT system (Promega) and quantified using Quantitect SybrGreen reagents (Qiagen Benelux, Venlo, the Netherlands, Cat.Nr.204145) on the VIIa7 (ThermoFisher, MA, USA, Cat.Nr.15596026) or using the GoTaq qPCR Master Mix (Promega) on the CFX384 Real-Time System (BioRad). SnoRNA and mRNA expression were normalized to U6 and GAPDH using the $2^{-\Delta Ct}$ method, respectively. All primers used are provided in Supplemental Table 1.

CRISPR/Cas9 of AF357425

We used the commercially available GeneArt CRISPR nuclease vector with OFP reporter (Invitrogen, ThermoFisher Scientific) to knock out AF357425. When using a single guide RNA did not yield any, surviving, knockout or mutant clones, we used a combination of four guide RNAs, two directed to the positive strand of the AF357425 gene and two directed to the negative strand. Guide RNAs were ordered as two separate DNA oligonucleotides each from Microsynth (Balgach, Switzerland), which were annealed in nuclease-free water using a thermal cycler, starting at 95°C for five minutes, and then decreasing the temperature in 5° steps for one minute each, until 10°C. The guide RNA sequences were then cloned into the GeneArt CRISPR nuclease vector, according to manufacturer's protocol and clones were checked for inserts using colony PCR. Positive clones were isolated using the PureYield Plasmid Miniprep System (Promega) followed by Sanger Sequencing (Microsynth). For each guide RNA, one clone containing the full and correct sequence was then grown overnight and the vector was purified using the PureYield Plasmid Midiprep System (Promega). Vectors containing the four different guide RNA sequences were then mixed in a 1:1:1:1 ratio. A separate, single, guide RNA was designed and cloned into the GeneArt CRISPR nuclease vector in order to knock out the mutant AF357425 in the BF6 clone. Guide RNA sequences are provided in Supplemental Table 2.

3T3 cells were transfected with the vector mix at a final concentration of 1 µg/µL, using the Calcium Phosphate Transfection Kit (Sigma-Aldrich) according to the manufacturer's

protocol. After 24 hours, the transfection medium was replaced by conditioned growth medium (medium collected from untransfected 3T3 cells after 24 hours of culture) and after another 24 hours, cells were trypsinised and replated in 96-well culture plates, using a serial dilution in conditioned medium. Wells containing a single cell were identified by visual inspection 24-48 hours after replating and left to grow into colonies. The presence of mutations in the AF357425 gene was verified using Sanger sequencing and AF357425 expression was checked by rt/qPCR. All primer sequences can be found in Supplemental Table 1.

Analysis of the BF6 clone

In order to obtain the DNA sequences of the heterozygous mutant BF6 clone, primers surrounding the AF357425 gene were used to amplify the BF6 AF357425 genes, which were cloned into the pCR2.1 vector, using the TA cloning kit (Invitrogen by Life Technologies) following the manufacturer's protocol. Clones were checked for inserts using colony PCR. PCR products were separated on a 3% agarose gel, to visualize longer and shorter inserts. One long and one short insert were analysed by Sanger sequencing to obtain sequence information on the two differently mutated alleles.

3GAs and GMs

3GAs were kindly provided by Idera Pharmaceuticals (Cambridge, MA, USA). 3GAs are made up of two identical strands of DNA-nucleotides with a phosphorothioate backbone, connected by a 5' phosphorothioate linker. GM consisted of five 2'Ome RNA-nucleotides, ten DNA-nucleotides and five more 2'Ome RNA-nucleotides with full phosphorothioate backbone, were custom designed and ordered from (Sigma Aldrich, MO, USA, or MicroSynth AG, Balgach, Switzerland). Sequences of 3GAs and GM are shown in Supplemental Table 3.

Transfection with 3GAs or GM

In order to synchronise the cell cycle, cells were treated with KN-93 (Sigma Aldrich, MO, USA, Cat.Nr.K1385), an inhibitor of CaMK-II (the multifunctional Ca2+/CaM kinase), to induce G1 cell cycle arrest[34]. KN-93 was added to the culture media (DMEM, 10% FCS and 1% P/S) at a concentration of 10 μM. After 48 hours, cells were washed with PBS and DMEM or MEM, depending on the cell type, without serum or PenStrep was added. Lipofectamine RNAiMAX Reagent (ThermoFisher, MA, USA, Cat.Nr.13778030) was used to create micelles loaded with 3GAs (200 nM) or GM (500 nM) against snoRNA AF357425 for transfection. 10% FCS was added to the cells after 1 hour of transfection. After 24 hours of transfection, cells were washed with PBS and used for further experiments and analyses.

RNA binding protein immunoprecipitation

RIP was performed using the EZMagna RIP kit (Millipore, Sigma Aldrich, MO, USA, Cat.Nr.17-701) according to the manufacturer's protocol. All steps were performed on ice and with prechilled buffers. In brief, GM and 3GA transfected PMFs were washed with PBS twice, trypsinised and centrifuged for 5 min at 1500 rpm to form a pellet. Cell pellets were resuspended in 0.1% formaldehyde in order to crosslink the RNA-protein interactions. After crosslinking, cells were centrifuged and pellets were resuspended in complete RIP lysis buffer. Next, cell lysates were incubated with magnetic beads conjugated with antibodies against fibrillarin (Abcam, Cambridge, UK Cat.Nr.ab5821) or a rabbit control IgG antibody (Millipore, Cat.Nr.PP64B) overnight at 4°C rotating. Prior to incubation with magnetic beads, 10% of the cell lysate was kept separate as an input reference for the immunoprecipitation. Samples with beads were placed in a magnetic separator before aspirating the supernatant. After 6 washing steps with RIP washing buffer, samples were treated with proteinase K for 30 minutes at 55°C while shaking. Next, samples were placed in a magnetic separator and the supernatant was further diluted to a final volume of 250 µl in RNAse free water. RNA was isolated using TRIzol LS Reagent (ThermoFisher, MA, USA, Cat.Nr.10296010) for liquid solutions. RNA concentration and purity were measured on the Nanodrop (Nanodrop Technologies) and Bioanalyzer prior to sending them for RNA sequencing.

RNA-Seq and analysis

RNA-Seq was outsourced to BGI (Hong Kong). DNBseq Eukaryotic Transcriptome resequencing was performed on the BGISEQ platform with PE100. We performed RNA-Seq, both on total RNA isolated from GM versus 3GA transfected PMFs and on the RNA isolated after the fibrillarin RIP. In the latter case, BGI performed an rRNA depletion step before sequencing.

Raw FASTQ files of long RNAseq samples and RIP-Seq samples were processed using the LUMC BioWDL RNAseq pipeline version 1.1.0 (https://github.com/biowdl/RNA-seq/tree/v1.1.0), which comprises FASTQ preprocessing, alignment and read quantification. Cutadapt (version 2.4) was used for adapters clipping. Reads were further aligned to the mouse reference genome GRCm38 using the STAR aligner (version 2.6.0c). Gene raw read quantification was performed using htseq-count (v0.9.1) with the Ensembl mouse gene annotation version 96. Only uniquely mapped reads are included. In addition, StringTie (v1.3.4) was used to calculate transcripts per million (TPM) of all genes with default settings.

For the long RNA-Seq, BLAST was used to identify 192 genes with a perfect conserved D' box seed antisense sequence AAACCCCAT in the coding region and 3' untranslated region (3'UTR). TPM values of these genes, generated from the long RNA seq. Genes without variants or genes which were not expressed in long RNA-Seq, were removed from the analysis.

In order to identify all potential targeted mRNAs, we downloaded mouse cDNA sequences from Ensembl FTP and identified all transcripts containing motif sequence AAACCCCAT using a customized Python script. To tolerate binding efficiency, we allowed one base mismatch in the first three bases and last three bases of this motif sequence. By crosschecking these potential binding transcripts with the genes with an increased expression, thus enriched in 3GA (high AF357425) versus GM (low AF357425) in the RIP-Seq samples (fold change expression >1), we identified 407 mouse genes of interest. We converted these murine genes to equivalent human genes, 285 in total. Using the same Python script, we identified 228 out of 285 human genes containing the motif sequence of AAACCCCAT and six of its variants (by allowing one base mismatch in the first three bases and last three bases of this motif sequence). Finally, we performed pathway enrichment analysis on the remaining set of potential target genes using PANTHER Classification System (v.16.0).

The RIP-Seq data were used to identify potential 2'Ome targets of the snoRNA, whereas the normal RNA-Seq was use to compare counts of different transcript variants (as published by Ensembl) within genes, in order to identify changes in mRNA splicing and 3'-end processing.

Detection and estimation of 2'Ome of RNA targets

For the detection of 2'-O-methylated nucleotides we used an adaptation of the RTL-Q method that was first described by *Dong et al*[26, 42]. Briefly, specific RT primers were designed around the site of interest. One forward primer was designed upstream of the possible methylation site (F_U) and one downstream of the methylation site (F_D). One reverse primer (R) was used for both F_U and F_D. The RT reaction was performed in two consecutive steps. First, a mixture of 20 ng RNA and 10 µM reverse primer was denatured at 70^{o}C for 5 minutes and incubated at 42^{o}C for 10 minutes as an initial annealing step. Then, a high (200 µM) or low (0,5 µM) concentration of dNTPs (Promega, Cat.Nr.U1511), 200U of M-MLV reverse transcriptase (Promega, Cat.Nr. M1705) and 20U of Recombinant RNasin Ribonuclease Inhibitor (Promega, Cat.Nr. N2515) added to the RT reaction. The RT reaction was incubated at 42^{o}C for 90 minutes followed by incubation at 75^{o}C for 15 minutes to deactivate the enzyme. Differences in primer extension efficiency were quantified using

SYBR green-based qPCR. To calculate the Estimated Methylated Fraction (EMF), we used an adaptation to the method described by Aschenbrenner et al[43].

$$Estimated\ Methylated\ fraction = 1 - E^{-\left(\Delta Ct_{\ FW-U\ (Low\ conc.-\ High\ conc.)} - \Delta Ct_{\ FW-D\ (Low\ conc.-\ High\ conc.)}\right)}$$

$$with\ E\ =\ PCR\ efficiency\ of\ FW-D\ at\ high\ dNTP\ concentration$$

Detection of processing/splicing variants

Differences in ratios between splice- and 3'-end processing variants of individual putative target genes were quantified using RT/qPCR. Where possible, we used the same forward primer, with a variable reverse primer in order to pick up the different variants. All primers are provided in Supplemental Table 1. We used Ensemble Genome Browser to look up transcript variants in the human genome (GRCh38.p13) and murine genome (GRCm39). Variants with or without AF357425/SNORD113-6 binding site were named variant 1 or variant 2, respectively (Supplemental Figure 2). Only relevant transcripts either with or without binding sites are shown. Ratio was calculated as variant 2 divided by variant 1. Of note, the product variant 2 is the sum of variant 1 and 2, as primers designed for variant 2 target exons/introns present in both variants, except for human *MAP2K1*, *DUSP7* and *EBPL* and murine *Dusp7*, for which both variants were measured with fully separate primer sets (Supplemental Table 1).

Western blotting

Cells were washed with PBS and lysed using liquid nitrogen. Proteins were denatured using Laemmli buffer (2x buffer: 0.125 M Tris base, 4% SDS, 20% glycerol, 10% beta-mercaptoethanol, 2mg bromophenol blue per ml buffer, pH approx. 6.8) and loaded onto Mini-PROTEAN® TGX™ Precast Protein gels (10-15%, Bio-Rad). After separation, proteins were transferred onto polyvinylidene difluoride membranes (0,45µm, Carl Roth). Membranes were blocked in 5% Non-Fat Milk buffer (BioRad) for 1 hour at room temperature and probed with the primary antibodies overnight at 4°C. The following primary antibodies were used:), rabbit polyclonal anti-MEK-1 ((MAP2K1) 1:1000, PA5-16556, Invitrogen, Thermo Fisher Scientific), rabbit polyclonal anti-CD61 ((ITGB3) 1:1000, PA5-85926, Invitrogen, Thermo Fisher Scientific), rabbit polyclonal anti-JAG1 (1:1000, PA5-72843, Invitrogen, Thermo Fisher Scientific), rabbit polyclonal anti-DUSP7 (1:1000,PA5-100490, Invitrogen, Thermo Fisher Scientific) and rabbit polyclonal anti-GAPDH (1:10.000-20.000, PA1-987, Invitrogen, Thermo Fisher Scientific). Membranes were washed with 0.1% Tween 20 PBS (PBST) and probed with the secondary HRP-conjugated anti-rabbit IgG

antibody (1:2500-5000) at room temperature for 2 hours. Protein levels were detected using chemiluminescence by SuperSignal West Femto Maximum Sensity Substrate (Invitrogen, Thermo Fisher Scientific). Intensities of the obtained signals were normalized to the intensities of the GAPDH control bands.

mRNA stability

In order to measure effects on mRNA stability, HUAFs and PMFs were treated with 10 µM KN-93 for 48 h and subsequently transfected with GMs against SNORD-113-6 or AF357425, respectively, or a negative control, as described earlier. After 24 h, cells were treated with 5 µg/µl Actinomycin D (Sigma Aldrich, Cat.Nr.A9415), to inhibit novel RNA transcription. We then measured mRNA expression at 2 (T2) and 6 (T6) hours after addition of Actinomycin D and calculated the decline in mRNA over time (T6-T2).

Fibroblast barrier function

Electric cell-substrate impedance sensing (ECIS, Model 1600R, Applied Biophysics, NY, USA) is a method to quantify cell function over time. Cells are seeded on an electrode and impedance is then used as a measure of electrode coverage, cell number and cell attachment[44]. For this assay 8 well/10 electrode plates were used (Ibidi, Gräfelfing, Germany, Cat.Nr.72010). Prior to seeding cells, electrodes were coated with 10 nM l-cysteine (Sigma, Steinheim, Germany, 30089-25G) and 1% gelatine (Merck, Darmstadt, Germany, 1040700500). Fibroblasts were collected 24 hours after KN-93 treatment and GM transfection and seeded at a density of 50.000 cells per well in DMEM (+10% FCS and 1% PenStrep). Impedance was measured over time at multiple frequencies 62-64000 Hz).

Collagen gel contraction

Extracellular matrix contraction was simulated by embedding fibroblasts in a collagen lattice gel as described by Ngo *et al*[45]. GM-transfected HUAFs were suspended in a 2 mg/mL collagen type I (Millipore, Sigma Aldrich, MO, USA, Cat.Nr.08-115) solution at a concentration of 1.5 x 10^5 cells/mL, together with 10 µM KN-93. We then poured 350 µL collagen gels in a 48-well plate and allowed the gels to solidify for 20 minutes at room temperature. Gels were dissociated from the mould and resuspended in DMEM (+10% FCS and 1% PenStrep). Pictures were taken at 0 (T0), 24 (T24) and 48 hours (T48) after dissociation, and contraction was analysed using ImageJ software (National Institutes of Health, Bethesda, Maryland, USA, https://imagej.nih.gov/ij/, 1997-2018).

Scratch wound healing assay

In order to investigate cell migration, HUAFs were treated with 10 µM KN-93 for 48 hours and subsequently transfected with GM against SNORD-113-6 or a negative control, as described earlier. A total of 24 h after transfection, a scratch was introduced by scraping a straight line using a p200 pipet tip in the cell monolayer. Cells were washed with PBS to remove any debris. Cells were incubated for 24 h in culture medium containing 10 µM KN-93 to inhibit cell proliferation. Pictures were taken under a phase-contrast microscope at 0 (T0) and 24 (T24) hours after introducing the scratch. Cell migration was analysed using ImageJ software (National Institutes of Health, Bethesda, Maryland, USA, https://imagej.nih.gov/ij/, 1997-2018).

Statistical analyses

Results are expressed as mean ± standard error of the mean (SEM). As knockdown efficiency varied per experiment, we performed paired t-tests to compare each treatment with its own control, within each individual experiment. Graphpad (v.8.4.2) was used to perform all statistical analyses. $P<0.05$ was considered significant and $P<0.1$ was considered a trend.

Data availability

All data are available in the main manuscript or in the Supplemental Material. RNA-Seq data are also available in the GEO under accession number GSE173099.

Acknowledgements

We kindly acknowledge Neda Ektefaie, Bart Boersma, Martijn Willemsen and Pleun Engbers for their technical support.

Funding

The study was supported by funding from the Rembrandt Institute of Cardiovascular Science (A.Y. Nossent and R.A. Boon) and the Austrian Science Fund FWF (A.Y. Nossent, Lise Meitner grant M2578-B30).

Author Contributions

EvI, DALvdH, VK, and NPM performed experiments, MLvdB and HM performed RNA-Seq data analyses, RAB and AYN designed experiments, EvI, DALvdH and AYN wrote the manuscript, RAB, PHAQ and JW critically reviewed the manuscript, RAB and AYN acquired funding.

Conflict of Interest

There are no conflicts of interest.

Abbreviations

DMRs: differentially methylated regions; ECIS: electric cell-substrate impedance sensing; FCS: fetal calf serum; 3GA: 3rd Generation Antisense oligonucleotides; GM: Gapmers; HUAFs: human umbilical arterial fibroblasts; lncRNAs: long noncoding RNAs; NEAA: non-essential amino acids; 2'Ome: 2'O-ribose methylation; PenStrep: penicillin/streptomycin; PMFs: primary murine fibroblasts; RIP: RNA-binding protein immunoprecipitation; rRNAs: ribosomal RNAs; RTL-Q: Reverse Transcription at Low dNTP concentration followed by Quantitative PCR; SEM: standard error of the mean; snoRNAs: small nucleolar RNAs; snoRNP: small nucleolar ribonucleoprotein complex; TPM: transcripts per million; 3'UTR: 3' untranslated region; Ψ: pseudouridylation.

References

1. Kiss, T. (2001). Small nucleolar RNA-guided post-transcriptional modification of cellular RNAs. *EMBO J* **20**: 3617-3622.
2. Monaco, P.L., Marcel, V., Diaz, J.J., and Catez, F. (2018). 2'-O-Methylation of Ribosomal RNA: Towards an Epitranscriptomic Control of Translation? *Biomolecules* **8**.
3. Jorjani, H., Kehr, S., Jedlinski, D.J., Gumienny, R., Hertel, J., Stadler, P.F., Zavolan, M., and Gruber, A.R. (2016). An updated human snoRNAome. *Nucleic Acids Res* **44**: 5068-5082.
4. Falaleeva, M., Welden, J.R., Duncan, M.J., and Stamm, S. (2017). C/D-box snoRNAs form methylating and non-methylating ribonucleoprotein complexes: Old dogs show new tricks. *Bioessays* **39**.
5. Håkansson, K.E.J., Goossens, E.A.C., Trompet, S., van Ingen, E., de Vries, M.R., van der Kwast, R., Ripa, R.S., Kastrup, J., Hohensinner, P.J., Kaun, C., et al. (2019). Genetic associations and regulation of expression indicate an independent role for 14q32 snoRNAs in human cardiovascular disease. *Cardiovascular research* **115**: 1519-1532.
6. Lin, S.P., Youngson, N., Takada, S., Seitz, H., Reik, W., Paulsen, M., Cavaille, J., and Ferguson-Smith, A.C. (2003). Asymmetric regulation of imprinting on the maternal and paternal chromosomes at the Dlk1-Gtl2 imprinted cluster on mouse chromosome 12. *Nat Genet* **35**: 97-102.
7. Boon, R.A., Hofmann, P., Michalik, K.M., Lozano-Vidal, N., Berghauser, D., Fischer, A., Knau, A., Jae, N., Schurmann, C., and Dimmeler, S. (2016). Long Noncoding RNA Meg3 Controls Endothelial Cell Aging and Function: Implications for Regenerative Angiogenesis. *J Am Coll Cardiol* **68**: 2589-2591.
8. Michalik, K.M., You, X., Manavski, Y., Doddaballapur, A., Zornig, M., Braun, T., John, D., Ponomareva, Y., Chen, W., Uchida, S., et al. (2014). Long Noncoding RNA MALAT1 Regulates Endothelial Cell Function and Vessel Growth. *Circ Res* **114**: 1389-1397.
9. Nossent, A.Y., Eskildsen, T.V., Andersen, L.B., Bie, P., Bronnum, H., Schneider, M., Andersen, D.C., Welten, S.M., Jeppesen, P.L., Hamming, J.F., et al. (2013). The 14q32 microRNA-487b targets the antiapoptotic insulin receptor substrate 1 in hypertension-induced remodeling of the aorta. *Ann Surg* **258**: 743-751; discussion 752-743.
10. van Ingen, E., Foks, A.C., Kroner, M.J., Kuiper, J., Quax, P.H.A., Bot, I., and Nossent, A.Y. (2019). Antisense Oligonucleotide Inhibition of MicroRNA-494 Halts Atherosclerotic Plaque Progression and Promotes Plaque Stabilization. *Molecular therapy Nucleic acids* **18**: 638-649.
11. Welten, S.M., Bastiaansen, A.J., de Jong, R.C., de Vries, M.R., Peters, E.A., Boonstra, M.C., Sheikh, S.P., La Monica, N., Kandimalla, E.R., Quax, P.H., et al. (2014). Inhibition of 14q32 MicroRNAs miR-329, miR-487b, miR-494, and miR-495 increases neovascularization and blood flow recovery after ischemia. *Circulation research* **115**: 696-708.
12. Welten, S.M., Goossens, E.A., Quax, P.H., and Nossent, A.Y. (2016). The multifactorial nature of microRNAs in vascular remodelling. *Cardiovascular research* **110**: 6-22.
13. Welten, S.M.J., de Jong, R.C.M., Wezel, A., de Vries, M.R., Boonstra, M.C., Parma, L., Jukema, J.W., van der Sluis, T.C., Arens, R., Bot, I., et al. (2017). Inhibition of 14q32 microRNA miR-495 reduces lesion formation, intimal hyperplasia and plasma cholesterol levels in experimental restenosis. *Atherosclerosis* **261**: 26-36.
14. Welten, S.M.J., de Vries, M.R., Peters, E.A.B., Agrawal, S., Quax, P.H.A., and Nossent, A.Y. (2017). Inhibition of Mef2a Enhances Neovascularization via Post-transcriptional Regulation of 14q32 MicroRNAs miR-329 and miR-494. *Molecular therapy Nucleic acids* **7**: 61-70.
15. Wezel, A., Welten, S.M., Razawy, W., Lagraauw, H.M., de Vries, M.R., Goossens, E.A., Boonstra, M.C., Hamming, J.F., Kandimalla, E.R., Kuiper, J., et al. (2015). Inhibition of MicroRNA-494 Reduces Carotid Artery Atherosclerotic Lesion Development and Increases Plaque Stability. *Annals of surgery* **262**: 841-847; discussion 847-848.
16. Cavaille, J., Seitz, H., Paulsen, M., Ferguson-Smith, A.C., and Bachellerie, J.P. (2002). Identification of tandemly-repeated C/D snoRNA genes at the imprinted human 14q32

domain reminiscent of those at the Prader-Willi/Angelman syndrome region. *Hum Mol Genet* **11**: 1527-1538.
17. Cavaille, J., Buiting, K., Kiefmann, M., Lalande, M., Brannan, C.I., Horsthemke, B., Bachellerie, J.P., Brosius, J., and Huttenhofer, A. (2000). Identification of brain-specific and imprinted small nucleolar RNA genes exhibiting an unusual genomic organization. *Proceedings of the National Academy of Sciences of the United States of America* **97**: 14311-14316.
18. Bortolin-Cavaillé, M.L., and Cavaillé, J. (2012). The SNORD115 (H/MBII-52) and SNORD116 (H/MBII-85) gene clusters at the imprinted Prader-Willi locus generate canonical box C/D snoRNAs. *Nucleic Acids Res* **40**: 6800-6807.
19. Prasasya, R., Grotheer, K.V., Siracusa, L.D., and Bartolomei, M.S. (2020). Temple syndrome and Kagami-Ogata syndrome: clinical presentations, genotypes, models and mechanisms. *Hum Mol Genet* **29**: R107-R116.
20. Kishore, S., Khanna, A., Zhang, Z., Hui, J., Balwierz, P.J., Stefan, M., Beach, C., Nicholls, R.D., Zavolan, M., and Stamm, S. (2010). The snoRNA MBII-52 (SNORD 115) is processed into smaller RNAs and regulates alternative splicing. *Hum Mol Genet* **19**: 1153-1164.
21. Kishore, S., and Stamm, S. (2006). Regulation of alternative splicing by snoRNAs. *Cold Spring Harb Symp Quant Biol* **71**: 329-334.
22. Kishore, S., and Stamm, S. (2006). The snoRNA HBII-52 regulates alternative splicing of the serotonin receptor 2C. *Science* **311**: 230-232.
23. Falaleeva, M., Pages, A., Matuszek, Z., Hidmi, S., Agranat-Tamir, L., Korotkov, K., Nevo, Y., Eyras, E., Sperling, R., and Stamm, S. (2016). Dual function of C/D box small nucleolar RNAs in rRNA modification and alternative pre-mRNA splicing. *Proceedings of the National Academy of Sciences of the United States of America* **113**: E1625-1634.
24. Huang, C., Shi, J., Guo, Y., Huang, W., Huang, S., Ming, S., Wu, X., Zhang, R., Ding, J., Zhao, W., et al. (2017). A snoRNA modulates mRNA 3' end processing and regulates the expression of a subset of mRNAs. *Nucleic Acids Res* **45**: 8647-8660.
25. Elliott, B.A., Ho, H.T., Ranganathan, S.V., Vangaveti, S., Ilkayeva, O., Abou Assi, H., Choi, A.K., Agris, P.F., and Holley, C.L. (2019). Modification of messenger RNA by 2'-O-methylation regulates gene expression in vivo. *Nature communications* **10**: 3401.
26. van der Kwast, R., van Ingen, E., Parma, L., Peters, H.A.B., Quax, P.H.A., and Nossent, A.Y. (2018). Adenosine-to-Inosine Editing of MicroRNA-487b Alters Target Gene Selection After Ischemia and Promotes Neovascularization. *Circulation research* **122**: 444-456.
27. Brameier, M., Herwig, A., Reinhardt, R., Walter, L., and Gruber, J. (2011). Human box C/D snoRNAs with miRNA like functions: expanding the range of regulatory RNAs. *Nucleic Acids Res* **39**: 675-686.
28. Håkansson, K.E.J., Sollie, O., Simons, K.H., Quax, P.H.A., Jensen, J., and Nossent, A.Y. (2018). Circulating Small Non-coding RNAs as Biomarkers for Recovery After Exhaustive or Repetitive Exercise. *Front Physiol* **9**: 1136.
29. Ploner, A., Ploner, C., Lukasser, M., Niederegger, H., and Huttenhofer, A. (2009). Methodological obstacles in knocking down small noncoding RNAs. *RNA* **15**: 1797-1804.
30. Ji, L., and Chen, X. (2012). Regulation of small RNA stability: methylation and beyond. *Cell Res* **22**: 624-636.
31. Motorin, Y., and Helm, M. (2010). tRNA stabilization by modified nucleotides. *Biochemistry* **49**: 4934-4944.
32. Jang, Y., Lincoff, A.M., Plow, E.F., and Topol, E.J. (1994). Cell adhesion molecules in coronary artery disease. *J Am Coll Cardiol* **24**: 1591-1601.
33. Filippova, J.A., Matveeva, A.M., Zhuravlev, E.S., Balakhonova, E.A., Prokhorova, D.V., Malanin, S.J., Shah Mahmud, R., Grigoryeva, T.V., Anufrieva, K.S., Semenov, D.V., et al. (2019). Are Small Nucleolar RNAs "CRISPRable"? A Report on Box C/D Small Nucleolar RNA Editing in Human Cells. *Front Pharmacol* **10**: 1246.

34. Tombes, R.M., Grant, S., Westin, E.H., and Krystal, G. (1995). G1 cell cycle arrest and apoptosis are induced in NIH 3T3 cells by KN-93, an inhibitor of CaMK-II (the multifunctional Ca2+/CaM kinase). *Cell Growth Differ* **6**: 1063-1070.
35. Downie Ruiz Velasco, A., Welten, S.M.J., Goossens, E.A.C., Quax, P.H.A., Rappsilber, J., Michlewski, G., and Nossent, A.Y. (2019). Posttranscriptional Regulation of 14q32 MicroRNAs by the CIRBP and HADHB during Vascular Regeneration after Ischemia. *Molecular therapy Nucleic acids* **14**: 329-338.
36. Bartel, D.P. (2004). MicroRNAs: genomics, biogenesis, mechanism, and function. *Cell* **116**: 281-297.
37. van, R.E., and Olson, E.N. (2012). MicroRNA therapeutics for cardiovascular disease: opportunities and obstacles. *Nat Rev Drug Discov* **11**: 860-872.
38. Yu, D., Iyer, R.P., Shaw, D.R., Lisziewicz, J., Li, Y., Jiang, Z., Roskey, A., and Agrawal, S. (1996). Hybrid oligonucleotides: synthesis, biophysical properties, stability studies, and biological activity. *Bioorg Med Chem* **4**: 1685-1692.
39. van der Kwast, R., Parma, L., van der Bent, M.L., van Ingen, E., Baganha, F., Peters, H.A.B., Goossens, E.A.C., Simons, K.H., Palmen, M., de Vries, M.R., et al. (2020). Adenosine-to-Inosine Editing of Vasoactive MicroRNAs Alters Their Targetome and Function in Ischemia. *Molecular therapy Nucleic acids* **21**: 932-953.
40. van der Kwast, R., Quax, P.H.A., and Nossent, A.Y. (2019). An Emerging Role for isomiRs and the microRNA Epitranscriptome in Neovascularization. *Cells* **9**.
41. Civitarese, R.A., Kapus, A., McCulloch, C.A., and Connelly, K.A. (2017). Role of integrins in mediating cardiac fibroblast-cardiomyocyte cross talk: a dynamic relationship in cardiac biology and pathophysiology. *Basic Res Cardiol* **112**: 6.
42. Dong, Z.W., Shao, P., Diao, L.T., Zhou, H., Yu, C.H., and Qu, L.H. (2012). RTL-P: a sensitive approach for detecting sites of 2'-O-methylation in RNA molecules. *Nucleic Acids Res* **40**: e157.
43. Aschenbrenner, J., and Marx, A. (2016). Direct and site-specific quantification of RNA 2'-O-methylation by PCR with an engineered DNA polymerase. *Nucleic Acids Res* **44**: 3495-3502.
44. Szulcek, R., Bogaard, H.J., and van Nieuw Amerongen, G.P. (2014). Electric cell-substrate impedance sensing for the quantification of endothelial proliferation, barrier function, and motility. *J Vis Exp*.
45. Ngo, P., Ramalingam, P., Phillips, J.A., and Furuta, G.T. (2006). Collagen gel contraction assay. *Methods Mol Biol* **341**: 103-109.

Supplementary data

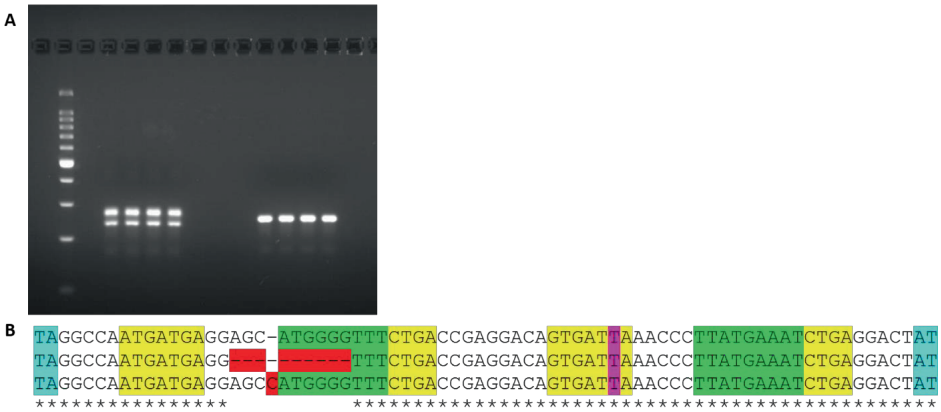

Supplemental Figure 1. BF6 Clone. (A) 2.5% Agarose gel with AF357425 PCR-product for Wildtype 3T3 (left four wells) and the BF6 clone (right four wells). (B) DNA Sequences of wildtype 3T3 (top line), BF6-short allele (middle line) and BF6-long allele (bottom line). Marked in blue are the self-binding ends of the snoRNA, marked in yellow from left to right the C box, D' box, C' box and D box, in green from left to right the D' box seed and the D box seed and in red the CRISPR/Cas9 induced in/dels. Stars mark full complementarity between sequences.

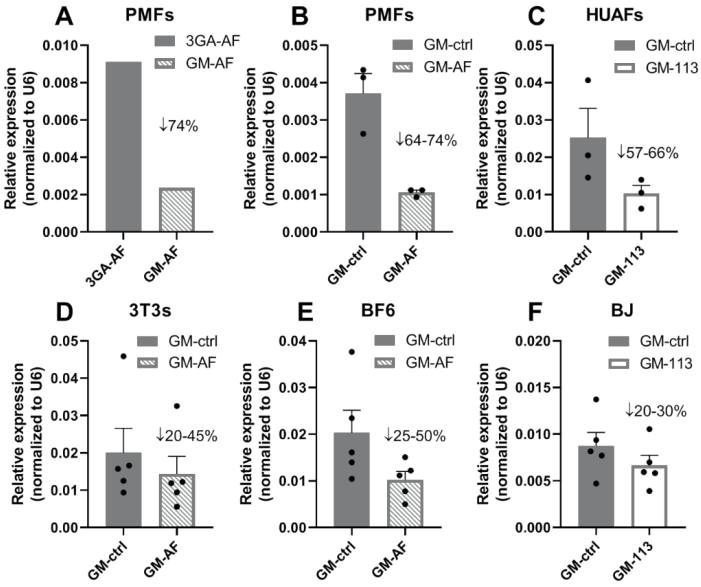

Supplemental Figure 2. SnoRNA overexpression and knockdown in primary cells and cell lines after 24 hours of transfection. (A) Relative AF357425 expression in primary murine fibroblasts (PMFs) treated with 3rd Generation Antisense (3GA) for overexpression or Gapmers against AF357425 (GM-AF) for inhibition. (B) Relative AF357425 expression in primary cells PMFs treated with Gapmer control (GM-ctrl) or GM-AF and (C) human umbilical arterial fibroblasts (HUAFs) treated with GM-ctrl or Gapmers against SNORD113-6 (GM-113). Relative AF357425 expression in cell lines (D) 3T3 and (E) BF6 and SNORD113-6 expression in (F) BJ cells treated with either GM-ctrl or GM-AF/113. Expression levels are relative to U6. Data are represented as mean ±SEM.

Supplemental Figure 3 Overview of all AF357425/SNORD113-6 binding sites located in (pre-)mRNAs

AF357425 (AF25)/SNORD113-6 binding sites in both human and murine variants are shown. Ensemble Genome Browser was used to define transcript variants in the human genome (GRCh38.p13) and murine genome (GRCm39). Ensemble transcript names are provided for each transcript. 2'O methylation (2'Ome) sites in exons, introns or 3' untranslated region (3'UTR) are shown as an asterisk. A zoom-in image shows the sequence of the binding site, a perfect sequence or with one mismatch, except for the middle three nucleotides. 2'Ome primers were designed around the sites shown as a zoom-in image. Only relevant transcripts either with or without binding sites are shown. Location of primer binding sites for quantification of the different variants are indicated by arrows (forward F and reversed R).

Jagged canonical Notch ligand 1 (JAG1)

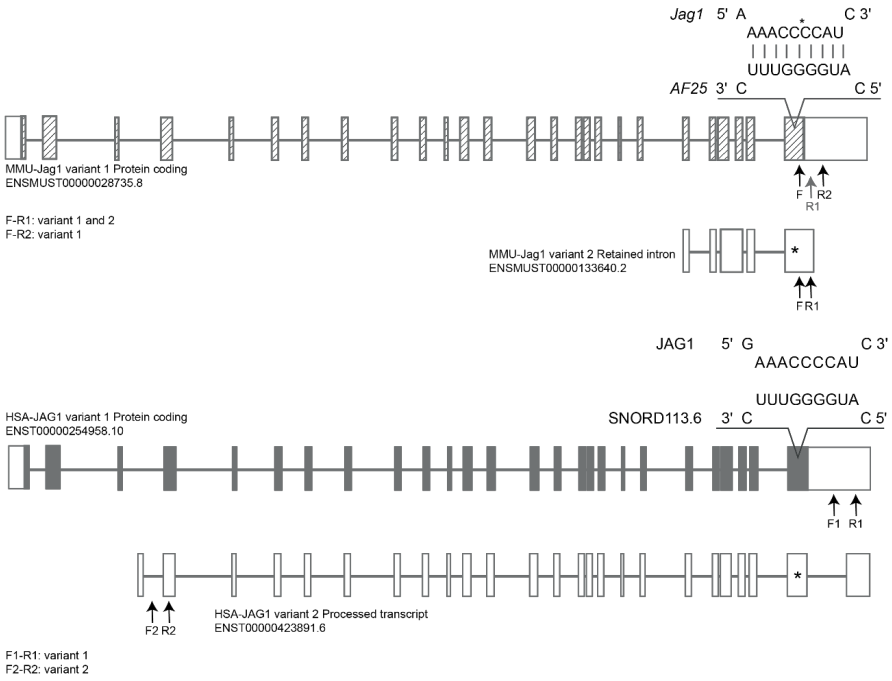

(Top) Murine *Jag1* variant 1 with a AF25 binding site located in the last exon and variant 2 with a binding site located in a retained intron (not protein coding).

(Bottom) Human *JAG1* variant 1 with a perfect SNORD113.6 binding site located in the last exon and variant 2 with the same binding site in a processed transcript (not protein coding).

Dual specificity phosphatase 7 (DUSP7)

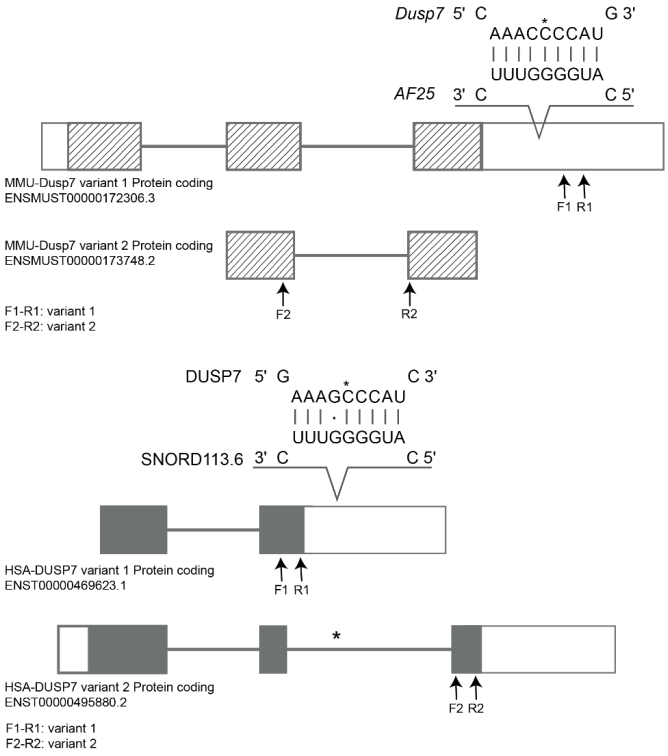

(Top) Murine *Dusp7* variant 1 with a AF25 binding site located in the 3'UTR and variant 2 without a binding site.

(Bottom) Human *DUSP7* variant 1 with a perfect SNORD113.6 binding site located in 3'UTR and variant 2 with a binding site in the last intron.

Emopamil binding protein-like (EBPL)

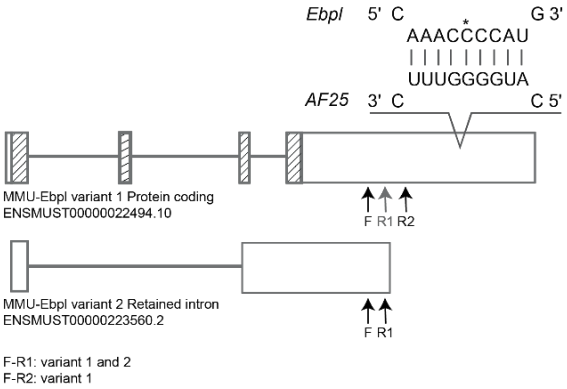

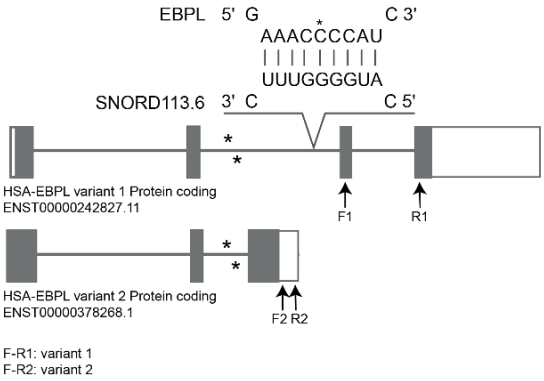

(Top) Murine *Ebpl* variant 1 with a AF25 binding site located in 3'UTR and variant 2 without a binding site (not protein coding).

(Bottom) Human *EBPL* variant 1 with three perfect SNORD113.6 binding sites located in the second intron and variant 2 without a third binding site.

Integrin beta 3 (ITGB3)

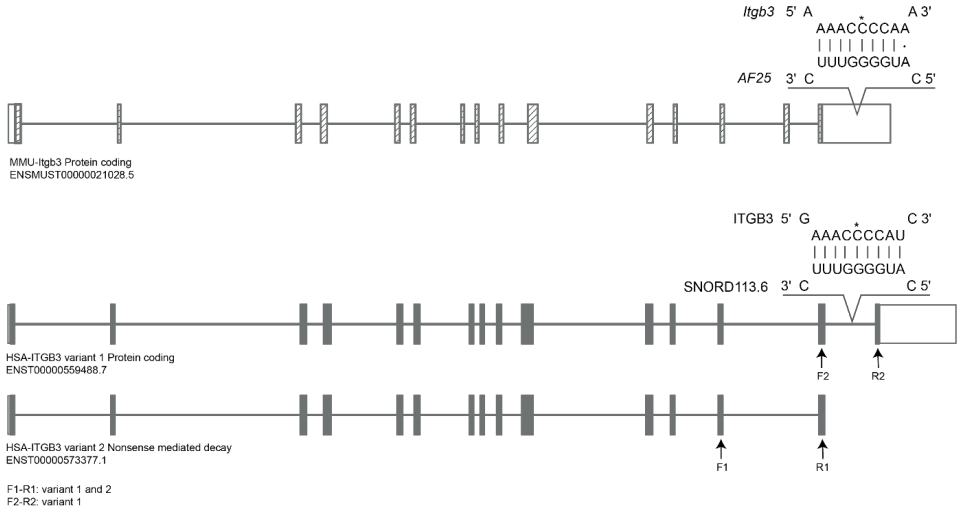

(Top) Murine *Itgb3* transcript with a perfect AF25 binding site located in the 3'UTR.

(Bottom) Human *ITGB3* variant 1 with a SNORD113.6 binding site located in the last intron. Variant 2 is marked for nonsense mediated decay and lacks the last intron and binding site.

Mitogen-activated protein kinase kinase 1 (MAP2K1)

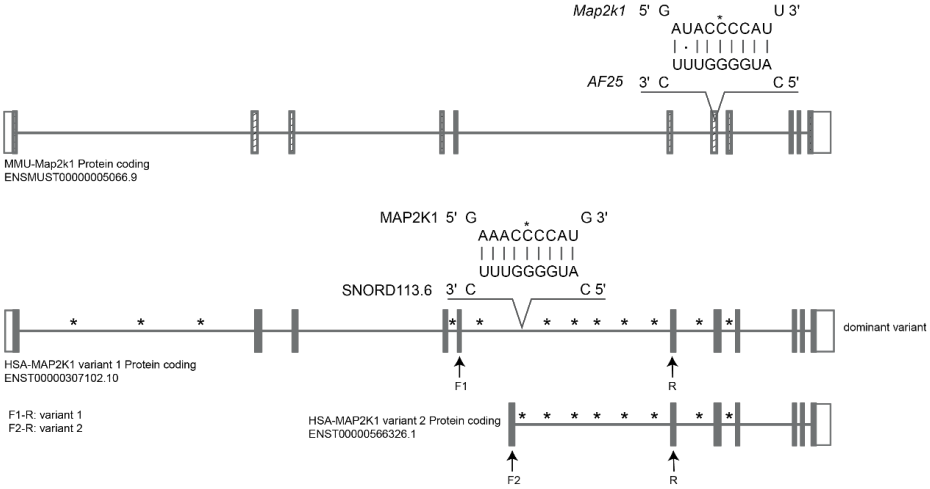

(Top) Murine *Map2k1* transcript with AF25 binding site located in an exon. One mismatch is present on the 2nd nucleotide of the antisense seed sequence.

(Bottom) Human *MAP2K1* variant 1 contains 12 intronic SNORD113.6 binding sites and variant 2 contains 6 intronic binding sites. All sites are perfect sequences.

Parvin beta (PARVB)

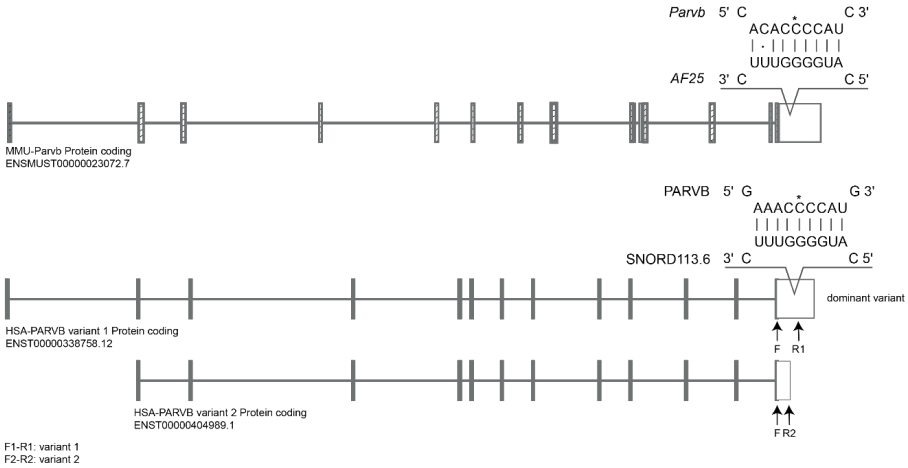

(Top) Murine *Parvb* transcript with a AF25 binding site, with one mismatch on the 2nd nucleotide, located in the 3'UTR.

(Bottom) Two transcript variants of human *PARVB.* SNORD113.6 binding site is located in the 3'UTR of variant 1. Variant 2 lacks that part of the 3'UTR and the binding site.

Integrin subunit alpha 7 (ITGA7)

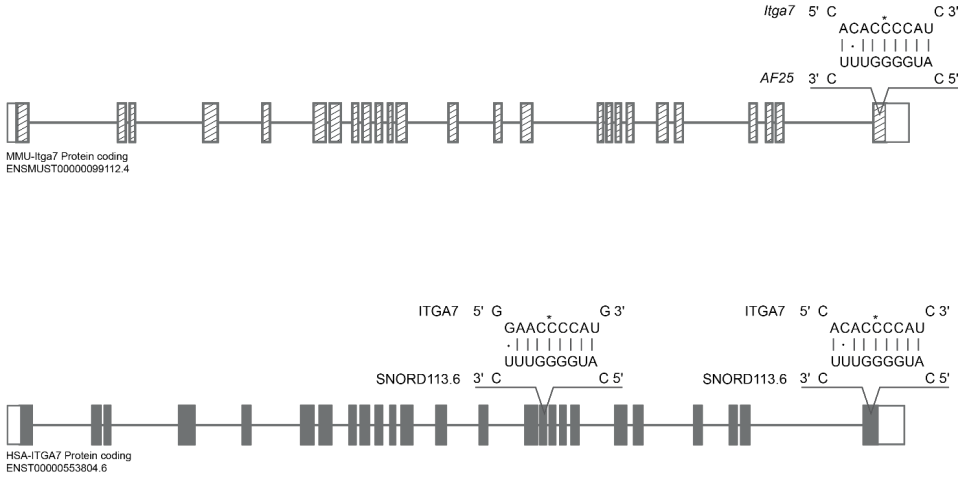

(Top) Murine *Itga7* transcript with a AF25 binding site located in the last exon.

(Bottom) Human *ITGA7* transcript with 2 SNORD113.6 binding sites, both with one mismatch, located in exons.

4

Filamin B (FLNB)

(Top) Murine *Flnb* transcript with a AF25 binding site, with one mismatch on the 2nd nucleotide, located in the 3'UTR.

(Bottom) Human *FLNB* transcript with a perfect SNORD113.6 binding site located in 3'UTR.

Collagen type IV alpha 4 chain (COL4A4)

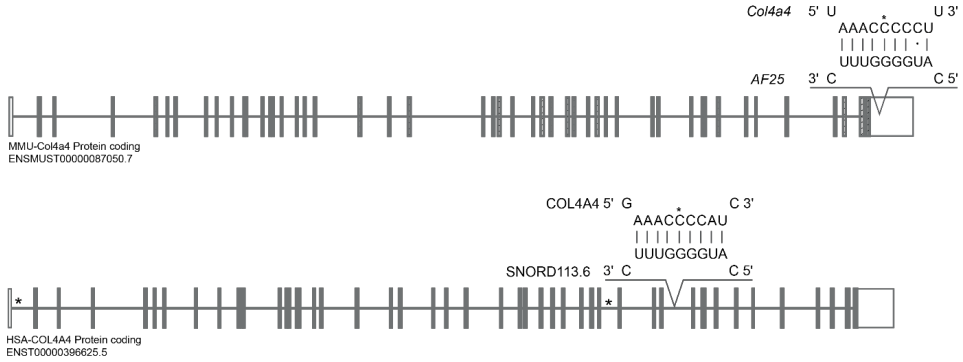

(Top) Murine *Col4a4* transcript with a perfect AF25 binding site located in 3'UTR.

(Bottom) Human *COL4A4* transcript with 2 perfect SNORD113.6 binding sites, both located in introns.

Netrin 4 (NTN4)

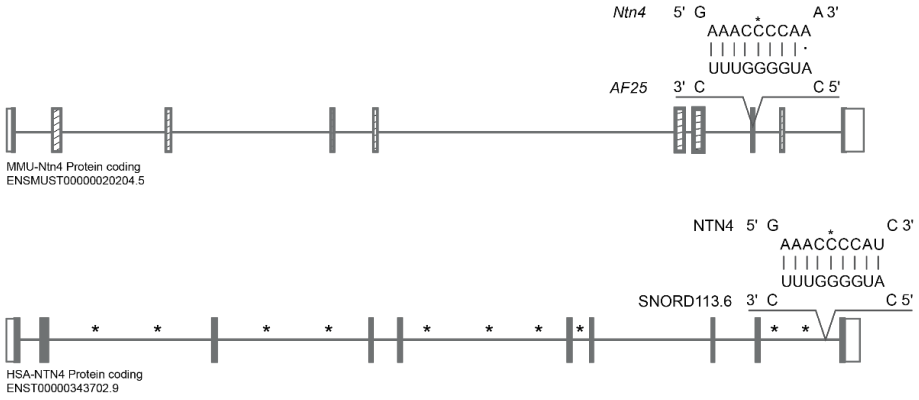

(Top) Murine *Ntn4* transcript with a perfect AF25 binding site located in an exon.

(Bottom) Human *NTN4* transcript with 10 perfect SNORD113.6 binding sites, all located in introns.

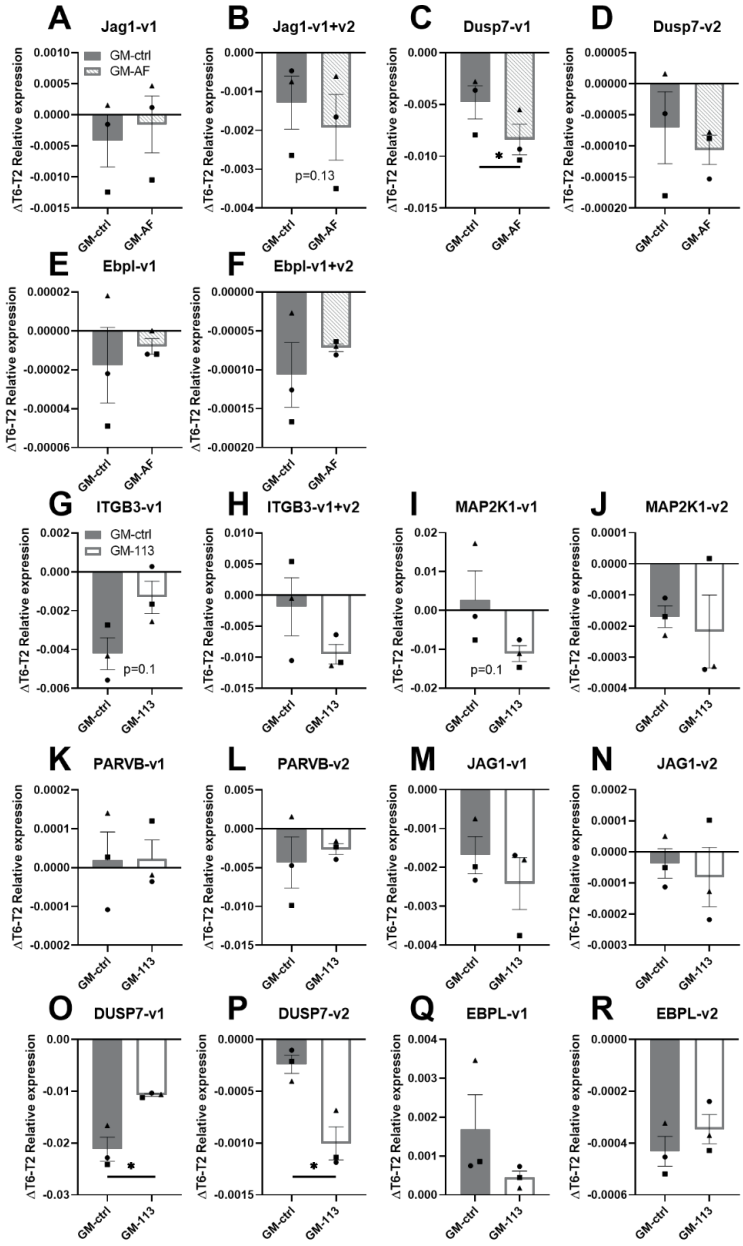

Supplemental Figure 4. Stability of SNORD113-6/AF357425 splice- and processing variants in primary cells. Primary murine fibroblasts (PMFs) or human umbilical arterial fibroblasts (HUAFs) were transfected with Gapmer control (GM-ctrl) or Gapmers against murine AF357425 (GM-AF) or human SNORD113-6 (GM113) for 24 hours. After 24 hours, cells were treated with Actinomycin D to inhibit novel RNA transcription. mRNA levels of SNORD113-6/AF357425 targets were measured 2 (T2) and 6 (T6) hours after addition of Actinomycin D. The decline in mRNA was calculated over time

as relative expression of T6 minus relative expression of T2 (ΔT6-T2). The primers used to quantify the decline in mRNA of the variants, target either one of the variants, variant 1 (v1) or variant 2 (v2), or both variants 1 and 2 (v1+v2). The decline in mRNA of murine targets (A) *Jag1* v1, (B) *Jag1* v1+v2, (C) *Dusp7* v1, (D) *Dusp7* v2, (E) *Ebpl* v1 and (F) *Ebpl* v1+v2) in PMFs transfected with GM-ctrl or GM-AF. The decline in mRNA of human targets (G) *ITGB3* v1, (H) *ITGB3* v1+v2, (I) *MAP2K1* v1, (J) *MAP2K1* v2, (K) *PARVB* v1, (L) *PARVB* v2, (M) *JAG1* v1, (N) *JAG1* v2, (O) *DUSP7* v1, (P) *DUSP7* v2, (Q) *EBPL* v1 and (R) *EBPL* v2 in HUAFs transfected with GM-ctrl or GM-113.6. A one-tailed paired t-test was performed to compare increased decline in GM-AF/113 compared to GM-ctrl, within each individual experiment. Data are represented as mean ±SEM. *$p<0.05$, compared to GM-ctrl.

Methylation primers MMU	
MMU-ITGA7-FW-U	CTGGGGCAACTCCCAGTG
MMU-ITGA7-RV	CTCCATCCCAAGGAGCCATC
MMU-ITGA7-FW-D	GACTGGCATCCTGAGCTGG
MMU-FLNB-FW-U	TGTATGATGACAAAGGAGAGCA
MMU-FLNB-RV	GAACCCAGAACCCAGTCGAG
MMU-FLNB-FW-D	ACACAGAGTGTGTGGCAAA
MMU-ITGB3-FW-U	AAGGCATGCAGAACACTCCA
MMU-ITGB3-RV	AGCCGCAATGAACTCTGGG
MMU-ITGB3-FW-D	TGGAATTCTGTACCTGCCTACT
MMU-COL4A4-FW-U	AGAACACACGTGCCTTGCTA
MMU-COL4A4-RV	CCGTGGGGTCTATACTTTGAAG
MMU-COL4A4-FW-D	CCTTCAGCCTTGCTGCTAGAAT
MMU-MAP2K1-FW-U	TCTGGTGGAGATGGCAGTTG
MMU-MAP2K1-RV	GGTCGGCTGTCCATTCCATA
MMU-MAP2K1-FW-D	CATTCCTCCTCCTGATGCCA
MMU-NTN4-FW-U	GGATTTTCTGCCCTCCGACA
MMU-NTN4-RV	AGCGTTCTCTTGCCTCGTAA
MMU-NTN4-FW-D	CTTATCAGCCCACGACAAAGG
MMU-DUSP7-FW-U	GCAAACCATCGATGTATTTTGTTTT
MMU-DUSP7-FW-D	AATGCATTTTGCACGTGTGT
MMU-DUSP7-RV	TCCTGATGCCCAGAGAGTGA
MMU-JAG1-FW-U	ACAACACCACCAACAATGTGC
MMU-JAG1-FW-D	ATCGAGAAACACGGAGCCAA
MMU-JAG1-RV	CCTCCACTTCCGAGTTGTGT
MMU-EBPL-FW-U	AGTGGTAAGGTTGAGTGACCTC
MMU-EBPL-FW-D	TCAGAACTGAGGTGTGGAGC
MMU-EBPL-RV	TTAATGCTACGTGGCTGGCT

Methylation primers HSA	
EVI-HSA-FLNB-FW-U	ATACAAAGCCCTCCAGCCTG
EVI-HSA-FLNB-FW-D	TGCTGTTGTAAAATGCCTTCAG
EVI-HSA-FLNB-RV	CCCCTGAACAAGCTTGCATT
EVI-HSA-ITGA7-FW-U	GAGGAACAACTGGGGCAGC
EVI-HSA-ITGA7-FW-D	CATCCTGGCTGCTGACGG
EVI-HSA-ITGA7-RV	AGCCCACTCTACCCTCTTCA
EVI-HSA-ITGB3-FW-U	TCAGGAGTTTGAGACCAGCC
EVI-HSA-ITGB3-FW-D	ATGGTGGTGTGTGCCTGTAG
EVI-HSA-ITGB3-RV	ACCTCCCCTGACTCAAGACA
EVI-HSA-pre-MAP2K1 I5-FW-U	AGCAGTTTTGAGACCAGCCT
EVI-HSA-pre-MAP2K1 I5-FW-D	AAAATTAGCTCGGCGTGGTG
EVI-HSA-pre-MAP2K1 I5-RV	CCTCCTGGGTTCAAGCAATTC
EVI-HSA-NTN4-FW-U	GGCAACATGATGAAACCCCA
EVI-HSA-NTN4-FW-D	AATTAGCTGGGAGTGGTGGC
EVI-HSA-NTN4-FW-RV	TCACTGCAGCCTCAATCTCC
EVI-HSA-NTN4-FW-U2	GTTCAGGAGCTCGAGACCAG
EVI-HSA-PARVB-FW-U	TCAGAAGTTCGAGACCAGCC
EVI-HSA-PARVB-FW-D	GGTATGTATGCCTGTAATCCCA
EVI-HSA-PARVB-RV	CAGTGGCATGATCTCAGCTCA
HSA-DUSP7-FW-U	CCCATTTAAGCACACCTCACT
HSA-DUSP7-FW-D	CAAGTGATAGTGTGGCCATCA
HSA-DUSP7-RV	GCTAGTCCCCAAGGCCTTAA
HSA-JAG1-FW-U	GGAGCAGCTGAACCAGATCAAA
HSA-JAG1-FW-D	ACACGGTCCCCATCAAGGAT
HSA-JAG1-RV	TGGTGTTTGTCCATGTCGTC
HSA-EBPL-FW-U	GACCAGCCTGGCCAACAT
HSA-EBPL-FW-D	TGGCGGGCACCTGTAAC
HSA-EBPL-RV	AGCAATTCTCCTGCCTCAGC

Transcript variants	
HSA-ITGB3-FW1	CCTGTATGTGGTAGAAGAGCCA
HSA-ITGB3-RV1	CGTGGATGGTGATGAGGAGT
HSA-ITGB3-FW2	ATTCTGCTCATTGGCCTTGC
HSA-ITGB3-RV2	TTGGTGAAGGTAGACGTGGC
HSA-PARVB-FW	CAGTTAGCGATCACAGGCCT
HSA-PARVB-RV-L	TGTCACATCTAAGCTTCTGGGA
HSA-PARVB-RV-S	AGCCCAGCCCAGGAGATC
EVI-HSA-MAP2K1-1-FW	AGGCCTGACATATCTGAGGGA
EVI-HSA-MAP2K1-2-FW	AGGCCTGGACTATGGAATGG
EVI-HSA-MAP2K1-RV	ACCCCAAAGTCACAGAGCTT
MMU-EBPL-FW	GCTCTTGAAGGGATGTCAAGC

MMU-EBPL-RV-1	AAGCTATTTACTTCATGGCGGC
MMU-EBPL-RV-2	CCCAGCACTTCAGAGGGTTA
MMU-JAG1-FW	GCCGCCATAGGTAGAGTTTGA
MMU-JAG1-RV-1	GCCTCAGACTGGAATAGGACA
MMU-JAG1-RV-2	TTCCCAGCCAACCACAGAAA
MMU-DUSP7-FW-1	GACTCCAACGAGGTTCACCC
MMU-DUSP7-RV-1	GGCCGCAATAGGTGTAGGTT
MMU-DUSP7-FW-2	CTCAACGTCACACCCAACCT
MMU-DUSP7-RV-2	CCATCTCCAAGGAACCCCAA
HSA-EBPL-FW-1	GAAATTCTGACCGTCGCCCT
HSA-EBPL-RV-1	TCTGCAGGAAATGCCGGTAA
HSA-EBPL-FW-2	CAGCTAGGATCTGTGTGGGG
HSA-EBPL-RV-2	GGAAGTACTAATGAGCCTACTCAA
HSA-JAG1-FW-1	TGAGGCCGTTGCTGACTTAG
HSA-JAG1-RV-1	TGAGATGCGGCACTCGATTT
HSA-JAG1-FW-2	CCTGTGATAAGAGCCAGGTCAG
HSA-JAG1-RV-2	GGAAAGGTGCTGTGAATGCT
HSA-DUSP7-FW-1	AGAAGTGTGGTGTCCTGGTG
HSA-DUSP7-RV-1	ACAAAGTCGTAGGCGTCGTT
HSA-DUSP7-FW-2	GTCACACCCAACCTACCCAA
HSA-DUSP7-RV-2	CACAGCACCTACCAATGAAGC

Housekeeping genes	
U6– MMU/HSA – FW	AGAAGATTAGCATGGCCCCT
U6– MMU/HSA – RV	ATTTGCGTGTCATCCTTGCG
GAPDH– MMU/HSA – FW	CACCACCATGGAGAAGGC
GAPDH– MMU/HSA – RV	AGCAGTTGGTGGTGCAGGA

SnoRNAs	
SNORD113-6 – FW	TGGACCAGTGATGAATATCATG
SNORD113-6 – RV	TGGACCTCAGAGTTGCAGATG
AF357425 – FW	AGGAGCATGGGGTTTCTGAC
AF357425 – RV	TTTCATAAGGGTTTAATCACTGTCC

Supplementary Table 1. Primer sequences

Guide RNA	Sequence
GA-AF357425-1+	+ GGCCAATGATGAGGAGCATGgtttt
	- CATGCTCCTCATCATTGGCCcggtg
GA-AF357425-2+	+ TTAAACCCTTATGAAATCTGtttt
	- CAGATTTCATAAGGGTTTAAcggtg
GA-AF357425-3-	+ AAGGGTTTAATCACTGTCCTtttt
	- AGGACAGTGATTAAACCCTTcggtg
GA-AF357425-4-	+ ATAGTCCTCAGATTTCATAAtttt
	- TTATGAAATCTGAGGACTATcggtg
GA-BF6+	+ GCCAATGATGAGGAGCCATGgtttt
	- CATGGCTCCTCATCATTGGCcggtg

Supplemental Table 2. sgRNAs for CRISPR/Cas9 of AF357425

Oligonucleotide	Sequence
3GA-AF357425	3'-[GGGTTTAATCACTGTCCTC]$_{D}$-X-[CTCCTGTCACTAATTTGGG]$_{D}$-3'
3GA-Control	3'-[TGTACGACTCCATAACGGT]$_{D}$-X-[TGGCAATACCTCAGCATGT]$_{D}$-3'
GM-AF357425	3'-[UUAAU]$_{2'OmeR}$[CACTGTCCTC]$_{D}$[GGUCA]$_{2'OmeR}$-5'
GM-AF357425-D'	3'-[GUCAG]$_{2'OmeR}$[AAACCCCATG]$_{D}$[CUCCU]$_{2'OmeR}$-5'
GM-BF6-D'	3'-[UCAGA]$_{2'OmeR}$[AACCCCATGG]$_{D}$[CUCCU]$_{2'OmeR}$-5'
GM-113-6-D'	3'-[CAGAA]$_{2'OmeR}$[ACCCCATGAT]$_{D}$[ATTCA]$_{2'OmeR}$-5'
GM-Control	3'-[AUCGA]$_{2'OmeR}$[TACCGTATAA]$_{D}$[UAACG]$_{2'OmeR}$-5'

Supplemental Table 3. Oligonucleotide sequences of 3rd Generation Antisense (3GA) and gapmers (GM). [nnn]$_{D}$ = DNA-nucleotides; [nnn]$_{2'OmeR}$ = 2'Ome-RNA nucleotides; X = phosphorothioate linker

Chapter 5

C/D box snoRNA SNORD113-6 guides 2´O-methylation and protects against site-specific fragmentation of tRNA^{Leu}(TAA) in human arterial fibroblasts

Eva van Ingen[1,2], Pleun A.M. Engbers[1,2], M. Leontien van der Bent[1,2], Hailiang Mei[3], Johann Wojta[4,6], Paul. H.A. Quax[1,2], A. Yaël Nossent[1,2,4-5]

Under review by Molecular Therapy Nucleic Acids

[1]Department of Surgery, [2]Einthoven Laboratory for Experimental Vascular Medicine and [3]Department of Biomedical Data Sciences, Leiden University Medical Center, The Netherlands. [4]Department of Internal Medicine II and [5]Department of Laboratory Medicine, Medical University of Vienna, Austria. [6]Ludwig Boltzmann Institute for Cardiovascular Research, Vienna, Austria.

Abstract

C/D box small nucleolar RNAs (snoRNAs) of the DLK1-DIO3 locus are associated with vascular remodelling and cardiovascular disease. None of these snoRNAs has any known targets yet, except for one, AF357425 in mice and SNORD113-6 in humans. We previously showed that this snoRNA targets mRNAs of the integrin signalling pathway and affects arterial fibroblast function. Here, we aimed to identify whether AF357425/SNORD113-6 can also target small RNAs. We overexpressed or inhibited AF357425 in murine fibroblasts and performed small RNA sequencing. Expression of tRNA fragments (tRFs) was predominantly regulated. Compared to overexpression, AF357425 knockdown led to an overall decrease in tRFs, but with an enrichment in smaller tRFs (<30 nucleotides). We focused on tRNA Leucine anti-codon TAA ($tRNA^{Leu}$(TAA)), that has a conserved predicted binding site for AF357425/SNORD113-6. Adjacent to this site, the tRNA is cleaved to form $tRF^{Leu\ 47\text{-}64}$, in both primary murine fibroblasts and human arterial fibroblasts. We show that AF357425/SNORD113-6 methylates $tRNA^{Leu}$(TAA) and thereby prevents the formation of $tRF^{Leu\ 47\text{-}64}$. Exposing fibroblasts to oxidative or hypoxic stress, increased AF357425/SNORD113-6 and $tRNA^{Leu}$(TAA) expression, but AF357425/SNORD113-6 knockdown did not increase $tRF^{Leu\ 47\text{-}64}$ formation under stress even further. Thus, independent of cellular stress, AF357425/SNORD113-6 protects against site-specific fragmentation of $tRNA^{Leu}$(TAA) via 2'O-ribose-methylation.

Introduction

Small nucleolar RNAs (snoRNAs) are a type of small noncoding RNA that mediate RNA modifications at post-transcriptional level. There are two types of snoRNAs, C/D box and H/ACA box snoRNAs, named after their conserved sequence motifs. C/D box snoRNAs guide 2'-O-ribose methylation (2'Ome) of their target RNAs, whereas H/ACA snoRNAs guide RNA pseudouridylation (Ψ). Both 2'Ome and Ψ are abundant site-specific RNA modifications and are mostly present on ribosomal (r)RNAs, where they function in rRNA folding and translational devotion[1-3].

C/D box snoRNAs associate with four conserved ribonucleoproteins NHP2L1, NOP56, NOP58 and Fibrillarin (FBL). FBL is the methyltransferase that catalyses 2'Ome. C/D box snoRNAs have two antisense boxes, located directly upstream of the D and D' boxes, which are not covered by ribonucleoproteins and are thus free to interact with target RNA sequences. C/D box snoRNAs hybridize to their target RNAs via Watson-Crick base-pairing. Once bound to the target RNA, the 5th nucleotide upstream of the D or D' box is positioned for 2'Ome[1, 2, 4]. Many expressed C/D box snoRNAs, however, lack antisense elements of known rRNA 2'Ome sites and are considered orphan snoRNAs[5]. Likely, these orphan C/D box snoRNAs target other types of RNA molecules than rRNA[6-8].

Besides rRNAs, transfer (t)RNAs are the most heavily modified cellular RNAs[9]. Their canonical function lies in protein translation, where they deliver amino acids to the translating peptide chain. However, recent reports show that tRNAs can be processed into tRNA-derived fragments (tRFs), which can perform other, noncanonical, functions. tRFs can derive from different regions of their parental tRNA, located anywhere from the 5' to 3' end, and have variable sizes up to ~50 nucleotides[10, 11]. Fragmentation of tRNAs can be induced under cellular stress, such as oxidative stress and hypoxia, which are important triggers of vascular remodelling processes[12-14]. Among others, Angiogenin (ANG) is a tRNA-processing endonuclease that is activated during cellular stress[12].

Recent findings show that RNA modifications guided by snoRNAs, 2'Ome and Ψ, can prevent tRNA cleavage and thereby regulate tRF formation[10, 15-18]. For instance, the former orphan SNORD97 induces 2'Ome on the wobble cytidine C34 of tRNA^{Met}(CAT), which protects against ANG-induced cleavage[15]. Loss of pseudouridine synthase 7 (PUS7), a pseudouridylation enzyme guided by H/ACA snoRNAs, results in loss of 5´tRFs of ~18 nucleotides in length, while the production of the larger 5´-tRNA halves increases[16].

The DLK1-DIO3 locus on the long arm of human chromosome 14, encodes a cluster of 41 C/D box snoRNAs (14q32; 12F1 in mice). We have demonstrated that this cluster of 14q32 C/D box snoRNAs is strongly associated with vascular remodelling and human cardiovascular disease[19-21]. The association with cardiovascular disease is both independent of and stronger than the 14q32 long noncoding RNAs (lncRNAs) and the cluster of 14q32 microRNAs that lie adjacent to the snoRNA genes[19]. Furthermore, plasma levels of 14q32 snoRNAs were associated with disease outcome in peripheral arterial disease (PAD) patients[20, 21]. However, all 14q32 C/D box snoRNAs are orphan snoRNAs and their molecular function is still unknown, except for one snoRNA. We recently demonstrated that one of the most abundantly expressed snoRNAs of the 14q32 cluster, human SNORD113-6 and its murine equivalent, AF357425, targets mRNAs of the integrin signalling pathway, influencing both pre-mRNA processing and 2'Ome. The D' antisense box of AF357425/SNORD113-6 is fully conserved between humans and mice. Fibroblast integrin signalling is important for cell-cell and cell-matrix interactions, but also acts in various forms of cardiovascular remodelling that can lead to cardiovascular disease[22]. Indeed, knockdown of SNORD113-6 altered human arterial fibroblast function[23]. Whether AF357425/SNORD113-6 also guides 2'Ome on small RNA molecules, however, is still unknown.

Here, we aimed to determine whether AF357425/SNORD113-6 can target small RNAs. We performed small RNA sequencing (sRNA-seq) on primary murine fibroblasts (PMFs) in which we either inhibited or overexpressed AF357425. We found that tRFs were the predominant group of small RNAs that changed in expression. Knockdown of AF357425 resulted in an apparent reduction of total tRFs, but an enrichment of smaller sized tRFs (18-30 nucleotides). We focused on one of these tRNAs, tRNA Leucine anti-codon TAA ($tRNA^{Leu}$(TAA)), which has a predicted binding site for AF357425 in mice and SNORD113-6 in human. sRNA-seq data showed that its dominant tRF, $tRF^{Leu\ 47\text{-}64}$, is formed just upstream of this site. Formation of $tRF^{Leu\ 47\text{-}64}$ was conserved in both PMFs and human umbilical arterial fibroblasts (HUAFs), and was investigated under oxidative, hypoxic and starvation stress. We show that AF357425/SNORD113-6 indeed methylates this tRNA and protects against site-specific $tRNA^{Leu}$(TAA) fragmentation.

Results

sRNA-seq in primary murine fibroblasts

In order to identify small RNA targets of AF357425/SNORD113-6, we performed sRNA-seq on PMFs in which we either inhibited or overexpressed AF357425. With this strategy, we aimed to obtain the largest possible difference in small RNA target expression. Gapmers were used to inhibit AF357425 expression (GM-AF25) and 3rd Generation Antisense (3GAs) to overexpress AF357425 (3GA-AF25). We showed previously that 3GAs directed against the 3'-end of AF357425 (3GA-AF25) induced snoRNA overexpression, likely through protection from degradation by endonucleases[19]. Expression of AF357425 was increased (>5-fold) in PMFs treated with 3GA-AF, compared to GM-AF25 (Supplemental Figure 1). By far most reads from the sRNA-seq in both samples were mapped to microRNAs. Read counts mapped to microRNAs, as well as those that mapped to the much lower expressed snoRNA and rRNA genes, were similar between AF25-High and AF25-Low cells. However, reads that mapped to tRNA genes, which are all tRFs of <45 nucleotides in length, appeared to be reduced in number in AF25-Low cells (Figure 1A and Supplemental Table 2). Where the longer tRFs (30-45 nucleotides) appeared enriched in AF25-High cells, smaller sized tRFs (18-29 nucleotides) were enriched in AF25-Low cells, particularly the 18-nucleotide tRFs (Figure 1B). These data indicate that AF357425 may direct tRNA fragmentation.

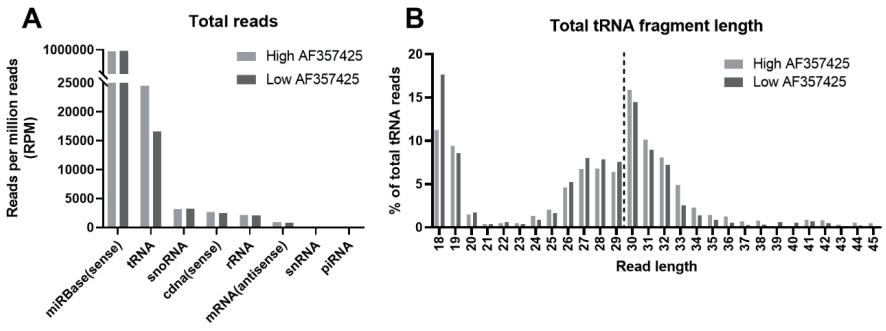

Figure 1. sRNA-seq. (A) Total reads mapped to small RNAs, normalized to reads per million (RPM) and (B) total tRNA fragment length (in nucleotides), shown as a percentage (%) of total tRNA reads in high AF357425 (overexpressed) and low AF357425 (inhibited) primary murine fibroblasts.

Fragmentation of tRNA^{Leu}(TAA)

In order to investigate the mechanisms through which AF357425/SNORD113-6 may influence tRNA fragmentation, we focused on a single tRNA. Among others, tRNA Leucine anti-codon TAA (tRNA^{Leu}(TAA)) had a predicted D' box antisense sequence for AF357425. This site was conserved in human tRNA^{Leu}(TAA) for the D' box antisense sequence of SNORD113-6. Except for the outer 2 nucleotides, a perfect reverse complementary sequence for the middle 7 nucleotides is present in both mouse and human tRNA^{Leu}(TAA) (AACCCCA; Figure 2A). A tRF cleaved just upstream of this predicted 2'Ome site (18 to 20 nucleotides; Figure 2A), tRF$^{Leu\ 47-64}$, was abundantly expressed in both AF25-High and AF25-Low cells (Figure 2B). However, the total tRFs generated from tRNA^{Leu}(TAA) were decreased in AF25-Low cells. In contrast, tRF$^{Leu\ 47-64}$ was more abundant relative to the total tRFs in AF25-Low (50%) compared to AF25-High cells (35%; Figure 2B, C). We confirmed expression of tRF$^{Leu\ 47-64}$ by Northern blot in both PMFs and in HUAFs. Expression of tRF$^{Leu\ 47-64}$ appeared enhanced under oxidative stress (Figure 2D, E).

Validation of tRNA^{Leu}(TAA) 2'Ome

Next, we performed RTL-Q to calculate the EMF, using site-specific primers for detection of 2'Ome. We confirmed 2'Ome of the mature full-length tRNA^{Leu}(TAA), located on the 5th nucleotide upstream of the D' antisense box, in both PMFs and HUAFs. Inhibition of AF357425/SNORD113-6 partly reduced 2'Ome at this site compared to GM-ctrl (p for trend=0.0725 in PMFs and 0.0968 in HUAFs; Figure 3). 2'Ome also appeared present on the precursor-(pre)tRNA^{Leu}(TAA) in HUAFs, but we could not confirm snoRNA-induced regulation of 2'Ome in the pre-tRNA^{Leu}(TAA), due to high Ct values above the detection threshold (>45 Ct; Supplemental Figure 2). The validation of 2'Ome in both mouse and human cells suggests that both are evolutionarily conserved features of tRNA^{Leu}(TAA).

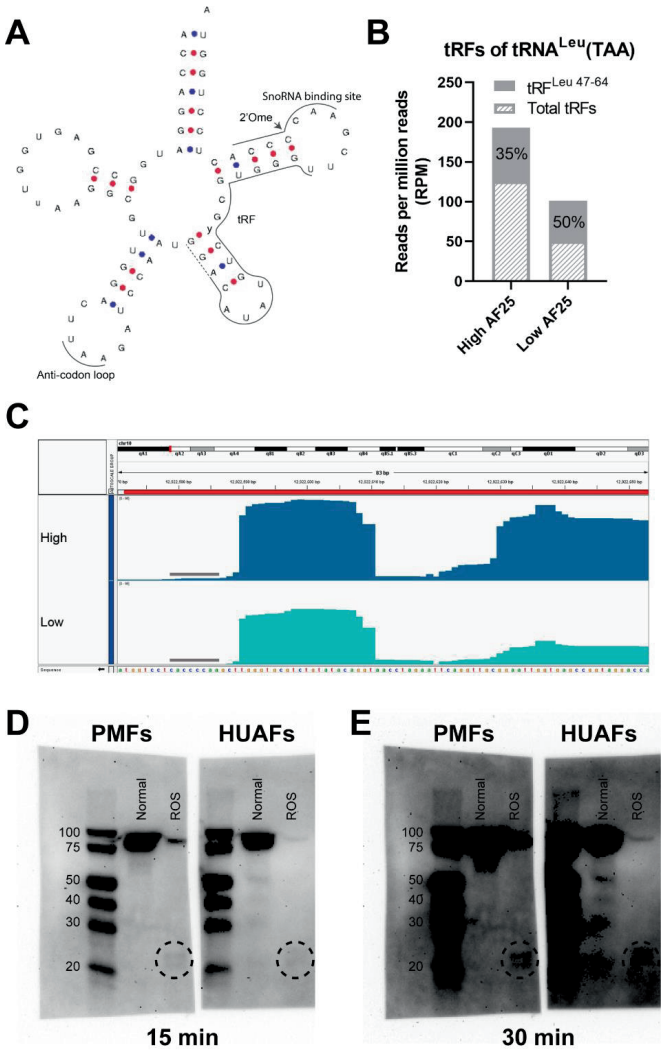

Figure 2. Fragmentation of tRNA^{Leu}(TAA). (A) Schematic overview of the mature tRNA^{Leu}(TAA) sequence in mouse and human. The AF357425/SNORD113-6 predicted binding site (snoRNA binding site), tRNA fragment generated upstream of the binding site, tRF$^{Leu\ 47\text{-}64}$, and the anti-codon loop are indicated with a line. The dashed line indicates length extension of tRF$^{Leu\ 47\text{-}64}$, representing 3 different sizes of generated tRFs. Arrow points at the predicted 2'O-methylation (2'Ome) site. γ represents U in mice and C in human. Figure adapted from GtRNAdb[35]. (B) The fragment of interest, tRF$^{Leu\ 47\text{-}64}$, shown as a percentage of total tRFs generated from tRNA^{Leu}(TAA). Data is normalized to reads per million reads (RPM). (C) Coverage plot of tRNA^{Leu}(TAA) in primary murine fibroblasts with either high or low AF357425 expression. The predicted AF357425 binding site is indicated with a line. Sequence is shown from 3' to 5'. Northern blots exposed for (D) 15 and (E) 30 min using the ChemiDoc-IT imaging system. Primary murine fibroblasts (PMFs) and human umbilical arterial fibroblasts (HUAFs) were cultured in normoxic and oxidative stress (ROS) conditions. A digoxigenin labeled probe was used to visualize tRFs. A circle indicates tRF$^{Leu\ 47\text{-}64}$.

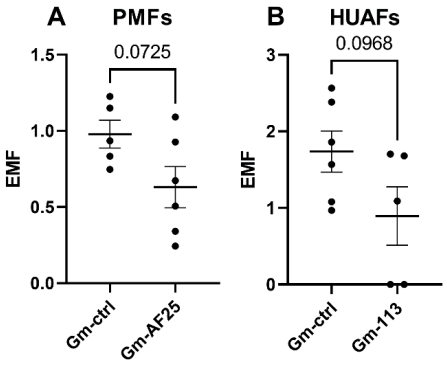

Figure 3. 2'O-methylation at predicted AF357425/SNORD113-6 binding sites on tRNA^{Leu}(TAA). For detection of 2'O-methyated nucleotides and to calculate the estimated methylated fraction (EMF), Reversed Transcription at Low dNTP concentration followed by Quantitative PCR (RTL-Q) was performed. Site-specific reversed primers were used exactly on and 1 nucleotide downstream of the predicted 2'Ome site to accurately determine the exact location of the 2'Ome site. (A) Primary murine fibroblasts (PMFs) or (B) human umbilical arterial fibroblasts (HUAFs) were transfected with Gapmers against AF357425 (GM-AF25)/ SNORD113-6 (GM-113) or a gapmer control (GM-ctrl) for 24 hours. N is represented by the individual dots. Data are represented as mean ±SEM. A two-tailed unpaired t-test was performed to compare GM-AF25/113 with GM-ctrl.

Fragmentation of tRNA^{Leu}(TAA) under cellular stress

As fragmentation of tRNAs can be induced during cellular stress[12-14], we cultured PMFs and HUAFs under different cellular stress conditions and measured expression levels of AF357425/SNORD113-6, mature tRNA^{Leu}(TAA) and tRF$^{Leu\ 47-64}$, by qPCR. Endogenous expression of AF357425/SNORD113-6 and mature tRNA^{Leu}(TAA) showed similar expression patterns in PMFs and HUAFs, with increased expression under both hypoxia and oxidative stress, compared to the normal culture condition control. Serum starvation, on the other hand, did not induce changes in either AF357425/SNORD113-6 or tRNA^{Leu}(TAA) expression compared to normal culture conditions. Expression of tRF$^{Leu\ 47-64}$ was only increased significantly under hypoxia in both PMFs and HUAFs, but appeared slightly elevated under oxidative stress as well (Figure 4).

Subsequently, PMFs and HUAFs were transfected with either GM-AF25/113 or a Gapmer control (GM-ctrl), and were cultured under the different cell stress conditions. The absolute Ct value of mature tRNA^{Leu}(TAA) was divided by the Ct value of tRF$^{Leu\ 47-64}$, in order to quantify expression of tRF$^{Leu\ 47-64}$ relative to mature tRNA^{Leu}(TAA), which it was generated from. The ratio was increased under AF357425/ SNORD113-6 inhibition under control conditions in both PMFs and HUAFs (Figure 5). In PMFs, the ratio was also increased under hypoxia and showed a trend towards an increased ratio under serum starvation (Figure 5A). This increased ratio

demonstrates that more $tRF^{Leu\ 47\text{-}64}$ is formed relative to its mature tRNA, when AF357425/SNORD113-6 is inhibited. When we quantified expression of ANG, we did not observe a difference between GM-AF25/113 and GM-ctrl (Supplemental Figure 3). However, ANG did increase under cellular stress, similar to the snoRNA, both in PMFs and HUAFs. We can neither confirm nor exclude that ANG is responsible for cleavage of $tRNA^{Leu}$(TAA), but we can conclude that ANG is not influenced by the snoRNA directly, and that changes in fragmentation are likely caused by changes in snoRNA-guided 2'Ome of the tRNA.

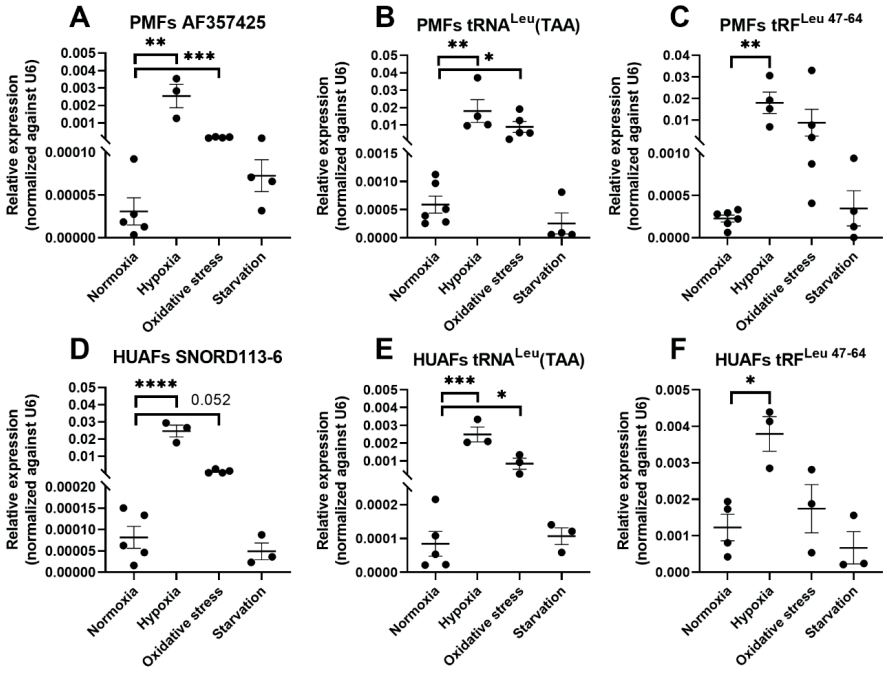

Figure 4. Relative snoRNA, $tRNA^{Leu}$(TAA) and $tRF^{Leu\ 47\text{-}64}$ expression during cellular stress. Relative expression levels in (A-C) primary murine fibroblasts (PMFs) and (D-F) human umbilical arterial fibroblasts (HUAFs) cultured in normoxic, hypoxic, oxidative stress and starvation conditions. Expression levels are normalized to U6. N is represented by the individual dots. Data are represented as mean ±SEM. A two-tailed unpaired t-test was performed to compare treatment with the control. *p<0.05, **p<0.01, ***p<0.005, compared to normoxia.

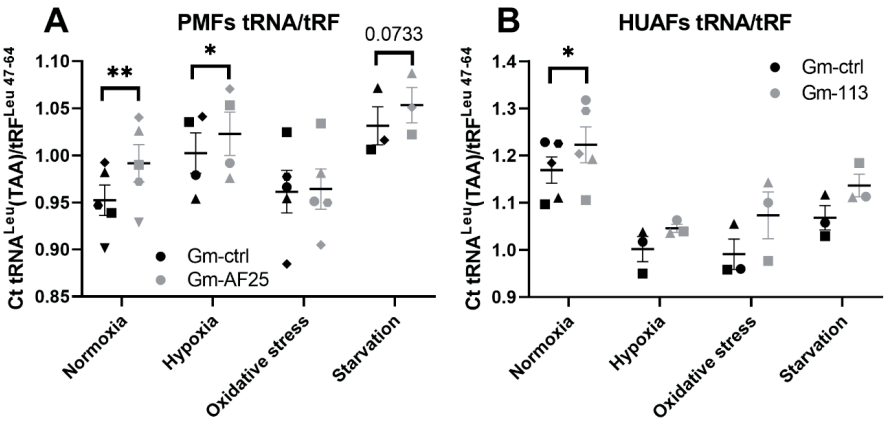

Figure 5. Ratio mature tRNA^{Leu}(TAA)/tRF$^{Leu\ 47\text{-}64}$ in primary cells exposed to different cell stress stimuli. (A) Primary murine fibroblasts (PMFs) and (B) human umbilical arterial fibroblasts (HUAFs) transfected with GM-AF25/113 or GM-ctrl, and cultured in normoxic, hypoxic, oxidative stress or starvation conditions. Expression levels were measured by qPCR. Ratios were calculated by dividing absolute Ct values of the mature tRNA by Ct values of the tRF. N is represented by the individual dots. Data are represented as mean ±SEM. A two-tailed paired t-test was performed to compare single treatment with the control, within each experiment. *p<0.05, **p<0.01, compared to GM-ctrl.

Effects of 2'Ome on tRNA stability

Ribonucleotide modifications in the structural core of the tRNA may stabilize the tRNA and reduce tRNA degradation rates[26]. After transfection with either GM-AF25/113 or GM-ctrl, cells were treated with a high concentration of Actinomycin D (5 µg/µl) for 1h, to inhibit novel tRNA transcription. In both PMFs and HUAFs, mature tRNA^{Leu}(TAA) was rapidly degraded, but no differences were observed between GM-AF25/113 and GM-ctrl (Figure 6A, C). In PMFs, the relative expression of mature tRNA^{Leu}(TAA) was lower to begin with in AF25-Low cells and remained lower after 1h, compared to GM-ctrl (Figure 6A). To rule out differences in degradation rates of housekeeping genes used (RPLP0 and U6) between the two groups, we also normalized the expression levels at 1h to 0h (T0; Figure 6B, D). Indeed, no differences in degradation rates between GM-AF25/113 or GM-ctrl were observed, indicating that a reduction of this single 2'Ome modification did not affect overall mature tRNA^{Leu}(TAA) stability, but only the site-specific fragmentation.

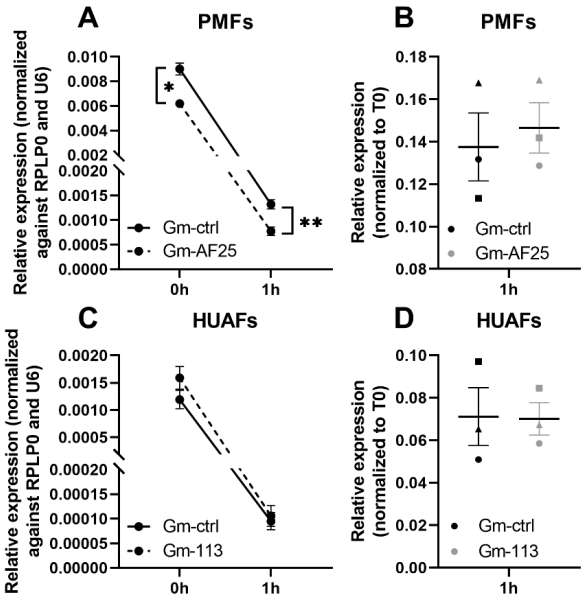

Figure 6. Stability of tRNA^{Leu}(TAA) in primary cells. (A,B) Primary murine fibroblasts (PMFs) and (C,D) human umbilical arterial fibroblasts (HUAFs) were transfected with Gapmers against AF357425 (GM-AF25)/ SNORD113-6 (GM-113) or a gapmer control (GM-ctrl) for 24 hours. After 24 hours, cells were treated for 1 hour with Actinomycin D to inhibit novel RNA transcription. Mature tRNA levels were measured 0 and 1 hour after addition of Actinomycin D. (A,C) Expression levels were normalized to RPLP0 and U6. (B,D) Expression levels at 1h were normalized to 0h (T0). Data are represented as mean ±SEM. *p<0.05, **p<0.01, compared to GM-ctrl.

Discussion

We here aimed to identify small RNA targets of AF357425/SNORD113-6. We found that tRNAs are the predominant small RNA target of AF357425. Inhibition of the snoRNA led to an overall decrease in tRFs, and compared to overexpression of the snoRNA, less larger (>30 nucleotides) and more smaller (<30 nucleotides) tRFs were formed. In order to investigate the underlying mechanisms of action, we focused on tRNA^{Leu}(TAA), which has a conserved binding site for the D' box seed sequence of AF357425/SNORD113-6. We showed that tRNA^{Leu}(TAA) is a 2'Ome target of AF357425/SNORD113-6 and that snoRNA inhibition led to an apparent reduction of 2'Ome at this site, both in murine and in human cells. Endogenous expression of AF357425/SNORD113-6 and mature tRNA^{Leu}(TAA), both increased under hypoxia and oxidative stress. Endogenous tRF$^{Leu\ 47\text{-}64}$ expression was also elevated under hypoxia. Knockdown of AF357425/SNORD113-6 resulted in an increased ratio of tRF$^{Leu\ 47\text{-}64}$ relative to its mature tRNA^{Leu}(TAA), particularly under normal culture conditions, without induction of cellular stress. 2'Ome by AF357425/SNORD113-6 was not important for the overall stability of the tRNA, however, we show that it acts via protecting against site-specific fragmentation of tRNA^{Leu}(TAA).

The same post-transcriptional modifications on tRNAs have been shown to both protect from and promote fragmentation[16, 17]. Our data suggest that AF357425/SNORD113-6 2'Ome protects the tRNA from cleavage into small fragments (~18 nucleotides in length), rather than promoting it. However, we found more tRFs in total, including all tRFs formed of tRNA^{Leu}(TAA), and longer fragments (>30 nucleotides) in AF357425-High cells than in AF357425-Low cells. Perhaps the presence or absence of modifications attracts different tRNA endonucleases, which produce different tRF species. However, the expression of mature tRNAs may also be different between AF357425-High and -Low cells and this could of course also affect total tRF production, e.g. expression of tRNA^{Leu}(TAA) decreased under knockdown of AF357425. The role of AF357425/SNORD113-6 2'Ome in cleavage of other tRNAs remains to be determined, but likely, its function is to prevent fragmentation of shorter tRFs (~18 nucleotides in length), as we demonstrated for tRNA^{Leu}(TAA).

Besides the stabilizing tertiary structure, little is known about other functions of post-transcriptional modifications in the structural core of tRNAs[26]. AF357425/SNORD113-6 targets and guides 2'Ome in the T-arm, the structural core, of tRNA^{Leu}(TAA). 2´Ome and the formation of tRF$^{Leu\ 47\text{-}64}$, were found in mouse and human cells, suggesting that both are evolutionarily conserved features of tRNA^{Leu}(TAA). Degradation rates of tRNA^{Leu}(TAA) were similar between GM-ctrl and GM-AF25/113 transfected cells, indicating that 2'Ome by

AF357425/SNORD113-6 is not important for the overall tRNA^{Leu}(TAA) stability. Of course, tRNAs are heavily modified and reduction of a single 2'Ome modification may not have direct consequences for their stability. Also, as knockdown of AF357425/SNORD113-6 only partly reduced 2'Ome and not completely, this reduction may not have been sufficient for decreasing tRNA stability. Nevertheless, we show that 2'Ome by AF357425/SNORD113-6 at least acts in preventing fragmentation of a specific site within tRNA^{Leu}(TAA).

The lack of effects on overall stability of tRNA^{Leu}(TAA) indicates that the presence of other modifications on the tRNA is similar between GM-ctrl or GM-AF25/113 treated cells, meaning that the single 2'Ome site is likely the only modification placed by AF357425/SNORD113-6 on this particular tRNA. The tRNA does, most likely, carry other modifications. This could pose a threat to the reliability of our measurements. Modifications on tRNAs may impede reverse transcription and limit detection of tRFs and tRNAs by rt/qPCR[27]. However, 2'Ome by AF357425/SNORD113-6 is located towards the 3' end of the tRNA. We designed qPCR primers for mature tRNA^{Leu}(TAA) upstream of that site, in order to limit confounding effects by presence or absence of 2'Ome. Furthermore, expression of tRF$^{Leu\ 47-64}$, that we initially found in the sRNA-seq, was confirmed by Northern blot and our qPCR results showed that tRF$^{Leu\ 47-64}$ and mature tRNA^{Leu}(TAA) were both abundantly expressed. We cannot control for effects of other modifications in our qPCRs, however, if reversed transcription was hampered by other modifications, these were likely similar between GM-AF25/113 and GM-ctrl.

Recent studies have shown that fragmentation of tRNAs increases under cellular stress[12-14, 28]. Similar cellular stress conditions, such as ischemia that leads to hypoxia in the underlying tissues, also trigger vascular remodelling processes. This implicates that the formation of tRFs may even play a role in vascular remodelling. Oxygen-glucose deprivation, which is an *in vitro* model for ischemic reperfusion injury, induced tRNA cleavage in neuronal cells[14]. Also, *in vivo* in ischemic brain tissue and in a hindlimb ischemia model, the formation of tRFs was strongly increased[13]. Similarly, we have previously shown that the 14q32 snoRNAs are regulated under ischemic conditions in PAD patients and during vascular remodeling[19]. In the current study, we show that expression of AF357425/SNORD113-6 indeed increased during hypoxia and oxidative stress, but not during serum starvation. Exposing cells to cellular stress did not result in an additional increase of tRF$^{Leu\ 47-64}$ to mature tRNA^{Leu}(TAA) ratio in AF357425/SNORD113-6 knockdown cells, whereas expression of mature tRNA^{Leu}(TAA) and ANG increased under both hypoxia and oxidative stress. In fact, the strongest increase in tRF$^{Leu\ 47-64}$/mature tRNA^{Leu}(TAA) ratio was observed in cells cultured under physiological conditions. An explanation could be that ANG and other endonucleases are being activated during cellular

stress[12, 28], which generate alternative tRF species from tRNA^{Leu}(TAA). We found no differences between GM-ctrl and GM-AF25/113 in relative ANG expression, and thus AF357425/SNORD113-6 does not directly regulate ANG expression. However, it could also be that the dramatic upregulation of the snoRNA under stress conditions completely overruled that relatively subtle knockdown of the snoRNA that we achieved with Gapmer treatment.
The question remains what the function of this AF357425/SNORD113-6-dependent tRF$^{Leu\ 47-64}$ could be. Assumingly, tRF$^{Leu\ 47-64}$ has an important role in cell physiology, as tRF$^{Leu\ 47-64}$ is also generated under physiological conditions and not exclusively during cellular stress. Our group, as well as others, have shown that tRFs have potential as circulating biomarkers in, for example, acute stroke[29-31]. It has also been demonstrated that tRFs can perform all sorts of regulatory functions, including regulation of protein translation, microRNA-like functions by base-pairing with mRNAs and interaction with RNA-binding proteins[32, 33]. Furthermore, tRFs have been shown to be functionally active in modulating cardiac and skeletal muscle function, endothelial function, but also in inhibition of angiogenesis[13, 34]. Which exact regulatory function(s) this particular tRF may have and how it impacts cellular function remains to be determined.

Taken together, we show that AF357425/SNORD113-6 targets predominantly tRNAs, protecting the tRNA from cleavage into small fragments. When zooming in on one specific tRNA, tRNA^{Leu}(TAA), we show that AF357425/SNORD113-6 induces 2'Ome of the mature tRNA, thereby protecting against site-specific tRNA fragmentation. The function of tRF$^{Leu\ 47-64}$, in general and in vascular remodelling in particular, remains to be elucidated.

Material and methods

Cell culture

Cells were cultured in a humidified incubator at 37°C under 5% CO_2. Cells were passaged at 70-90% confluency and used up to passage 6. DMEM, supplemented with 10% heat-inactivated foetal calf serum (FCSi) and 1% Pen/Strep, was used as culture media and was refreshed every 2-3 days.

Primary murine fibroblasts (PMFs) isolation

Ear tissues from C57BL/6-J mice, about 3 weeks of age, were clipped into smaller pieces and embedded in 0.2% gelatine in 6-well plates. DMEM supplemented with 20% FCSi and 1% non-essential amino acids (NEAA; Thermo Fisher, MA, USA, Cat.Nr.11140050), was added to the embedded ear-clippings. After 7 days, skin fibroblasts were grown out of the tissues onto the bottom of the culture plates. PMFs were expanded in culture media up to passage 3. PMFs were then used for further analysis or frozen down and stored in liquid nitrogen for later use.

Primary human umbilical arterial fibroblasts (HUAFs) isolation

Umbilical cords from full-term pregnancies were collected, stored in sterile PBS at 4°C, and within 7 days used for HUAFs isolation. The two arteries were isolated from the umbilical cord. Endothelial cells were removed by gently rolling the artery over a blunted needle. After that, the tunica adventitia and tunica media were separated using surgical tools. The tunica adventitia was incubated overnight in culture media supplemented with 10% heat inactivated human serum (PAA, Pasching, Austria) and 1% NEAA. The next day, the tunica adventitia was treated with 2 mg/ml collagenase type II solution (Worthington; OH, USA, Cat.Nr.NC9693955) at 37°C. The resulting cell suspension was filtered over a 70 µm cell strainer and centrifuged at 400g for 10 minutes. Cells were plated in 6-wells plates and media was refreshed after 90 minutes to remove slow adhering non-fibroblasts cells. HUAFs were expanded up to passage 3, used for further analysis or frozen down and stored in liquid nitrogen for later use.

Cellular stress conditions

Oxidative stress in both PMFs and HUAFs was induced by adding 10 µM of ROS mimic tert-butyl hydroperoxide (tBHT; Luperox, 458139, Sigma Aldrich, MO, USA) to the culture media for 24h. To serum starve the cells, DMEM with 1% PenStrep, supplemented with 1% FCSi for PMFs or 3% FCSi for HUAFs, was added to the cells for 24h. To induce hypoxia, cells in normal culture media were kept in a humidified incubator at 37°C under 1% O_2 for 24h.

RNA isolation and RT/qPCR

RNA was isolated by standard TRIzol (Thermo Fisher, MA, USA, Cat.Nr.15596026) chloroform extractions. RNA concentration and purity were measured using Nanodrop (Nanodrop Technologies, DE, USA) or the Bioanalyzer (2100 Bioanalyzer Instrument, Agilent, CA, USA). Reversed transcription of total RNA was performed with the high-capacity RNA-to-cDNA reverse transcription kit (Applied Biosystems, Thermo Fisher, MA, USA, Cat.Nr.4388950). Quantitect SybrGreen reagents (Qiagen Benelux, Venlo, the Netherlands, Cat.Nr.204145) were used for quantifications. Custom designed TaqMan small RNA assays (Thermo Fisher, Cat.Nr.4398987) were used for reversed transcription and quantifications of tRFs. Expression levels were normalized to U6 using the $2^{-\Delta Ct}$ method. All primers used are provided in Supplemental Table 1.

3rd Generation Antisense and Gapmers

3rd Generation Antisense oligonucleotides (3GAs) were kindly provided by Idera Pharmaceuticals (Cambridge, MA, USA). 3GAs directed to AF357425, consisted of two identical strands of DNA-nucleotides with a full phosphorothioate backbone, connected by a 5' phosphorothioate linker. Gapmers (GM) were custom designed against AF357425 (GM-AF25) or SNORD113-6 (GM-113; Sigma Aldrich, MO, USA). GM were made up out of five 2'Ome RNA-nucleotides, ten DNA-nucleotides and five more 2'Ome RNA-nucleotides with full phosphorothioate backbone. Sequences of 3GAs and GM are provided in Supplemental Table 1.

Transfection with 3rd Generation Antisense and Gapmers

Prior to transfections, G1 cell cycle arrest was induced by treating cells with KN-93 (Sigma Aldrich, MO, USA, Cat.Nr.K1385), an inhibitor of CaMK-II (the multifunctional Ca2+/CaM kinase). KN-93 was added to the culture media at a concentration of 10 μM for 48h. After cell synchronization, cells were washed with PBS and basal DMEM was added. Meanwhile, lipofectamine RNAiMAX Reagent (ThermoFisher, MA, USA, Cat.Nr.13778030) was used to create micelles loaded with 3GAs (200 nM) or GM (500 nM) against snoRNA AF357425 or SNORD113-6 for transfection. Micelles were added to the cells and after 1h of transfection, 10% FCSi was supplemented to the transfected cells. After 24h of transfection, cells were washed with PBS and used for further experiments or analyses.

RNA sequencing and analysis

RNA was isolated from PMFs transfected with 3GA or GM against AF357425. Isolated RNA was shipped to BGI for DNBseq sRNA-seq (GEO: GSE190537). Generated sRNA-seq files in

FASTQ format are processed using the sRNAbench tool[24]. Bowtie aligner was used to align reads to various reference genome and databases, such as GRCm38, mirbase small database, and RNAcentral. The expression of multiple classes of small RNA are quantified in the single assignment based approach where reads mapping to multiple loci are assigned to the locus that has the highest expression. RPM (Read per million) normalized counts are further generated that are used for downstream analysis.

Northern blotting

Total RNA samples were diluted in Novex Tris-borate-EDTA (TBE)-Urea sample buffer (ThermoFisher, Cat.Nr.LC6876), denatured at 95^{o}C for 5 minutes and put on ice. 15% Mini-PROTEAN TBE-Urea gels (BioRad, Cat.Nr.4566053) in TBE buffer were pre-run at 200 V for 20 minutes. After that, RNA samples and digoxigenin (DIG)-labeled Blue Color Marker for small RNA (DynaMarker, BioDynamics, Cat.Nr.DM270-125uL) were loaded on the gel. Gels were electrophoresed at 200 V for ~1h. Next, RNA was transferred from the gel to a Hybond N+ membrane (GE Healthcare, Cat.Nr.RPN203B) at 200 mA for 1h. A Mini Trans-Blot Electrophoretic Transfer Cell (Biorad) system with an ice element and stirrer were used for RNA transfer. Next, RNA was crosslinked to the membrane with freshly prepared 1-ethyl-3-(3-dimethylaminopropyl) carbodiimide (EDC; Sigma, Cat.Nr.E1769) 1-methylimidazole (Sigma, Cat.Nr.336092) crosslinking solution (pH 8) for 1h at 60^{o}C. Membranes were pre-hybridized in ULTRAhyb Oligo Hybridization Buffer (Invitrogen, Cat.Nr.AM8663) at 37^{o}C for 30 min while gently shaking. Dual DIG-labelled DNA probes (designed and ordered at Integrated DNA Technologies, NJ, USA) were denatured at 95^{o}C for 1 min, added to the hybridization buffer (final concentration 5 nM) and left overnight at 37^{o}C. The next day, membranes were washed with low stringency wash buffer (2x SSC, 0.1% SDS), high stringency was buffer (0.1x SSC, 0.1% SDS) at 37^{o}C and then washed with 2x SSC buffer at room temperature. Then, membranes were washed and blocked with the DIG Wash and Block Buffer Set (Roche, Cat.Nr.11585762001) according to the manufacture's protocol. After blocking for 3h at room temperature while shaking, Anti-Digoxigenin-AP, Fab fragments (Roche, Cat.Nr.11093274910) in blocking buffer (1:15.000) were added to the membranes. CDP-star Development Reagent (Roche, Cat.Nr.CDP-RO) was added to the membranes and images were acquired using ChemiDoc-IT imaging system. Dual DIG-labelled DNA probes are listed in Supplemental Table 1.

Detection of 2'Ome

For detection of 2'Ome nucleotides we used an adaptation of the Reverse Transcription at Low dNTP concentration followed by Quantitative PCR (RTL-Q) method that was described by

Dong et al. To accurately determine the exact location of the 2'Ome site on mature tRNA, a reversed primer downstream of the 2'Ome site (R_D) and a reversed primer on the 2'Ome site (R_U) were designed to the +1 and 0 nt downstream of the predicted 2'Ome nucleotide, respectively. The RT reaction was performed in two consecutive steps. First, a mixture of 20 ng RNA and 10 µM R_D or R_U primers was denatured at 70^{o}C for 5 minutes and incubated at 42^{o}C for 10 minutes as an initial annealing step. Then, a high (200µM) or low (0,5µM) concentration of dNTPs (Promega, Cat.Nr.U1511), 200U of M-MLV reverse transcriptase (Promega, Cat.Nr.M1705) and 20U of Recombinant RNasin Ribonuclease Inhibitor (Promega, Cat.Nr.N2515) was added to the RT reaction. The RT reaction was incubated at 42^{o}C for 90 minutes followed by incubation at 75^{o}C for 15 minutes. When a 2'Ome site is present, the extension of the R_D primer pauses at this site when low dNTP concentrations are used, whereas the R_U primer does not. Primer extensions are not affected by 2'Ome sites when performing RT at high dNTP concentrations. The differences in RT products were quantified by SYBR green-based qPCR. The estimated methylated fraction (EMF) was calculated using the following formula.

EMF = (Ct Low dNTP R_D – Ct High dNTP R_D) – (Ct Low dNTP R_U – Ct High dNTP R_U)
>0 means that methylation is present
≤0 means that no methylation is present

The sequence of the human precursor tRNA (pre-tRNA) was obtained from publicly available RNA sequencing data performed by Gogakos et al[25]. RT primers were designed around the predicted 2'Ome site. One reverse primer was designed upstream of the possible 2'Ome site (R_U) and one downstream of the 2'Ome site (R_D). One forward primer (FW) was used for both R_U and R_D. The same RTL-Q conditions were used as for mature tRNA. All primer sequences are provided in Supplemental Table 1.

Degradation assay

HUAFs and PMFs were treated with KN-93 for 48h and then transfected with GM-113 or GM-AF25, respectively, or a negative GM-ctrl, as described above. After 24h of transfection, cells were treated with 5 µg/µl Actinomycin D (Sigma Aldrich, Cat.Nr.A9415) to inhibit novel RNA transcription for 1h. The decline of mature tRNA and the tRF levels over time were quantified by qPCR.

Statistical analyses

Results are expressed as mean ± standard error of the mean (SEM). An unpaired t-test was performed to compare single treatment with the control. As knockdown efficiency varied per experiment, for these experiments a paired t-test was performed to compare each treatment with its own control, within each individual experiment. Graphpad (v.9.0.1) was used to perform all statistical analysis. $p<0.05$ was considered significant and $p<0.1$ was considered a trend.

Author contributions

E.V.I., P.H.A.Q. and A.Y.N. designed the experiments; E.V.I., P.A.M.E., M.L.B. and H.M. conducted the experiments; E.V.I., J.W., P.H.A.Q. and A.Y.N. wrote, reviewed and edited the paper; A.Y.N. acquired funding; A.Y.N. and P.H.A.Q. supervised.

Conflict of interest

There are no conflicts of interest.

Key words

tRNA fragments; C/D box small nucleolar RNAs; orphan; 14q32 locus; DLK1-DIO3 locus; cardiovascular disease

References

1. Watkins, N.J., and Bohnsack, M.T. (2012). The box C/D and H/ACA snoRNPs: key players in the modification, processing and the dynamic folding of ribosomal RNA. *Wiley Interdiscip Rev RNA* **3**: 397-414.
2. Kiss, T. (2001). Small nucleolar RNA-guided post-transcriptional modification of cellular RNAs. *The EMBO journal* **20**: 3617-3622.
3. Decatur, W.A., and Fournier, M.J. (2002). rRNA modifications and ribosome function. *Trends Biochem Sci* **27**: 344-351.
4. Ojha, S., Malla, S., and Lyons, S.M. (2020). snoRNPs: Functions in Ribosome Biogenesis. *Biomolecules* **10**.
5. Jorjani, H., Kehr, S., Jedlinski, D.J., Gumienny, R., Hertel, J., Stadler, P.F., Zavolan, M., and Gruber, A.R. (2016). An updated human snoRNAome. *Nucleic Acids Res* **44**: 5068-5082.
6. Falaleeva, M., Welden, J.R., Duncan, M.J., and Stamm, S. (2017). C/D-box snoRNAs form methylating and non-methylating ribonucleoprotein complexes: Old dogs show new tricks. *Bioessays* **39**.
7. Elliott, B.A., Ho, H.T., Ranganathan, S.V., Vangaveti, S., Ilkayeva, O., Abou Assi, H., Choi, A.K., Agris, P.F., and Holley, C.L. (2019). Modification of messenger RNA by 2'-O-methylation regulates gene expression in vivo. *Nature communications* **10**: 3401.
8. Nostramo, R.T., and Hopper, A.K. (2019). Beyond rRNA and snRNA: tRNA as a 2'-O-methylation target for nucleolar and Cajal body box C/D RNPs. *Genes & development* **33**: 739-740.
9. Pereira, M., Francisco, S., Varanda, A.S., Santos, M., Santos, M.A.S., and Soares, A.R. (2018). Impact of tRNA Modifications and tRNA-Modifying Enzymes on Proteostasis and Human Disease. *Int J Mol Sci* **19**.
10. Krishna, S., Raghavan, S., DasGupta, R., and Palakodeti, D. (2021). tRNA-derived fragments (tRFs): establishing their turf in post-transcriptional gene regulation. *Cell Mol Life Sci* **78**: 2607-2619.
11. Keam, S.P., and Hutvagner, G. (2015). tRNA-Derived Fragments (tRFs): Emerging New Roles for an Ancient RNA in the Regulation of Gene Expression. *Life (Basel)* **5**: 1638-1651.
12. Fu, H., Feng, J., Liu, Q., Sun, F., Tie, Y., Zhu, J., Xing, R., Sun, Z., and Zheng, X. (2009). Stress induces tRNA cleavage by angiogenin in mammalian cells. *FEBS Lett* **583**: 437-442.
13. Li, Q., Hu, B., Hu, G.W., Chen, C.Y., Niu, X., Liu, J., Zhou, S.M., Zhang, C.Q., Wang, Y., and Deng, Z.F. (2016). tRNA-Derived Small Non-Coding RNAs in Response to Ischemia Inhibit Angiogenesis. *Scientific reports* **6**: 20850.
14. Elkordy, A., Mishima, E., Niizuma, K., Akiyama, Y., Fujimura, M., Tominaga, T., and Abe, T. (2018). Stress-induced tRNA cleavage and tiRNA generation in rat neuronal PC12 cells. *J Neurochem* **146**: 560-569.
15. Vitali, P., and Kiss, T. (2019). Cooperative 2'-O-methylation of the wobble cytidine of human elongator tRNA(Met)(CAT) by a nucleolar and a Cajal body-specific box C/D RNP. *Genes & development* **33**: 741-746.
16. Guzzi, N., Cieśla, M., Ngoc, P.C.T., Lang, S., Arora, S., Dimitriou, M., Pimková, K., Sommarin, M.N.E., Munita, R., Lubas, M., et al. (2018). Pseudouridylation of tRNA-Derived Fragments Steers Translational Control in Stem Cells. *Cell* **173**: 1204-1216.e1226.
17. Lyons, S.M., Fay, M.M., and Ivanov, P. (2018). The role of RNA modifications in the regulation of tRNA cleavage. *FEBS Lett* **592**: 2828-2844.
18. Clouet d'Orval, B., Bortolin, M.L., Gaspin, C., and Bachellerie, J.P. (2001). Box C/D RNA guides for the ribose methylation of archaeal tRNAs. The tRNATrp intron guides the formation of two ribose-methylated nucleosides in the mature tRNATrp. *Nucleic Acids Res* **29**: 4518-4529.
19. Håkansson, K.E.J., Goossens, E.A.C., Trompet, S., van Ingen, E., de Vries, M.R., van der Kwast, R., Ripa, R.S., Kastrup, J., Hohensinner, P.J., Kaun, C., et al. (2019). Genetic associations and regulation of expression indicate an independent role for 14q32 snoRNAs in human cardiovascular disease. *Cardiovascular research* **115**: 1519-1532.

20. Håkansson, K.E.J., Sollie, O., Simons, K.H., Quax, P.H.A., Jensen, J., and Nossent, A.Y. (2018). Circulating Small Non-coding RNAs as Biomarkers for Recovery After Exhaustive or Repetitive Exercise. *Front Physiol* **9**: 1136.
21. Nossent, A.Y., Ektefaie, N., Wojta, J., Eichelberger, B., Kopp, C., Panzer, S., and Gremmel, T. (2019). Plasma Levels of snoRNAs are Associated with Platelet Activation in Patients with Peripheral Artery Disease. *Int J Mol Sci* **20**.
22. Civitarese, R.A., Kapus, A., McCulloch, C.A., and Connelly, K.A. (2017). Role of integrins in mediating cardiac fibroblast-cardiomyocyte cross talk: a dynamic relationship in cardiac biology and pathophysiology. *Basic Res Cardiol* **112**: 6.
23. Ingen, E., Homberg, D.A.L., Bent, M.L., Mei, H., Papac-Milicevic, N., Kremer, V., Boon, R.A., Quax, P.H.A., Wojta, J., and Nossent, A.Y. (2021). C/D box snoRNA SNORD113-6/AF357425 plays a dual role in integrin signalling and arterial fibroblast function via pre-mRNA processing and 2'O-ribose methylation. *Human molecular genetics*.
24. Aparicio-Puerta, E., Lebrón, R., Rueda, A., Gómez-Martín, C., Giannoukakos, S., Jaspez, D., Medina, J.M., Zubkovic, A., Jurak, I., Fromm, B., et al. (2019). sRNAbench and sRNAtoolbox 2019: intuitive fast small RNA profiling and differential expression. *Nucleic Acids Res* **47**: W530-w535.
25. Gogakos, T., Brown, M., Garzia, A., Meyer, C., Hafner, M., and Tuschl, T. (2017). Characterizing Expression and Processing of Precursor and Mature Human tRNAs by Hydro-tRNAseq and PAR-CLIP. *Cell reports* **20**: 1463-1475.
26. Motorin, Y., and Helm, M. (2010). tRNA stabilization by modified nucleotides. *Biochemistry* **49**: 4934-4944.
27. Potapov, V., Fu, X., Dai, N., Corrêa, I.R., Jr., Tanner, N.A., and Ong, J.L. (2018). Base modifications affecting RNA polymerase and reverse transcriptase fidelity. *Nucleic Acids Res* **46**: 5753-5763.
28. Yamasaki, S., Ivanov, P., Hu, G.F., and Anderson, P. (2009). Angiogenin cleaves tRNA and promotes stress-induced translational repression. *J Cell Biol* **185**: 35-42.
29. Nguyen, T.T.M., van der Bent, M.L., Wermer, M.J.H., van den Wijngaard, I.R., van Zwet, E.W., de Groot, B., Quax, P.H.A., Kruyt, N.D., and Nossent, A.Y. (2020). Circulating tRNA Fragments as a Novel Biomarker Class to Distinguish Acute Stroke Subtypes. *Int J Mol Sci* **22**.
30. Ishida, T., Inoue, T., Niizuma, K., Konno, N., Suzuki, C., Inoue, T., Ezura, M., Uenohara, H., Abe, T., and Tominaga, T. (2020). Prediction of Functional Outcome in Patients with Acute Stroke by Measuring tRNA Derivatives. *Cerebrovasc Dis* **49**: 639-646.
31. Magee, R., Londin, E., and Rigoutsos, I. (2019). TRNA-derived fragments as sex-dependent circulating candidate biomarkers for Parkinson's disease. *Parkinsonism Relat Disord* **65**: 203-209.
32. Su, Z., Wilson, B., Kumar, P., and Dutta, A. (2020). Noncanonical Roles of tRNAs: tRNA Fragments and Beyond. *Annu Rev Genet* **54**: 47-69.
33. Magee, R., and Rigoutsos, I. (2020). On the expanding roles of tRNA fragments in modulating cell behavior. *Nucleic Acids Res* **48**: 9433-9448.
34. Liapi, E., van Bilsen, M., Verjans, R., and Schroen, B. (2020). tRNAs and tRNA fragments as modulators of cardiac and skeletal muscle function. *Biochim Biophys Acta Mol Cell Res* **1867**: 118465.
35. . GtRNAdb tRNAscan-SE analysis of complete genomes. June 2021 ed.

Supplementary data

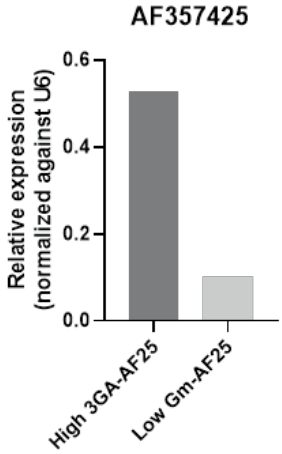

Supplemental Figure 1: Relative AF357425 expression in small RNA-seq samples. Primary murine fibroblasts were transfected with 3rd Generation Antisense (High 3GA-AF25) or Gapmers (Low Gm-AF25) against AF357425 for 24 hours. Expression levels are normalized to U6.

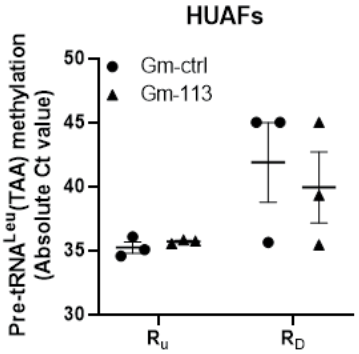

Supplemental Figure 2. Precursor (pre-)tRNA^{Leu}(TAA) methylation in human arterial fibroblasts (HUAFs). For detection of 2'O-methyated nucleotides, Reversed Transcription at Low dNTP concentration followed by Quantitative PCR (RTL-Q) was performed. Reversed primers were designed upstream (R_U) and downstream (R_D) of the predicted 2'O-methylation (2'Ome) site. RT was performed at low dNTP concentrations. When a 2'Ome site is present, the extension of the R_D primer pauses at this site when low dNTP concentrations are used, whereas the R_U primer does not. Results are shown in absolute Ct values. Ct values above the detection threshold are shown as 45 Ct. N is represented by the individual dots.

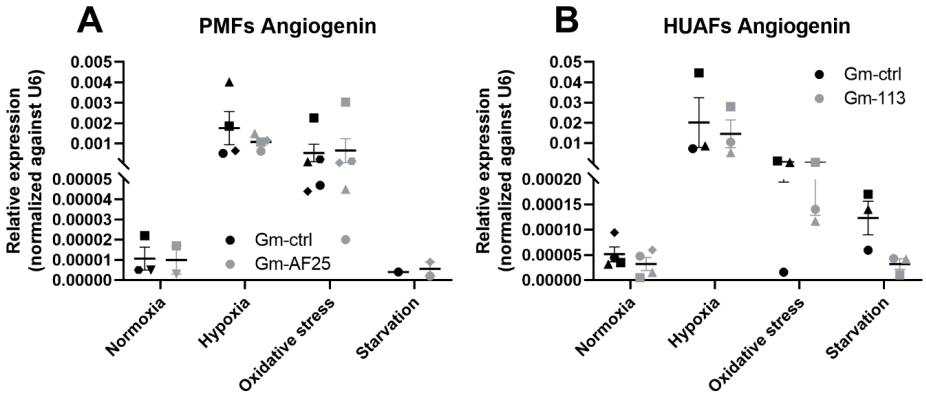

Supplemental Figure 3. Angiogenin expression in primary cells during cellular stress. (A) Primary murine fibroblasts (PMFs) and (B) human umbilical arterial fibroblasts (HUAFs) were transfected with either Gm-ctrl or Gm-AF25/113 and cultured in normoxic (control), hypoxic, oxidative stress or starvation conditions for 24h. Relative expression levels are normalized to U6. N is represented by the individual dots.

Oligonucleotide	
3GA-AF357425	3’-[GGGTTTAATCACTGTCCTC]$_D$-X-[CTCCTGTCACTAATTTGGG]$_D$-3’
GM-AF357425-D’	3’-[GUCAG]$_{2'OmeR}$[AAACCCCATG]$_D$[CUCCU]$_{2'OmeR}$-5’
GM-113-6-D’	3’-[CAGAA]$_{2'OmeR}$[ACCCCATGAT]$_D$[ATTCA]$_{2'OmeR}$-5’
GM-Control	3’-[AUCGA]$_{2'OmeR}$[TACCGTATAA]$_D$[UAACG]$_{2'OmeR}$-5’
Northern blot	
Dual DIG-labelled DNA probes	/5Dig/ACCCACGCAGACATATGT/3Dig/
Methylation primers	
Mature tRNA^{Leu}(TAA) HSA/MMU FW	CCGAGTGGTTAAGGCGTTG
Mature tRNA^{Leu}(TAA) HSA/MMU R$_D$	TGGTACCAGGAGTGG
Mature tRNA^{Leu}(TAA) HSA/MMU R$_U$	GGTACCAGGAGTGGG
pre-tRNA^{Leu}(TAA) HSA FW	AAACAAGGTTCAACGTCTGCA
pre-tRNA^{Leu}(TAA) HSA R$_D$	ACCTAAAGCTACCAGGAGTGG
pre-tRNA^{Leu}(TAA) HSA R$_U$	CGAACCCACGCGGACATATG
qPCR primers	
Mature tRNA^{Leu}(TAA) FW	CCGAGTGGTTAAGGCGTTG
Mature tRNA^{Leu}(TAA) RV	CAGGAGTGGGGTTCGAAC
Taqman Custom designed	
tRF$^{47-64}$ MMU	UGGACAUAUGUCUGCGUGGGU
tRF$^{47-64}$ HSA	UGGACAUAUGUCCGCGUGGGU
Housekeeping genes	
U6– MMU/HSA – FW	AGAAGATTAGCATGGCCCCT
U6– MMU/HSA – RV	ATTTGCGTGTCATCCTTGCG
RPLP0 HSA FW	TCCTCGTGGAAGTGACATCG
RPLP0 HSA RV	TGTCTGCTCCCACAATGAAAC
RPLP0 MMU FW	GTGATGCCCAGGGAAGACAG
RPLP0 MMU RV	TCTGCTCCCACAATGAAGCA
SnoRNAs	
SNORD113-6 – FW	TGGACCAGTGATGAATATCATG
SNORD113-6 – RV	TGGACCTCAGAGTTGCAGATG
AF357425 – FW	AGGAGCATGGGGTTTCTGAC
AF357425 – RV	TTTCATAAGGGTTTAATCACTGTCC
Angiogenin	
HSA FW	CTGGGCGTTTTGTTGTTGGTC
HSA RV	GGTTTGGCATCATAGTGCTGG
MMU FW	CCAGGCCCGTTGTTCTTGAT
MMU RV	GCAAACCATTCTCACAGGCAATA

Supplemental Table 1. Oligonucleotide and primer sequences. 3rd Generation Antisense (3GA) and gapmers (GM). [nnn]$_D$ = DNA-nucleotides; [nnn]$_{2'OmeR}$ = 2’Ome-RNA nucleotides; X = phosphorothioate linker.

antiCodon	High RPM	Low RPM	FoldChange
AlaAGC	342	317	1,08
AlaCGC	169	198	0,85
AlaTGC	334	387	0,86
ArgACG	686	338	2,03
ArgCCG	304	188	1,61
ArgCCT	1000	637	1,57
ArgTCG	786	376	2,09
ArgTCT	235	227	1,04
AsnGTT	446	101	4,40
AspGTC	1109	628	1,77
CysGCA	159	106	1,50
GlnCTG	144	150	0,96
GlnTTG	85	79	1,07
GluCTC	1153	735	1,57
GluTTC	640	489	1,31
GlyACC	22	13	1,67
GlyCCC	167	179	0,94
GlyGCC	817	806	1,01
GlyTCC	322	445	0,72
HisATG	2	2	1,09
HisGTG	213	160	1,33
IleAAT	957	811	1,18
IleGAT	11	7	1,66
IleTAT	20	16	1,20
LeuAAG	256	382	0,67
LeuCAA	255	178	1,43
LeuCAG	272	221	1,23
LeuTAA	238	121	1,97
LeuTAG	157	217	0,72
LysCTT	1758	1357	1,30
LysTTT	1241	1156	1,07
MetCAT	984	437	2,25
PheGAA	250	99	2,53
ProAGG	853	347	2,46
ProCGG	726	355	2,04
ProTGG	2659	1319	2,02
SeC(e)TCA	16	7	2,19
SeCTCA	1	1	0,67
SerAGA	470	406	1,16
SerCGA	77	44	1,75
SerGCT	139	74	1,88
SerGGA	25	8	2,95
SerTGA	161	144	1,12

SupTTA	3	1	2,42
ThrAGT	203	192	1,06
ThrCGT	148	87	1,69
ThrTGT	280	188	1,49
TrpCCA	333	245	1,36
TyrGTA	1610	736	2,19
ValAAC	233	178	1,30
ValCAC	328	261	1,26
ValTAC	88	85	1,04

Supplemental Table 2. Expression of tRNA fragments in reads per million (RPM). Small RNA sequencing was performed on primary murine fibroblasts with AF357425 overexpression (High) and knockdown (Low). Fold change is calculated by dividing High by Low RPM. Read counts are quantified in the single assignment approach where reads that map to multiple loci are assigned to the locus that has the highest expression.

Chapter 6

General Discussion

General discussion

Cardiovascular disease (CVD) is considered to be one of the most alarming health problems globally. CVD affects the quality of life and life expectancy of many patients[1]. Over the past few decades, major improvements have been made in both the prevention and treatment of CVD. Nevertheless, a rapidly ageing population, increasing prevalence of CVD, rising numbers of risk factors (e.g. obesity), and the great economic burden, emphasize the urgent need for novel therapies to improve prevention and treatment of CVD[1, 2].

Over the past few years, ncRNAs have emerged as potential therapeutical targets for different cardiovascular pathologies[3]. One type of small ncRNA that received much attention is the microRNA. MicroRNAs have the ability to fine-tune expression of multiple target genes simultaneously. They may act as master switches in complex diseases as CVD. Another type of small ncRNA is the snoRNA. C/D box snoRNAs have long been known to guide 2'-O-methylation (2'Ome) of ribosomal RNA (rRNA)[4]. However, half of the human C/D box snoRNAs lack a known target and their function is unknown[5]. Numerous C/D box snoRNAs have been associated with diseases, including CVD[6, 7]. This implies they have a regulatory role in disease.

The 14q32 ncRNA cluster (12F1 in mice) transcribes the largest known human microRNA cluster, a cluster of 54 microRNA genes. MiR-494-3p and miR-329-3p, both 14q32 microRNAs, have been shown to be involved in different processes of vascular remodeling[8-11]. In a previous study, inhibition of miR-494-3p reduced lesion development in a mouse model with early atherosclerosis[11]. This study focused on early lesion development. Patients at risk of (recurrent) cardiovascular events however, generally present with advanced and symptomatic lesions. Patients often also receive plasma cholesterol lowering drugs (e.g. statins) in order to reduce the risk of a (recurrent) cardiovascular event[12]. In this thesis, we therefore aimed to investigate 14q32 microRNA inhibition in a mouse model that more closely resembles the human clinical setting. We used mice with advanced atherosclerosis and treated them with either 3rd Generation Antisense against miR-494-3p (3GA-494) or miR-329-3p (3GA-329). We simultaneously lowered plasma lipids by changing their diet from high-fat high-cholesterol to regular chow.

Macrophages have a key role in the onset and progression of atherosclerosis[13]. In a follow-up study, we investigated whether miR-494-3p directly influences macrophage activation and polarization. Whether this affects atherosclerotic plaque stability was unknown.
Adjacent to the cluster of microRNA genes lies a cluster of 41 C/D box snoRNA genes[7]. This cluster of C/D box snoRNAs is strongly associated with CVD. This association is both

independent of and stronger than that of the 14q32 microRNAs. Expression of 14q32 snoRNAs is regulated under ischemic conditions in PAD patients and during vascular remodeling[7, 14]. Compared to the 14q32 microRNAs however, much less is known about the 14q32 snoRNAs. The canonical function of C/D box snoRNAs is to guide 2'Ome of rRNA[4]. However, none of the 14q32 snoRNAs has a known RNA target. Direct binding to the methyltransferase fibrillarin does suggest a canonical function of 2'Ome, but possibly on noncanonical RNA targets[7]. We therefore aimed to elucidate both the function and RNA targets of 14q32 snoRNAs. We focused on one of the most abundantly expressed 14q32 snoRNAs, SNORD113-6 in humans and its equivalent AF357425 in mice. First, we investigated several mRNAs of the integrin pathway that AF357425/SNORD113-6 targets via two mechanisms, pre-mRNA processing and 2'Ome. As integrin signaling is important for cell-cell and cell-matrix interactions[15], we also examined human arterial fibroblast function. Second, we aimed to determine whether AF357425/SNORD113-6 can also target small RNAs. We found that tRNAs were predominantly targeted by AF357425/SNORD113-6 and investigated whether 2'Ome by AF357425/SNORD113-6 affects fragmentation of tRNAs.

MicroRNA-494-3p and microRNA-329-3p in advanced atherosclerosis

In **chapter 2**, LDLr$^{-/-}$ mice with advanced atherosclerosis were treated with 3GA-494, 3GA-329 or a scrambled sequence control (3GA-ctrl). A subset of mice (baseline) was sacrificed directly after 10 weeks of high-fat high-cholesterol diet. We show that inhibition of miR-494-3p and, in part, miR-329-3p halted plaque progression in the carotid artery and promoted plaque stability in the aortic root. Plasma cholesterol levels were strongly reduced after changing diet from high-fat high-cholesterol to regular chow. Although we combined plasma lipid lowering with 3GA treatment, plaque sizes from either 3GA-494 or 3GA-329 mice were not reduced compared to baseline mice. This indicates that even though plaque progression was reduced, plaque regression did not occur in this setup.

Unlike the carotid artery plaques, plaque sizes in the aortic root did not differ between groups. Plaque stability however, is just as, or even more important than plaque size in reducing the risk of cardiovascular events. Collagen provides structural support in the fibrotic cap. Inhibition of miR-494-3p increased intra-plaque collagen and reduced macrophage content in advanced aortic root plaques. The number of plaque macrophages was reduced by diet switch alone and was further reduced when mice were treated with miR-494-3p inhibitors.

We observed a reduction in circulating platelets in particular, but also in pro-atherogenic Ly6C^{hi} monocytes and neutrophils in 3GA-494 treated mice. Platelets are highly involved in

proinflammatory responses and facilitate monocyte and neutrophil extravasation into the lesion[16-18]. Reducing their numbers may have contributed to the decrease in plaque macrophages and thus, is favorable in arresting plaque progression. Platelets are essential in blood clotting, which is often the direct cause of acute ischemic diseases like ischemic stroke and myocardial infarction[19]. Perhaps lowering their numbers would reduce the risk of an acute cardiovascular event as well. However, a dramatic decrease in platelets is likely accompanied by an increased bleeding risk, even though this was not (yet) observed in the 3GA-494 treated mice. Another concern is the enlarged spleen in these mice. We found a strong increase in number of splenic megakaryocytes, the progenitor cells of platelets. This is likely a compensatory mechanism to prevent severe thrombocytopenia. Treatment with 3GA-494 led to hyper-activation of human platelets *in vitro* and could be the underlying cause of rapid platelet clearance *in vivo*.

MicroRNA-494-3p in macrophage polarization

Inhibition of miR-494-3p resulted in smaller lesions with increased stability, both in early[11] and advanced atherosclerosis (**chapter 2**). Aortic root lesions contained less macrophages and numbers of pro-atherogenic Ly6C^{hi} monocytes were reduced in the circulation. Based on these findings, we hypothesized that miR-494-3p directly influences macrophage polarization in atherosclerosis. This was investigated in **chapter 3**.

First, we showed that endogenous miR-494-3p is being regulated during macrophage polarization. MiR-494-3p expression was decreased in proinflammatory M1 and increased in anti-inflammatory M2 polarization. Second, key polarization markers at mRNA and protein levels, were regulated by miR-494-3p. 3GA-494 treatment inhibited miR-494-3p expression in M1 macrophages and dampened M1 polarization. 3GA-494 treatment simultaneously enhanced M2 polarization, while miR-494-3p expression was increased in M2 macrophages. Both are favorable in reducing plaque formation and increasing stability. This is correspondingly shown in **chapter 2**. In **chapter 3**, we also showed that inhibition of miR-494-3p in atherosclerotic plaques *in vivo* led to an apparent reduction of the proinflammatory marker C-C motif chemokine receptor-2 (CCR2).

Pathway enrichment analysis predicted that miR-494-3p has more than 70 targets involved in macrophage polarization. The pathway containing most assigned genes was the Wnt signaling pathway. MiR-494-3p indeed regulates expression of multiple Wnt signaling components, including LRP6 and TBL1X. In canonical Wnt signaling, non-phosphorylated β-catenin is translocated into the nucleus, where it induces downstream transcription[20]. Wnt signaling

appeared activated through increased non-phosphorylated β-catenin, in both cultured M1 macrophages and in plaques of hypercholesterolemic mice treated with 3GA-494. The dampened M1 polarization is thus, at least in part, regulated via activated Wnt signaling.

Wnt signaling is mostly known from determining (stem) cell fates and involvement in diseases, such as cancer. Some studies, however, suggest a protective role of Wnt signaling against atherosclerosis[21-23]. Wnt signaling may have a role in limiting cholesterol accumulation in atherosclerotic plaques, for example[22, 24]. Findings from previous studies and this thesis indicate that miR-494-3p inhibition affects cholesterol metabolism. Efflux of high-density lipoprotein (HDL)[11] for instance, was increased in miR-494-3p inhibited macrophages[11]. MiR-494-3p inhibition reduced necrotic core sizes in early atherosclerotic plaques[11] and lowered plasma cholesterol levels *in vivo* (**chapter 2**). TREM2 is a marker for anti-inflammatory foamy lipid-laden macrophages involved in cholesterol metabolism[13]. Even though not a direct miR-494-3p target, TREM2 expression increased in M2 polarized macrophages treated with 3GA-494. 3-Hydroxy-3-methylglutaryl-coenzyme A synthase 1 (HMGCS1) is a putative miR-494-3p target and involved in cholesterol synthesis. Out of four human donors, three donors showed differential expression of HMGCS1 after 3GA-494 treatment, in both cultured M1 and M2 macrophages (**chapter 3**). MiR-494-3p is therefore likely involved in the regulation of cholesterol metabolism genes. Investigations on exact mechanisms remain to be performed in future research though, and also whether they involve the Wnt signaling pathway or other relevant pathways.

Polarization of macrophages towards M2 induced miR-494-3p expression. MiR-494-3p expression was even further induced in response to 3GA-494 treatment (**chapter 3**). This phenomenon was also observed in both platelets and the whole spleen after treatment with 3GA-494 (**chapter 2**). Perhaps miR-494-3p regulates expression of RNA binding proteins and RNA binding proteins in turn regulate miR-494-3p processing. RNA binding protein Mef2A, for example, directly binds to pri-miR-494-3p[10]. Which precise mechanism underlies this subset-, cell-, and tissue-specific autoregulation, however, remains to be determined.

Summarizing, the first part of this thesis shows that miR-494-3p contributes to the progression of atherosclerosis. Its inhibition halts plaque progression and increases stability of advanced lesions. MiR-329-3p inhibition has a less profound effect on the progression of atherosclerosis. Furthermore, miR-494-3p directly modulates macrophage activation and polarization. Inhibition of miR-494-3p reduces M1 polarization, while M2 polarization is

enhanced. A graphical representation of the findings from the first part of this thesis is shown in **Figure 1**.

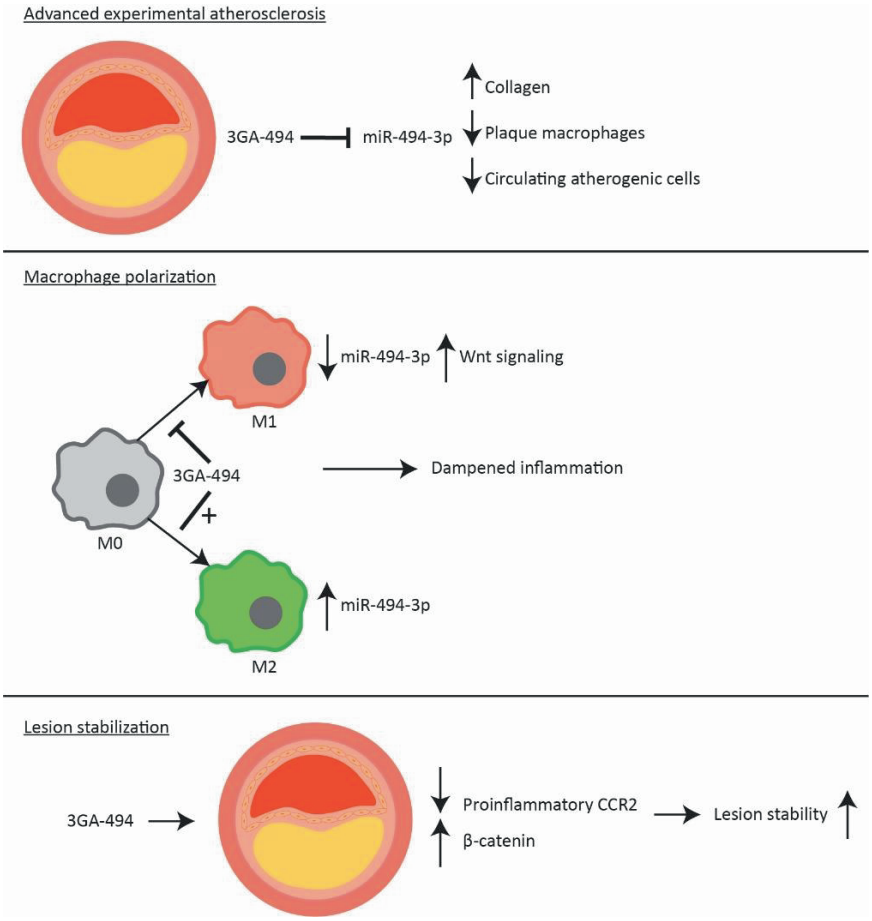

AF357425/SNORD113-6 targets mRNAs via pre-mRNA processing and 2'Ome

Figure 1. Graphical representation of miR-494-3p in advanced experimental atherosclerosis and macrophage polarization. 3rd Generation Antisense against miR-494-3p (3GA-494) was used to inhibit microRNA expression. (Top) 3GA-494 treatment in advanced atherosclerosis. (Middle) 3GA-494 dampens M1 polarization, while enhancing M2 polarization. (Bottom) Treatment with 3GA-494 reduces proinflammatory M1 marker C-C motif chemokine receptor-2 (CCR2) and increases non-phosphorylated β-catenin, via activated Wnt signaling, in atherosclerotic plaques. This likely contributed to increased lesion stability.

C/D box snoRNAs that have no known targets are called orphan snoRNAs. Since they lack known targets, their function is also unknown. Orphan C/D box snoRNAs have been described to guide fibrillarin-dependent 2'Ome on noncanonical RNA targets like mRNAs, microRNAs and tRNAs[25-27]. Completely different functions, e.g. directing alternative splicing and regulating gene expression in a microRNA-like manner, have also been described for orphan C/D box snoRNAs[28, 29].

In **chapter 4**, we aimed to lift the orphan status of one of the 14q32 snoRNAs, SNORD113-6 and its mouse equivalent AF357425. The D' box seed of this snoRNA is fully conserved between mice and humans. SNORD113-6/AF357425 and 14q32 snoRNAs in general, are highly expressed in fibroblasts. We aimed for AF357425 knockout fibroblasts. Unfortunately, those could not be obtained due to the lack of any viable AF357425-knockout clones. This either suggests that our CRISPR/Cas9 strategy was not successful or, more likely, that AF357425 is essential for cell survival. We therefore used antisense technology to knockdown or overexpress AF357425 in murine fibroblasts, followed by two different RNA sequencing (RNA-seq) strategies. In one strategy, RNA-seq was performed on whole cell lysates to examine alternative splicing and processing. In the other strategy, RNA from a fibrillarin pulldown and depleted from rRNA, was sequenced to identify fibrillarin-associated targets.

We found an enrichment of AF357425 binding sites (i.e. the reversed complement of the D' antisense box) in the last exon and the 3'UTR of (pre)mRNAs. We identified 46 genes with putative snoRNA binding sites that showed differential expression of splice- or processing-variants between AF357425 overexpression and knockdown cells. Of these genes, 20 genes had a conserved putative binding site in humans. We selected three genes, DUSP7, JAG1 and EBPL, and confirmed altered processing under SNORD113-6/AF357425 knockdown. It appeared that the location of the snoRNA binding site determines whether pre-mRNA processing is affected by SNORD113-6/AF357425 knockdown or not. A binding site in the last exon and 3'UTR, but not in introns, resulted in increased expression of the dominant variant (defined by the variant with a binding site in exon/3'UTR, the protein coding variant or the variant with most binding sites) over the alternative variant under SNORD113-6/AF357425 knockdown.

We identified 7 genes from the integrin pathway, MAP2K1, ITGB3, ITGA7, FLNB, NTN4, PARVB and COL4A4, that are fibrillarin-dependent 2'Ome mRNA targets of AF357425/SNORD113-6. The integrin pathway is important for cell-cell and cell-matrix interactions[15]. Binding sites of these genes were conserved both in mouse and human, albeit for some on different locations

(last exon/3'UTR in mouse versus introns in human). We focused on the integrin pathway since it had the strongest enrichment of targeted genes. However, we also found putative targets involved in other cardiovascular relevant pathways. After blocking novel transcription, mRNA degradation rates increased under knockdown of AF357425/SNORD113-6. 2'Ome by AF357425/SNORD113-6 is therefore important for stability of these mRNA targets. The effects on protein levels were ambiguous though and most likely depend on several factors. The location of the binding site and whether binding of AF357425/SNORD113-6 leads to 2'Ome or not, could affect protein translation. On the one hand, we show that 2'Ome protects the mRNA from degradation. More mRNA is thus present to be translated into protein. On the other hand, 2'Ome placed on the mRNA may hamper binding of the ribosome, which results in less protein[25]. When we examined fibroblast function, we found an increased barrier function, increased ability to contract extracellular matrix and increased migration in SNORD113-6 knockdown fibroblasts. Both the integrin pathway and fibroblast function are important in cardiovascular remodeling and disease[15]. How fibroblast function regulated by SNORD113-6 affects cardiovascular remodeling and disease exactly, remains to be determined in future research. A graphical representation of the findings from **chapter 4** is shown in **Figure 2**.

AF357425/SNORD113-6 directs fragmentation of tRNAs via 2'Ome

In **chapter 4**, we show that AF357425/SNORD113-6 targets a broad range of mRNAs and influences their expression through two mechanisms, pre-mRNA processing and 2'Ome. Recent studies have shown that post-transcriptional modifications guided by snoRNAs, 2'Ome and pseudouridylation Ψ, on tRNAs can direct their cleavage into smaller tRNA-derived fragments (tRFs)[27, 30]. In **chapter 5**, we aimed to determine whether AF357425/SNORD113-6 can also target small RNAs.

Small RNA sequencing (sRNA-seq) was performed on cell lysates from either AF357425 inhibited or overexpressed murine fibroblasts. The small RNAs that changed most in expression were tRFs. The overall formation of tRFs was reduced in AF357425 knockdown fibroblasts. When stratified by fragment length, the smaller sized tRFs (18-30 nucleotides) were enriched and the longer sized tRFs (30-45 nucleotides) depleted in these cells.

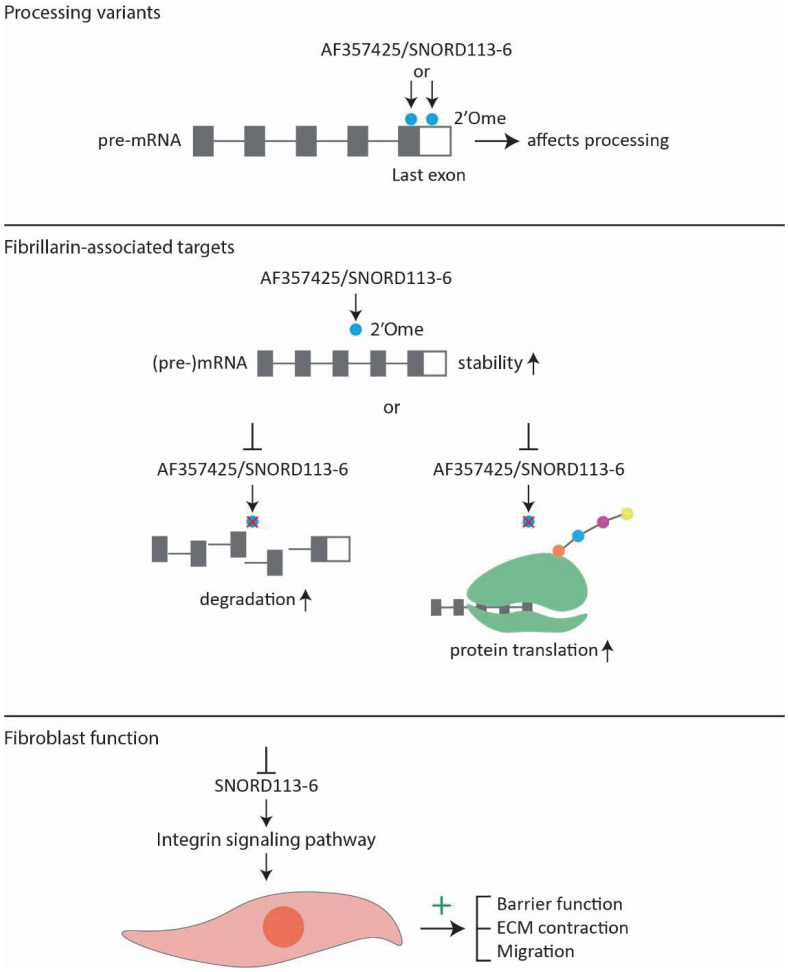

Figure 2. Graphical representation of AF357425/SNORD113-6 in 3'end processing/splicing, 2'-O-methyatlion (2'Ome) of mRNA targets and fibroblast function. RNA sequencing was performed on whole cell lysates to examine alternative splicing and processing of putative targets. RNA from fibrillarin pulldown was sequenced to identify fibrillarin-associated targets. (Top) An enrichment of SNORD113-6/AF357425 binding sites was found in the last exon and 3'UTR of (pre)mRNAs. It appears that snoRNA binding sites in the last exon and 3'UTR, but not in introns, affects pre-mRNA processing. (Middle) 2'Ome by SNORD113-6/AF357425 is important for stability of mRNAs. Inhibition of SNORD113-6/AF357425 reduces 2'Ome on its mRNA targets. This could lead to either decreased or increased protein translation via two proposed mechanisms. 2'Ome protects the mRNA from degradation. Fewer mRNAs are thus present to be translated into protein. Alternatively, 2'Ome placed on the mRNA may hamper binding of the protein. Fewer 2'Ome could therefore lead to increased protein. (Bottom) SNORD113-6 targets mRNAs of the integrin signaling pathway and affects fibroblast function.

We focused on one of the tRNAs, tRNA Leucine anti-codon TAA (tRNA^{Leu}(TAA)), in order to investigate the underlying mechanism-of-action. TRNA^{Leu}(TAA) has a predicted binding site for AF357425/SNORD113-6, which was indeed methylated by AF357425/SNORD113-6. AF357425/SNORD113-6 knockdown did not affect degradation rates of tRNA^{Leu}(TAA). This single 2'Ome site is therefore not essential for the overall stability of the tRNA. The dominant tRF of tRNA^{Leu}(TAA), tRF$^{Leu\ 47-64}$, is formed adjacent to the 2'Ome site. Knockdown of AF357425/SNORD113-6 increased the ratio of tRF$^{Leu\ 47-64}$ to tRNA^{Leu}(TAA). This suggests that 2'Ome by AF357425/SNORD113-6 acts in preventing site-specific fragmentation of tRNAs into small fragments (~18 nucleotides in length).

It has been shown that fragmentation of tRNAs increases under cellular stress, including hypoxia and oxidative stress. Plasma levels of 14q32 snoRNAs are also regulated under ischemic conditions in PAD patients[7]. As expected, exposing cells to cellular stress increased expression of AF357425/SNORD113-6, but also tRNA^{Leu}(TAA) and tRF$^{Leu\ 47-64}$. However, inducing cellular stress did not increase the ratio of tRF$^{Leu\ 47-64}$ relative to mature tRNA^{Leu}(TAA) even further in AF357425/SNORD113-6 knockdown cells. In fact, the strongest increase in this ratio was in cells cultured under physiological conditions, without induction of cellular stress. An explanation could be that other endonucleases are being activated during cellular stress and produce alternative tRF species from tRNA^{Leu}(TAA). It could also be that the upregulation of AF357425/SNORD113-6 under cellular stress, counters the effects of snoRNA knockdown.

This particular tRF$^{Leu\ 47-64}$ may have an important role in cell physiology as it is produced under physiological conditions and not exclusively during cellular stress. All different sorts of regulatory functions have been described for tRFs. They regulate protein translation, perform microRNA-like functions and interact with RNA-binding proteins[31, 32]. TRFs can also regulate cell phenotypes, including cardiac muscle cells, skeletal muscle cells and endothelial cells, and complex vascular processes like angiogenesis[31-34]. The exact function of this AF357425/SNORD113-6-dependent tRF$^{Leu\ 47-64}$ and its role in vascular remodeling is not known yet and therefore remains to be determined in future research. A graphical representation of the findings from **chapter 5** is shown in **Figure 3**.

Summarizing, the second part of this thesis shows that SNORD113-6/AF357425 targets a broad range of mRNAs and affects their expression via two mechanisms, pre-mRNA processing and 2'Ome. Both mechanisms stabilize mRNAs and affect fibroblast phenotype. Furthermore, SNORD113-6/AF357425 guides 2'Ome and thereby affects fragmentation of tRNAs in general and of tRNA^{Leu}(TAA) in particular. These insights in the function of

SNORD113-6/AF357425 and how this snoRNA affects fibroblast function, may provide novel therapeutical opportunities in the treatment of CVD.

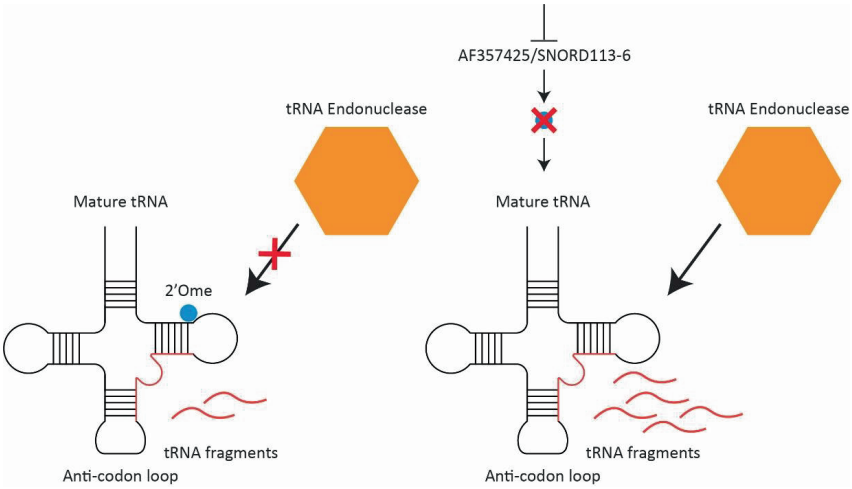

Figure 3. Graphical representation of 2'-O-methylation (2'Ome) by AF357425/SNORD113-6 in preventing site-specific fragmentation of tRNAs. TRNA endonucleases can cleave mature tRNAs into smaller tRNA fragments (tRFs). TRNA Leucine anti-codon TAA (tRNA^{Leu}(TAA)) has a conserved binding site for AF357425/SNORD113-6. The dominant tRF of tRNA^{Leu}(TAA), tRF$^{Leu\ 47\text{-}64}$, is formed adjacent to the 2'Ome site. 2'Ome by AF357425/SNORD113-6 prevents formation of tRF$^{Leu\ 47\text{-}64}$. Inhibition of AF357425/SNORD113-6 reduces 2'Ome and leads to increased formation of tRF$^{Leu\ 47\text{-}64}$.

Future perspectives

This thesis has uncovered (part of) the contribution of 14q32 microRNAs and snoRNAs to the progression of CVD. We have also explored their therapeutical potential. In the first part of the thesis we have demonstrated that targeting miR-494-3p has potential in reducing atherosclerosis. In the second part, we investigated both the function and RNA targets of one 14q32 snoRNA, human SNORD113-6 and its mouse equivalent AF357425. This provided novel insights in human arterial fibroblast function. There are still numerous hurdles to overcome for this fundamental knowledge to be developed into medicine. However, a better understanding of the underlying pathogenesis of the disease, to which this thesis contributed, does create new therapeutic opportunities in CVD.

A key challenge in the development of RNA therapeutics, and drug development in general, is to prevent or at least minimize adverse off-target effects. In principle, sequence-specific RNA inhibitors can only be biologically active in those cells that express the targeted RNA. A target microRNA or snoRNA is therefore ideally only expressed in the diseased vessel and not in other cells and tissues (e.g. healthy vessels). Both 14q32 microRNAs and snoRNAs have location-specific expression patterns throughout the human vasculature[35]. In complex diseases as CVD however, many different cell types of both the cardiovascular and immune system are involved[36]. The ideal therapeutical agent would therefore target multiple aspects of the disease, in order to maximize the therapeutic effect, without affecting physiological processes.

MicroRNAs facilitate a modest downregulation of their target genes rather than a full knockdown. They are promising candidates in that respect. In **chapter 2**, we explored miR-494-3p as a therapeutical target for reducing advanced experimental atherosclerosis. MiR-494-3p is an abundantly expressed microRNA in many different cell types. We indeed found effects of 3GA-494 treatment at a multicellular level, e.g. in plaque macrophages and circulating pro-atherogenic Ly6C^{hi} monocytes, neutrophils and platelets. 3GA-494 even had distinct anti-atherogenic effects in different subsets of macrophages (**chapter 3**). All of these effects together most likely contribute to maximize the therapeutic effect of 3GA-494 and reduced atherosclerosis.

The dramatic decline in circulating platelets in 3GA-494 treated mice was an unexpected off-target effect. Reducing platelet numbers may be favorable in arresting plaque progression and reducing the risk of an acute cardiovascular event. However, a strong decline in platelets is likely accompanied with an increased risk of bleeding. In previous studies, 3GA-494 treated

mice neither had reduced numbers of circulating platelets nor enlarged spleens[8-11]. These mice received 3GA-injections less frequently compared to the study in **chapter 2**, indicating that 3GA-494-induced depletion of platelets is a time- and dose-dependent response. Platelets have no nucleus and lack novel transcription. We therefore investigated whether 3GA-494 could directly target miR-494-3p expression in these anucleate cells. MiR-494-3p expression was initially downregulated by 3GA-494 treatment, followed by an upregulation. The primary miR-494-3p transcript, pri-miR-494-3p, was rapidly depleted in response to the miR-494-3p inhibition.

3GA-494 thus directly targets miR-494-3p expression in platelets and triggered hyperactivation compared to 3GA-ctrl treated platelets (**chapter 2**). The question remains whether altered miR-494-3p expression directly led to hyperactivation or not. It could also be that the hyperactivation of the platelets is triggered by the composition of the 3GAs. Antisense oligonucleotides have been reported to trigger hypersensitive platelets and thrombocytopenia[37-39]. These effects have been linked to several types of nucleic acids and the phosphorothioate (PS) backbone of antisense oligonucleotides[38, 39]. We did not observe a decline in circulating platelets in our 3GA-ctrl treated group. 3GA-ctrl is similar as 3GA-494 in chemical composition and structure, except for the targeted sequence. This suggests that 3GA-494-induced hyperactivation of platelets is triggered by the specific sequence rather than the chemical composition and structure of the 3GAs themselves.

The question remains how exactly 3GA-494, and antisense oligonucleotides in general, affect hypersensitivity of platelets and more importantly, how this could be avoided to prevent severe thrombocytopenia. More research into the exact mechanisms is therefore needed to overcome this current limitation for therapies using antisense oligonucleotides.

Another surprising observation in both **chapter 2** and **chapter 3** is the upregulated miR-494-3p expression in specific tissues, cell types and even in cell subsets, after treatment with 3GA-494. We found an increased expression of miR-494-3p *in vivo* in the spleen and platelets in **chapter 2**, but also in cultured human M2 polarized macrophages in **chapter 3**, after 3GA-494 treatment. MicroRNAs can regulate expression of RNA-binding proteins, which in turn can regulate processing of microRNAs. RNA-binding protein Mef2A for example, directly binds to pri-miR-494-3p[10]. Whether Mef2A or other RNA-binding proteins are responsible for the cell type- and subset-specific autoregulation of miR-494-3p, is yet to be determined.

MicroRNAs have cell type-specific target genes[40]. We showed in **chapter 3** that even subsets of the same cell type, the macrophages, have distinct Wnt pathway genes that were targeted by miR-494-3p. 3GA-494 treatment dampened M1 polarization, while M2 polarization was enhanced. The effects in both subsets are favorable in reducing atherosclerosis. However, distinct effects of miR-494-3p, and microRNAs in general, in different tissues, cells and cell subsets, are important to take into account when developing (micro)RNA therapeutics. It remains a technical challenge to specifically target cells or even their subsets, but could avoid unwanted side effects in future studies. More research is therefore needed to overcome this technical restriction that has important implications for the potential future use of (micro)RNA therapeutics.

The cluster of 14q32 C/D box snoRNAs is strongly associated with vascular remodeling and human CVD[7, 14, 41]. Plasma levels of 14q32 snoRNAs were associated with disease outcome in peripheral arterial disease (PAD)[7, 14]. These findings indicate a regulatory role of 14q32 snoRNAs in CVD. In the second part of the thesis, in **chapter 4** and **chapter 5**, we aimed to unravel the function of SNORD113-6/AF357425. Even though we succeeded to identify mRNA targets as well as tRNA targets of this snoRNA, the full function remains to be elucidated. We focused in **chapter 4** on mRNA targets from the integrin signaling pathway, but found also enrichments of mRNA targets in other cardiovascular relevant pathways, including blood coagulation and interleukin signaling. We showed that 2'Ome by AF357425/SNORD113-6 acts in stabilization of mRNAs, but effects on protein level were quite ambiguous. More research is therefore needed to fully explore the function of 2'Ome by AF357425/SNORD113-6. Furthermore, SNORD113-6/AF357425 has two antisense boxes and we now focused on just one, the D' antisense box, for target prediction. The question whether the other antisense box is active or not, still needs to be answered.

What complicates the research in (orphan) C/D box snoRNAs is that it can be challenging to reliably knockdown these snoRNAs[42]. We aimed to overcome this issue by generating an AF357425 knockout model. Our knockout strategy however, proved unsuccessful. This suggests nevertheless that AF357425 is essential for cell survival. AF357425 likely also acts in cell proliferation. Prior treatment with KN93 in order to synchronize the cell cycle, was needed to reproducibly knockdown AF357425 using oligonucleotides. How and by which exact mechanism SNORD113-6/AF357425 expression is being regulated in cell survival and proliferation, remains elusive for now.

Of course, the technical challenges in snoRNA knockdown also complicate investigating the function of AF357425/SNORD113-6 *in vivo*. Targeting AF357425 in, for example, a hind limb ischemia model (a model for PAD) would explore the therapeutical potential of AF357425. Knockdown of SNORD113-6 affected human arterial fibroblast phenotype and increased barrier function, extracellular contraction and cell migration. In **chapter 5**, we showed that exposing both human and murine fibroblasts to hypoxia and oxidative stress upregulated SNORD113-6/AF357425 expression. Both are important triggers of vascular remodeling processes. Perhaps modulating AF357425 expression *in vivo* would consequently also affect entire processes like angiogenesis.

In **chapter 5** it was demonstrated that 2'Ome by SNORD113-6/AF357425 regulates tRNA fragmentation. We focused on the formation of $tRF^{Leu\ 47\text{-}64}$ in particular. The question remains what the function of this AF357425/SNORD113-6-dependent tRF could be. TRFs have been shown to be functionally active in cardiac and skeletal muscle cells, but also in inhibition of processes like angiogenesis[33, 34]. The function and targets of $tRF^{Leu\ 47\text{-}64}$ as well as its role in vascular remodeling remains to be identified in future studies.

Even though many questions still need to be answered, we managed to lift the orphan status of AF357425/SNORD113-6. Like a microRNA, AF357425/SNORD113-6 facilitates a modest regulation of its targets, but affects many target genes simultaneously. Modulation of AF357425/SNORD113-6 can thus be powerful in complex diseases as CVD. SnoRNAs or tRNA fragments that act like microRNAs or that perform functions completely different from their canonical function, increases the complexity of ncRNAs. It also provides a new regulatory layer to their function that may yield novel therapeutical targets. We explored the function of one of the 14q32 snoRNAs in humans. Still, more research into the remaining 40 14q32 snoRNAs remains to be done.

Research over the past few years has led to more understanding of CVD. Atherosclerosis, the underlying cause of most CVDs, is no longer considered to be just a lipid-driven disease. The inflammatory component of atherosclerosis is now being recognized as a major contributor to the progression of the disease. The CANTOS trial is a prominent example proving the role of the immune system in CVD, independent of lipid lowering[36, 43]. Advances in sequencing techniques created new angles for therapeutic strategies to combat CVD. A large part of the noncoding human genome is no longer considered non-functional. In fact, the role of ncRNAs in regulating gene expression and in different cardiovascular pathologies is now increasingly being recognized[3]. The use of mRNA vaccines in the current COVID-19 pandemic may also

pave the way for RNA therapeutics in clinical practice[44]. Many steps still have to be taken before ncRNA therapies will be used to treat CVD. However, this thesis showed that 14q32 microRNAs and snoRNAs may be promising therapeutical targets to treat and prevent CVD.

References

1. Organization, W.H. (2017). https://www.who.int/news-room/fact-sheets/detail/cardiovascular-diseases-(cvds).
2. Timmis, A., Townsend, N., Gale, C., Grobbee, R., Maniadakis, N., Flather, M., Wilkins, E., Wright, L., Vos, R., Bax, J., et al. (2018). European Society of Cardiology: Cardiovascular Disease Statistics 2017. *European heart journal* **39**: 508-579.
3. Poller, W., Dimmeler, S., Heymans, S., Zeller, T., Haas, J., Karakas, M., Leistner, D.M., Jakob, P., Nakagawa, S., Blankenberg, S., et al. (2018). Non-coding RNAs in cardiovascular diseases: diagnostic and therapeutic perspectives. *European heart journal* **39**: 2704-2716.
4. Watkins, N.J., and Bohnsack, M.T. (2012). The box C/D and H/ACA snoRNPs: key players in the modification, processing and the dynamic folding of ribosomal RNA. *Wiley Interdiscip Rev RNA* **3**: 397-414.
5. Jorjani, H., Kehr, S., Jedlinski, D.J., Gumienny, R., Hertel, J., Stadler, P.F., Zavolan, M., and Gruber, A.R. (2016). An updated human snoRNAome. *Nucleic Acids Res* **44**: 5068-5082.
6. Taulli, R., and Pandolfi, P.P. (2012). "Snorkeling" for missing players in cancer. *The Journal of clinical investigation* **122**: 2765-2768.
7. Håkansson, K.E.J., Goossens, E.A.C., Trompet, S., van Ingen, E., de Vries, M.R., van der Kwast, R., Ripa, R.S., Kastrup, J., Hohensinner, P.J., Kaun, C., et al. (2019). Genetic associations and regulation of expression indicate an independent role for 14q32 snoRNAs in human cardiovascular disease. *Cardiovascular research* **115**: 1519-1532.
8. Welten, S.M., Bastiaansen, A.J., de Jong, R.C., de Vries, M.R., Peters, E.A., Boonstra, M.C., Sheikh, S.P., La Monica, N., Kandimalla, E.R., Quax, P.H., et al. (2014). Inhibition of 14q32 MicroRNAs miR-329, miR-487b, miR-494, and miR-495 increases neovascularization and blood flow recovery after ischemia. *Circulation research* **115**: 696-708.
9. Welten, S.M.J., de Jong, R.C.M., Wezel, A., de Vries, M.R., Boonstra, M.C., Parma, L., Jukema, J.W., van der Sluis, T.C., Arens, R., Bot, I., et al. (2017). Inhibition of 14q32 microRNA miR-495 reduces lesion formation, intimal hyperplasia and plasma cholesterol levels in experimental restenosis. *Atherosclerosis* **261**: 26-36.
10. Welten, S.M.J., de Vries, M.R., Peters, E.A.B., Agrawal, S., Quax, P.H.A., and Nossent, A.Y. (2017). Inhibition of Mef2a Enhances Neovascularization via Post-transcriptional Regulation of 14q32 MicroRNAs miR-329 and miR-494. *Molecular therapy Nucleic acids* **7**: 61-70.
11. Wezel, A., Welten, S.M., Razawy, W., Lagraauw, H.M., de Vries, M.R., Goossens, E.A., Boonstra, M.C., Hamming, J.F., Kandimalla, E.R., Kuiper, J., et al. (2015). Inhibition of MicroRNA-494 Reduces Carotid Artery Atherosclerotic Lesion Development and Increases Plaque Stability. *Annals of surgery* **262**: 841-847; discussion 847-848.
12. Stone, N.J., Robinson, J.G., Lichtenstein, A.H., Bairey Merz, C.N., Blum, C.B., Eckel, R.H., Goldberg, A.C., Gordon, D., Levy, D., Lloyd-Jones, D.M., et al. (2014). 2013 ACC/AHA guideline on the treatment of blood cholesterol to reduce atherosclerotic cardiovascular risk in adults: a report of the American College of Cardiology/American Heart Association Task Force on Practice Guidelines. *Circulation* **129**: S1-45.
13. Willemsen, L., and de Winther, M.P. (2020). Macrophage subsets in atherosclerosis as defined by single-cell technologies. *J Pathol* **250**: 705-714.
14. Håkansson, K.E.J., Sollie, O., Simons, K.H., Quax, P.H.A., Jensen, J., and Nossent, A.Y. (2018). Circulating Small Non-coding RNAs as Biomarkers for Recovery After Exhaustive or Repetitive Exercise. *Front Physiol* **9**: 1136.
15. Civitarese, R.A., Kapus, A., McCulloch, C.A., and Connelly, K.A. (2017). Role of integrins in mediating cardiac fibroblast-cardiomyocyte cross talk: a dynamic relationship in cardiac biology and pathophysiology. *Basic Res Cardiol* **112**: 6.
16. Badrnya, S., Schrottmaier, W.C., Kral, J.B., Yaiw, K.C., Volf, I., Schabbauer, G., Soderberg-Naucler, C., and Assinger, A. (2014). Platelets mediate oxidized low-density lipoprotein-

induced monocyte extravasation and foam cell formation. *Arteriosclerosis, thrombosis, and vascular biology* **34**: 571-580.
17. da Costa Martins, P., Garcia-Vallejo, J.J., van Thienen, J.V., Fernandez-Borja, M., van Gils, J.M., Beckers, C., Horrevoets, A.J., Hordijk, P.L., and Zwaginga, J.J. (2007). P-selectin glycoprotein ligand-1 is expressed on endothelial cells and mediates monocyte adhesion to activated endothelium. *Arteriosclerosis, thrombosis, and vascular biology* **27**: 1023-1029.
18. Lisman, T. (2018). Platelet-neutrophil interactions as drivers of inflammatory and thrombotic disease. *Cell Tissue Res* **371**: 567-576.
19. Nording, H., Baron, L., and Langer, H.F. (2020). Platelets as therapeutic targets to prevent atherosclerosis. *Atherosclerosis* **307**: 97-108.
20. Nusse, R., and Clevers, H. (2017). Wnt/β-Catenin Signaling, Disease, and Emerging Therapeutic Modalities. *Cell* **169**: 985-999.
21. Ackers, I., Szymanski, C., Silver, M.J., and Malgor, R. (2020). Oxidized Low-Density Lipoprotein Induces WNT5A Signaling Activation in THP-1 Derived Macrophages and a Human Aortic Vascular Smooth Muscle Cell Line. *Front Cardiovasc Med* **7**: 567837.
22. Borrell-Pagès, M., Romero, J.C., and Badimon, L. (2015). LRP5 deficiency down-regulates Wnt signalling and promotes aortic lipid infiltration in hypercholesterolaemic mice. *Journal of cellular and molecular medicine* **19**: 770-777.
23. Cheng, W.L., Yang, Y., Zhang, X.J., Guo, J., Gong, J., Gong, F.H., She, Z.G., Huang, Z., Xia, H., and Li, H. (2017). Dickkopf-3 Ablation Attenuates the Development of Atherosclerosis in ApoE-Deficient Mice. *Journal of the American Heart Association* **6**.
24. Borrell-Pages, M., Carolina Romero, J., and Badimon, L. (2015). LRP5 and plasma cholesterol levels modulate the canonical Wnt pathway in peripheral blood leukocytes. *Immunol Cell Biol* **93**: 653-661.
25. Elliott, B.A., Ho, H.T., Ranganathan, S.V., Vangaveti, S., Ilkayeva, O., Abou Assi, H., Choi, A.K., Agris, P.F., and Holley, C.L. (2019). Modification of messenger RNA by 2'-O-methylation regulates gene expression in vivo. *Nature communications* **10**: 3401.
26. van der Kwast, R., van Ingen, E., Parma, L., Peters, H.A.B., Quax, P.H.A., and Nossent, A.Y. (2018). Adenosine-to-Inosine Editing of MicroRNA-487b Alters Target Gene Selection After Ischemia and Promotes Neovascularization. *Circulation research* **122**: 444-456.
27. Vitali, P., and Kiss, T. (2019). Cooperative 2'-O-methylation of the wobble cytidine of human elongator tRNA(Met)(CAT) by a nucleolar and a Cajal body-specific box C/D RNP. *Genes & development* **33**: 741-746.
28. Kishore, S., Khanna, A., Zhang, Z., Hui, J., Balwierz, P.J., Stefan, M., Beach, C., Nicholls, R.D., Zavolan, M., and Stamm, S. (2010). The snoRNA MBII-52 (SNORD 115) is processed into smaller RNAs and regulates alternative splicing. *Human molecular genetics* **19**: 1153-1164.
29. Brameier, M., Herwig, A., Reinhardt, R., Walter, L., and Gruber, J. (2011). Human box C/D snoRNAs with miRNA like functions: expanding the range of regulatory RNAs. *Nucleic Acids Res* **39**: 675-686.
30. Guzzi, N., Cieśla, M., Ngoc, P.C.T., Lang, S., Arora, S., Dimitriou, M., Pimková, K., Sommarin, M.N.E., Munita, R., Lubas, M., et al. (2018). Pseudouridylation of tRNA-Derived Fragments Steers Translational Control in Stem Cells. *Cell* **173**: 1204-1216.e1226.
31. Su, Z., Wilson, B., Kumar, P., and Dutta, A. (2020). Noncanonical Roles of tRNAs: tRNA Fragments and Beyond. *Annu Rev Genet* **54**: 47-69.
32. Magee, R., and Rigoutsos, I. (2020). On the expanding roles of tRNA fragments in modulating cell behavior. *Nucleic Acids Res* **48**: 9433-9448.
33. Liapi, E., van Bilsen, M., Verjans, R., and Schroen, B. (2020). tRNAs and tRNA fragments as modulators of cardiac and skeletal muscle function. *Biochim Biophys Acta Mol Cell Res* **1867**: 118465.

34. Li, Q., Hu, B., Hu, G.W., Chen, C.Y., Niu, X., Liu, J., Zhou, S.M., Zhang, C.Q., Wang, Y., and Deng, Z.F. (2016). tRNA-Derived Small Non-Coding RNAs in Response to Ischemia Inhibit Angiogenesis. *Scientific reports* **6**: 20850.
35. Goossens, E.A.C., de Vries, M.R., Simons, K.H., Putter, H., Quax, P.H.A., and Nossent, A.Y. (2019). miRMap: Profiling 14q32 microRNA Expression and DNA Methylation Throughout the Human Vasculature **6**.
36. Lutgens, E., Atzler, D., Döring, Y., Duchene, J., Steffens, S., and Weber, C. (2019). Immunotherapy for cardiovascular disease. *European heart journal* **40**: 3937-3946.
37. Crooke, S.T., Baker, B.F., Witztum, J.L., Kwoh, T.J., Pham, N.C., Salgado, N., McEvoy, B.W., Cheng, W., Hughes, S.G., Bhanot, S., et al. (2017). The Effects of 2'-O-Methoxyethyl Containing Antisense Oligonucleotides on Platelets in Human Clinical Trials. *Nucleic Acid Ther* **27**: 121-129.
38. Flierl, U., Nero, T.L., Lim, B., Arthur, J.F., Yao, Y., Jung, S.M., Gitz, E., Pollitt, A.Y., Zaldivia, M.T., Jandrot-Perrus, M., et al. (2015). Phosphorothioate backbone modifications of nucleotide-based drugs are potent platelet activators. *J Exp Med* **212**: 129-137.
39. Zaslavsky, A., Adams, M., Cao, X., Yamaguchi, A., Henderson, J., Busch-Østergren, P., Udager, A., Pitchiaya, S., Tourdot, B., Kasputis, T., et al. (2021). Antisense oligonucleotides and nucleic acids generate hypersensitive platelets. *Thromb Res* **200**: 64-71.
40. Rogg, E.M., Abplanalp, W.T., Bischof, C., John, D., Schulz, M.H., Krishnan, J., Fischer, A., Poluzzi, C., Schaefer, L., Bonauer, A., et al. (2018). Analysis of Cell Type-Specific Effects of MicroRNA-92a Provides Novel Insights Into Target Regulation and Mechanism of Action. *Circulation* **138**: 2545-2558.
41. Nossent, A.Y., Ektefaie, N., Wojta, J., Eichelberger, B., Kopp, C., Panzer, S., and Gremmel, T. (2019). Plasma Levels of snoRNAs are Associated with Platelet Activation in Patients with Peripheral Artery Disease. *Int J Mol Sci* **20**.
42. Ploner, A., Ploner, C., Lukasser, M., Niederegger, H., and Hüttenhofer, A. (2009). Methodological obstacles in knocking down small noncoding RNAs. *Rna* **15**: 1797-1804.
43. Ridker, P.M., Everett, B.M., Thuren, T., MacFadyen, J.G., Chang, W.H., Ballantyne, C., Fonseca, F., Nicolau, J., Koenig, W., Anker, S.D., et al. (2017). Antiinflammatory Therapy with Canakinumab for Atherosclerotic Disease. *The New England journal of medicine* **377**: 1119-1131.
44. Kim, Y.C., Dema, B., and Reyes-Sandoval, A. (2020). COVID-19 vaccines: breaking record times to first-in-human trials. *NPJ Vaccines* **5**: 34.

Appendix

Nederlandse Samenvatting

Introductie

Hart- en vaatziekten

Hart- en vaatziekten zijn wereldwijd één van de meest voorkomende doodsoorzaken en vertegenwoordigen 31% van alle sterfgevallen ter wereld. Het hart en de bloedvaten, die het cardiovasculaire systeem worden genoemd, circuleren bloed door het lichaam om zuurstof en voedingsstoffen af te geven en afvalstoffen te verwijderen. 'Hart- en vaatziekten' is een verzamelnaam voor verschillende ziektes die het cardiovasculaire systeem aantasten. Hieronder vallen een hartinfarct, beroerte en perifeer vaatlijden.

Atherosclerose

De onderliggende oorzaak van de meeste hart- en vaatziekten is atherosclerose. Atherosclerose is een chronische ontstekingsziekte die wordt gekenmerkt door een progressieve opbouw van plaques in de slagaderwand. Plaques zijn samengesteld uit lipiden en ontstekingscellen. Plaques ontwikkelen zich in grote en middelgrote slagaders. De meeste plaques die zich tijdens het leven van een persoon ontwikkelen blijven onopgemerkt. Patiënten krijgen doorgaans pas symptomen wanneer de slagader ernstig vernauwd raakt (bij een stenose van meer dan 70%) of wanneer een plaque scheurt. Dit laatste veroorzaakt een acute verstopping van de slagader. Die patiënten vertonen vaak ernstiger symptomen die zelfs fataal kunnen zijn, bijvoorbeeld in geval van een hartinfarct of ischemische beroerte. Volledige ruptuur van een plaque of plaque-erosie (wanneer een oppervlakkig stukje van de plaque afbreekt) leidt tot het vormen van een bloedprop in de slagader. De bloedprop sluit de slagader gedeeltelijk of volledig af, blokkeert de bloedstroom en veroorzaakt een acuut tekort aan zuurstof en voedingsstoffen in het achterliggende gebied. Dit heet een infarct. Zuurstof en voedingsstoffen zijn van cruciaal belang voor het overleven en functioneren van weefsel. Daarom moet onmiddellijk worden ingegrepen om de bloedstroom te herstellen en de nadelige gevolgen, waaronder celdood en blijvende schade in de ischemische weefsels, te beperken.

Risicofactoren en huidige behandelingen

Risicofactoren voor door atherosclerose veroorzaakte hart- en vaatziekten zijn hoog cholesterol, diabetes, obesitas, genetische aanleg, hoge bloeddruk en leeftijd. Veel van deze risicofactoren kunnen het gevolg zijn van een ongezonde levensstijl, zoals een hoge vet-, cholesterol- en zoutinname, roken en een gebrek aan lichaamsbeweging. Gezonde veranderingen in de levensstijl kunnen daarom helpen in de preventie van hart- en vaatziekten. Plasma lipiden-verlagende geneesmiddelen (bv. statines), bloedplaatjesremmers

en antihypertensiva zijn voorbeelden van veel gebruikte geneesmiddelen om het risico op een (recidief) cardiovasculair event te verlagen.

Zodra zich een cardiovasculair event heeft voorgedaan (bv. een hartinfarct), zijn de therapieën gericht op het herstellen van de bloedstroom, met als doel herhaling te voorkomen en het getroffen orgaan, zoals het hart, te ondersteunen. Bloedstolsel oplossende geneesmiddelen (trombolytica) en chirurgische ingrepen zijn de huidige therapieën om de arteriële blokkade te verwijderen en de bloedstroom te herstellen.

Ondanks verbeteringen in zowel de preventie als behandelingen van hart- en vaatziekten, vertonen de huidige behandelingen ook tekortkomingen. Zo is er een risico op terugkerende occlusies bij endovasculaire ingrepen of bypass operaties, of brengen chirurgische ingrepen, zoals een endarterectomie, perioperatieve risico's met zich mee. De verwachting bestaat dat het aantal patiënten over de jaren heen alleen maar toe zal nemen. Dit komt onder andere door een groei van het aantal risicofactoren, veelal veroorzaakt door een ongezonde leefstijl en door vergrijzing van de samenleving. De totale kosten voor patiënten met hart- en vaatziekten zijn hoog en zullen naar verwachting nog veel verder stijgen. Dit benadrukt de urgentie tot het ontwikkelen van nieuwe therapieën die zowel de preventie als de behandelingen van hart- en vaatziekten verbeteren.

Niet-coderend RNA

Niet-coderende RNA's (ncRNA's) zijn RNA's die niet in eiwitten worden vertaald. Meer dan 97% van het menselijke genoom codeert voor ncRNA's. Jarenlang werden delen van het humane genoom die niet coderen voor eiwitten beschouwd als junk-DNA. De laatste 2 decennia zijn er echter steeds meer aanwijzingen dat ncRNA's van cruciaal belang zijn voor de regulering van genexpressie en de vervulling van functies bij verschillende ziekten, waaronder hart- en vaatziekten. NcRNA's reguleren de expressie van andere RNA's. Op basis van hun grootte worden ncRNA soorten ingedeeld in ofwel kleine ofwel lange ncRNAs (respectievelijk korter of langer dan 200 nucleotiden). Er zijn veel verschillende soorten ncRNA's, die op hun beurt verschillende functies vervullen. In dit proefschrift ligt de nadruk op microRNA's, small nucleolar RNA's (snoRNA's) en transfer RNA's (tRNA's).

Een type klein ncRNA dat veelal wordt bestudeerd in cardiovasculaire processen, is de microRNA. MicroRNA's reguleren de expressie van meerdere genen tegelijk. In complexe ziekten zoals hart- en vaatziekten, waarin meerdere genen betrokken zijn, kan het veranderen van de expressie van één microRNA daarom resulteren in een groot effect.

Een ander type klein ncRNA is de snoRNA. Van C/D box snoRNA's is al lang bekend dat zij 2'-O-methylering (2'Ome) van ribosomaal RNA (rRNA) begeleiden. Voor de helft van de menselijke C/D box snoRNA's ontbreekt echter een bekend target en hun functie is onbekend. Talrijke C/D box snoRNA's zijn wel in verband gebracht met verschillende ziekten, waaronder hart- en vaatziekten. Dit impliceert dat zij een regulerende rol hebben hierin.

Het 14q32 cluster

Een cluster op de lange arm van chromosoom 14 van het humane genoom (14q32) codeert voor talrijke ncRNA's. Het 14q32 cluster, ook DLK1-DIO3 locus genoemd naar de eiwit-coderende genen DLK1 en DIO3, is sterk geconserveerd bij de mens en de muis. Het equivalent bij muizen bevindt zich op chromosoom 12 (12F1). Het 14q32 cluster transcribeert het grootste bekende humane microRNA-cluster, een cluster van 54 microRNA-genen. Het 14q32 cluster codeert naast zijn drie eiwit-coderende genen en 54 microRNA's, voor een cluster van 41 C/D box snoRNA's, drie lange niet-coderende RNA's (lncRNA's), MEG3, MEG8 en MEG9, en Piwi-interacterende RNA's (piRNA's). Genetische associatie analyses hebben aangetoond dat de 14q32 microRNA's, snoRNA's en lncRNA's, onafhankelijk van elkaar, sterk geassocieerd zijn met hart- en vaatziekten.

14q32 microRNA-494-3p en microRNA-329-3p in atherosclerose

MiR-494-3p en miR-329-3p, beide 14q32 microRNA's, zijn betrokken bij verschillende processen van vasculaire remodellering. In een eerdere studie verminderde remming van miR-494-3p de ontwikkeling van plaques in een muismodel met vroege atherosclerose. Deze studie richtte zich op de vroege ontwikkeling van plaques. Patiënten die risico lopen op (terugkerende) cardiovasculaire aandoeningen hebben echter meestal vergevorderde en symptomatische plaques. Patiënten krijgen vaak ook plasma-cholesterolverlagende medicijnen (bv. statines) om het risico op een (recidief) cardiovasculair event te verminderen. In dit proefschrift wilden we daarom 14q32 microRNA remming onderzoeken in een muismodel dat meer lijkt op de menselijke klinische setting. We gebruikten muizen met gevorderde atherosclerose en behandelden hen met ofwel 3e generatie antisense tegen miR-494-3p (3GA-494) of miR-329-3p (3GA-329). Tegelijkertijd verlaagden we hun plasma lipiden door hun dieet te veranderen van vet- en cholesterolrijk naar normaal voedsel.

Macrofagen spelen een belangrijke rol bij het ontstaan en de progressie van atherosclerose. In een vervolgstudie hebben we onderzocht of miR-494-3p direct invloed heeft op macrofaag activatie en polarisatie. Of dit een invloed heeft op de stabiliteit van atherosclerotische plaques was onbekend.

De functie en RNA-targets van 14q32 snoRNA's

De expressie van 14q32 snoRNA's wordt gereguleerd onder ischemische omstandigheden bij patiënten met perifeer vaatlijden en tijdens vasculaire remodellering. In vergelijking met de 14q32 microRNA's, is er echter veel minder bekend over de 14q32 snoRNA's. Normaliter is de functie van C/D box snoRNA's het begeleiden van 2'Ome op rRNA. Geen van de 14q32 snoRNA's heeft echter een bekend RNA-target. C/D box snoRNA's die geen bekende RNA-targets hebben, worden ''wees'' snoRNA's genoemd. Aangezien zij geen bekende RNA-targets hebben, is hun functie ook onbekend. Directe binding van 14q32 snoRNA's aan methyltransferase fibrillarine suggereert wel de functie van 2'Ome, maar mogelijk op andere RNA-targets dan rRNA. Daarom was ons doel om zowel de functie als de RNA-targets van 14q32 snoRNA's op te helderen. Wij richtten ons op één 14q32 snoRNA die hoog tot expressie komt, SNORD113-6 bij de mens en zijn equivalent AF357425 bij de muis. We laten zien dat AF357425/SNORD113-6 een breed scala van mRNAs target en hun expressie beïnvloedt via twee mechanismen, pre-mRNA processing en 2'Ome. Vervolgens hebben we mRNAs van de integrine pathway geïdentificeerd als targets van AF357425/SNORD113-6. Aangezien integrine signalering belangrijk is voor cel-cel en cel-matrix interacties, onderzochten we ook of inhibitie van SNORD113-6 de functie van humane arteriële fibroblasten veranderde. Ten tweede wilden we bepalen of AF357425/SNORD113-6 ook kleine RNA's kan targeten. We vonden dat tRNA's voornamelijk werden getarget door AF357425/SNORD113-6 en onderzochten of 2'Ome door AF357425/SNORD113-6 de fragmentatie van tRNA's beïnvloedt.

Proefschrift

Het doel van het eerste deel van dit proefschrift is om inhibitie van microRNA-494-3p en microRNA-329-3p in gevorderde atherosclerose te onderzoeken. Het doel van het tweede deel is om zowel de functie als RNA-targets van één 14q32 snoRNA, humaan SNORD113-6 en de muis equivalent AF357425, te onderzoeken.

MicroRNA-494-3p en microRNA-329-3p in gevorderde atherosclerose

In **hoofdstuk 2** werden LDLr$^{-/-}$ muizen met gevorderde atherosclerose behandeld met 3GA-494, 3GA-329 of een scrambled sequence controle (3GA-ctrl). Een subset van muizen (baseline) werd direct na het tien weken volgen van een vet- en cholesterolrijk dieet opgeofferd. Wij tonen aan dat remming van miR-494-3p en, gedeeltelijk, miR-329-3p de progressie van plaque in de halsslagader stopte en de plaque stabiliteit in de aorta bevorderde. Plasma cholesterol niveaus werden sterk verlaagd na het veranderen van dieet van vet- en cholesterolrijk naar normaal voedsel. Hoewel we de behandeling met 3GA combineerden met het verlagen van plasma lipiden, werd de grootte van de plaque van zowel

3GA-494 als 3GA-329 muizen niet verminderd in vergelijking met de baseline muizen. Dit geeft aan dat, hoewel de plaque progressie werd verminderd, plaque regressie niet optrad in deze opzet.

In tegenstelling tot de plaques in de halsslagaders, verschilden de plaque groottes in de aorta niet tussen de groepen. De stabiliteit van de plaque is echter net zo belangrijk als, of zelfs belangrijker dan de grootte van de plaque voor het verminderen van het risico op cardiovasculaire events. Collageen biedt structurele support in de fibrotische kap van de plaque. Inhibitie van miR-494-3p verhoogde het collageen en verminderde het aantal macrofagen in de gevorderde aorta plaques. Het aantal plaque macrofagen werd verminderd door alleen het dieet te veranderen en werd verder verminderd wanneer muizen werden behandeld met miR-494-3p remmers.

Muizen behandeld met 3GA-494 hadden niet alleen een sterk verminderd aantal circulerende bloedplaatjes, maar ook een verminderd aantal pro-atherogene Ly6C^{hi} monocyten en neutrofielen in de circulatie. Bloedplaatjes zijn sterk betrokken bij pro-inflammatoire reacties en vergemakkelijken de extravasatie van monocyten en neutrofielen in de plaque. Vermindering van hun aantal kan hebben bijgedragen aan de afname van plaque macrofagen, hetgeen gunstig is bij het stoppen van plaque progressie. Bloedplaatjes zijn essentieel in de bloedstolling. Een bloedprop is vaak de directe oorzaak van acute ischemische aandoeningen zoals ischemische beroerte en myocardinfarct. Wellicht zou een verlaging van hun aantal ook het risico op een acute cardiovasculaire events verminderen. Een drastische daling van het aantal bloedplaatjes gaat echter waarschijnlijk gepaard met een verhoogd risico op bloedingen, hoewel dit (nog) niet werd waargenomen bij de met 3GA-494 behandelde muizen. Een ander punt van zorg is de vergrote milt bij deze muizen. Wij vonden een sterke toename van het aantal megakaryocyten in de milt, de voorlopercellen van bloedplaatjes. Dit is waarschijnlijk een compensatiemechanisme om ernstige trombocytopenie te voorkomen. Behandeling met 3GA-494 leidde tot hyper-activatie van menselijke bloedplaatjes *in vitro* en zou de onderliggende oorzaak kunnen zijn van de snelle klaring van bloedplaatjes *in vivo*.

MicroRNA-494-3p in macrofaag polarisatie

Remming van miR-494-3p resulteerde in kleinere plaques met een verhoogde stabiliteit, zowel in vroege als in gevorderde atherosclerose (**hoofdstuk 2**). Aorta plaques bevatten minder macrofagen en het aantal pro-atherogene Ly6C^{hi} monocyten waren ook verminderd in de circulatie. Gebaseerd op deze bevindingen stelden wij de hypothese dat miR-494-3p

direct invloed heeft op macrofaag polarisatie in atherosclerose. Dit werd onderzocht in **hoofdstuk 3**.

Ten eerste toonden we aan dat endogene miR-494-3p gereguleerd wordt tijdens macrofaag polarisatie. MiR-494-3p expressie was verlaagd in pro-inflammatoire M1 en verhoogd in anti-inflammatoire M2 polarisatie. Ten tweede werden belangrijke polarisatie markers op mRNA en eiwit niveau gereguleerd door miR-494-3p. 3GA-494 behandeling remde miR-494-3p expressie in M1 macrofagen en dempte M1 polarisatie. 3GA-494 behandeling versterkte tegelijkertijd M2 polarisatie, terwijl miR-494-3p expressie verhoogd werd in M2 macrofagen. Beide zijn gunstig in het verminderen van plaque vorming en het verhogen van de stabiliteit. Dit komt overeen met de resultaten in **hoofdstuk 2**. In **hoofdstuk 3** toonden we ook aan dat remming van miR-494-3p in atherosclerotische plaques *in vivo* leidde tot een duidelijke vermindering van de pro-inflammatoire marker C-C motief chemokine receptor-2 (CCR2).

Pathway enrichment analyse voorspelde dat miR-494-3p meer dan 70 targets heeft die betrokken zijn bij macrofaag polarisatie. De pathway met de meeste toegewezen genen was de Wnt signalling pathway. MiR-494-3p reguleert inderdaad de expressie van meerdere Wnt signalling genen, waaronder LRP6 en TBL1X. Bij activatie van de Wnt signalling pathway wordt niet-gefosforyleerd β-catenine getransponeerd naar de kern, waar het downstream transcriptie induceert. De Wnt signalling pathway bleek inderdaad geactiveerd na behandeling met 3GA-494. Niet-gefosforyleerd β-catenine was verhoogd zowel in gekweekte M1 macrofagen als in plaques van hypercholesterolemische muizen. De gedempte M1 polarisatie wordt dus, althans gedeeltelijk, gereguleerd via geactiveerde Wnt signalling.

Wnt signalling is vooral bekend van (stam)cel differentiatie en de betrokkenheid bij ziekten, zoals kanker. Sommige studies suggereren echter een beschermende rol van Wnt signalling tegen atherosclerose. Wnt signalling zou bijvoorbeeld een rol kunnen spelen in het beperken van cholesterol-ophoping in atherosclerotische plaques. Bevindingen uit eerdere studies en uit dit proefschrift wijzen erop dat miR-494-3p remming cholesterolmetabolisme beïnvloedt. Efflux van high-density lipoproteïne (HDL) bijvoorbeeld, was verhoogd in miR-494-3p geremde macrofagen. MiR-494-3p inhibitie verminderde ook de grootte van de necrotische kern in vroege atherosclerotische plaques en verlaagde het plasma cholesterolgehalte *in vivo* (**hoofdstuk 2**). TREM2 is een marker voor ontstekingsremmende lipide-geladen macrofagen die betrokken zijn bij cholesterolmetabolisme. Hoewel geen direct miR-494-3p target, nam de expressie van TREM2 toe in M2 gepolariseerde macrofagen behandeld met 3GA-494. 3-Hydroxy-3- methylglutaryl-coenzyme A synthase 1 (HMGCS1) is een vermoedelijk miR-494-3p

target en is betrokken bij de cholesterolsynthese. Van de vier humane donoren, toonden drie donoren een differentiële expressie van HMGCS1 na 3GA-494 behandeling, in zowel gekweekte M1 als M2 macrofagen (**hoofdstuk 3**). MiR-494-3p is daarom waarschijnlijk betrokken bij de regulatie van cholesterol metabolisme genen. De precieze mechanismen, en ook of Wnt signalling of andere relevante pathways hierbij betrokken zijn, zal echter nog uitgezocht moeten worden in toekomstig onderzoek.

Polarisatie van macrofagen naar M2 induceerde miR-494-3p expressie. MiR-494-3p expressie werd echter nog verder geïnduceerd in reactie op behandeling met miR-494-3p remmers (**hoofdstuk 3**). Dit onverwachte fenomeen werd ook waargenomen in zowel de bloedplaatjes als de gehele milt na behandeling met 3GA-494 (**hoofdstuk 2**). Mogelijk reguleert miR-494-3p de expressie van RNA-bindende eiwitten en reguleren RNA-bindende eiwitten op hun beurt de processing van miR-494-3p. RNA-bindend eiwit Mef2A, bijvoorbeeld, bindt direct aan pri-miR-494-3p. Welk mechanisme precies aan de basis ligt van deze subset-, cel-, en weefselspecifieke autoregulatie, moet echter nog worden onderzocht.

Samenvattend, het eerste deel van dit proefschrift toont aan dat miR-494-3p bijdraagt aan de progressie van atherosclerose. Remming ervan stopt plaque progressie en verhoogt de stabiliteit van gevorderde plaques. Remming van miR-329-3p heeft een minder ingrijpend effect op de progressie van atherosclerose. Bovendien reguleert miR-494-3p ook rechtstreeks de activering en polarisatie van macrofagen. Inhibitie van miR-494-3p vermindert M1 polarisatie, terwijl M2 polarisatie wordt versterkt. Beide zijn gunstig in het afremmen van atherosclerose.

AF357425/SNORD113-6 target mRNA's via pre-mRNA-processing en 2'Ome

Van sommige ‘’wees’’ C/D box snoRNA's, die dus geen bekende rRNA-targets hebben, is beschreven dat zij 2'Ome op andere type RNAs sturen, zoals mRNA's, microRNA's en tRNA's. Geheel andere functies, b.v. het sturen van alternatieve splicing en het reguleren van genexpressie expressie op een microRNA-achtige manier, zijn ook beschreven voor ‘’wees’’ C/D box snoRNAs.

In **hoofdstuk 4** hebben we één van de 14q32 snoRNAs, SNORD113-6 en zijn muizen equivalent AF357425, onderzocht. Met de D’ antisense box bindt het snoRNA aan zijn RNA targets. De D' box antisense box van SNORD113-6/AF357425 is volledig geconserveerd tussen mens en muis. SNORD113-6/AF357425 en 14q32 snoRNA’s in het algemeen, komen sterk tot expressie in fibroblasten. Daarom was ons eerste plan om AF357425 knock-out fibroblasten te

gebruiken. Deze konden echter niet worden verkregen, omdat AF357425-knockout klonen niet levensvatbaar bleken te zijn. Dit suggereert ofwel dat onze CRISPR/Cas9 strategie niet succesvol was of, meer waarschijnlijk, dat AF357425 essentieel is voor cel overleving. Daarom gebruikten we een antisense technologie om AF357425 in muizen fibroblasten te inhiberen (knockdown) of tot overexpressie te brengen. Vervolgens hebben we twee verschillende RNA sequencing (RNA-seq) strategieën toegepast op deze cellen. In één strategie, werd RNA-seq uitgevoerd op hele cel lysaten om alternatieve splicing en processing te onderzoeken. In de andere strategie werd RNA afkomstig van fibrillarine pulldown geïsoleerd. Vervolgens werd dit RNA vrijgemaakt van rRNA en gesequenced om fibrillarine-geassocieerde targets te identificeren.

Wij vonden een verrijking van AF357425 bindingsplaatsen (d.w.z. het omgekeerde complement van de D' antisense box) in het laatste exon en de 3'UTR van (pre)mRNAs. We identificeerden 46 genen met vermoedelijke snoRNA bindingsplaatsen. Deze vertoonden differentiële expressie van splice- of processing-varianten tussen AF357425 overexpressie en knockdown cellen. Van deze genen, hadden vermoedelijk 20 genen een geconserveerde bindingsplaats bij de mens. We selecteerden drie genen, DUSP7, JAG1 en EBPL, en bevestigden inderdaad veranderde processing onder SNORD113-6/AF357425 knockdown. Het bleek dat de locatie van de snoRNA-bindingsplaats bepaalt of de processing van het pre-mRNA al dan niet wordt beïnvloed door SNORD113-6/AF357425-knockdown. Een bindingsplaats in het laatste exon en 3'UTR, maar niet in introns, resulteerde in verhoogde expressie van de dominante variant (gedefinieerd door de variant met een bindingsplaats in exon/3'UTR, de eiwit-coderende variant of de variant met de meeste bindingsplaatsen) boven de alternatieve variant onder SNORD113-6/AF357425 knockdown.

Ook identificeerden we 7 genen uit de integrine pathway, MAP2K1, ITGB3, ITGA7, FLNB, NTN4, PARVB en COL4A4, die fibrillarine-afhankelijke 2'Ome mRNA targets zijn van AF357425/SNORD113-6. De integrine pathway is belangrijk voor cel-cel en cel-matrix interacties. Bindingsplaatsen van deze genen waren zowel bij muis als mens geconserveerd, zij het voor sommige op verschillende locaties (laatste exon/3'UTR bij muis versus introns bij mens). We richtten ons op de integrine pathway, omdat deze de sterkste verrijking van targets had. We vonden echter ook mogelijke targets die betrokken zijn bij andere relevante cardiovasculaire pathways. Na het blokkeren van transcriptie, werd het mRNA van de targets sneller afgebroken onder knockdown van AF357425/SNORD113-6. 2'Ome door AF357425/SNORD113-6 is dus belangrijk voor de stabiliteit van deze mRNA targets. De effecten op eiwitniveaus waren echter dubbelzinnig en hangen waarschijnlijk af van

verschillende factoren. De plaats van de bindingsplaats en de vraag of binding van AF357425/SNORD113-6 leidt tot 2'Ome of niet, zou de translatie van eiwitten kunnen beïnvloeden. Aan de ene kant laten we zien dat 2'Ome het mRNA beschermt tegen degradatie. Er is dus meer mRNA aanwezig om in eiwit te worden vertaald. Anderzijds kan 2'Ome op het mRNA de binding van het ribosoom belemmeren, wat resulteert in minder eiwit. Om meer duidelijkheid te krijgen in wat dit betekent voor de functie van fibroblasten, hebben we een aantal functionele assays uitgevoerd met humane arteriële fibroblasten. We vonden een verhoogde barrièrefunctie, een verhoogd vermogen om extracellulaire matrix samen te trekken en een verhoogde migratie in SNORD113-6 knockdown fibroblasten.

Zowel de integrine pathway als de fibroblast functie zijn belangrijk in cardiovasculaire remodellering en ziekte. Hoe de door SNORD113-6 gereguleerde fibroblastfunctie de cardiovasculaire remodellering en ziekte precies beïnvloedt, moet nog worden bepaald in toekomstig onderzoek.

AF357425/SNORD113-6 reguleert fragmentatie van tRNAs via 2'Ome

In **hoofdstuk 4** laten we zien dat AF357425/SNORD113-6 een breed scala van mRNAs target en hun expressie beïnvloedt via twee mechanismen, pre-mRNA processing en 2'Ome. Recente studies hebben aangetoond dat post-transcriptionele modificaties geleid door snoRNAs, 2'Ome en pseudouridylering Ψ, op tRNAs kunnen leiden tot hun splitsing in kleinere tRNA-afgeleide fragmenten (tRFs). In **hoofdstuk 5** wilden we daarom bepalen of AF357425/SNORD113-6 ook kleine RNAs kan targetten.

Small RNA sequencing (sRNA-seq) werd uitgevoerd op cel lysaten van ofwel AF357425 geremde of tot overexpressie gebrachte AF357425 muizen fibroblasten. De kleine RNA's die het meest in expressie veranderden waren tRF's. De totale vorming van tRFs was verminderd in AF357425 knockdown fibroblasten. Wanneer gestratificeerd naar fragmentlengte, waren de kleinere tRFs (18-30 nucleotiden) verrijkt en de langere tRFs (30-45 nucleotiden) verminderd in deze cellen.

Wij focuste ons op één van de tRNA's, tRNA Leucine anti-codon TAA ($tRNA^{Leu}$(TAA)), om het onderliggende werkingsmechanisme te onderzoeken. $TRNA^{Leu}$(TAA) heeft een voorspelde bindingsplaats voor AF357425/SNORD113-6, die inderdaad door AF357425/SNORD113-6 bleek te worden gemethyleerd. AF357425/SNORD113-6 knockdown had geen invloed op de degradatie van $tRNA^{Leu}$(TAA). Deze enkele 2'Ome site is dus niet essentieel voor de algemene stabiliteit van het tRNA. De dominante tRF van $tRNA^{Leu}$(TAA), $tRF^{Leu\ 47\text{-}64}$ wordt gevormd

aangrenzend aan de 2'Ome site. Knockdown van AF357425/SNORD113-6 verhoogde de verhouding van $tRF^{Leu\ 47\text{-}64}$ tot $tRNA^{Leu}$(TAA). Dit suggereert dat 2'Ome door AF357425/SNORD113-6 plaats-specifieke fragmentatie van tRNAs in kleine fragmenten (~18 nucleotiden in lengte) voorkomt.

Het is aangetoond dat fragmentatie van tRNAs toeneemt onder cellulaire stress, zoals hypoxie en oxidatieve stress. Plasmaniveaus van 14q32 snoRNA's zijn ook gereguleerd onder ischemische condities bij perifeer vaatlijden patiënten. Zoals verwacht verhoogde blootstelling van cellen aan cellulaire stress de expressie van AF357425/SNORD113-6, maar ook van $tRNA^{Leu}$(TAA) en $tRF^{Leu\ 47\text{-}64}$. Echter, het induceren van cellulaire stress verhoogde de verhouding van $tRF^{Leu\ 47\text{-}64}$ ten opzichte van het volwassen $tRNA^{Leu}$(TAA) niet verder in AF357425/SNORD113-6 knockdown cellen. In feite was de sterkste toename van deze verhouding in cellen gekweekt onder fysiologische omstandigheden, zonder inductie van cellulaire stress. Een verklaring zou kunnen zijn dat andere endonucleasen geactiveerd worden tijdens cellulaire stress en alternatieve tRF soorten produceren uit volwassen $tRNA^{Leu}$(TAA). Het zou ook kunnen dat de opregulatie van AF357425/SNORD113-6 onder cellulaire stress, de effecten van snoRNA knockdown compenseert.

Dit specifieke $tRF^{Leu\ 47\text{-}64}$ kan een belangrijke rol spelen in de celfysiologie, aangezien het onder fysiologische omstandigheden wordt geproduceerd en niet uitsluitend tijdens cellulaire stress. Voor tRF's zijn allerlei regulerende functies beschreven. Zij reguleren de translatie van eiwitten, vervullen microRNA-achtige functies en hebben interactie met RNA-bindende eiwitten. TRFs kunnen zowel cel fenotypes reguleren, bv. hartspiercellen, skeletspiercellen en endotheelcellen, als ook volledige complexe vasculaire processen reguleren zoals angiogenese. De exacte functie van deze AF357425/SNORD113-6-afhankelijke $tRF^{Leu\ 47\text{-}64}$ en zijn rol in vasculaire remodellering is nog niet bekend en moet dus nog in toekomstig onderzoek worden vastgesteld.

Samenvattend blijkt uit het tweede deel van dit proefschrift dat SNORD113-6/AF357425 een breed scala van mRNA's target en hun expressie beïnvloedt via twee mechanismen, pre-mRNA processing en 2'Ome. Beide mechanismen stabiliseren mRNA's en beïnvloeden het fenotype van fibroblasten. Verder laten we zien dat SNORD113-6/AF357425 ook tRNA's target via 2'Ome en dat dit de fragmentatie beïnvloedt. We hebben ingezoomd op het mechanisme van $tRNA^{Leu}$(TAA). Deze inzichten in de functie van SNORD113-6/AF357425 en hoe dit snoRNA de fibroblastfunctie beïnvloedt, kunnen nieuwe therapeutische mogelijkheden bieden bij de behandeling van hart- en vaatziekten.

Conclusie

Dit proefschrift heeft (een deel van) de bijdrage van 14q32 microRNAs en snoRNAs aan de progressie van hart- en vaatziekten laten zien. We hebben ook hun therapeutisch potentieel onderzocht. In het eerste deel van het proefschrift hebben we aangetoond dat remmen van miR-494-3p potentieel heeft in het verminderen van atherosclerose. In het tweede deel onderzochten we zowel de functie als de RNA targets van één 14q32 snoRNA, het humane SNORD113-6 en zijn muizen equivalent AF357425. Dit leverde nieuwe inzichten op in de functie van menselijke arteriële fibroblasten. Er moeten nog talrijke hindernissen worden overwonnen voordat deze fundamentele kennis in de geneeskunde kan worden toegepast. Een beter begrip van de onderliggende pathogenese van de ziekte, waartoe dit proefschrift heeft bijgedragen, creëert echter wel nieuwe therapeutische mogelijkheden voor hart- en vaatziekten.

Appendix

List of publications

1. **E van Ingen**, PAM Engbers, ML van der Bent, H Mei, J Wojta, PHA Quax, AY Nossent. C/D box snoRNA SNORD113-6 guides 2'-O-methylation and protects against site-specific fragmentation of $tRNA^{Leu}$(TAA) in human arterial fibroblasts. *Molecular Therapy Nucleic Acids*; under review

2. V Kremer, L Stanicek, **E van Ingen**, DI Bink, S Hilderink, A Tijsen, AY Nossent, RA Boon. Long non-coding RNA MEG8 induces endothelial barrier through regulation of microRNA-370 and -494 processing. *Journal of Cell Science*; under review

3. **E van Ingen***, DAL van den Homberg*, ML van der Bent, N Papac-Milicevic, V Kremer, RA Boon, PHA Quax, J Wojta, AY Nossent. C/D box snoRNA SNORD113-6/AF357425 plays a dual role in integrin signalling and arterial fibroblast function via pre-mRNA processing and 2'O-ribose methylation. *Human Molecular Genetics* 2022 Mar 31;31(7):1051-1066
   *authors contributed equally

4. V Kremer, DI Bink, L Stanicek, **E van Ingen**, T Gimbel, S Hilderink, S Günther, AY Nossent, RA Boon. MEG8 regulates Tissue Factor Pathway Inhibitor 2 (TFPI2) expression in the endothelium. *Scientific Reports* 2022 Jan 17;12(1):843

5. **E van Ingen**, AC Foks, T Woudenberg, ML van der Bent, A de Jong, PJ Hohensinner, J Wojta, I Bot, PHA Quax, AY Nossent. Inhibition of microRNA-494-3p activates Wnt signaling and reduces proinflammatory macrophage polarization in atherosclerosis. *Molecular Therapy Nucleic Acids* 2021 Nov 4;26;1228-1239

6. RVCT van der Kwast, L Parma, ML van der Bent, **E van Ingen**, F Baganha, HAB Peters, EAC Goossens, KH Simons, M Palmen, MR de Vries, PHA Quax, AY Nossent. Adenosine-to-Inosine editing of vasoactive microRNAs alters their targetome and function in ischemia. *Molecular Therapy Nucleic Acids* 2020 Sep 4;21:932-953

7. **E van Ingen**, AC Foks, MJ Kröner, J Kuiper, PHA Quax, I Bot*, AY Nossent*. Antisense oligonucleotide inhibition of microRNA-494 halts atherosclerotic plaque progression and promotes plaque stabilization. *Molecular Therapy Nucleic Acids* 2019 Dec 6;18:638-649
   *authors contributed equally

8. KEJ Håkansson*, EAC Goossens*, S Trompet*, **E van Ingen**, MR de Vries, RVCT van der Kwast, RS Ripa, J Kastrup, PJ Hohensinner, C Kaun, J Wojta, S Böhringer, S Le Cessie, JW Jukema, PHA Quax, AY Nossent. Genetic associations and regulation of expression indicate an independent role for 14q32 snoRNAs in human cardiovascular disease. *Cardiovascular Research* 2019 Aug 1;115(10):1519-1532
   *authors contributed equally

9. MJ Hernandez, R Gaetani, VM Pieters, NW Ng, AE Chang, TR Martin, **E van Ingen**, EA Mol, JPG Sluijter, KL Christman. Decellularized extracellular matrix hydrogels as a delivery platform for microRNA and extracellular vesicle therapeutics. *Advanced Therapeutics* 2018 Jul;1(3):1800032

10. RVCT van der Kwast, **E van Ingen**, L Parma, HAB Peters, PHA Quax PHA, AY Nossent. Adenosine-to-Inosine editing of microRNA-487b alters target gene selection after ischemia and promotes neovascularization. *Circulation Research* 2018 Feb 2;122(3):444-456

Appendix

Curriculum Vitae

Eva van Ingen werd geboren op 3 juli 1992 te Utrecht. In 2010 behaalde zij haar vwo-diploma aan Het Nieuwe Lyceum in Bilthoven. Dat jaar begon zij aan haar studie Biomedische Wetenschappen aan de Universiteit Utrecht. Na het succesvol afronden van haar Bachelor (BSc), startte Eva in 2014 aan de Master Regenerative Medicine and Technology, een samenwerking tussen de Graduate school of Life Sciences van de Universiteit Utrecht en de faculteit Biomedical Engineering van de Technische Universiteit Eindhoven. Tijdens het eerste jaar heeft Eva een onderzoeksstage gedaan bij de groep van prof. dr. Sluijter, de afdeling Experimentele Cardiologie in het Universitair Medisch Centrum Utrecht. Tijdens het tweede jaar heeft zij een onderzoeksstage gedaan bij de groep van dr. Christman aan de University of California San Diego (UCSD), Department of Bioengineering. Hiervoor kreeg zij een beurs uit het Jo Kolk Studiefonds. In 2017 behaalde Eva haar Master diploma (MSc). Dat jaar is zij ook begonnen als promovenda onder leiding van prof. dr. Quax en dr. Nossent, op de afdeling Vaatchirurgie in het Leids Universitair Medisch Centrum. Zij is aangesteld op een beurs van het Rembrandt Institute for Cardiovascular Science (RICS), een samenwerking binnen cardiovasculair onderzoek tussen Leiden en Amsterdam. De beurs is verkregen door dr. Nossent en prof. dr. Boon, van de afdeling fysiologie in het Amsterdam UMC. Eva heeft tijdens haar promotie de rol van 14q32 niet-coderende RNA's onderzocht in hart- en vaatziekten. Haar resultaten staan beschreven in dit proefschrift. In 2019 heeft Eva tijdens haar promotie 3 maanden de groep van dr. Wojta, aan de Medical University of Vienna, Department of Internal Medicine II, bezocht. Zij heeft hier de rol van 14q32 niet-coderende RNA's in macrofagen onderzocht. Zij heeft hiervoor een beurs uit het Prins Bernhard Cultuurfonds en uit het Leids Universitair Fonds Study Trip gekregen. Tijdens haar promotie is Eva meerdere keren geselecteerd om haar werk te presenteren op congressen en symposia. In 2021 is Eva gestart als postdoc bij de groep van prof. dr. Kuiper, Division of BioTherapeutics in het Leiden Academic Centre for Drug Research. Hier is zij verder gegaan in het onderzoek naar atherosclerose.

Dankwoord

Iedereen die heeft bijgedragen aan de totstandkoming van mijn proefschrift wil ik bedanken. In het bijzonder gaat mijn dank uit naar de volgende mensen.

Mijn promotor, prof. dr. Paul Quax, bedankt voor alle jaren binnen de onderzoeksgroep. Je was een betrokken begeleider en ik kon op D6 altijd even binnenwandelen om iets te vragen of gewoon voor een kopje koffie.

Mijn copromotor, dr. Yaël Nossent, bedankt voor alle steun en het in mij gestelde vertrouwen. Met jouw enthousiaste manier van begeleiden heb je mij wegwijs gemaakt in de RNA wereld en kreeg ik altijd weer energie om door te gaan.

Tom, mijn broertje. Onze band is altijd heel sterk geweest. We begrijpen elkaar, hebben dezelfde humor en kunnen elkaar goed helpen. Ook al weet je niet veel van de inhoud van dit proefschrift, de cover heb ik aan jou te danken. Ik ben heel trots en dankbaar dat jij vandaag mijn paranimf bent.

Eveline, ik leerde je kennen toen ik begon aan mijn promotie in 2017. We hadden gelijk een klik en waren dan ook vaak samen te vinden op D6, in de celkweek of aan de RNA bench. Ondanks dat jij in 2019 het onderzoek inruilde voor de kliniek, bleef jij toch mijn RNA-partner-in-crime. Ik ben dan ook heel blij en dankbaar dat je vandaag naast mij staat als paranimf.

Erna, dank je wel voor het meedenken en helpen met experimenten en het begeleiden van studenten. En natuurlijk ook dank voor alle fietstips.

Daphne, dank je wel voor de samenwerking en je inzet bij het snoRNA paper. Veel succes bij je eigen promotie en verdere carrière.

Margreet, Licheng, Alwin, Thijs, Tamar, Judith, Taya, I will never forget the beach day and especially the horseback riding. Thanks for all the work-related help, but also all the fun times we had in the lab.

Leontien, Laura, Regi, Valérie, Fabiana, the previous C7 crew. Thanks for all the scientific help, laughs, gossips, great dancing skills and fun during my PhD.

Annelieke, Michèle, Fenna en Ruth, ook al is de oude D6 nu al even verleden tijd, dank voor jullie gezelligheid, de lunches en (iets te lange) koffiemomentjes.

Bart, Gaia, Martijn en Pleun: jullie als mijn studenten wil ik graag bedanken voor je inzet en hulp in het lab. Ik wens jullie veel succes met de afronding van jullie studie en verdere carrière.

Leon, thanks a lot for your help with the bioinformatics part of this thesis. Your help was of great value to the snoRNA papers.

Veerle en prof. dr. Reinier Boon, bedankt voor de nuttige meetings, input op experimenten en een geslaagde Rembrandt samenwerking.

Dr. Ilze Bot, dr. Amanda Foks en prof. dr. Johan Kuiper, bedankt voor jullie samenwerking en input op dit proefschrift. En natuurlijk ook dat ik nu deel uit mag maken van jullie groep.

Vriendinnen, vrienden en familie, dank jullie wel voor jullie steun, interesse in mijn promotie en natuurlijk al het leuks buiten het werk om. Met alle weekendjes weg, borrels, etentjes, paardrijden en fietstochten, is het leven één groot feest. Jullie zijn mij heel dierbaar.

Papa en mama, jullie kijken al jaren uit naar deze dag en nu gaat het dan echt gebeuren. Jullie zijn er altijd voor me. Om mij te helpen of om zomaar even te kletsen. Bedankt voor jullie steun en dat jullie altijd in mij geloven. Opa's Jan en oma Riet, ik weet dat jullie ontzettend trots zouden zijn geweest dat ik als eerste van de familie een doctorstitel behaal. Ik denk aan jullie. Oma Tineke, ik ben ontzettend dankbaar dat jij, mijn omaatje, bij deze bijzondere dag kan zijn.

Olivier, ook al vind je het nog steeds lastig om uit te leggen waar dit proefschrift over gaat (gênant), je blijft altijd geïnteresseerd en denkt met alles mee. Met jouw kalmte en humor weet je mij altijd weer gerust te stellen en aan het lachen te krijgen. Je bent mijn grote liefde en steun.